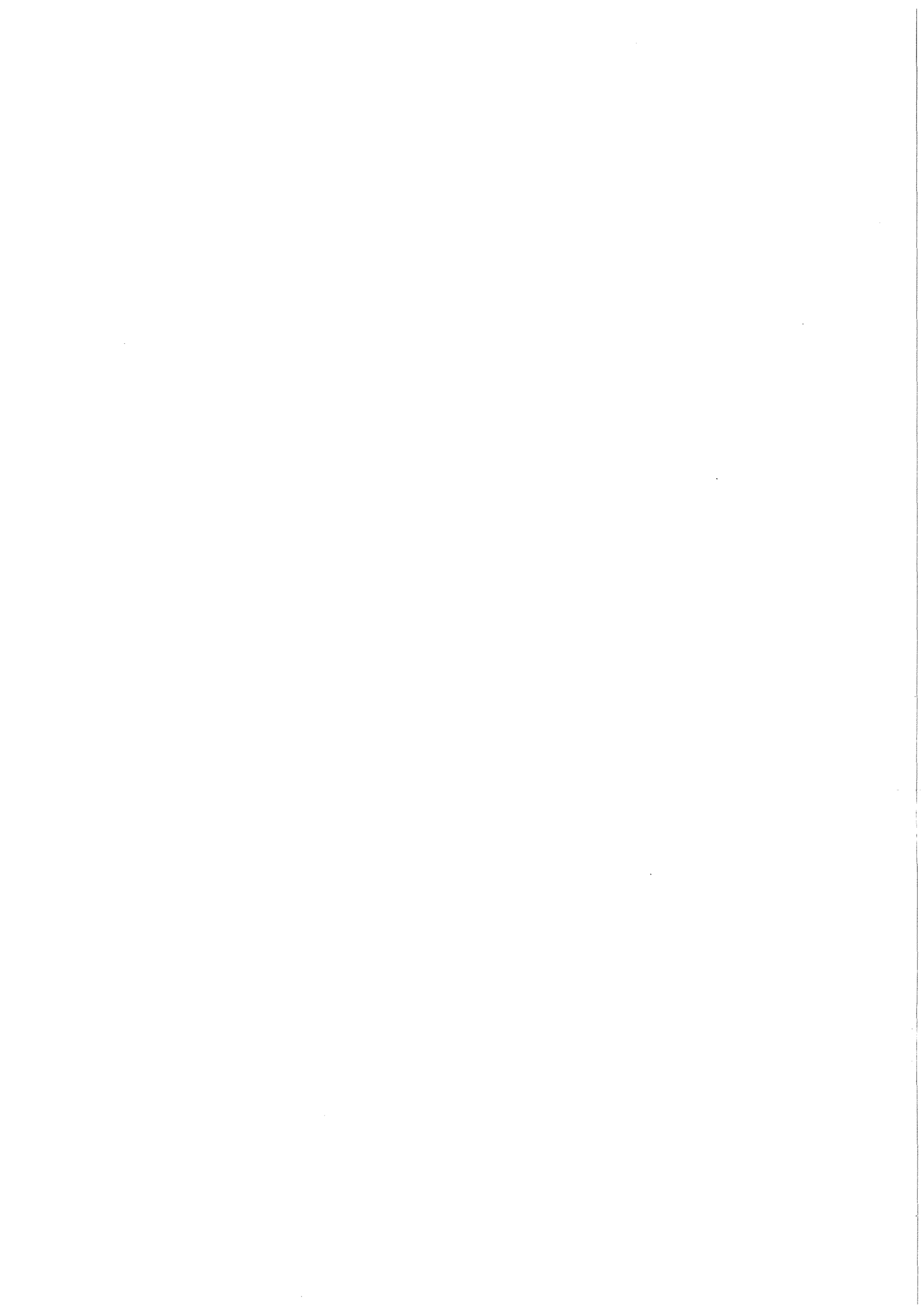


KfK 3749
Juni 1984

Microprocessor-Based Integrated LMFBR Core Surveillance

Editor: L. Gmeiner
Institut für Datenverarbeitung in der Technik
Projekt Schneller Brüter

Kernforschungszentrum Karlsruhe



KERNFORSCHUNGSZENTRUM KARLSRUHE

Institut für Datenverarbeitung in der Technik
Projekt Schneller Brüter

KfK 3749

Microprocessor-Based Integrated LMFBR Core Surveillance

by

Lothar Gmeiner
(Editor)

Kernforschungszentrum Karlsruhe GmbH, Karlsruhe

Als Manuskript vervielfältigt
Für diesen Bericht behalten wir uns alle Rechte vor

Kernforschungszentrum Karlsruhe GmbH
ISSN 0303-4003

Microprocessor-Based Integrated LMFBR Core Surveillance

Abstract:

This report results from a joint study of KfK and INTERATOM. The aim of this study is to explore the advantages of microprocessors and microelectronics for a more sophisticated core surveillance, which is based on the integration of separate surveillance techniques.

Due to new developments in microelectronics and related software an approach to LMFBR core surveillance can be conceived that combines a number of measurements into a more intelligent decision-making data processing system.

The following techniques are considered to contribute essentially to an integrated core surveillance system:

- subassembly state and thermal hydraulics performance monitoring,
- temperature noise analysis,
- acoustic core surveillance,
- failure characterization and failure prediction based on DND- and cover gas signals, and
- flux tilting techniques.

Starting from a description of these techniques it is shown that by combination and correlation of these individual techniques a higher degree of cost-effectiveness, reliability and accuracy can be achieved.

The proposed data processing system is organized in five levels:

the reactor instrumentation level, the common communication level, the signal evaluation level, the decision making level, and the output generation level.

This layered architecture is modular and therefore allows to integrate or substitute individual parts if this should be necessary due to technological developments.

In addition, a complementary approach to core surveillance and fault diagnosis based on methods of parameter and state estimation is considered.

This complementary approach can be integrated in the signal evaluation level of our proposed data processing system, too.

Part of this study was funded by the European community under contract ECI-909-B-7222-82-D.

Ein integriertes, mikroprozessorgesteuertes System zur Kernüberwachung bei Schnellen Brutreaktoren

Zusammenfassung

Dieser Bericht beschreibt eine gemeinsame Studie zwischen KfK und INTERATOM. Ziel dieser Studie ist es, den Vorteil der Mikroprozessortechnologie für eine fortgeschrittene Kernüberwachung von Brutreaktoren aufzuzeigen.

Aufgrund neuerer Entwicklungen der Mikroelektronik und der Softwaretechnologie wird ein Konzept vorgestellt, in dem eine Reihe von individuellen Überwachungsverfahren zu einem integrierten Messwertverarbeitungssystem zusammengestellt werden.

Die folgenden Überwachungsverfahren liefern wesentliche Beiträge zur integrierten Kernüberwachung:

- Temperaturüberwachung der einzelnen Brennelemente
- Temperaturrauschen
- Akustische Überwachungsverfahren
- Messung und Überwachung der verzögerten Neutronen sowie des Schutzgases.

Ausgehend von einer Beschreibung dieser Verfahren wird gezeigt, daß durch eine Kombination bzw. eine Korrelation dieser individuellen Verfahren ein höherer Grad an Zuverlässigkeit, Kosteneffizienz und Genauigkeit erreicht werden kann.

Das vorgeschlagene Datenverarbeitungssystem besteht aus fünf Ebenen: der Reaktorinstrumentierungsebene, der Kommunikationsebene, der Signalauswertungsebene, der globalen Entscheidungsebene sowie der Ausgabebene.

Diese schichtenweise Organisation ist modular und erlaubt es, individuelle Teile zu integrieren oder zu ersetzen, sofern dies notwendig sein sollte.

Darüberhinaus wird ein komplementärer Ansatz zur Kernüberwachung und Fehlerdiagnose behandelt, der auf Methoden der Parameterschätzung basiert. Dieser komplementäre Ansatz kann innerhalb der Signalauswertungsebene in das vorgeschlagene Datenverarbeitungssystem integriert werden.

Ein Teil dieser Arbeiten wurde von der Europäischen Gemeinschaft unter ECI-909-B-7222-82-D gefördert.

Table of contents:

	Page
1. Introduction W. Glauner, PSB-PL; A. Holick, INTERATOM	1
2. Current activities	7
2.1 A Microprocessor-based system for the evaluation of fuel element outlet temperatures U. Voges, IDT	8
2.2 Subassembly state and performance monitoring M. Edelmann, INR	22
2.3 Detection of cooling channel disturbances by measurement and analysis of temperature fluctuation signals at the outlet of an LMFBR G. Weinkötz, L. Krebs, IRB	40
2.4 Acoustic noise detection H. Rohrbacher, IRE	53
2.5 Detection of failed fuel elements S. Jacobi, IRE	61
2.6 Location of failed fuel elements by flux tilting S. Jacobi, IRE	72
2.7 Neutron-noise analysis	89
3. Integrated approach L. Gmeiner, U. Voges, IDT	90
4. Concept of "Global LMFBR Core Surveillance Procedure" (GCSP) A. Holick, INTERATOM	98
5. Performance tests by means of simulation A. Holick, INTERATOM	180
6. Preliminary verification with KNK-II experiments A. Holick, INTERATOM	229
7. Conclusions	284

1. Introduction

W. Glauner, KfK-PSB
A. Holick, Interatom

This study is based on R+D-work for the German Fast Breeder Reactor. Cooling disturbances within the core are a major concern for safety and availability considerations. A fault propagation diagram has been set up and the potential of different individual advanced measuring techniques and analysis procedures is explored.

The aim of this study is now to explore the advantage of microprocessors for a more sophisticated core supervision. Efficient utilization of the information contained in the measurements is a basic concern of the surveillance methodologies. The availability of microprocessors provides an opportunity for applying advanced concepts of "information technology" to the enhancement of the availability and safety of fast breeder plants in particular. The CEC sponsored joint study on "Integrated LMFBR-Core Surveillance" from KfK and Interatom has chosen an approach, where a number of individual monitoring techniques are combined for the purpose of exploring the power of advanced microprocessor-based information processing concepts. The resulting protection and control system is expected to approach the state of the art in real time information processing and will contribute to increasing the cost effectiveness of LMFBR plants.

KfK's contribution to this study (chapter 2 and 3) focusses on the advanced individual methods, including the application of microprocessors to on-line signal evaluation. In a next step, the integral system will be considered and the surveillance variables associated with the various measurement channels will be provided simultaneously to a single decision making entity, where correlation techniques and cause-consequence analysis will be employed to support the early warning capability of the protection system.

The KfK-approach rests upon the results of the R+D-work for the German Fast Breeder Reactor and, in particular, upon conclusions to be drawn from accident analysis. It aims mainly at the early detection of cooling disturbances and the identification of pin failures. The rationale of the approach is introduced in the following in some more detail.

If we omit - for this study - the so-called hypothetical accidents, we then have to deal mainly with cooling disturbances in fuel subsassemblies. They may be caused by pin failures, pin bowing, foreign materials, spacer failures, or inadequate clearances and tolerances (see Fault Propagation Diagram, Fig. 1-1). These could lead to blockages in the fissile zone (internal blockages) or at the subassembly inlet (external blockages). The chemical reaction between fuel and sodium is of particular importance with respect to blockage formation around defective fuel pins.

The increased volume of the reaction product could lead to a temperature increase within the blocked area and to a further propagation of the defect by affecting adjacent pins etc. Also the release of fuel or the fuel-coolant compound from the defect area and its deposition on the down-stream spacergrid is a possible blockage mechanism.

Up to now, we will have the surveillance of:

- the mean coolant outlet temperature from each fuel element (chapter 2.1),
- delayed neutrons (DND-technique) in the coolant, which indicates the possible release of fission products from defected fuel pins (chapters 2.5, 2.6).

The mean coolant temperature from each fuel element and the fission product release measurements, made by the DND-systems are connected to the automatic shutdown system, in a conventional way.

A good status of knowledge for released fission product monitoring has been reached by a series of loop and in-core measurements with artificially and naturally defected fuel pins. In addition to the DND-technique, other methods, especially for released fission gases are studied.

Whereas the temperature monitoring supervises each individual fuel subassembly the DND-systems observes only the total coolant flow of the primary system. This does not allow to localize the defective fuel element, and other means are to be investigated to identify the faulty position. This can be achieved by the "flux-tilting" procedure, which is a part of this study and will be found in chapter 2.6.

A probabilistic risk analysis has shown a very low probability for the occurrence of different blockage scenarios, and by the installation of sensitive measuring devices, the probability for a defect propagation between fuel elements is expected to be $\leq 10^{-6}/a$.

Besides blockages and possible consequences on defect propagation, the release of fission products and fuel into the coolant is also undesirable from the viewpoint of system contamination and maintenance.

Whereas the mean temperature and the DN-supervision are already part of the breeder design, further R+D-work on new methods for sensitive coolant disturbance detection is performed, namely

- temperature fluctuation analysis: coolant disturbances (blockages) within a fuel element bundle cause an increase of the turbulences, measurable by an increase of temperature noise at the fuel element outlet (chapter 2.3),
- advanced methods for sensitive measurement of the mean coolant temperature from a fuel element: even large total local blockages within the fuel bundle cause only a small decrease of the total flow rate or only a slight increase of the mean outlet temperature, which is difficult to determine due to natural background fluctuation from coolant flow, neutron power etc.

The so-called "compensation method" allows the elimination of undesired noise-contributions and a more precise measurement of the mean outlet temperature (chapter 2.2)

- acoustic boiling detection: in case a blockage causes sodium boiling in a fuel-assembly, measurement of the acoustic signal will be a means to detect it (chapter 2.4).

Furthermore, the general potential of neutron-noise analysis for the detection of different phenomena in the core has been investigated (chapter 2.7). Within the frame of this study, the application is made only for the "compensation method" for sub-assembly state and performance monitoring (chapter 2.2).

Fig. 1-1 shows the principal detection potential of these methods at the different stages of the fault development process. In many cases, diverse detection of specific events is possible.

The status of the R+D-work of these new methods is such, that the basic phenomenological effects are investigated and are understood, from out-pile and in-pile experiments. On the other hand, reactor experience is still lacking. Here the KNK-II reactor will serve to get some more experience on the long term behaviour of the reactor itself and of the measuring chains also.

The measuring methods developed correspond to the phenomena to be observed - so we use thermocouples, neutron sensors, special microphones and different fission product detection devices.

The signal analysis methods are individually tailored for the problem under investigation. Except for fission product release monitoring (DND, fission gas measurements etc.), no attempt up to now has been made to combine or correlate the results from the different new measurement methods. It is thought that this could be a next step in the R+D-work, which needs some efforts to identify the possible chains of events, their possible time scales and probabilities. The use of microelectronics should be incorporated into this task. Chapter 3 proposes the concept of a micro-processor based integrated core surveillance system.

The installation of an integrated core surveillance system in the SNR 300 is not planned up to now. However, the advantages of having such an integrated system are obvious.

Interatom's contribution (chapters 4,5,6,7) focusses on the application of parameter and state estimation to the measurements from the out-of-core instrumentation, excluding the DND-signal, covergas monitoring and acoustic measurements. The expected gain in employing on-line estimation techniques lies in the opportunity to maximise the amount of information which can be extracted from the standard out-of-core measurements and can be provided to the decision-making subsystems. The concept provides a global picture of core dynamics and will be called, therefore, "Global Core Surveillance Procedure" (GCSP) for easy reference.

The GCSP aims at monitoring cooling - and reactivity-anomalies by means of two basically different modules:

- . Estimator for core state (i.e. fuel temperature and thermo-hydraulic core parameters (chapter 4.4, 4.5)
- . Estimator for the various reactivity contributions and reactivity parameters (chapter 4.6, 4.7).

There is a rather large number of estimation/identification methods available. Dynamic data systems methodology (DDS) has been applied already to simulated and real LMFBR data in an attempt to assess the feasibility of on-line monitoring systems and to non-nuclear large scale problems. It seems feasible, therefore, to place the estimation technique employed in this study within this frame.

The basis of the DDS approach is the auto-regressive moving average (ARMA) analysis of time ordered signals. In the most simple case, when only scalar measurement samples are considered, the ARMA-model can be looked upon as a digital filter whose input is a wide noise sequence and whose output is the observed sequence.

The ARMA-model has been generalized in the literature to the so-called ARMAX-model, which includes non-zero mean random input processes. Its most general form is based on a state space formulation.

The objective of on-line estimation is here to find the elements of the state vector and of the state-transition matrix from the measured system response to the input disturbance.

One has to cope with a combined parameter- and state-estimation task. Its solution can be found, for instance, with the "mutual interactive state and parameter estimation procedure" (MISP). MISP makes use of alternatively two Kalman-filters, one in state space and one in parameter space. The two filters interact recursively in performing optimal estimation in such a way, that the result is unbiased. Consistency is especially important for the estimate of system order.

Interatom's parameter adaptive approach to core surveillance requires also that a combined parameter and state estimation problem in state space formulation (ARMAX-model) is to be solved. But the solution method can be greatly simplified - as compared with MISP - because of the following arguments:

- . The coefficients of the ARMAX-model are derived from a physical model of core thermohydraulics, whose validity has been already tested. Hence, model order is known a priori and the coefficients are known in terms of the physical model parameters (section 4.1); deviations of the actual plant behaviour from the (model based) predicted behaviour will be sensed and indicated (section 4.8).

- . The standard out-of-core instrumentation and, especially, the standard analog-to-digital conversion equipment does not allow for preserving the process noise properties in computing the surveillance variables, hence, it is not possible to rely on system excitation solely due to process noise, even if the noise amplitudes would suffice. External excitation is needed during well defined calibration control intervals (section 4.3). Excitation profile and duration bear close resemblance to automatic feedback control signals.
- . Recursive interaction between parameter and state estimation, which is a characteristic feature of MISP, has been omitted and an analytical separation between the two tasks has been achieved (section 4.2). The significance of the bias problem in the least square algorithms is greatly reduced, because of the prefiltering of data needed to smooth quantization noise (appendix A4.3 and section 7.2.) Note again, that model order is known a priori.

Interatom's choice of method is characterized by analytical separation of the parameter from the state estimation task (increased failure tolerance level), by external excitation of the core (automatic calibration) and by insensitivity against process noise distortion (no need for special instrumentation). Neither the least square algorithms nor the Kalman filter need to be modified.

Fuel temperature was found to be a sensitive indicator of cooling anomalies (section 4.5). The coefficients of the prediction model (section 4.1) will be automatically updated, if the residual observation exceeds a prespecified bound (section 4.4). Detection and identification of slug flow requires modification of the Kalman filter (appendix A4.1).

Reactivity monitoring concepts are under development in USA, France and Germany. R.A. Harris (see chapter 6) showed, that systematic errors have to be expected in the reactivity balance and may reach magnitudes which are much larger than the actual signal. Therefore, the method relies heavily upon costly calibration schemes for slowly developing bias errors, whose origin cannot be identified.

Gauthier et al. (chapter 6) report good performance of the French concept during stationary operation and aim at extending the algorithms to the non-stationary case. The German concept for reactivity balance monitoring is similar to the US and French approach and is still being tested at the KNK II-plant.

In chapter 6 of this report, the conventional reactivity monitoring concept is briefly described and the coefficients of the prediction model are analytically expressed in terms of core state and physical core parameters.

Section 4.6 and 4.7 describe a new concept based on parameter and state estimation, which is characterized by the independence of the reactivity feedback model coefficients of the thermohydraulic core state.

The diagnostic potentials of the "Global Core Surveillance Procedure" and the need for automating the diagnostic process within the frame of artificial intelligence is discussed in section 4.7.

Convergence and consistency of the recursive parameter and state estimation procedures are tested in chapter 5 by means of simulation. Thermohydraulic monitoring performance is illustrated in terms of, for instance, a partial blockage with simultaneous perturbation of the radial power distribution, slug flow in a particular fuel element and continuous estimation of subassembly flow. Simultaneous estimation of all relevant thermohydraulic parameters has also been achieved with high accuracy. Estimation of reactivity parameters and itemized reactivity contributions is discussed in the sections 5.4, 5.5 and 5.6. It seems worthwhile emphasizing, that the reactivity contributions of the control rods are continuously determined without having to rely on rod position measurements. Performance tests for reactivity surveillance during non-stationary reactor operation is also treated.

In chapter 6, comparisons are made between the parameter adaptive Global Core Surveillance Procedure (GCSP) and other known monitoring methods, mainly in terms of sensitivity, adaptiveness to different reactors and time varying conditions, the need for special instrumentation and inherent diagnostic capabilities. The data base for the comparison is tables of surveillance variables which can be attributed to the various methods, plus timing constraints and the accuracies attainable. A discussion on the expected gain in coverage by adding the DND-signal, covergas monitoring, and acoustic measurements is also presented in chapter 6.

Experimental verification has been started with the off-line analysis of data from the KNK-plant. The experiment consists of disturbing the bank position or the flow rate manually in accordance with a given sequence of alternating constant and ramplike functions over a total of several minutes (section 6.1). Preprocessing schemes for the measured data are described in section 6.2. The objective is to reduce the effect of error sources which are typical for the out-of-core instrumentation system. The prediction model of the parameter estimation algorithms is identical to the on-line simulator and it is verified by comparison with measurements during small core transients. It is surprising how well the measurements can be reproduced with a very elementary model. The non-ideal thermocouple is introduced in terms of a time constant and a gain factor (first order lag) which are considered unknown and are estimated in context with the core parameters. The model of the thermocouple is embedded into the core model.

It is shown, that the input-disturbance profile chosen for this experiment does not excite the core sufficiently and that, therefore, the core transient response does not contain sufficient information on all thermohydraulic parameters to be estimated. However, realizable excitation functions are found which guarantee observability. Finally, section 6.4 is concerned with the parameter estimation task under the restrictions posed by the particular experimental conditions.

2. Current activities

This chapter summarizes different KfK-activities in the area of early failure detection methods.

2.1 A Microprocessor-Based System
for the Evaluation of Fuel Element Outlet Temperatures

U. Voges

Institut für Datenverarbeitung in der Technik

Abstract

A microprocessor-based reactor safety shut-down system is described which is monitoring the fuel element outlet temperatures of a fast reactor for the purpose of detecting local cooling disturbances and initiating automatic shut-down of the reactor (scram) in case of possible emergency situations. The system consists of four functional different subsystems each of which consists of three redundant microprocessors which communicate with each other for error detection and fault tolerance. The licensing of this system is one of the main objectives of this project.

2.1.1 Introduction

Up to now there is only limited use of programmable computers in safety-oriented parts of a reactor. This is mainly due to the fact that neither industry nor licensing authorities push this cause since, among other reasons, there exists only little experience with the validation of software.

We attempt to overcome these difficulties and we show a way to demonstrate the reliability of software. This attempt is made for a computerised reactor safety shut-down system which is monitoring the fuel element outlet temperatures at an LMFBR for cooling disturbances.

In chapter 2.1.2 the purpose of the protection system will be explained. Chapter 2.1.3 gives some details on the shut-down algorithms to be applied. Chapter 2.1.4 introduces the hardware design, chapter 2.1.5 the software structure. In chapter 2.1.6 the validation methodology will be outlined and chapter 2.1.7 will present some conclusions.

2.1.2 Purpose of the system

We are in the process of developing a safety shut-down system for the liquid metal fast breeder reactor KNK II at Karlsruhe. Currently there exists a hardwired safety system which we want to duplicate with a computerised system.

Enhanced algorithms shall be realised in this new system, which will first run in parallel to the existing system, but only in an open-loop fashion. Depending on the running experience it may later be working in closed-loop operation in parallel to the hardwired system or even replacing the old system.

The purpose of the system is the inspection of the coolant outlet temperature at each individual fuel element in order to detect local cooling disturbances. In case of emergency, that is if the temperature is exceeding certain fixed or calculated set points, either a message to the operators is given or an immediate automatic shut-down is initiated.

At the KNK II there are 29 fuel elements, each of which is instrumented with three redundant thermocouples. The measurement of these thermocouples has to be scanned cyclically. The total reaction time of the system has to be less than about five seconds for the time between temperature exceeding set points and shut-down (control rods in final position).

Although the design for the KNK II is presented in this paper, the same methodology can be applied for other LMFBRs. Similar systems have been in discussion for the SNR300, eg.

2.1.3 Shut-down algorithms

Five different shut-down algorithms shall be applied. Some of them are exactly the ones used in the existing hardwired system, some are more sophisticated ones which were discussed for the SNR300. Part of these limits are constant, the other part are floating limits which are newly calculated in every cycle. An overview on the algorithms is given in table 2.1-1.

The first algorithm is concerned with only some of the fuel elements, the elements within the test zone. For them individual fixed upper limits exist. If they are exceeded again a shut-down is initiated. No lower limit exists in this case. This is a rather KNK II special feature algorithm which probably will have no counterpart in normal reactors.

The second algorithm is calculating a floating limit. For this the fuel elements are grouped together according to their behaviour dependence on their position and the position of the control rods. For the small KNK II only two groups are formed. For larger cores like the SNR300 some five groups could be necessary. For each group the mean value is calculated. If the temperature of a group member is too much above the group mean value, scram is initiated, if it is diverging too much below this mean value, an alarm message is printed.

The third algorithm is mainly a kind of plausibility check. The major fixed limits are considered. If the upper limit of 650 degree is exceeded, a shut-down is initiated. If the temperature is below the lower limit, the inlet temperature, an alarm message to the operators is given, since this is probably a defect in the measuring system.

So far the algorithms were only concerned with the actual measurement value, no history was involved. The following are keeping a memory of the measurement values and do some kind of digital filtering.

The fourth algorithm is calculating some mean value over the last 10 or so measurement cycles. If the actual measurement is deviating too much from this mean value a shut-down (too high) or an alarm message (too low) is initiated.

Finally, the fifth algorithm is similar to the previous one, but not only 10 but about 100 cycles are used and a global mean value is calculated, not an individual one. Again, in case of deviation of the local mean value from the global mean value scram or alarm are the result.

2.1.4 Hardware design

The system was subdivided into four subsystems, each with a different purpose. Each subsystem itself consists of three redundant microprocessors. These are connected with each other. Among these subsystems an extensive exchange of information is taking place. This shall provide each single system with good error recognition capability. In addition, failure of single components (e. g. communication lines or computers) can be tolerated to a certain degree since redundant information is available.

The safety and availability is not influenced by this, but early failure detection is necessary to eliminate double failure which could result in a fail-safe reaction, that is shut-down.

The structure of the system is shown in figure 2.1-1.

The first group (M1,M2,M3) receives the process data, makes some plausibility checks and calculates the mean value of the three redundant input channels which is then sent to the next groups (A and F).

The second group (A1,A2,A3) takes the actual measurements and calculates therefrom the floating set points and evaluates whether at any position a floating or a fixed setpoint is exceeded. The algorithms I to III are performed in this group. The results of this evaluation are given to group four (K).

The third group (F1,F2,F3) takes not only the actual measurements but applies a digital filtering technique, thereby taking into account also the history. This is the realisation of algorithms IV and V. Again the floating set points are calculated and an evaluation is made with the results given to the fourth group (K).

The fourth group (K1,K2,K3) makes a final combined evaluation of the results of groups A and F. This evaluation is just a simple check whether at any position there is a scram situation detected by one of the algorithms. No correlation analysis is carried out at the time being, but investigations on its value seem to be usefull. The output is a simple binary result, either '1' (keep on going) or '0'

(shut-down).

This signal is then used by the final hardware two-out-of-three voter to act on the control rods. This voter is designed inherently fail-safe. This is necessary because it is the bottle-neck of the design which cannot be redundant.

In addition there is a protocol unit which is taking the alarm messages and other information from the individual units, provides the operators with information, and conducts some data logging.

The twelve microprocessors within the system are mainly identical, the only difference is the amount of i/o-ports.

For our realisation we have chosen the Siemens SMP E8, a single board computer based on the Intel 8088 microprocessor chip. This microcomputer was selected due to the good price-performance relation. It is based on a powerful 16-bit microprocessor and shows a small and compact board design. In addition the indirect connections to the bus via plugs and the probably good earth quake resistance are features which improve the validation and licensing procedures.

Each single computer consists of

- chassis with power supply
- CPU
- up to 64k byte main memory (EPROM + RAM)
- I/O interfaces (parallel and serial).

There is no peripheral unit associated to a computer. Only for maintenance there is the possibility to connect some diagnostic aid to an otherwise unused i/o-port.

The connection of the microprocessors is not via a common bus, but by separate point to point connections. Thereby the probability of a common mode failure due to the bus system is eliminated.

Each redundant line (M1, A1, F1, K1; M2, A2, F2, K2; M3, A3, F3, K3) will be in a separate compartment and finally also in a separate room. This again is to minimize the probability of common mode failures.

Minicomputers are generally more powerful than microcomputers, but require also a more complex operating system and have a more complex structure. Therefore more effort is needed during the validation and verification process for licensing.

The use of microcomputers has a considerable influence on the complexity of the single units and the whole system, too.

The separation of tasks is leading to smaller units with lower complexity, and the possibility of error propagation is rather limited compared with a solution incorporating minicomputers.

2.1.5 Software structure

The software of the microprocessors can be separated into the following four parts

- supervisor/operating system
- communication software
- application software
- self-testing software.

For validation purposes the operating system will be kept at a minimum. Since the hardware structure is not too complex, not too many functions are needed of the operating system. The main functions needed from the software side are i/o-drivers and task-management. Since several tasks are running in one processor, the correct scheduling and also the time control are important subjects.

The communication software incorporates the protocol mechanism and thereby also features for error detection. The protocol itself can be rather simple, since we have only point to point connections and not a bus structure. There is only the computer internal local bus. The amount and kind of information to be exchanged is also fixed. Only the amount of messages in case of errors is changing. A certain amount of redundancy is incorporated into the transferred data for error detection (e.g. parity, control words).

The application software contains the actual problem solving programs. This is the part which will vary between the different groups while

the other three parts remain identical in groups M, A, F, and K.

The self-testing software is running in the spare time of each processor. Its purpose is to control the correct functioning of the hardware, to check the constant part of the memory and to test the interprocessor communication lines. In addition a certain amount of neighbor checking is performed. The results of these checks are reported to a central protocol processor as well as to the following group. By these self-tests errors shall be detected as soon as possible in order to have a very low probability of double error within one unit between maintenance phases.

2.1.6 Validation methodology

Since licensing is involved in this project, large portions of the work go into validation and verification. The validation procedure which will be applied in this project consists of constructive and analytical parts. Both parts will be explained in more detail in the following.

2.1.6.1 Constructive methods

Starting at the beginning of the development cycle the use of a formal specification language has to be mentioned. Error analysis studies have shown that many errors have their origin in the specification /Endres75, Gmeiner78/. Either the specification was not precise enough or it was incomplete or contradictory. Without a formal specification language the detection of these errors is quite hard. Therefore we are trying to eliminate as many of these specification errors as possible by the use of the specification language ESPRESO /Eckert81/ for the software specification of the system.

After the formal specification the implementation is done in high level programming languages. Similar to the redundancy in hardware we apply diverse programming in the software.

In our case we selected PASCAL, PL/M and IFTRAN /IFTRAN79/ (a structured FORTRAN) as implementation languages for the application software. These implementations are done by independent teams. By means of this technique we attempt to eliminate common mode errors

which might arise if the same software is loaded to the redundant computers and an overlooked coding or design error is activated.

But not only the probability of common mode software errors is decreasing by this technique. Also the probability of occurrence of the same hardware error at the same time is at least diminished since different software will activate different hardware functions in the redundant computers.

2.1.6.2 Analytical methods

We mainly distinguish between reviews and testing techniques.

In order to use review techniques the software development cycle has to be marked with milestones to which certain documents are associated. The reviews are performed by following a checklist. The new documents are compared with the previous ones. By this iterative kind of checking the consistency between the different documents of the separate development phases can be guaranteed.

Our reviews will be conducted in two phases. The first step consists of a review within the development team. The second step is made together with the licensing authority.

The main advantage of the review technique is that every document and every phase of the development cycle (specification, design, program, e.g.) is controlled. So possible errors should be detected as early as possible.

The testing techniques are mainly concerned with the program code. Our approach consists of three steps:

- module test
- program test
- system test.

During the module test the programmer will test his program according to his own standards until he considers his program error-free.

The program test will be conducted by an independent test team. The test data will be derived from the program structure and the design

description, and the expected test results will be derived from the program specification or the requirements specification. This is assisted by the use of automated testing tools like RXVP80TM /RXVP80, Geiger80/, which can do a static and dynamic analysis of the program.

There is no coupling to the process during the program test. The program will be tested off-line by bottom-up integration. Thereby the amount of extra test bed design can be minimised. Part of this test can even be made on a host computer.

During the system test the complete system, including the hardware, is tested under real-time conditions. The necessary test data are now chosen application- and specification-oriented.

During the specification-oriented system test the different test cases are derived from the program specification in order to exercise all different cases and functions. This is aided by the use of a decision-table-like combination table.

The above mentioned process applies mainly to the special developed application software. For the other parts a slightly different approach will be taken. The operating system is a manufacturer made system which is also used in other application areas. Part of the validation will be substituted by this operating experience. The communication software is self-made and has to undergo rigid testing. Since the scope of it is limited, this should be possible to a large extent. The self-testing software has a well-defined objective. It has to be demonstrated that it is capable of detecting certain errors, and that these are the most common errors.

The final phase of the system test is done by using the original process data. Since in our case a hardwired protection system already exists and the process is available, the coupling to the process can be done. The final test will therefore be a long term test on-line open-loop, i. e. the original process data are used. In addition to this, since the emergency probability is very low, some emergency situations have to be simulated by changing some of the process data. But until the final license is achieved no immediate shut-down may be initiated, but only a message will be given to the operators.

2.1.7 Conclusions

We introduced the design of a microprocessor-based reactor shut-down system and the associated approach for validation and licensing. By the use of single board computers a simple hardware structure is achieved. Combined with the functional separation of the tasks and distribution to independent processors this supports and eases the validation process.

The use of constructive techniques for the software in connection with analytical validation methods shall provide a good result and convince the licensing authority of the quality and reliability of the final product.

Hardware and software have to be looked at together. This integrated approach shall demonstrate that hardware and software solutions for fault tolerance and error recognition can assist each other and help to achieve the required overall reliability.

As an advantage of the computer-based protection system as compared to the existing hard-wired system the following can be pointed out. The modification of the $f(i)$ -values which is necessary about every month is more easy and also easier to protocol. The threshold values can be adopted according to the operating experience. It is possible to change the algorithms and even extend the system to some new ones. No additional cabling is necessary, 'only' some reprogramming. An extension in the direction of correlated analysis of the different realised algorithms could be made quite easily. Therefore the effort necessary to license such a system consisting of hardware and software is considered worthwhile.

2.1.8 References

/Eckert81/

Eckert, K., and Ludewig, J.: ESPRESO-W, ein Werkzeug für die Spezifikation von Prozeßrechner-Software. In: Werkzeuge der Programmieretechnik, IFB43, Springer-Verlag, Berlin, 1981, 101-112.

/Endres75/

Endres, A.: An Analysis of Errors and their Causes in System Programs, IEEE Trans. Softw. Eng. SE-1 (1975) 140-149.

/Geiger80/

Geiger, W. and Gmeiner, L.: Automatische Test- und Dokumentationshilfsmittel für FORTRAN-Programme, KfK-Nachrichten 12 (1980), No. 1-2, 23-28 (in German).

/Gmeiner78/

Gmeiner, L.: unpublished report 1978

/IFTRAN79/

IFTRAN Structured Programming for FORTRAN, User's Manual, General Research Corporation, Santa Barbara, 1979.

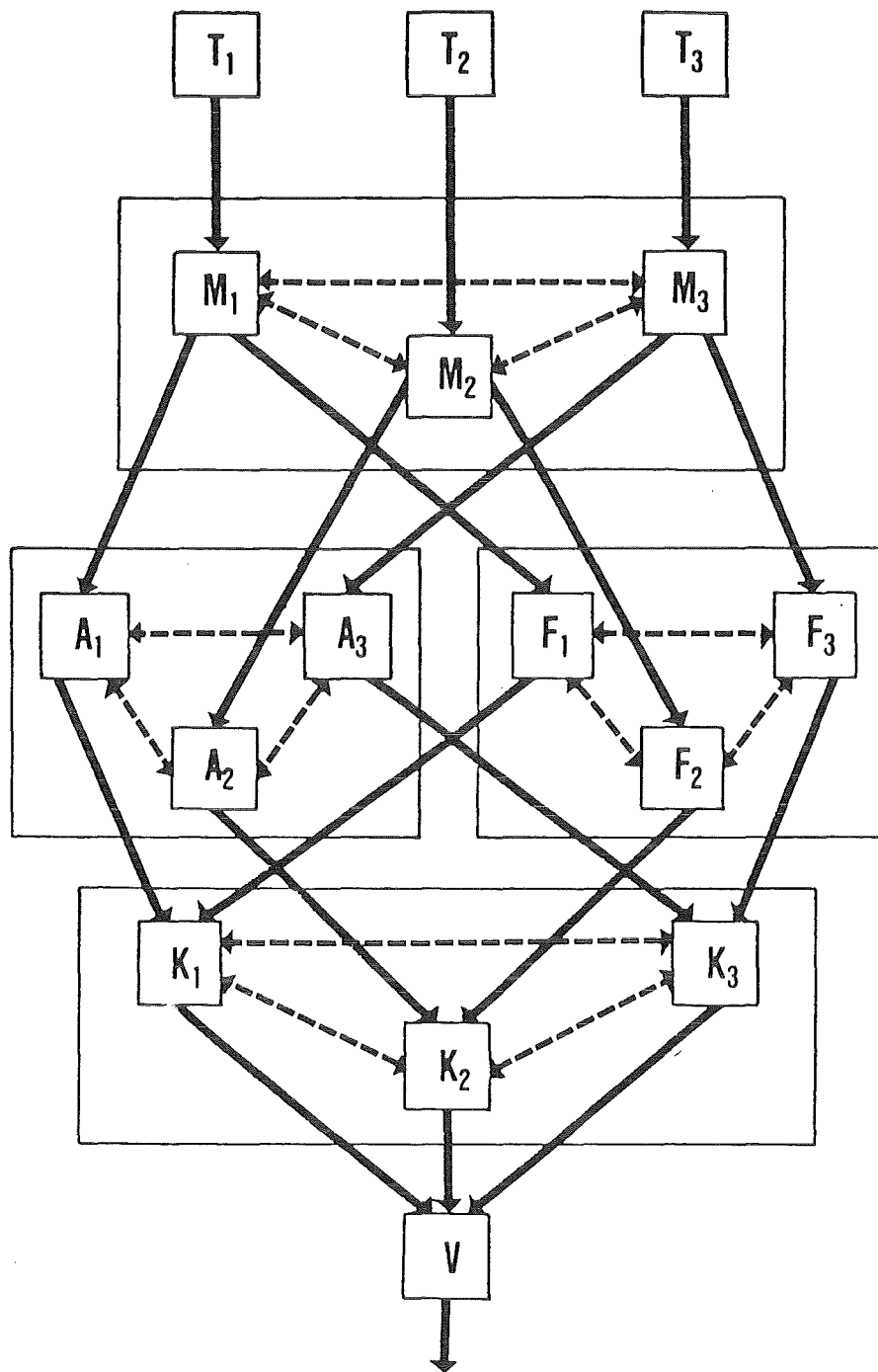
/RXVP80/

RXVP80 User's Manual, General Research Corporation, Santa Barbara, 1980.

- I $\text{temperature}(i) > \text{fixed_limit}(i)$
 for all test zone fuel element positions i
 with individual $\text{fixed_limits}(i)$
- II $\text{delta_temp}(i) > f(i) * \text{group_mean_value}(\text{group_num})$
 + $\text{delta}(2)$
 for all fuel element positions i belonging to
 group group_num
 for all groups
 $\text{group_mean_value}(\text{group_num}) = (1 / ||\text{n}(\text{group_num})||) *$

 $\text{delta_temp}(i)$
 $i \in \text{group}(\text{group_num})$
- III $\text{temperature}(i) > 650$ degrees centigrade
 for all fuel element positions i
- IV $\text{delta_temp}(i) > \text{short_term_temp}(i,k) + \text{delta}(4)$
 for all fuel element positions i
- $\text{short_term_temp}(i,k) = 1/S * \text{delta_temp}(i)$
 + $(S-1)/S * \text{short_term_temp}(i,k-1)$
 k : cycle number
 S : integration range (in the range of 10)
- V $\text{long_term_temp}(i,k) > f(i) * \text{long_term_mean_value}(k) + \text{delta}(5)$
 for all fuel element positions i
 with cycle number k
- $\text{long_term_temp}(i,k) = 1/L * \text{delta_temp}(i)$
 + $(L-1)/L * \text{long_term_temp}(i,k-1)$
- $\text{long_term_mean_value}(k) = 1/N * \sum_i \text{long_term_temp}(i,k)$
- N : number of fuel elements
 L : integration range (about 100)
- $\text{delta_temp}(i) = \text{outlet_temperature}(i) - \text{inlet_temperature}$
 $\text{delta}(j)$: individual algorithm threshold

Table 2.1-1: SHUT-DOWN ALGORITHMS



---> Communication for redundancy and control
—> Data flow

- T Thermocouples
- M Microprocessor for mean value calculation
- A Microprocessor for limit control taking actual values
- F Microprocessor for limit control taking filtered values
- K Microprocessor for criteria evaluation
- V Hardware 2-out-of-3 voter

Fig. 2.1-1: Structure of the Reactor Shut-Down System

Beitrag zur EG-Studie 82/83, Teil 1

Microprocessor-based Integrated Core Surveillance System

Udo Voges, KFK/IDT

21. 7. 1983

A Microprocessor-Based System for the
Evaluation of Fuel Element Outlet Temperatures

2.2 Subassembly State and Performance Monitoring

M. Edelmann

Institut für Neutronenphysik und Reaktortechnik

Abstract

In the following chapter a method is described by which local loss of cooling in LMFBR subassemblies can be detected with improved sensitivity, i. e. at an early stage of a developing blockage. It is expected that in general a blockage can be detected before it causes boiling of coolant in the wake behind it. In addition, thermal hydraulic fuel element parameters as, for instance, an integral heat transfer coefficient between fuel and coolant can be monitored. Using individual subassembly (SA) outlet temperature signals the method provides for indirectly monitoring SA coolant flow with high precision. In Fig. 1-1 it is indicated by the symbols TM and FI at which stages of fault propagation local loss of coolant might be detected in this way.

2.2.1. General Considerations on SA State and Performance Monitoring

Fast reactor fuel elements due to their high power densities are sensitive to cooling disturbances. In future LMFBR's therefore the coolant flow rate through the subassemblies will be monitored indirectly by individual temperature instrumentation. However, with conventional monitoring narrow tolerance bands are not feasible for individual fuel element outlet temperatures because of significant changes of outlet temperatures under normal operating conditions. This is due to power and inlet temperature noise, load variation and burn-up.

On the other hand, local cooling disturbances within a fuel element, i. e. local blockages, swelling or bowing of fuel pins, may lead to thermal overload of fuel or cladding without producing a significant additional pressure drop. In this case the total flow rate of coolant and therefore also the outlet temperature would not change significantly.

Consequently, the coolant flow through the subassemblies has to be measured with high precision to detect local cooling disturbances. For this measurement simple and reliable techniques are required. At present only temperature instrumentation seems to be practicable in commercial fast breeder reactors. Individual redundant and high precision flow instrumentation for all subassemblies is prohibitive for technical and economic reasons. Therefore, the only way to detect local loss of cooling in a fast reactor subassembly before local boiling of sodium or pin failure may occur will be by more sophisticated surveillance of outlet temperatures. Several different techniques are investigated in this respect as, for instance, using dynamic references for outlet temperatures /Jacobi 76/ or the analysis of outlet temperature noise /Weinkötz 79/.

The major reason why conventional outlet temperature monitoring is only moderately sensitive to cooling disturbances in a single subassembly is due to the fairly large variations of reactor power and inlet temperature under normal operating conditions. These may cause changes in SA outlet

temperatures of more than 10 K. Correspondingly, alarm or scram levels have to be set around 15 K temperature rise. This is equivalent to about 10 % reduction of coolant flow.

From investigations at the sodium cooled test reactor KNK at Karlsruhe it is concluded that SA outlet temperatures would deviate by no more than 1 K from their stationary mean values if there were no changes in SA power and inlet temperature. This corresponds to less than 1 % flow variation for a typical temperature rise of the coolant of about 200 K in fast reactor fuel elements. Consequently, SA outlet temperature monitoring would be much more sensitive to loss of cooling if the effect of power and inlet temperature variations on SA outlet temperature could be eliminated.

In an earlier paper /Edelmann 77/ a novel method of monitoring individual SA coolant flow using SA outlet temperature signals was proposed. In this method high sensitivity and quick response to cooling disturbances is achieved by balancing-out the operational variations of SA outlet temperatures. The principle of this method consists of simulating normal fuel element performance and intercomparing model-predicted outlet temperatures to actually measured ones.

For simulating the individual thermal hydraulic performance of the fuel elements a very simple theoretical model turned out to be sufficient. As shown earlier /Edelmann 79/ a fairly good estimate of SA outlet temperatures is obtained by low-Pass filtering and delaying a neutron detector signal (being proportional to SA power) and adding an inlet temperature signal. Digital filter algorithms are simple and fast enough for on-line simulating the whole core of an LMFBR on a small digital computer in this way.

Subtracting the model-predicted outlet temperatures from the measured ones provides "balanced" (zero mean) temperatures which only depend on SA coolant flow. An increase of a balanced outlet temperature would be a clear sign of a loss of cooling in the corresponding SA as long as the SA model parameters remain constant. Since the model parameters may change over long periods of reactor operation they have to be verified and readjusted from time to time.

Besides the temperature rise a local blockage in a SA would produce some other effects that might be utilized to detect it. So, for instance, it might cause additional (high frequency) outlet temperature noise or even a DND (delayed neutron detector) signal if the blockage consists of fissile material from failed fuel. At later stages a growing blockage also might be detected by acoustic sensors if sodium boiling occurs in the wake behind the blockage. Sodium boiling might be detected by monitoring the reactivity or power noise of the reactor, too.

It can be expected that combining the various signals that might be affected by a cooling disturbance would enable more sensitive and more reliable techniques of monitoring individual SA performance. This has been demonstrated already for detecting of sodium boiling by neutron and acoustic noise /Wright 75/. In this case it was found that individual drawbacks or limitations of the single measurement techniques can be overcome or reduced at least by using cross correlation techniques for a combined analysis of independent signals. An integrated core surveillance system would use all of the available informations and highly sophisticated techniques for their optimum evaluation in order to provide early and reliable indications of developing malfunctions or deviations from normal reactor operating conditions.

Such a system, in addition, might be used to obtain useful information on physical plant parameters also under normal operating conditions. So, for instance, simulating of individual SA performance as discussed before does not only provide a means for sensitive monitoring of coolant flow relative to subassembly power. It could also be applied to measure fuel element parameters such as absolute coolant flow and power as well as average fuel temperature and heat transfer coefficients by fitting simulator outputs to actual plant signals. No special or additional instrumentation is needed for these measurements. They are based on the inherent noise of reactor power only and use only normally available plant signals. Therefore the measurements can be performed at any time during normal reactor operation. The change of fuel element parameters with time and reactor operating conditions can also be measured in this way.

2.2.2. Thermal Hydraulic Fuel Element Model for Predicting SA Outlet Temperatures

The theoretical model used to describe the fuel element thermal hydraulics is the same as developed earlier /Edelmann 77/ for KNK I. However, in the following a more general approximation of the SA power-to-outlet temperature transfer function is derived for simulating individual SA performance.

In the model a fuel element consists of two regions. One is representing the fuel rod bundle being the heat source, the other one, the heat sink, is comprising the coolant and all subassembly structure with negligible heat generation. In the following only the active zone of the subassembly is considered. Axial blankets and subassembly structure is not accounted for. The system is completely determined by the temperatures and heat capacities of the two regions, an integral heat transfer coefficient between them and the heat generation rate as well as by the heat removed per unit time by the coolant. The heat balance between the two regions is given by the following equations,

$$C_f \dot{T}_f(t) = P(t) - k(T_f(t) - T_c(t)) \quad (1)$$

$$C_c \dot{T}_c(t) = k(T_f(t) - T_c(t)) - 2hF(T_c(t) - T_i(t)) \quad (2)$$

with

T_f mean temperature of fuel region

$T_c = \frac{T_o + T_i}{2}$ mean coolant temperature

T_i, T_o inlet and outlet temperature

C_f, C_c	heat capacity of fuel and coolant region
P	subassembly power
k	overall heat transfer coefficient between fuel and coolant region
h	specific heat of coolant
F	coolant mass flow rate

For stationary operating conditions only inlet temperature and power are independent variables of time. Non-stationary conditions can be included to a first approximation by allowing small variations of the parameters in the stationary solutions.

The Laplace transforms of Eqs. (1) and (2) can be solved explicitly. For the mean coolant temperature one obtains in the frequency domain

$$T_c(j\omega) = H(j\omega) \cdot \frac{P(j\omega)}{2hF} + H_i(j\omega) \cdot T_i(j\omega) \quad (3)$$

wherein

$$H(j\omega) = \frac{1-\gamma}{(1+j\omega\tau_1) \cdot (1+j\omega\tau_2)^{-\gamma}} \quad (4)$$

$$H_i(j\omega) = (1+j\omega\tau_1) \cdot H(j\omega) \quad (5)$$

$$\gamma = \frac{k}{k+2hF} \quad (6)$$

$$\tau_1 = \frac{C_F}{k} \quad (7)$$

$$\tau_2 = \frac{\gamma C_c}{k} = \frac{C_c}{k+2hF} \quad (8)$$

The relationship between the coolant temperature T_c and subassembly power and inlet temperature are described by the two transfer functions (4) and (5) representing modified (feedback) low-pass characteristics of second and first order, respectively. The two time constants defined in Eqs. (7) and (8) are assigned to the fuel and coolant region, respectively, because of their proportionality to the corresponding heat capacities. The model parameter given by Eq. (6) also has a physical meaning. For the stationary mean values of fuel and coolant temperature, T_f and T_c , it follows directly from Eq. (2)

$$\frac{\bar{T}_c - \bar{T}_i}{\bar{T}_f - \bar{T}_i} = \gamma$$

The third parameter (6) of the transfer function (4) therefore represents the ratio of average stationary temperature rises in coolant and fuel.

From the quantities in Eq. (3) only T_c and T_i can be measured directly. Subassembly power and coolant flow rate in general are not available in absolute units. Only the ratio of their stationary mean values $P(o)/2hF$ is known through the temperature rise $T_c(o) - T_i(o)$. In a fast reactor the signal of a power monitor can be considered proportional to subassembly power, too. The corresponding calibration factor needs not to be known explicitly. Its value relative to the outlet temperature signals is

automatically accounted for by relating the temperature signals to a neutron detector signal instead of the original physical quantities. The other model parameters can be calculated according to Eqs. (6) through (8) if the necessary fuel element data are known with sufficient accuracy. This is not true for the heat transfer coefficient k . This parameter strongly depends on the heat conductance between fuel and cladding which is known only with very low certainty.

The model parameters can also be determined experimentally by fitting Eq. (4) to a measured transfer function. The power-to-outlet temperature transfer function of a fuel element can be measured easily by noise analysis techniques /Schlitt 72/ during normal reactor operation if there is sufficiently high power noise in the relevant frequency range. Otherwise the power fluctuations had to be increased by external reactivity modulation. This is also possible during normal power operation because only small amplitude reactivity oscillation is required. Since the fuel heat capacity is known fairly well the over-all heat transfer coefficient k can be obtained from the fitted fuel time constant τ_1 . From this coefficient in turn the specific heat conductance between fuel and cladding (gap conductance) can be determined if the other heat conductances (fuel, cladding, cladding/coolant) are given. This method has the further advantage that all thermal parameters remain unchanged during the measurement because the power and temperature fluctuations are very small in comparison to their stationary mean values.

Theoretical estimations showed, and measurements at KNK II confirmed, that in general, only the fuel time constant τ_1 is significantly influencing the SA transfer functions. The coolant time constant τ_2 is by more than a factor of ten less than the fuel time constant (and the response time of thermocouples used for SA outlet temperature measurements). Furthermore, typical fast reactor power noise is limited to frequencies far below the corner frequency of a low pass with a time constant equal to τ_2 . Inlet temperature noise is limited to even lower frequencies. Thus, the measurement of SA transfer functions will normally provide a single time constant only.

Whereas the lack of high frequency content in power and inlet temperature noise imposes difficulties in determining both time constants it favours simple approximations of the transfer functions (3) and (4). For KNK-II at frequencies $f \ll 1$ Hz second-order terms of ω could be neglected and the transfer functions H and H_i to a good approximation are given by

$$H(j\omega) \approx \tilde{H}(j\omega) = \frac{1}{1+j\omega\tau_o} \quad (10)$$

and

$$H_i(j\omega) \approx \tilde{H}_i(j\omega) = \frac{1+j\omega\tau_1}{1+j\omega\tau_o} \quad (11)$$

wherein

$$\tau_o = \frac{\tau_1 + \tau_2}{1 - \gamma} \quad (12)$$

Thus, the power to outlet temperature transfer function is reduced to a first-order low-pass characteristics with the time constant τ_o . Since the coolant time constant τ_2 in typical fast reactor fuel elements is much smaller than the fuel time constant it will have no significant effect on the amplitude of SA outlet temperature noise. It will only cause a phase shift which can be approximated by a small delay between power and outlet temperature noise. Therefore, the time constant obtained by fitting the gain of the transfer function (4) to measured curves would be

$$\tau_o = \frac{\tau_1}{1 - \gamma} \quad (13)$$

rather than that defined in Eq. (12). For similar reasons $H_i(j\omega) = 1$ is a good approximation in practical applicaitons.

From the Eqs. (6) and (13) we find the relationship

$$k = \frac{C_f}{\tau_o - \frac{C_f}{2hF}} \quad (14)$$

which can be used to determine the over-all heat transfer coefficient from the measured time constant, calculated heat capacity of the fuel rod bundle and nominal coolant flow rate of the subassembly.

For completeness, it should be mentioned here that at KNK-I as shown in ref. /Edelmann 77/ a further simplification was applied to Eq. (10) because of a too low level of power noise around the fuel corner frequency f_0 corresponding to the fuel time constant τ_1 . For the lower frequency noise the gain of the transfer function is not frequency dependent, only a linear phase shift representing a time delay according to the time constant (12) is left. This delay is not attenuated by a slow thermocouple like the magnitude of the temperature fluctuations. To the contrary, the time delay is increased by the time constant of the thermocouple. From the measured delay time between power and outlet temperature noise signals the fuel time constant and therefore the heat transfer coefficient can be obtained, too if the time delay of the thermocouple and the involved signal channel are known.

If the measurements are performed with slow thermocouples having time constants not much smaller than those of the fuel element the thermocouple has to be included in the theoretical model as well as in the fuel element simulator. To a good approximation the transmission properties of a thermocouple can be described by a first-order low-pass characteristics

$$G(j\omega) = \frac{1}{1+j\omega\tau} \quad (15)$$

with the time constant τ . Thus, we finally obtain for the simulated outlet temperature signal T_s

$$T_s(j\omega) = U(j\omega) \frac{P(j\omega)}{hF} + G(j\omega) \cdot T_i(j\omega) \quad (16)$$

with

$$U(j\omega) = G(j\omega) \cdot \tilde{H}(j\omega) = \frac{1}{(1+j\omega\tau) \cdot (1+j\omega\tau_0)} \quad (17)$$

Thus far the transit time of the coolant from the point subassembly model located near to the core midplane to the thermocouple is not yet included in the theoretical model. It is accounted for separately in the time domain only when measured and simulated temperature signals are intercompared. The transit time of the coolant between the thermocouples at the reactor inlet and subassembly outlet causes a delay of the inlet temperature component in the outlet temperature signals relative to the inlet temperature signal. For the extremely low frequencies of the inlet temperature noise this difference is negligible in general and in the second term of Eq. 16 we can set $G(j\omega) \equiv 1$.

2.2.3 Fuel Element Simulation and Outlet Temperature Monitoring

In which way a fuel element is to be simulated depends on the intended application. For monitoring of stationary coolant flow the simplified transfer function (10) or possibly a pure time delay is sufficient to derive an outlet temperature signal from a neutron detector signal. Which one of these possibilities has to be chosen depends on the required sensitivity and false alarm rate of a balanced temperature signal with respect to changes of coolant flow as well as on the spectral composition of power noise and on the actual values of the fuel element time constants. This interdependence is described in /Edelmann 77/ in more detail.

The balanced outlet temperature signal T_b to be monitored is formed by subtracting the simulated signal from the measured one. The simulated outlet temperature signal is obtained by filtering and amplifying a neutron detector signal in a single active low-pass filter with the time constant τ_0 and adding an inlet temperature signal. If necessary an additional low-pass filter is used to simulate the thermocouple. The corresponding signal processing procedures can be realized using either individual analog devices for each subassembly or preferably a small digital computer for the whole core.

The principle of sensitive SA outlet temperature monitoring is represented schematically by the block diagram shown in Fig. 2.2-1. It comprises the procedures for the outlet temperature simulation and the surveillance of both original and balanced outlet temperatures with respect to their statistical parameters. This principle was realized and tested with the experimental SA surveillance system KASUMOS /Edelmann 82/ developed at KfK Karlsruhe. Experience obtained with this System at the sodium cooled test reactor KNK II confirmed that using balanced outlet temperatures instead of the originally measured ones provides for significantly increased sensitivity in SA coolant flow monitoring. At KNK II in this way a sensitivity of less than 1 % relative change in SA coolant flow was achieved as opposed to some 10 % attainable with conventional outlet temperature monitoring.

This improvement is essentially due to the fact that the balanced outlet temperature signal is not sensitive to changes in coolant temperatures caused by changes of total reactor power. This in turn is possible only when outlet temperature signals are being combined with neutron detector signals for SA coolant flow monitoring. Thus, we have here a first example of how an integrated core surveillance system by combining different plant signals can provide more precise information on plant operating parameters. From the improved accuracy in monitoring system parameters one can expect earlier indications of developing malfunctions or failures.

This was also demonstrated in practical applications of the balanced outlet temperature monitoring using KASUMOS during anomalies that occurred in the primary cooling system of KNK II. These anomalies were caused by cover gas entrained in the coolant /Hoppé 79/. Power and temperature signals measured during such events are shown in Fig. 2.2-2.

When passing the core the gas reduces the coolant density for a few seconds, thus causing a power drop (because of the negative reactivity effect) and a loss of cooling simultaneously. The outlet temperature decreased at all SA outlets. The power drop was always overriding the loss

of cooling effect. Therefore the conventional monitoring of outlet temperatures does not provide any information on the individual loss of flow in a SA. In the balanced signals the power drop effect is removed. They would clearly increase if the gas content would reach 1 % or more.

This was not observed in general. Only during a few extremely large anomalies an increase of balanced temperatures was found at all SA outlets. It has to be concluded therefore that the gas is not passing a single or a few of the SA's only, but rather it must be distributed uniformly over the whole core. This means that the KNK II primary cooling system anomaly does not have any consequences on proper SA cooling. This was demonstrated with KASUMOS for a large number of events of this kind.

The general scheme of SA state and performance monitoring within an integrated core surveillance system is outlined in Fig. 2.2-3. In addition to producing dynamic reference signals and balanced outlet temperatures for each SA according to the functional diagram shown in Fig. 2.2-1 it includes procedures for the estimation of the SA model parameters necessary for individual outlet temperature prediction. The parameter estimation module could be operated continuously for monitoring the thermal-hydraulic fuel element parameters, e. g. heat transfer coefficient between fuel and coolant. From time to time it has to be run to check or up-date the data base of the temperature prediction module.

The Surveillance module in a first approach would provide a series of early warnings in the case that any one of the balanced SA outlet temperatures as produced by the dynamics compensation module would exceed prescribed fixed levels corresponding to various degrees of coolant flow reduction.

For a more detailed diagnosis the original and balanced temperature signals could be compared to more complex signal patterns. For this purpose a fault patterns and criteria library is included in the general scheme. An integrated core surveillance system would extend this diagnostic potential by including additional plant signals and procedures for their combined analysis and evaluation.

2.2.4. Conclusion

From theoretical considerations and first practical experience it is found that monitoring balanced outlet temperatures represents a very sensitive method for detecting local loss of cooling in fast reactor fuel elements. The method is based on modeling individual thermal hydraulics performance of the fuel elements. It can be extended to monitoring other thermal-hydraulics SA parameters by continuously adapting the model parameters during normal reactor operation. The diagnostics potential of this technique mainly results from a combined analysis of neutron and temperature measurements. It is expected that including other plant variables in an integrated core surveillance system would enable to further improve both the sensitivity and the reliability in diagnosing local loss of cooling in LMFBR's.

2.2.5 References

- /Jacobi 76/ S. Jacobi, K. Schleisiek, D. Smidt, M. Straka
Kühlungsstörungen in Brennelementen natriumgekühlter
Reaktoren und davon abgeleitete Anforderungen an das
Brennelement-Schutzsystem,
Tagungsbericht DATF Reaktortagung Düsseldorf, 1976,
Deutsches Atomforum e. V.,
Bonn (1976), p. 312
- /Weinkötz 83/ This study report, chapter 2.3
- /Edelmann 77/ M. Edelmann
Noise and DC Balanced Outlet Temperature Signals for
Monitoring Coolant Flow in LMFBR Fuel Elements
Proc. SMORN-II, Gatlinburg, Tenn., USA
Sept. 19 - 23, 1977
in: Progress in Nucl. En. Vol. 1, No. 2 - 4
(1977), 543 - 552
- /Edelmann 79/ M. Edelmann
Simulation of Fuel Element Thermal Hydraulics for
Sensitive Monitoring of Coolant Flow
Report GRS-19 (1979), Gesellschaft für
Reaktorsicherheit, Köln, FRG
- /Wright 75/ S. A. Wright, R. W. Albrecht, M. Edelmann
Cross Correlation of Neutronic and Acoustic Noise
Signals From Local Boiling,
Ann. Nucl. Energy 2, 367 (1975)

/Schlitt 72/

H. Schlitt, F. Dittrich
Statistische Methoden der Regelungstechnik
B.I. - Hochschultaschenbücher Nr. 526,
Bibliogr. Inst. Mannheim/Wien/Zürich (1972)

/Edelmann 82/

M. Edelmann, H. Massier
Functions and Structure of the Karlsruhe Subassembly
Monitoring System KASUMOS
Proc. SMORN III, Tokyo, Oct. 26 - 30, 1981 in: Progr.
Nucl. Eng., Vol. 9, 389 - 398 (1982)

/Hoppé 79/

P. Hoppé, H. Massier, F. Mitzel, W. Väth
Untersuchungen zum Gaseintrag an KNK-II
KfK-Bericht 2867, November 1979
Kernforschungszentrum Karlsruhe

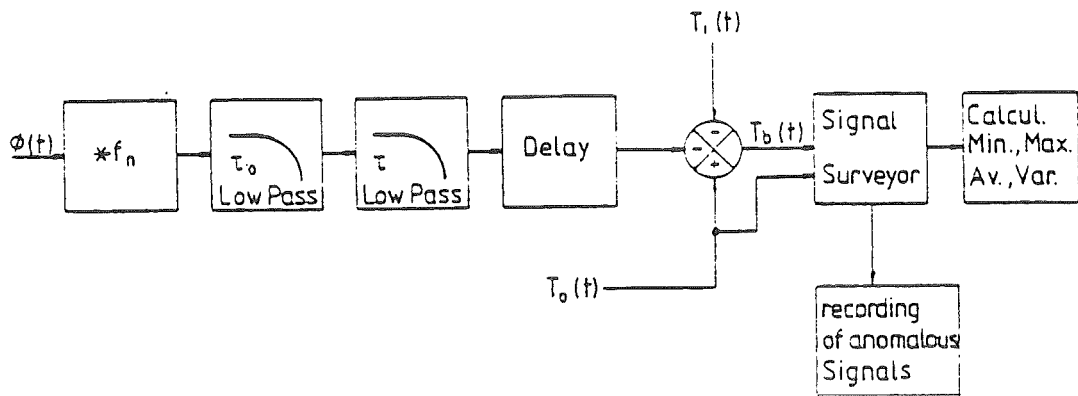


Fig. 2.2-1 Principle of sensitive coolant flow monitoring

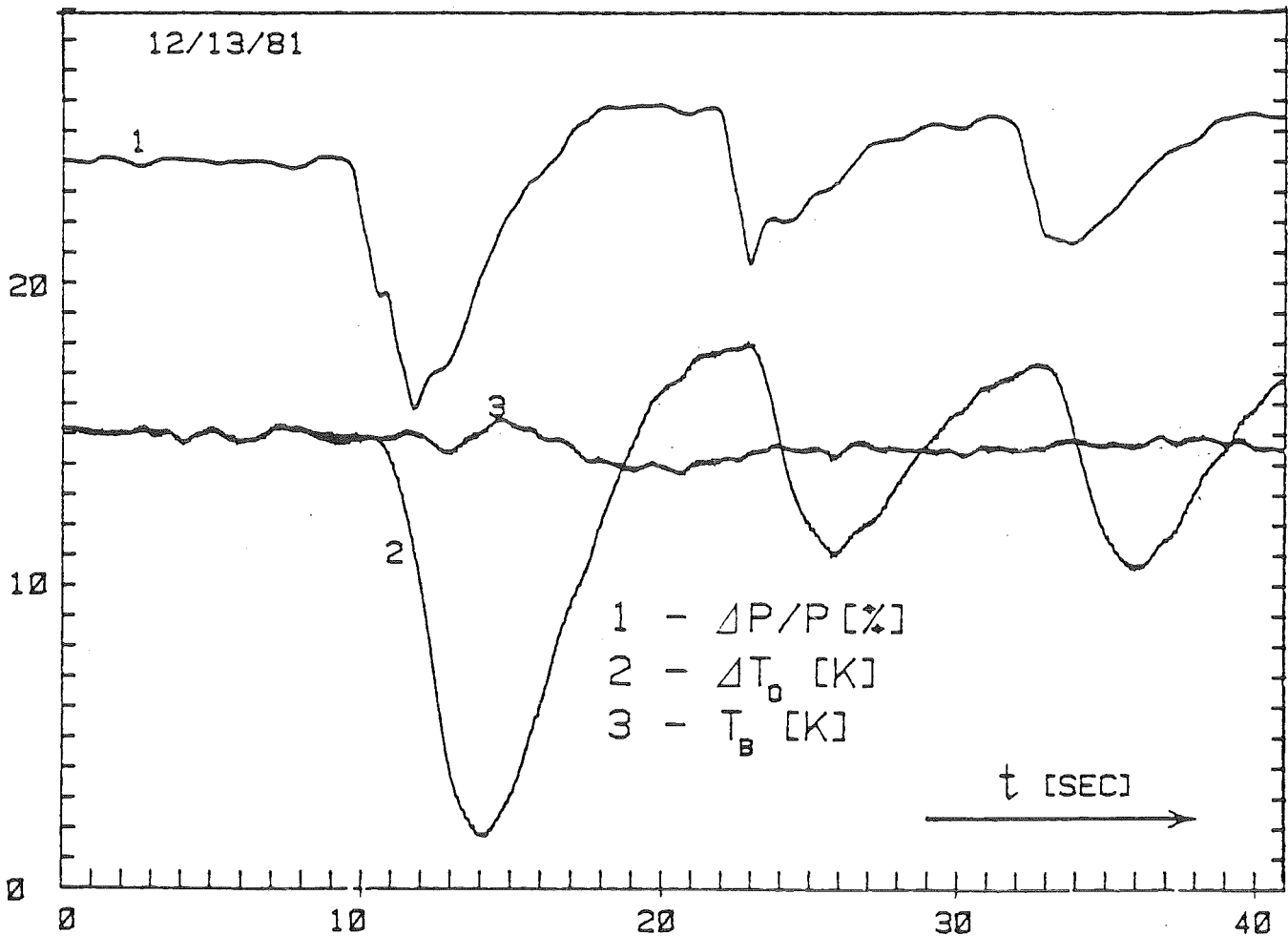


Fig. 2.2-2 KNK II signals recorded during a primary coolant flow anomaly

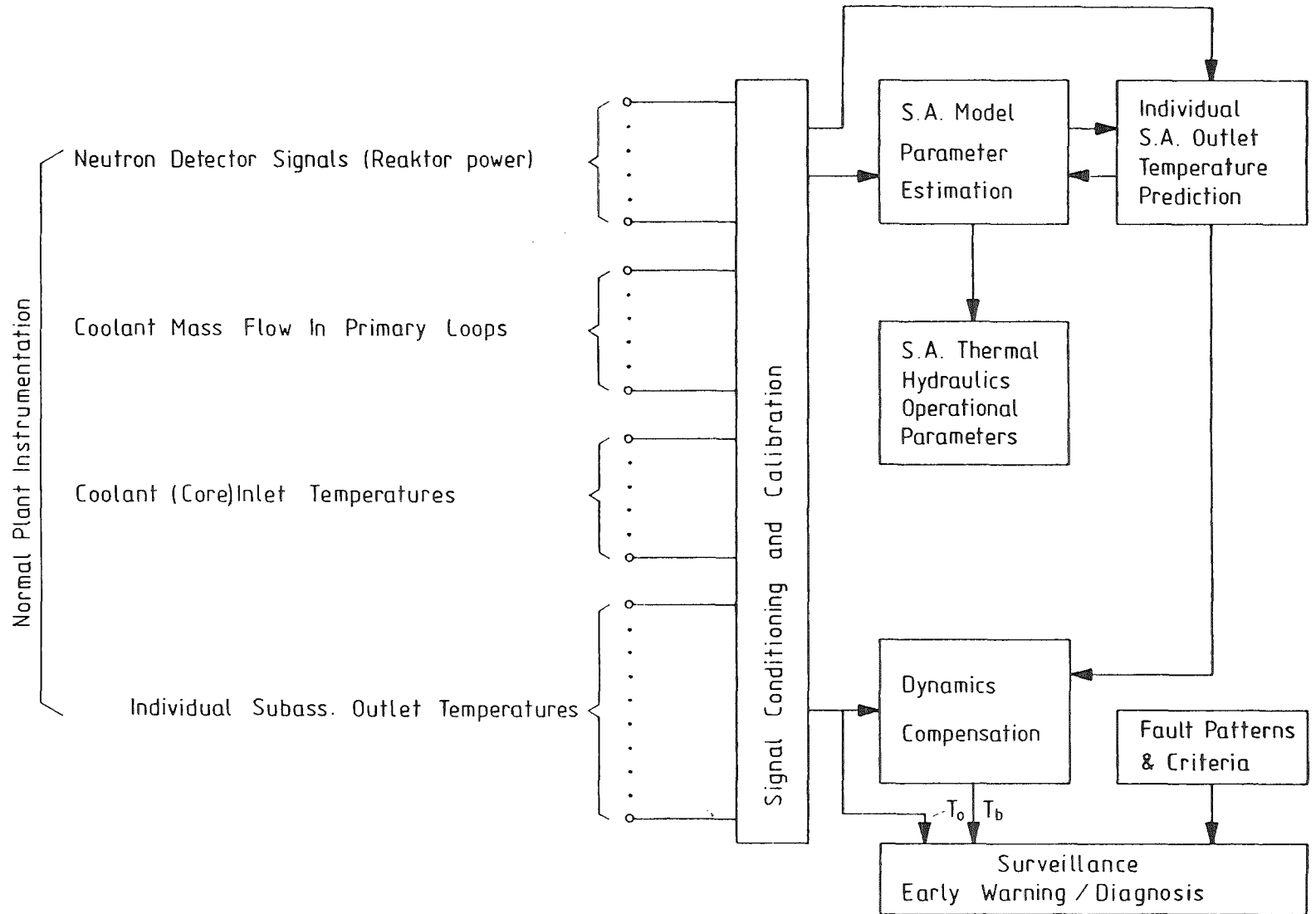


Fig. 2.2-3 Scheme of S.A. state and performance monitoring

2.3 Detection of Cooling Channel Disturbances by Measurement and
Analysis of Temperature Fluctuation Signals at the Outlet of
an LMFBR

G. Weinkötz, L. Krebs
Institut für Reaktorbauelemente

Abstract

Coolant disturbances within a fuel element subassembly of an LMFBR produce temperature fluctuations with higher level than in the undisturbed case. A promising method for detection of coolant disturbances by measurement of the temperature fluctuations downstream of the subassembly outlet is discussed in this chapter. Theoretical and experimental studies show that the RMS-value of the temperature fluctuations is more significant than the mean temperature. Using fast response steel-sodium thermocouples higher frequency signal parts of the temperature fluctuations in the coolant lead additionally to more sensitivity. This detection method is indicated by Temperature Noise (TN) in the Local Faults Propagation in Fig. 1.-1.

2.3.1 Introduction

The early detection of cooling disturbances in the core of a Liquid Metal-cooled Fast Breeder Reactor (LMFBR) constitutes an effective means of reducing the risk of a damage propagation in the fuel element and thus of enhancing the safety of the plant.

Thermocouples are a significant element of reactor instrumentation for the surveillance of fuel elements during operation. As a matter of fact, the temperature signal $T(t)$ measured by a thermocouple can be separated into two portions, the time averaged linear mean value of the temperature \bar{T} and the temperature fluctuation signal $\delta(t)$ always superposed to this temperature mean value.

$$T(t) = \bar{T} + \delta(t) \quad (1)$$

At present, only the temperature mean value \bar{T} is evaluated as a signal variable in reactor plants.

In addition the analysis of the temperature fluctuation signals is considered to be a successful surveillance method for the detection of a local cooling disturbance in an individual fuel element.

Investigations performed on the electrically heated fuel element simulator /Weinkötz 82b/ have shown that the cooling disturbances in the fuel element which were produced by cooling channel blockages can be detected with a higher sensitivity by analyzing the temperature fluctuation signals than by exclusive measurement of the temperature mean value.

However, an analysis of the temperature fluctuation signals with a view to detecting cooling channel disturbances in a fuel element calls for a precise knowledge of the physical process producing temperature fluctuations and of signal transmission parameters.

2.3.2 Analysis of the Temperature Fluctuation Signals

The spread of cooling disturbances downstream of a fuel element is strongly influenced by the velocity field behind the fuel element outlet. Using the results of basic research on a water test section /Krebs 81/ and on a similar sodium test section /Krebs 82/ the decay of temperature mean value and temperature fluctuations can be calculated.

Temperature fluctuations at the outlet of the fuel element are generated by temperature gradients within the coolant. These temperature gradients can be caused by different fuel rod loadings, dissimilar cooling channel geometries in the sub-channels of the fuel elements or in the case of an incident by coolant channel blockages. However, the nature of the fluctuating signals is stochastic which means that they can be described with the help of the probability laws. The frequency of the temperature fluctuation signals depends on the velocity of the coolant and on the place where they are measured. The dependance of the frequency response on the velocity and the thermocouple location was analyzed in water and sodium experiments /Krebs 79, Weinkötz 79b/.

To analyze and evaluate the onset of cooling channel disturbances the following parameters and characteristic functions are of importance:

Parameters:

Temperature mean value
$$\bar{T} = \frac{1}{2 t_M} \int_{-t_M}^{+t_M} T(t) \cdot dt \quad (2)$$

RMS value
$$\sigma = \sqrt{\frac{1}{2 t_M} \int_{-t_M}^{+t_M} \delta^2(t) \cdot dt} \quad (3)$$

Characteristic functions:

Autocorrelation
(time domain)
$$\Phi_{\delta\delta}(\tau) = \lim_{t_M \rightarrow \infty} \frac{1}{2 t_M} \int_{-t_M}^{+t_M} \delta(t) \delta(t-\tau) \cdot dt \quad (4)$$

Power density spectrum
(frequency domain)
$$S_{\delta\delta}(f) = \int_{-\infty}^{+\infty} \Phi_{\delta\delta}(\tau) \cdot e^{-j2\pi f\tau} \cdot d\tau \quad (5)$$

where $2t_M$ = time of analysis.

Among the steady-state variables similar to the temperature mean value the RMS value can be composed at little expenditure in terms of measuring technology and signal processing. This is important above all for the surveillance of a great number of fuel elements. Since the RMS value at the same time constitutes a sensitive indicator of cooling disturbances in the fuel element of an LMFBR, it is particularly suited for reactor instrumentation. The skewness and the flatness are also of interest, but they give additional information only in special cases. Therefore they will not be discussed further in this more general paper.

Since the characteristic functions (Eqs. (4) and (5)) require more expenditure in computer hardware and in computation time, these functions are applied only if a cooling channel disturbance detected by the RMS value must be further analyzed.

However, the RMS value of the temperature fluctuation signals at the bundle outlet depends on the response behavior of the temperature measuring probes used and on the respective operating conditions of the reactor. Therefore these parameters must be taken into account in the detection of cooling disturbances in the fuel element based on the RMS value of the temperature fluctuation signals. The operating conditions (i.e. reactor power R_N and the coolant flow Q at the respective moment) influence the coolant temperature rise ΔT between the fuel element inlet and outlet. For instance, at the reactor KNK II the coolant flow Q is controlled by the reactor power R_N and the temperature rise ΔT depends on both parameters as it is shown in Fig. 2.3-1a. Within the power range 0 - 30 % R_N , the temperature rise ΔT is proportional to the reactor power with the coolant flow Q_{\min} remaining constant, and in the power range 30 % - 100 % R_N , the coolant flow is proportional to the reactor power with the temperature rise ΔT remaining constant.

In Fig.-1b the dependence has been plotted of the RMS value of the temperature fluctuation signal versus the reactor power R_N considering the response behavior of the temperature measuring probe. It is assumed that the temperature probe is capable of transmitting without signal decay the fluctuation signals appearing at maximum coolant flow.

This means:

The cut-off frequency of the temperature measuring probe TC is greater than the frequency of the temperature fluctuation signals occurring at maximum coolant flow.

$$f_g(\text{TC}) > f_g(\delta(t)_{Q_{\max}}) \quad (6)$$

Then the following relations are obtained for the RMS value of the temperature fluctuations σ :

$$\begin{aligned} \sigma &\sim R_N \sim \Delta T \quad \text{for} \quad 0 - 30 \% \quad R_N \\ \sigma &\sim \sqrt{R_N} \quad \text{for} \quad 30 - 100 \% \quad R_N \end{aligned}$$

In summary, taking into account different functional relationships depending on the reactor operating conditions poses some difficulties in signal analysis.

By low-pass filtering of the temperature fluctuation signal the influence of coolant flow variation on the RMS value can be eliminated. This has been represented in plot (c) of Fig. 2.3-1. Assuming that the cut-off frequency of the temperature probe is smaller than the cut-off frequency at minimum coolant flow

$$f_g(\text{TC}) < f_g(\delta(t)_{Q_{\min}}) \quad (7)$$

we obtain for the RMS value of the temperature fluctuations σ :

$$\begin{aligned} \sigma &\sim R_N \sim \Delta T && \text{for } 0 - 30 \% R_N \\ \sigma &= \text{const.} && \text{for } 30 - 100 \% R_N \end{aligned}$$

These relations have been confirmed by measurements with three-wire thermocouples with steel/sodium junctions, made above the fuel element central position of KNK II.

Normalizing the RMS value of the temperature fluctuations by the temperature rise ΔT gives on the assumption above a parameter termed k-value which is independent of the respective reactor operating conditions. In plot (d) of Fig.-1 the development of the parameter k has been represented as a function of the reactor power.

$$k = \frac{\text{RMS value (low-pass filtered)}}{\text{coolant temperature rise}} \quad (8)$$

As has been shown by out-of-pile measurements /Weinkötz 79. a,b/ the k-value undergoes variations only if a cooling disturbance occurs within the fuel element.

As a second example Fig. 2.3-2 shows the results of measurement in case the

parameter k is applied in the signal analysis of temperature fluctuations at a fuel element simulator accommodating 28 electrically heated rods. The figure allows a comparison to be made between the case of undisturbed bundle geometry (bundle without blockage) with the measurements made in a disturbed coolant flow (bundle with 34 % blockage).

In the right part of the figure the scheme of the 28-rod bundle is shown together with the flow mixer and the thermocouple plane 7 as well as the bundle cross section with the thermocouple positions projected to the heater rods. The lower plot in Fig. 2.3-2 shows the temperature mean values of the eight thermocouples installed on plane 7. The measured temperature mean values differ but slightly. This is mainly caused by different inlet temperatures during the two experiments.

The upper plot shows the k -values of the respective temperature fluctuation signals determined by relation (7). By contrast the k -values of the temperature fluctuations differ considerably from that of the bundle with undisturbed bundle geometry. The k -value averaged over all measuring positions is about four times greater for the 34 % blockage than for the unblocked bundle.

2.3.3 Temperature Measuring Probes

Thermocouples are a significant element of reactor instrumentation. To record the temperature mean values most of the LMFBRs are provided with thermocouples at the fuel element outlet. These thermocouples normally have a diameter of 1.5 mm or more which implies long response times. The cut-off frequency of these thermocouples is less than 1 Hz. Since in turbulent coolant flow of these reactors temperature fluctuations occur at a cut-off frequency of more than 20 Hz, a considerable part of these fluctuation signals are not recorded /Weinkötz 82.a/. This substantially reduces the sensitivity of detection of cooling channel disturbances in the fuel element. The problem can be solved by use of the three-wire thermocouple. A temperature measuring probe with a three-wire thermocouple for recording the temperature fluctuation signals is shown in Fig. 2.3-3. The three-wire thermocouple consists of an isolated Cr-Al junction for the measurement of the temperature mean value and a fast responding steel-sodium junction for recording the temperature fluctuation signals.

Moreover, a reference thermocouple T_2 for the steel-sodium junction T_1 has been installed within the probe. This reference measuring point must be surrounded by stagnant sodium so that no temperature fluctuation signals appear at this point.

A temperature measuring probe of the design shown in Fig. 2.3-3 was installed to record temperature fluctuation signals at KNK II. Fig. 2.3-4 shows a comparison of the signal response behavior of this probe with the operating measuring probe used at KNK II. In the left part of Fig. 2.3-4 the power density spectra have been plotted of a 1.5 mm diameter operating thermocouple with chromel-alumel junction for 30 % and 95 % reactor power and in the right part the spectra are shown of the 1.5 mm diameter three-wire thermocouple with steel-sodium junction. Both thermocouples had been fixed at the outlet of the KNK II central element. The steel-sodium thermocouple transmits at 30 % R_N temperature fluctuation signals with a cut-off frequency of 6 Hz related to the spectral power density of the temperature fluctuation signal at 1.5 Hz. The cut-off frequency of the temperature fluctuation rises to approx. 12 Hz at 95 % reactor power. By contrast, the power spectra of the operation thermocouple differ but slightly at 30 % and 95 % reactor power. Moreover, the steel-sodium thermocouple shows a signal power of the measured temperature fluctuations which is greater by a factor 5 at 1.5 Hz as compared to the operating thermocouple although the steady-state thermoelectric voltage ($\mu\text{V}/\text{K}$) of the chromel-alumel thermocouple is greater by approximately the factor 3 than of the steel-sodium thermocouple.

2.3.4 Signal Processing

On the basis of the foregoing statements and the experimental investigations in Sections 2 and 3 a concept is indicated for fuel element surveillance which relies on the analysis of the temperature fluctuation signals. On account of the multitude of fuel elements to be surveyed and since a coolant disturbance occurring in a fuel element shall be recorded as quickly as possible, it is necessary to process the temperature signals generated both in a parallel mode and in a serial mode. Therefore, the proposed concept for a fuel element surveillance system has been subdivided in Fig. 2.3-5 into an analog signal process for parallel data processing and a

digital signal process for serial data processing.

On the left hand side of Fig.-5 the analog part is shown for temperature signal processing including the following steps:

- amplification of the temperature signals $T(t)$,
- separation of the temperature fluctuation $\sigma(t)$ from the temperature mean value \bar{T} ,
- high and low-pass filtering of the temperature fluctuation signals,
- determination of the RMS value of the temperature fluctuation signal,
- determination of the temperature rise ΔT at the fuel element on the basis of the coolant inlet temperature T_E and the coolant outlet temperature T_A at each fuel element.

By parallel signal processing the number of the system elements entered in the analog process part depends on the number of the fuel elements to be surveyed in a reactor.

Serial data processing takes place in a digital data processing system. The following tasks were assigned to this system:

- Serial recording and processing of the signal variables present in the analog process part (RMS value σ and ΔT) of n fuel elements.
- Computation of the k -values from σ and ΔT for n fuel elements and display on a monitor.
- Alarm signal in case the limit value is exceeded.
- Sampling and recording of the fluctuating signal of the disturbed fuel element and computation and representation of the characteristic functions $\phi(\tau)$ and $S(f)$ and/or other values and functions.

2.3.5 Conclusions

In this contribution the potential of the analysis of temperature fluctuations at the fuel element outlet of LMFBR's is discussed for reactor surveillance. Considering the results of out-of-pile experiments on a 28-rod bundle and in-pile experiments at KNK II, it has been demonstrated, that the RMS-value normalized by the temperature rise of the fuel element, - the k -value - is suitable, for detection of cooling disturbances, especially

blockages. Using fast responding thermocouples the sensitivity of the method has been increased, but it is not yet well known, how sensitive this method can be made. This is a point of further investigation, and in addition the development of an suitable data processing is also proposed in this paper.

2.3.6 References

- /Weinkötz 79a/ G. Weinkötz, H. Martin, "Detection of different coolant blockage sizes in an LMFBR subassembly by measurement of the RMS value of temperature fluctuations". Int. Meeting on Fast Reactor Safety Technology, Seattle, Wash. Aug. 19-23, (1979). ANS, Vol. IV p. 1716
- /Weinkötz 79b/ G. Weinkötz, H. Martin, L. Krebs, "Detection of Coolant Disturbances in the Fuel Elements of an LMFBR by Temperature Fluctuation Analysis" Procedures and Systems for Assisting an Operator During Normal and Anomalous Nuclear Power Plant Operation Situations. IAEA/NPPCI Specialists' Meeting, München, December 5-7, (1979). GRS-19. p. 483
- /Weinkötz 82a/ G. Weinkötz, L. Krebs, H. Martin, "Analysis of Temperature Fluctuations at the Subassembly Outlet of the KNK II Reactor". Proceedings of the LMFBR Safety Topical Meeting, Lyon, July 19-23, (1982).
- /Weinkötz 82b/ G. Weinkötz, L. Krebs, H. Martin, "Measurement and Analysis of Temperature Fluctuations at the Outlet of an Electrically Heated 28-Rod Bundle without and with Flow Blockage". Tenth Meeting of the Liquid Metal Boiling Working Group (LMBWG) Kernforschungszentrum Karlsruhe, October 27-28, (1982).
- /Krebs 79/ L. Krebs, "Ausbreitung von Temperaturstörungen in begrenzter Strömung hinter einem Düsenblock". KfK-Bericht 2846, Dezember (1979).

/Krebs 81/

L. Krebs, K. Bremhorst, U. Müller, "Measurement and Prediction of the Mean and Fluctuating Temperature Field Downstream of a Multi-Bore Jet Block in which one Jet is Heated". Int. J. Heat Mass Transfer, Vol. 24, No. 8, pp. 1305-1312, (1981).

/Krebs 82/

L. Krebs, K. Bremhorst, "Mean and Fluctuating Temperature Fields in Sodium Flow Downstream of a Multi-Bore Jet Block Comparison of Gradient Diffusion Model and Experiment". Tenth Meeting of the Liquid Metal Boiling Working Group (LMBWG), Kernforschungszentrum Karlsruhe, October 27-28, (1982).

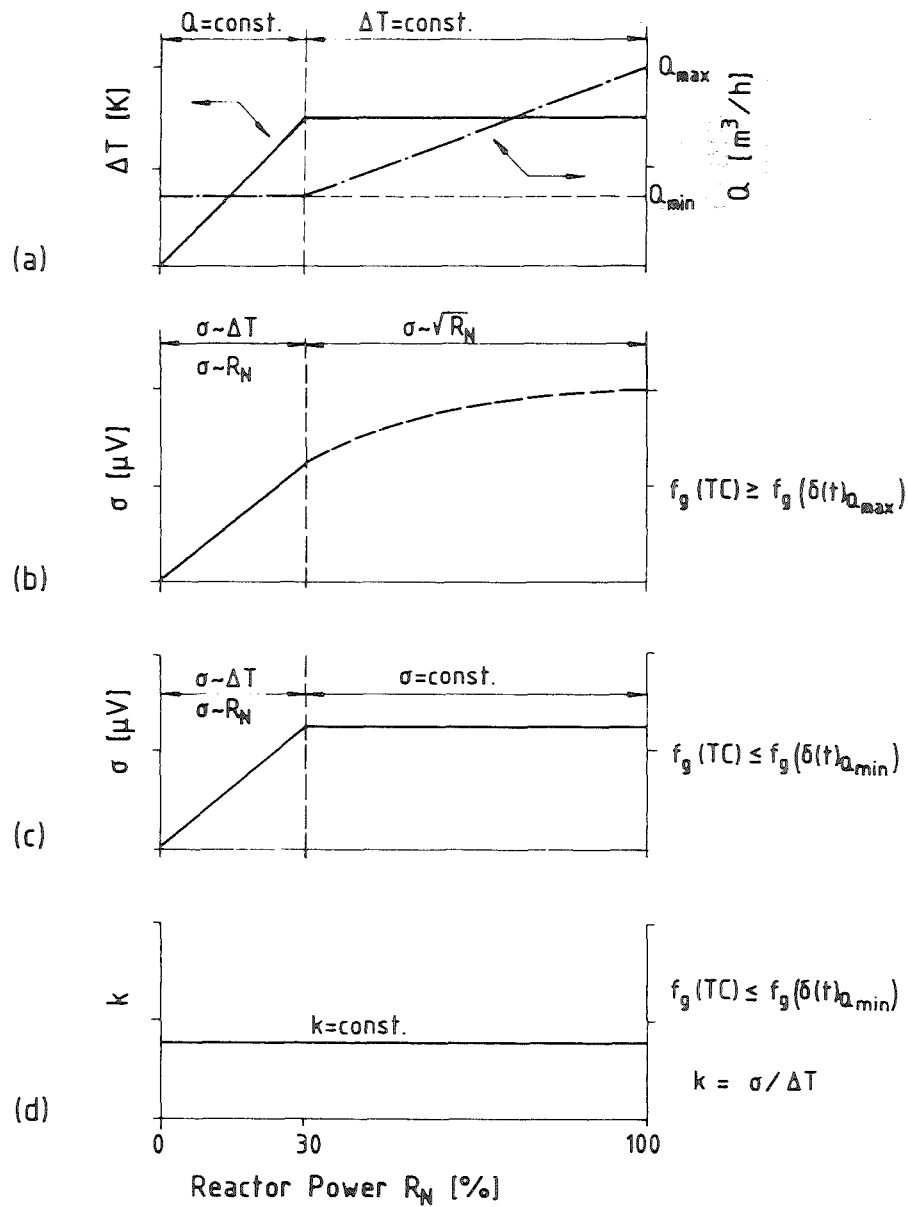


Fig. 2.3-1 Dependence of RMS-and k-Value of Temperature Fluctuations on Reactor Power R_N

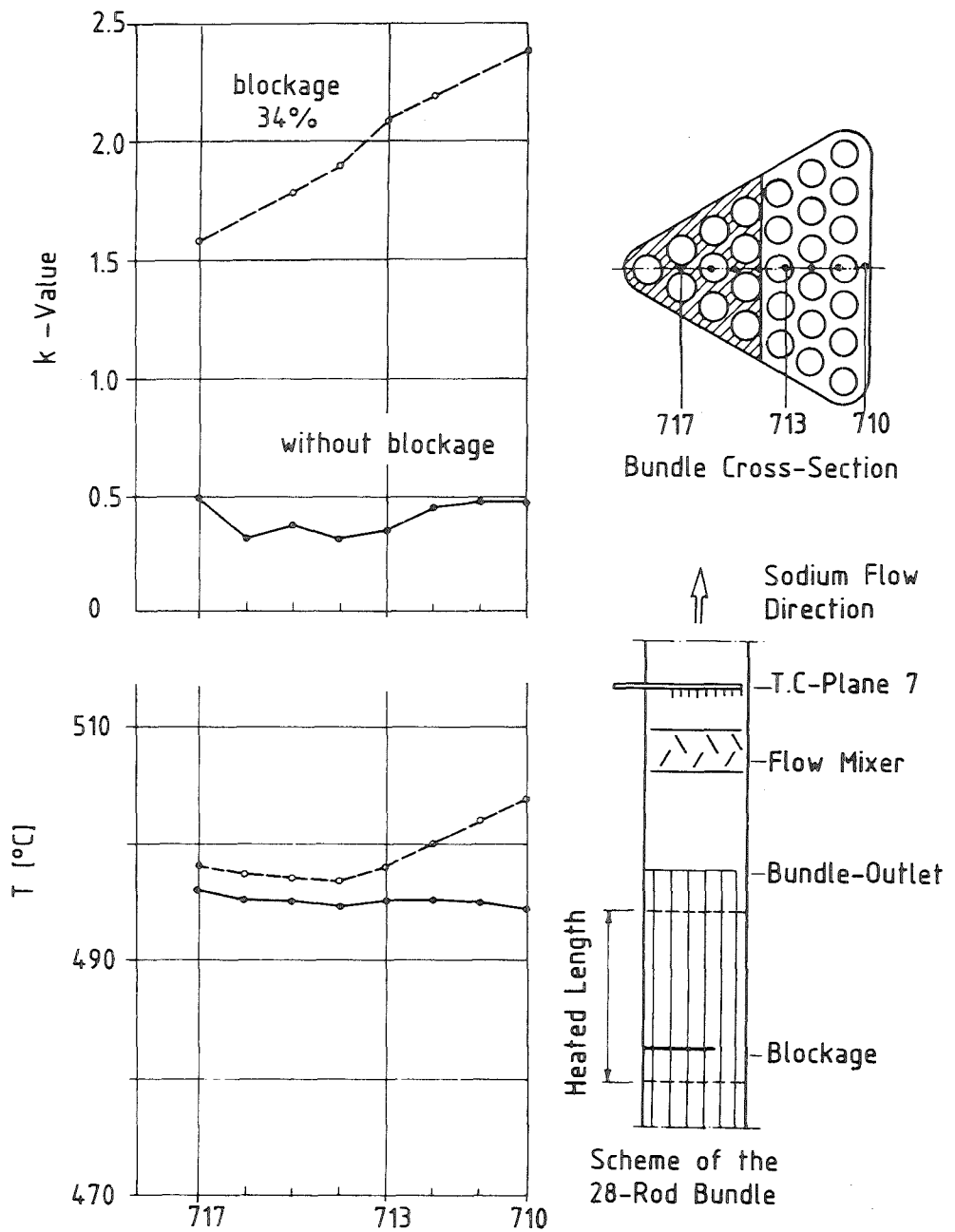


Fig. 2.3-2 Influence of Coolant Channel Blockage on the Mean Temperature and k-Value

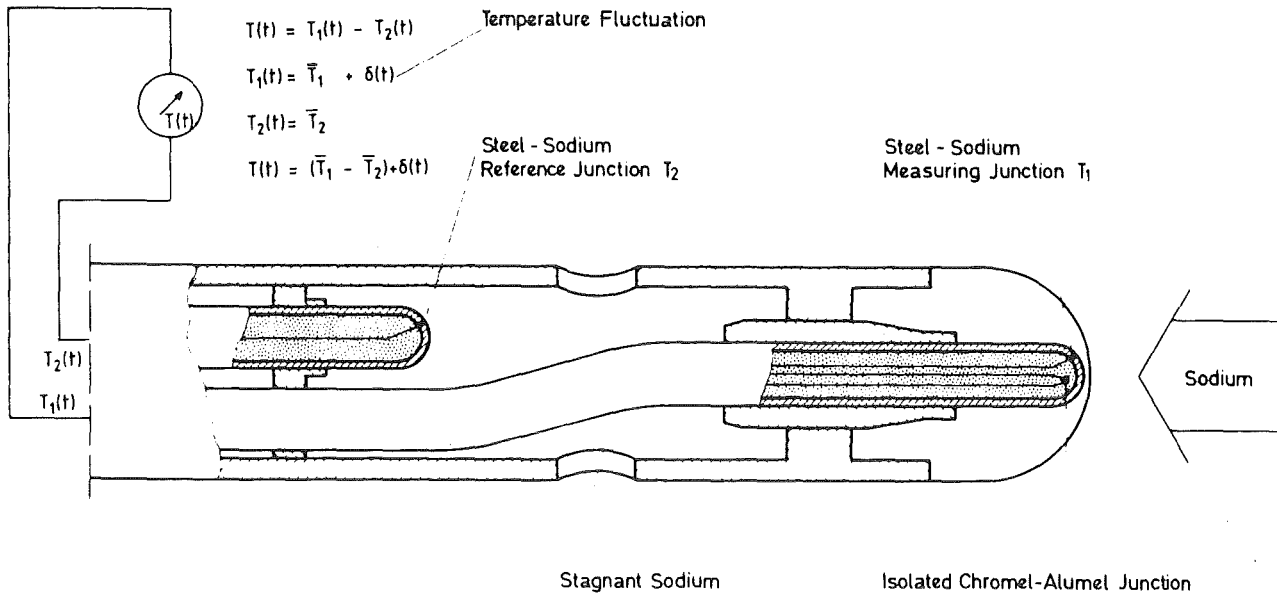


Fig. 2.3-3 Principle of a Three-Wire Thermocouple with Steel-Sodium Junction

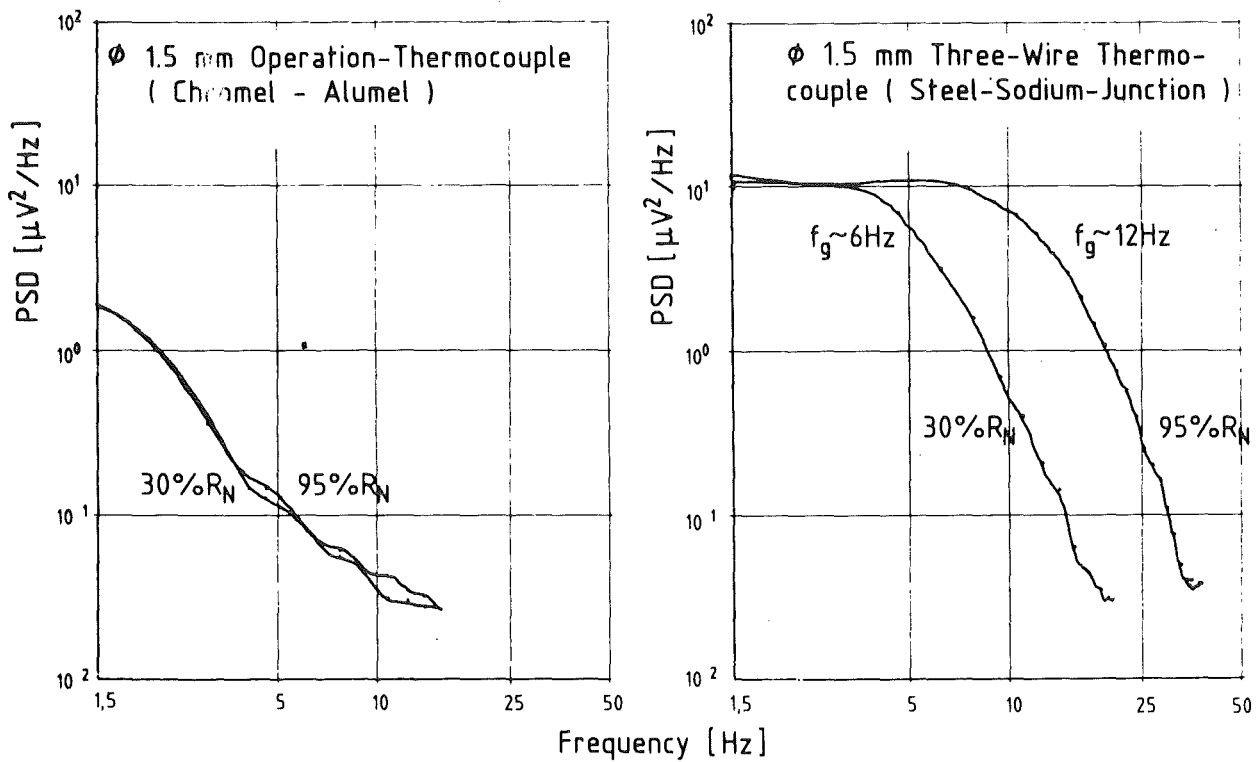


Fig. 2.3-4 PSD of Temperature Fluctuations Downstream of the Central Subassembly of KNK II

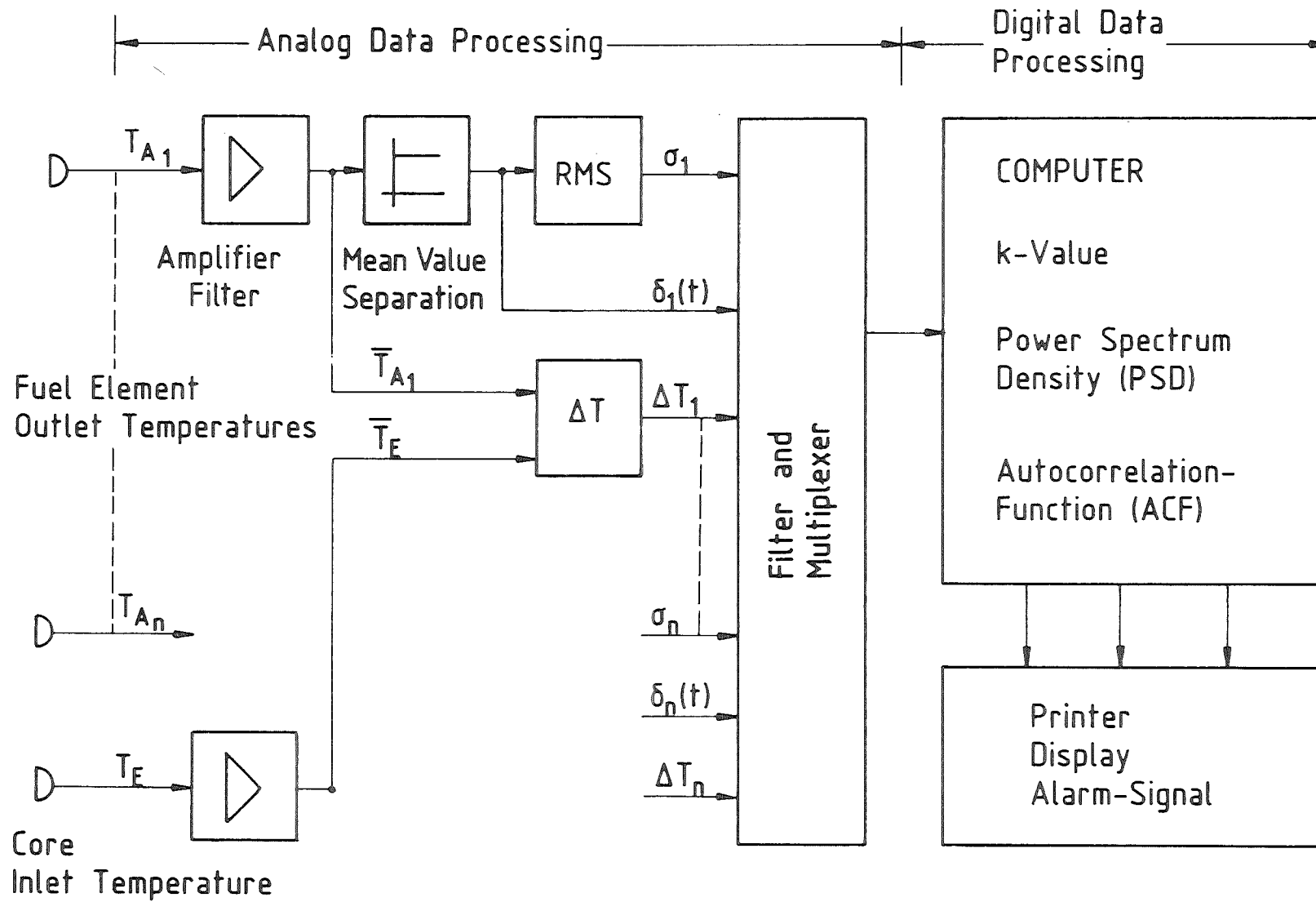


Fig. 2.3-5 Temperature Noise Processing System

2.4 Acoustic Noise Detection

H.A. Rohrbacher
Institut für Reaktorentwicklung

Abstract

Acoustic noise detection methods (AN) for an early boiling or loose parts detection offer a new and redundant possibility for the incore safety surveillance [NIEMANN 71], [NIEMANN 74]. The method is based on a continuously updated catalog for the acoustic background and it uses the pattern recognition technique for separating the derived incore signals from the reactor noise. Acoustic signals may become cross correlated to neutronic noise. Although a large number of datas per time must be analyzed and calculated, the acoustic system responds within one second.

General

The possibility of application of an acoustic noise analysis system in sodium cooled reactors is a redundant technique allowing correlation to already existing and classic measuring methods.

2.4.1 Boiling Detection

As it is known from experiments that sodium boiling can become detected by acoustics even in a high background noise level which is normally present in a reactor under working conditions [Rohrbacher 82].

Acoustic boiling spectra are found in a broadband range from up to 200 kHz. Originally, the acoustic source is a white noise generator in a much higher frequency span.

The source signal transfer is a reactor individual signal transport from the source to the sensors positioned in the sodium plenum, i.e. in the sodium outlet domain.

2.4.2 Frequency Window

To get separated from the high energy acoustic background, it was found the frequency-window from 40 kHz to 80 kHz to be an optimal detection range for boiling detection. Different reactors may show different window bandwidths, moreover, it is typical that more than but only one frequency window is used as a consequence of the complex transfer function for the acoustic transport.

2.4.3 Background Patterns

The acoustic background from 0 to 200 kHz changes its spectral composition and its stochastic behaviour as a function of time, temperature span and power rate. Consequently, a background catalogue must be set up for each instrumented acoustic sensor position. Let be N the number of sensors, P the periodicity of updating the background and S the number of samples for a given background bandwidth, the total minimum number of datapoints D per time unit (sec) is given by:

$$D = N \cdot P \cdot S \quad \text{Samples, average value per second}$$

or, for a fixed total bandwidth ΔF (s^{-1}) following the SHANNON minimum requirements:

$$D = N \cdot P \cdot S \Delta F \quad \text{Samples/sec}$$

For a coarse assumption with $N = 20$, $P = 0,017$ (10 min. update) and $\Delta F = 200$ kHz, the data rate R_d for an acoustic background pattern is:

$$R_d = 8 \cdot 10^6 \quad \text{samples/for each 10 minutes}$$

Since the first 20 kHz of the background spectra risk to interfere the boiling signals due to their high dynamic signal contents they must be cut off by filtering so that they do not contribute data for the background pattern catalogue. Above 20 kHz, signal dynamics are restricted to about 46 dB, thus, the samples need to be drawn at a resolution of 1 by 200 or at 8 bits for each sample.

2.4.4 Creating an Updated Sample Average

The information of an acoustic catalogue for all background signals cannot be drawn from a single R_d -value but only from an minimum number of repetitive R_d -rates and their average taken in an suitable time

interval T_S . A sufficient number of R_d -values is $N_R = 16$ for a time-interval $T_S = 100$ seconds. Averaging the N_R times R_d -rates forms the shape of the new updated acoustic background information which is the reference for each sensor position making a comparison to all detected sound until the following update.

The updating process therefore claims for an online spectrum analysis of $N_R \cdot R_d = 1,28 \cdot 10^8$ samples for the named example and it refers to the presence of 20 sensors.

2.4.5 Uninterrupted Background Pattern Comparison

In order to ensure a gapless signal comparison to the catalogue during the update time and its associated averaging delay the previous catalogue content must be held effective in the memory until the total update which takes 100 seconds has been completed and the new catalogue is ready to be shifted from a buffer to the main memory. The shift delay may not exceed 100 milliseconds to avoid a justifiable dead time.

2.4.6 Background Analysis

The background signals from each individual sensor are processed by use of a spectrum analyzer which could be a part of the computer system. A twenty channel analyzer executing fast Fourier Transform (FFT) and having the capability for cross correlation is a substantial component for the data evaluation described in 2.4.2 to 2.4.5.

2.4.7 Signal to Background Coherence

The patterns from boiling signals are unrelated to the measured and stored background information, therefore the relevant coherence is much below 1.

In case of appearance of a number of anomalous signals which do not meet a minimum coherence in the frame of the preset frequency windows or of certain repetition rates and/or of the programmed RMS-contents which all is part of the analysis software for the pattern recognition technique [Niemann 81], the acoustic diagnosis must lead to a pre-alarm. The occurrence of single acoustic signals such as bursts or sharp impulses and their relevant low spectral density as well as their non-repetitive status within a preset time interval are valuation datas for a discriminating system suppressing disturbances and interference signals,

electrical noise peaks and non periodic single events from mechano-acoustic sources. The latter ones are formed by thermal stress and cracks and they must become separated from boiling noise by means of an additional pre-filtering incorporated in the pattern recognition system.

2.4.8 Correlating Acoustic Signals

The occurrence of boiling noise is detected from a large part of the sodium immersed transducers in the upper plenum simultaneously. Depending from their individual geometrical position the acoustic transducers will sense the sound pressure wave fronts emitted from the boiling source at different propagation time delays and thus expressed by a number of individual phase displacements. The time phase shift as a consequence from different sound transfer paths offers an additional potential for a signal to noise separation by means of the time discriminating technique. A signal pick-up from more than one sensor position with an undue phase delay or single pulses from only one sensor in the plenum are then ignored by the correlator.

2.4.9 Out-of-Tank Noise Sensors

Most of periodic noise is generated by the pumps and other rotating components such as motor drives and cooling fans. In many cases a higher frequent noise distribution is known from the sodium flow at different flow rates and temperatures. Some of the named 20 microphones must be used to sense the most prominent noise sources from out of the tank area, i.e. the rotating sodium pumps. Their acoustic signals form a base for the pattern field and relevant background catalogue update.

2.4.10 Correlated non-acoustic External Datas

The acoustic background is controlled by a number of variables of state which are fundamental patterns for its catalog. Hence, the following operating datas are needed:

- Pump speed from all sodium pumps in each circuit
- Total primary Flow Rate
- Inlet Temperature (Na)
- Outlet Temperature (Na)

- Outlet Temperature (Na)
- Neutron flux
- Reactor Power
- Control Rods: Position and displacement activity

Accordingly, about 12 non-acoustic datas are requested for the acoustic data processing device.

2.4.11 Data Format from Acoustic Sensors

Acoustic sensors transform mechanical pressure transients into analog electrical signals at very low levels (0 to 10 mV max). Pre- and mainamplifieres provide for a galvanically isolated analog amplification up into the volt domain, associated with a suitable bandpass-Filtering.

2.4.12 Data Format from External Signals

Analogous to the acoustic signals the signals from the reactors operating system are expected to be already conditioned 0 - 10 Volts datas. Their source impedances must be less 500 Ohms.

2.4.13 Alarm-Signal

The acoustic alarm signal is created in a alarm generator associated to the acoustic pattern recognition system. The alarm trigger may consist by a relais contact and/or a TTL-output step signal connected to the main processor.

2.4.14 Acoustic Data Chain

Fig. 2.4-1 shows the block diagram of the acoustic noise detection system, its data transfer into the analyzer and the pattern recognition processor incorporated. The analog part consists by the pre/main-amplifiers 1 + 2 and the multiplexer section 3 followed by the AD-converter and the digital FTT system. The buffers 5 arranged in the batch mode serving as intermediate memories are connected to the pattern recognition analyzer system 6 which responds by an alarm generator 7. Its output, however, represents the cross section to the processing unit 8. That one working in connection to all other reactor detection and measuring systems like neutron noise surveillance 9 which offers in some cases a cross correlation with acoustics.

2.4.15 Diagnostic Potential

The results available to this date from background measurements in the reactor performed over extended periods of time and knowledge derived from out-of-pile boiling experiments in bundle geometry as well as from quite a number of model experiments lead to the conclusion that the evaluation of acoustic boiling concentrates on three methods:

- Creating the autocorrelated Power-Density-Spectrum (PSD) and analyzing the peak-spectrum up to 200 kHz
- Calculation for the RMS-values within the named signal-spectrum with the aim to improve the S/N-ratio. Since high spikes and most of the electric pulse peaks occurring temporarily have normally but a low energy content they are filtered by the RMS-evaluation as pure interferences.
- One-dimensional Pattern Recognition method using well known algorithms for the statistical problem.

Both, spectrum analysis and RMS data evaluation represent the classic methods for an acoustic surveillance system in a reactor. However, it was shown [Pridöhl 80] that a surveillance system based only on the spectrum analysis is not recommended for a severe background-noise situation. In contrast to these methods, Pattern Recognition supported by modern computer standards offers an already experienced method in the area of military acoustic and sonar surveillance systems and in the medical field [Quante 78].

In the UK [SMEDLEY 83] acoustic leak detection systems based on the detection of high frequency impingement noise have been tested in test rigs and on the PFR. The data have enabled the writing of a leak detection algorithm using pattern recognition which will give detection of escalating microleaks with a spurious detection rate of less than 0.5 per reactor operating year.

2.4.16 Nomenclature

N	= Number of Sensors
N _e	= Number of Data rates for averaging
P	= Periodicity of updating
S	= Number of Samples
D	= Number of Data points per time

ΔF = Bandwidth of background
 R_d = Data rate (Samples / time)
 T_s = Time interval

2.4.17 Reference

[Rohrbacher 82_]

J. Aberle, R. Bartholomay, H. Rohrbacher, K. Schleisiek:
"Potential and Problem of Acoustic Boiling Detection 10 th Meeting
of the Liquid Metal Boiling Working Group.
Karlsruhe, October 27-29, 1982

[Niemann 71_] H. Niemann:

An Improved Series Expansion for Pattern Recognition,
NTZ 24(1971) 473-477

[Niemann 74_] H. Niemann:

Methoden der Mustererkennung, Akademische Verlagsgesellschaft,
Frankfurt 1974

[Niemann 81_] H. Niemann:

Pattern Analysis, Springer, Berlin, Heidelberg, New York 1981

[Pridöhl 80_] E. Pridöhl, Akustische Detektion von Wasserlecks in natrium-
beheizten Dampferzeugern unter Verwendung von Methoden der statisti-
schen Entscheidungstheorie,

Akademie der Wissenschaften der DDR, Zentralinstitut für Kernforschung
Rossendorf bei Dresden, ZfK-428, 1980

[Quante 78_] F. Quante et al.:

System zur automatischen Herzschall-Analyse, Realisierung und
Anwendung

Institut für Informations-Verarbeitung in Technik und Biologie,
Karlsruhe 1978, 20-26

[SMEDLEY 83_] J.A. Smedley et al.:

Theoretical and Experimental Work on Steam Generator Integrity on
Reliability with particular Reference to Leak Development and Detection
UK Status Report, October 1983

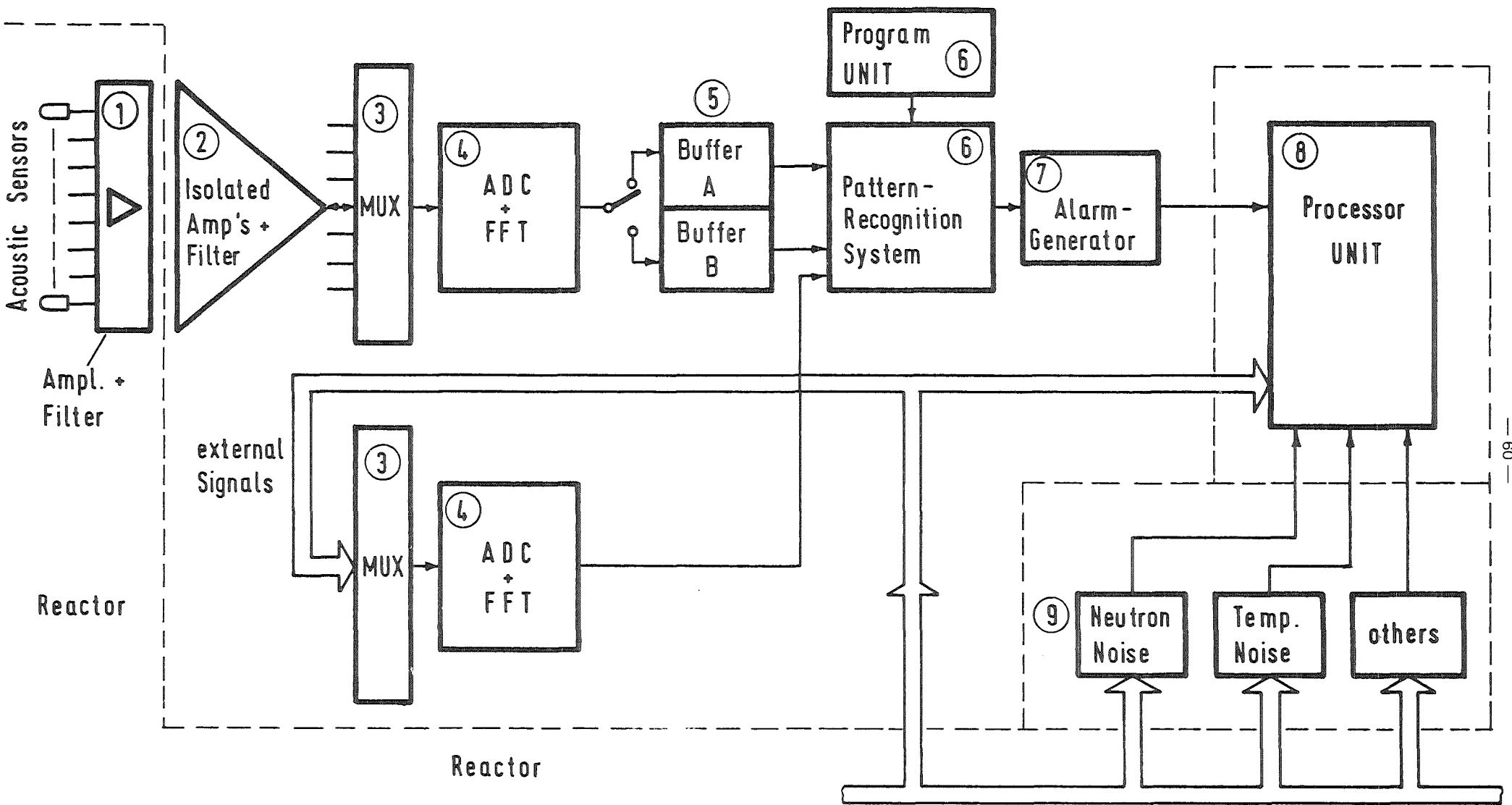


Fig. 2.4-1 Block Diagram of Acoustic Noise Detection System

2.5 DETECTION OF FAILED FUEL ELEMENTS

by

S. Jacobi

Institut für Reaktorentwicklung

Abstract

The operation of a nuclear power plant with a failed fuel element requires, especially in case of an LMFBR, comprehensive knowledge for evaluating the situation in the proper way. This knowledge is needed as regards several differing subject areas:

- science and technology of nuclear fuels,
- behaviour of failed fuel subassemblies during plant operation,
- mechanisms governing the release and transport of fission products,
- techniques for detection and location of failed fuel subassemblies,
- safety and availability of the plant during operation with failed fuel elements,
- plant specific requirements.

Since an expert provided with these requirements cannot be available at every moment, the attempt is made to substitute him by the most recent data processing technology. Both the theoretical knowledge and experience already derived and still to be derived from plant operation and experiments should be stored in a formalised manner. The said system receives further data from the plant as instantaneous measured values without the necessity of installing additional sensors which is a noticeable feature. At the final stage of development the system, in the same way as an expert now, shall give to the operator recommendations for the subsequent operation of the plant based on a linking of all data available. The system in this way becomes a "Consulting Core Surveillance System".

2.5.1 Introduction

It is an experience established worldwide that failures of the cladding tubes of fuel subassemblies cannot be avoided in nuclear power plants. Cladding tube failures in this context mean a leak in the confinement of the fissile material and of the radioactive fission products generated during nuclear fission. The causes of such leaks may vary considerably and can be broken down into the following groups:

- a) Defects already existing at the beginning of operation:
 - defects in manufacturing not detected in the course of the various controls;
 - defects caused during handling prior to first use.
- b) Early defects originating at low burnup:
 - defects in manufacturing;
 - unfavorable manufacturing tolerances for cladding tube and fuel.
- c) Late defects originating approximately upon attainment of the target burnup:
 - chemical and mechanical interactions of cladding tube, fuel and fission products;
 - chemical interaction of cladding tube, coolant and its impurities;
 - embrittlement of cladding tube material as a result of irradiation.
- d) Defects due to overload or disturbances in cooling.

Groups a) and b) are the Begin-of-Life (BOL) defects whilst group c) constitutes the End-of-Life (EOL) defects. But in every case a cladding tube failure implies a contamination of the primary cooling circuit with radioactive fission products, in case of major defects also a contamination with fuel, which can be tolerated up to defined limits only.

In principle, the statements above apply to all reactor types but they are greatly mitigated in case of light water reactors on account of the high chemical resistance of UO_2 to cooling water. By contrast, Liquid Metal Cooled Fast Breeder Reactors (LMFBRs) are in a less advantageous position due to the chemical reaction taking place between the sodium coolant and the mixed oxide $(U, Pu)O_2$ and the oxygen contained in the sodium and fuel, respectively: $Na_3(U, Pu)O_4$ is formed which makes grow small primary defects or gives rise to secondary defects [Adamson 76].

In the worst case such a defect of a fuel pin could develop to a disturbance in cooling necessitating a shutdown of the plant [Smidt 76].

The main problem is the proper choice of the time of reactor shutdown which, especially for an LMFBR, calls for extensive expert knowledge [Brudermüller 81, Jacobi 82]. Regarding reactor shutdown the main consequences of a wrong decision are:

Unnecessary Shutdown

- Thermal stresses on the plant,
- 0.5 mio \$/day for substitute electricity,
- If too often and too long: negative public image.

Shutdown too Late

- High fission product contamination of the primary loop, ^{x)}
- Fuel in the primary loop, ^{x)}
- Potential start of a disturbance in cooling.

^{x)} problems of repair and maintenance

After a cladding tube failure has appeared, i.e., after it has been detected, it is of paramount importance to locate the defect. Besides the methods of individual coolant sampling or tagging, flux tilting will become increasingly important in the future because of the specific problems associated with the methods mentioned first (see separate chapter on that subject and [Jacobi 82]). Under the flux tilting method variations in power within various core zones allow one to determine those core positions where the failure has occurred. But this method calls for a particular wealth of expert knowledge and can hardly be realized in large reactors without the use of computers.

To improve this situation an expert would have to be permanently available at each LMFBR with knowledge and experience gathered in

- Failed Fuel Detection (FFD),
- Various methods of Failed Fuel Location (FFL),
- Behaviour of defective fuel elements during reactor operation,
- Problems of safety and availability as regards a failed fuel element and plant operation.

Since these conditions cannot be fulfilled in the future at each plant and at any time, a Microprocessor-based Integrated Core Surveillance System, supplemented by appropriate expert knowledge and on-line signal evaluation, shall give advice to the operator in decision making. A part of this system will be the Consulting Core Surveillance System COCOSS, a subsystem for detection and location of failed fuel elements, see also chapter 2.6 LOCATION OF FAILED FUEL ELEMENTS and [Hoffmann 83].

2.5.2 Fission Products as an Indicator of Failed Fuel Elements

If leaks occur in the claddings of individual fuel rods during operation of LMFBRs fission products and possibly, also fuel may be released into the coolant [Jacobi 82]. When analyzing such phenomena, different mechanisms of fission product releases must be taken into account.

- Releases into the coolant by recoil.
- Releases into the coolant by diffusion.
- Releases by recoil into open fuel pores and on into the coolant.
- Releases by diffusion into the plenum and on into the coolant.
- Releases into the coolant by knock-out mechanisms.
- Releases by knock-out mechanisms into open fuel pores and on into the coolant.

2.5.3 Releases into the Coolant by Recoil

In releases of radioactive fission products caused by recoil mechanisms it is assumed that fission products formed in a layer of the thickness L_i right underneath the defect area F are spontaneously released into the coolant by recoil in a fraction δ . After an equilibrium condition has become established, the following equation holds:

$$R_i^R = \delta \cdot F \cdot L_i \cdot \lambda_i \cdot v_i \cdot S \quad (1) \text{ Model A}$$

R_i^R [s⁻²] Activity release rate of nuclide i into the coolant by recoil.

δ [1] Geometric escape coefficient.

F [cm²] Geometric defect area.

L_i [cm] Recoil length of nuclide i .

λ_i [s⁻¹] Decay constant of nuclide i .

v_i [1] Cumulative fission yield of nuclide i .

S [s⁻¹cm⁻³] Specific fission rate.

2.5.4 Releases Into the Coolant by Diffusion

If radioactive fission products are released by diffusion, the fission products generated are assumed to migrate through the fuel up to the fuel rod defect and on into the coolant as a result of a concentration gradient.

Under the additional assumptions of a linear, one-dimensional geometry and the absence of any repercussions on diffusion processes in the fuel of the concentration of fission products in the coolant, it follows, after an equilibrium condition has become established:

$$R_i^D = F \cdot v_i \cdot S \cdot \sqrt{\lambda_i} \cdot \sqrt{D_i} \quad (2) \text{ Model B}$$

R_i^D $\left[\text{s}^{-2} \right]$ Activity release rate of nuclide i into the coolant by diffusion.

D_i $\left[\text{cm}^2 \text{s}^{-1} \right]$ Diffusion coefficient of nuclide i in the fuel region.

2.5.5 Releases by Recoil into Open Fuel Pores and on into the Coolant

For releases of radioactive fission products by recoil mechanisms into open fuel pores and on into the coolant, the following model is assumed to be valid: Fission products formed in a layer of the thickness L_i and an area F^P , which surrounds the open porosity, are released spontaneously into the free pores by recoil in a fraction δ . Fission product noble gases also released carry part of the fission products from the open porosity through the rod defect into the coolant. An Arrhenius type release is assumed to prevail. After an equilibrium has been established, it is found that

$$R_i^{RP} = \frac{\lambda_i \cdot \lambda_e}{\lambda_i + \lambda_e} \cdot \delta \cdot L_i \cdot F^P \cdot v_i \cdot S \quad (3) \text{ Model C}$$

R_i^{RP} $\left[\text{s}^{-2} \right]$ Activity release rate of nuclide i by recoil into the open porosity and on into the coolant.

λ_e $\left[\text{s}^{-1} \right]$ Escape coefficient.

F^P $\left[\text{cm}^2 \right]$ Surface of open porosity in the region of the fuel rod defect.

The other three release mechanisms mentioned above are not at present treated mathematically and numerically.

2.5.6 The k-Factor

The fissuring factor, k , has been defined as the ratio of the effective recoil area to the geometric defect area, in which case fission product release by recoil was assumed [Jacobi 77]. For a specific nuclide it can be expressed as follows:

$$k_i = \frac{R_i^G}{R_i^R} \quad (4)$$

k_i [] Fissuring factor relative to nuclide i .

R_i^G [s⁻²] Measured radioactivity release rate of nuclide i .

R_i^R [s⁻²] Radioactivity release rate of nuclide i calculated by means of a recoil model.

If the real radioactivity release is diffusion controlled, R_i^G can be expressed as follows in accordance with Eq. (2):

$$R_i^G = F \cdot \sqrt{D_i} \cdot \lambda_i^{1/2} \cdot v_i \cdot S \quad (5)$$

With Eqs. (5) and (1), Eq. (4) is transformed into

$$k_i = \frac{1}{\delta \cdot L_i} \cdot \left(\frac{D_i}{\lambda} \right)^{1/2} \quad (6)$$

Eq. (6) can be converted into

$$D_i = L_i^2 \cdot \delta^2 \cdot \lambda_i \cdot k_i^2 \quad (7)$$

In deriving Eq. (6) it has been assumed that the fuel will not change chemically after the occurrence of the defect. However, this condition does not always exist if sodium is used as a coolant because, when certain oxygen concentrations in the fuel and the sodium are exceeded, part of the fuel will be converted into Na₃MO₄ or similar compounds. The letter M in this case stands for metal, i.e., U or Pu. Since also the density of the fissile material taken into account changes in this transformation also different specific fission

ratios must be substituted in Eq. (5) and (1). For this general case one obtains:

$$k_i = \frac{S^R}{\delta \cdot L_i \cdot S^B} \cdot \left(\frac{D_i^R}{\lambda_i} \right)^{1/2} \quad (8)$$

S^R [s⁻¹ cm⁻³] Specific fission rate in the Na₃MO₄ reaction layer.
 S^B [s⁻¹ cm⁻³] Specific fission rate in MO₂ fuel.
 D_i^R [cm² s⁻¹] Diffusion coefficient of nuclide i in the reaction layer.

Eq. (8) can be changed into:

$$D_i = L_i^2 \cdot \delta^2 \cdot \lambda_i \cdot \left(\frac{S^B}{S^R} \right) \cdot k_i^2 \quad (9)$$

However, if the actual radioactivity release is controlled by recoil into open pores, it holds for R_i^G according to Eq. (3):

$$R_i^G = \frac{\lambda_e}{\lambda_i + \lambda_e} \cdot \delta \cdot L_i \cdot F^P \cdot \lambda_i \cdot v_i \cdot S^B \quad (10)$$

With Eq. (10) and (1), Eq. (4) changes into

$$k_i = \frac{\lambda_e}{\lambda_i + \lambda_e} \cdot \frac{F^P}{F} \quad (11)$$

If this type of release prevails, it is assumed that there has been no chemical conversion of the fuel or that such (Na₃MO₄) reaction layer has been reduced again.

2.5.7 Instrumentation for Failed Fuel Detection and Location

The instrumentation of LMFBRs for failed fuel detection and location is very similar in all these reactors. Therefore the following brief description of the instrumentation of the KNK II)^x may serve as a typical example.

KNK II has two systems for failed fuel element detection. The first system consists of two DND (= Delayed Neutron Detector) monitors, one of each is attached to the two main primary sodium pipes (Fig. 1) downstream of their

outlet from the reactor vessel. Each monitor contains eight ^3He counters connected in pairs to an amplifier. Three pairs make up three redundancies in the DND system, one pair serves for standby purposes. The counting tubes are enclosed in a moderator block made of polyethylene and are strongly shielded against γ -radiation and core neutrons. Each DND measuring station has a γ -dose rate monitor and is equipped with a temperature sensor. If a calculated limit value of the DND counting rate of 2000 cps is exceeded, the reactor will be scrambled. Alarm is given by 1500 cps.

The second system consists of measuring the fission product gas concentration in the primary cover gas. For this purpose, the KNK-II facility has a separate gas circuit (Fig. 2) for failed fuel detection. It contains two NaI(Tl) detectors equipped with amplifiers, single-channel discriminators and ratemeters, a computerized on-line γ -measuring station with high purity germanium detector, multi-channel analyzer as well as three different types of precipitators [Richard 82].

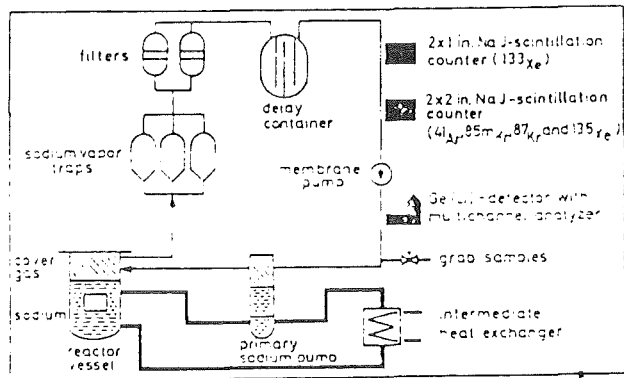
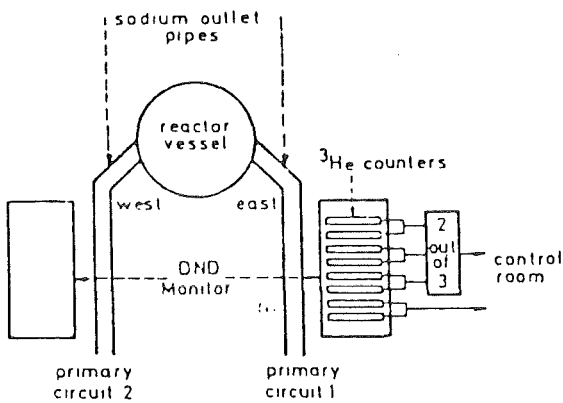


Fig. 1. DND Monitoring System KNK II

Fig. 2. Failed Fuel Detection System on the Cover Gas KNK II

)x Kompakte Natriumgekühlte Kernreaktoranlage Karlsruhe (KNK II), 20 MWe

2.5.8 Codes Established to Date

To calculate the expected count rates of the DND detectors the FICTION (Fission Product Signal Calculation) code was written, Table 1. Recoil of the fission products into the coolant was assumed as the release mechanism. In addition, the k-factor was programmed. The following formulae were used [Hoffmann 82]:

$$N_i = \delta \cdot L_i \cdot F \cdot k \cdot \lambda_i \cdot v_i \cdot \mu_i \cdot S \quad (12)$$

N_i [s⁻²] Neutron activity release rate of nuclide i into the coolant

μ_i [1] Emitted neutrons per nuclide disintegration.

$$C = \eta \cdot \rho^N \cdot V^P \cdot \sum_{i=1}^{10} \left(\frac{N_i}{Q} \cdot e^{-\lambda_i \cdot t^1} \right) \quad (13)$$

C [s⁻¹] Count rate of DND detector

η [1] Neutron sensitivity of DND detector

V^P [cm³] Volume of Na sample vessel

Q [g/s] Sodium flow

ρ^N [g/cm³] Sodium density

t^1 [s] Transit time of sodium from the defect point to the DND detector.

For short sodium recirculation times it holds that

$$C^R = \eta \cdot \rho^N \cdot V^P \cdot \sum_{j=1}^m \cdot \sum_{i=1}^{10} \left(\frac{N_i}{Q} \cdot e^{-\lambda_i (t^1 + j \cdot t^u)} \right) \quad (14)$$

C^R [s⁻¹] Count rate of DN detector taking account of sodium recirculation

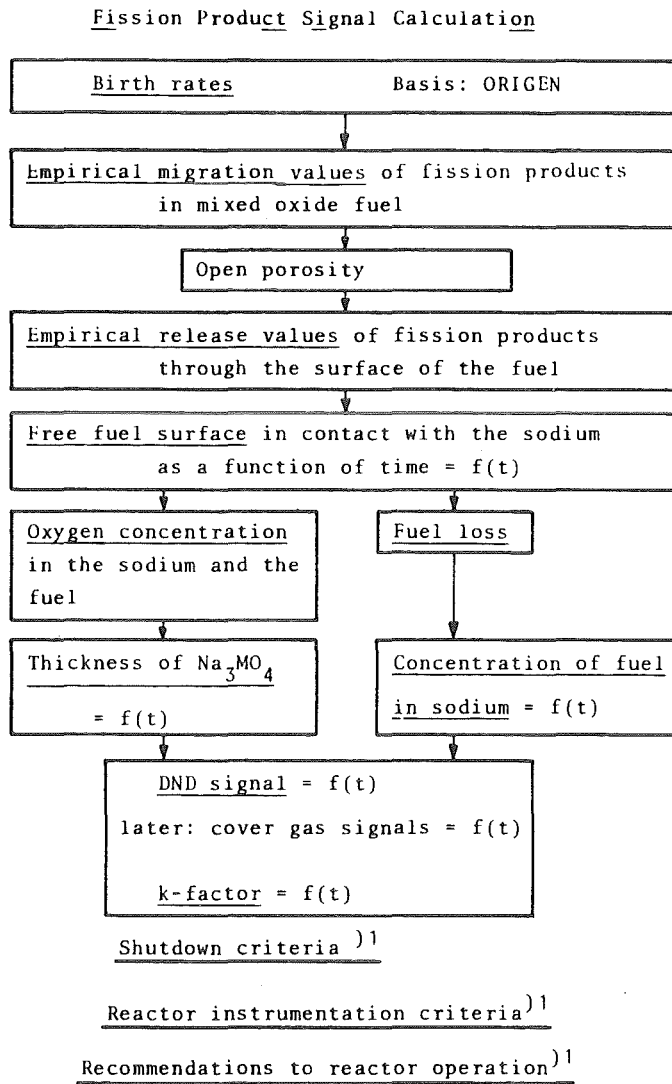
t^u [s] recirculation time of sodium

with

$$m = \frac{5 \cdot \ln 2}{t^u \cdot \lambda(\text{Br-87})}$$

The variable input quantities include F , K , S , η , ρ^N , V^P , Q , t^l and t^u .
 The following nuclides are taken into account: Br-87, Br-88, I-137, Br-89, Rb-93, I-138, As-85, Br-90, Rb-94 and I-139.

Table 1. FICTION Code



)¹ Not part of the code, but application

References

- [Adamson 76] M.G. Adamson: Sodium-Fuel Reaction Studies: Fuel Pellet Swelling Behavior and Alkalimetal-Oxide Fuel Reaction Thermodynamics. GEAP-14093, UC-79b, March 1976
- [Smidt 77] D. Smidt, K. Schleisiek: Fast Breeder Safety against Propagation of Local Failures, Nucl. Eng. Des., 40(1977) 393
- [Brudermüller 81] G. Brudermüller et al.: 18 Days KNK II Operation with a Failed Fuel Element Based on In-Pile Loop Experiments. Topical Meeting on Reactor Safety Aspects of Fuel Behavior, August 2-6, 1981, Sun Valley, Idaho
- [Jacobi 82] S. Jacobi, Editor: Fuel Failure Detection and Location in LMFBRs. Proc. of Int. Atomic Energy Agency Specialists' Meeting, Karlsruhe, May 11-14, 1981, KfK 3203, June 1982
- [Hoffmann 83] G. Hoffmann, S. Jacobi, G. Schmitz: Transfer of Expert Knowledge to the Consulting Core Surveillance System COCOSS at KNK II. Fifth Power Plant Dynamics, Control and Testing Symposium, March 21-23, 1983, Knoxville, Tenn.
- [Jacobi 77] S. Jacobi, K.-D. Letz, G. Schmitz: Release and Detection of Fission Products from defective Fuel Pins. Nucl. Eng. Design 44(1977) 125
- [Richard 82] H. Richard et al.: Experience of Failed Fuel Detection and Localization at KNK II, Proc. of Int. Atomic Energy Agency Specialists' Meeting, Karlsruhe, May 11-14, 1981, KfK 3203, June 1982, p. 93
- [Hoffmann 82] G. Hoffmann, S. Jacobi, G. Schmitz: Fuel Failure Detection and Location in Fast Breeder Reactors. In [Jacobi 82], p. 215

2.6 LOCATION OF FAILED FUEL ELEMENTS
BY FLUX TILTING

by

S. Jacobi

Institut für Reaktorentwicklung

Abstract

This chapter 2.6 is the direct continuation of the previous chapter 2.5 DETECTION OF FAILED FUEL ELEMENTS. After the information that anywhere in the core a failed fuel element exists, that means after the detection the location of the subassembly with the failed fuel element is the next important step. From this and the following information about size and type of the failure significant decisions are derived for the further operation of the plant. The instrument for this task will be the Consulting Core Surveillance System COCOSS, described in this chapter.

2.6.1 State of the Art

Regarding failed fuel elements a great deal of complex knowledge has been obtained from in-pile tests and LMFBR operation. Compared to this, the information provided by the failed fuel detection systems is not adequate, especially as far as the evaluation and derivation of decisions are concerned. This is illustrated by the following examples:

- Few applications of computers or microprocessors to failed fuel subassembly detection and location.
- Conventional hardwired electronic devices are currently used.
- No correlation and linking of measurements and operational parameters.
- A harmless momentary burst of fission products may give rise to an unnecessary scram.
- Global scram levels for the whole core without taking into account individual subassembly conditions.
- Especially flux tilting calls for an expert to interpret the complex fission product signals (explanations on the flux tilting method will be given in the next chapter).
- Owing to the complexity of signal evaluation computer aided recommendations are not available for the subsequent operation of the plant, e.g.,

immediate or temporary shutdown, reduction in power, decisions in favor of campaigns for locating the failure.

Thus, for plant operation with defective fuel elements

the decisions rely on the special knowledge of the operators and/or the availability of experts.
--

It should be mentioned here that quite a number of attempts have been made to install disturbance analysis systems at nuclear power plants. Examples cited here are the publications by W. Bastl, C.D. Heising and A.B. Long [Bastl 82, Heising 82, Long 80]. Unlike the goals pursued with the Consulting Core Surveillance System COCOSS which will be discussed here, all systems previously described have in common:

- They have been designed to apply to the whole "nuclear power plant" system. An application to the "failed fuel detection and location" partial area accompanied by recommendations for subsequent plant operation has not been described until this date.
- The system serve the purpose of status surveillance and disturbance analysis, e.g., Disturbance Analysis System DAS [Long 80] and Störungs-analyse-Rechner (disturbance analysis computer) STAR [Bastl 82].
- The previous systems are solely intended to lend assistance to the operator in decision making in a disturbance by means of a cause-consequence analysis and reduction of data without providing recommendations based on signal evaluation.
- Disturbance prediction is still lacking, i.e., the anticipated subsequent development of the disturbance in case that one or the other intervention in the plant is performed or omitted, is not known.

2.6.2 Flux Tilting

2.6.2.1 Experience Gathered at KNK II

Unlike collecting individual samples from each fuel subassembly or tagging involving investment costs on the order of several millions of \$, flux tilting constitutes a method of failure location not requiring additional expenditure in equipment [Jacobi 82]. Since this method will play a major role in this paper, some explanations will be given below.

The rate of fission product generation is proportional to the fission power of a given volume of fuel. Leaving aside quite a lot of other effects, the rate of fission product release from a failed fuel pin into the coolant is thus proportional to the local fission power. By an appropriate instrumentation measuring out of pile the fission product activity concentration in the coolant signal changes will be recorded in case of power changes at the point of cladding tube failure. This effect is utilized in flux tilting with a view to locate the failure.

Initially, all control rods are immersed to the same depth; the distribution of power density in the core is symmetric. While this symmetric distribution is maintained, the entire reactor power is strongly reduced. 30 % of the nominal power is a realistic value; in the first of these experiments performed at KNK II the average reactor power was only 15 % of the nominal power because particular care had been taken [Richard 82]. Evidently, the reduction of fission power implies a similar reduction of the fission product signal emanating from the defective fuel pin. The subsequent actions depend on the number of main coolant pipings leaving the reactor tank. KNK II is equipped with two main coolant pipings with one monitor each installed for Delayed Neutron Detection (DND) allowing to detect fission products in the sodium [Jacobi 79 and 82a]. The main coolant pipings leave the tank in the western and eastern directions (Fig. 1).

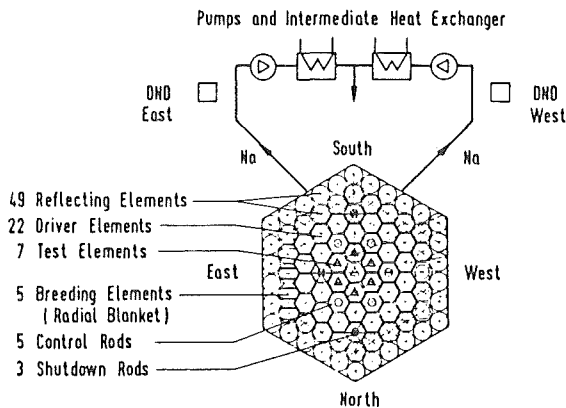


Fig. 1. KNK II. Cross-section of core configuration and primary coolant circuits.

Thanks to the configuration shown in Fig. 1 reductions and increases, respectively, in power are possible by insertion and withdrawal, respectively, of the control rods into and from the opposite core halves, namely North-South and East-West (see upper half of Fig. 2).

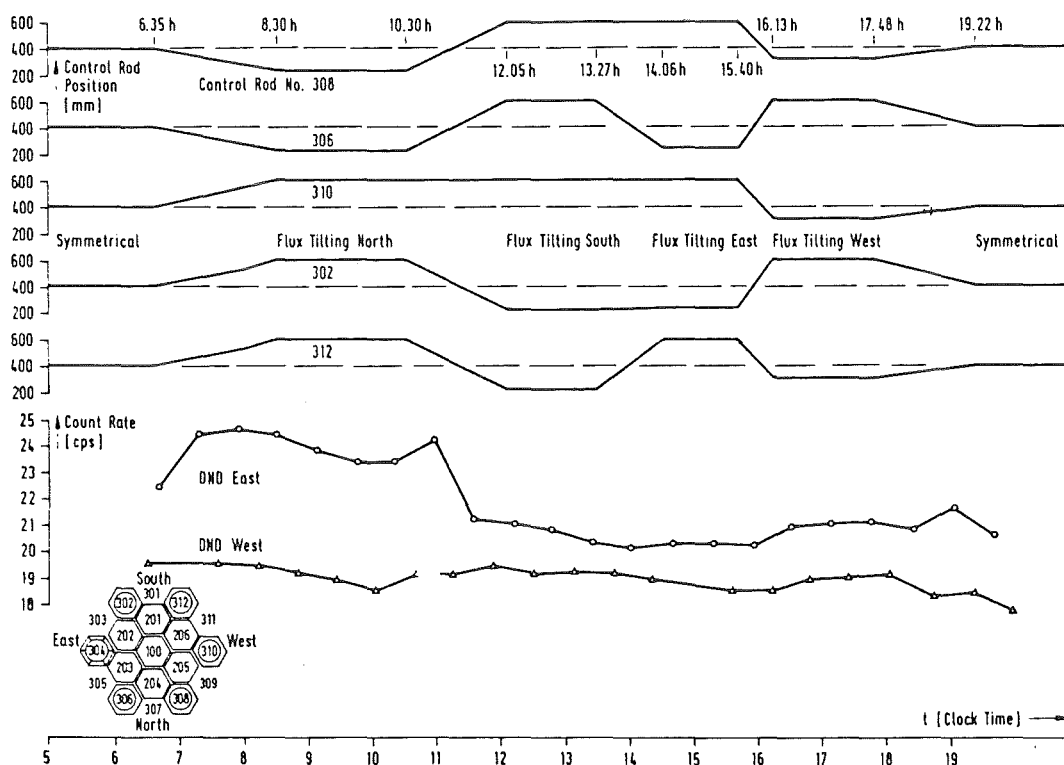


Fig. 2: KNK II. Control rod positions above bottom of the core (cold) and DND-signals during flux tilting on August 28, 1980 from 6.35 h to 19.22 h. Bottom left the central part of the core, control rods No. 302, 306, 308, 310, 312, shut down rod No. 304 and the surrounding subassemblies, compare Fig. 1.

Parallel to these changes in the control rod positions the fission power near the already detected but not yet located fuel pin failure changes accordingly. Consequently, the rate of fission product release and thus also the signals DND-West and DND-East (Fig. 2, bottom half) undergo variations. It can be noted from the signal developments in case of flux tilting North and West that the signal DND-East rises. Other details such as the decay of signal DND-East during flux tilting North or the peaks of DND-East upon transition of flux tilting North to flux tilting South and of flux tilting West to symmetric rod position fit the familiar picture of failed fuel element behavior. In this way, an expert, referring to a number of very different criteria of selection, will be in a position to locate the failed fuel subassembly with the help of the plots shown in Fig. 2. The failed fuel subassembly in this example was in core position 202 (Fig. 2, "bottom left) [Richard 82]. This expert knowledge shall be implemented later-on in COCOSS.

2.6.2.2 From the Experimental Reactor to the Large Power Station

The target of all breeder development work consists in realizing a large power station of more than 1000 MWe. Whilst at KNK II the interpretation of the DND-signals during flux tilting is already a relatively complex task, the use of computers seems to be indispensable in a large power station because of the necessity of operating control rods also individually. Table 1 will give an impression of the development work and indicate the development trend regarding COCOSS.

Table 1: The Three Development Stages of the LMFBR

	Experimental Power Plant, e.g. KNK II	Prototype Plant, e.g. SNR 300	Large Power Plant, e.g. Super Phenix
Electric power (MWe)	20	300	1200
Number of fuel subassemblies	29	205	364
Number of control rods	8	12	24
Number of cooling circuits	2	3	4

2.6.3 The Consulting Core Surveillance System COCOSS

2.6.3.1 Purpose and Target of COCOSS

COCOSS is presently developed at KNK II and it is intended to test it at this plant. However, it should be underlined that all activities are being carried out with a view to application at a large power station. COCOSS is permanently operated on-line during reactor operation. Its major tasks during the final stage of realization will include:

- a) Avoidance of unnecessary or too late shutdowns; see INTRODUCTION.
- b) Core surveillance during operation without failed fuel subassemblies:
 - Information about the status of the plant,
 - Automated test of the measuring chains,
 - Plausibility consideration of the measuring signals,
 - Recording of background signals which undergo changes for various reasons (may be important above all during flux tilting because the signal amplitudes are small in that case).
- c) Diagnosis upon occurrence of fission product signals caused by cladding tube failures:
 - Correlation of all relevant measuring signals available,
 - Access to data banks where expert knowledge has been stored regarding types of failure and their behaviour with time as a function of different operating conditions of the plant,
 - Comparison of present measuring signals with information derived from the data banks above,
 - Correction of transient background signals and their subtraction from the measured value,
 - Information to the operator concerning the most probable status of the failed fuel subassembly: nature and size of failure and core zone affected,
 - Observation of the subsequent development of the failure and permanent updating of information to be provided to the operator.
- b) Prediction of disturbance, i.e., comparison of the respective actual condition with the expert knowledge stored in the data banks concerning the development with time of previous cladding tube failures. Information about the most probable subsequent development of the failure.
- e) Recommendations for subsequent reactor operation, derived from the prediction of disturbance, e.g.:
 - Immediate shutdown of the plant,

- Shutdown of the plant at a time recommended by COCOSS,
 - Immediate or soon reduction of power.
- f) Recommendations for diagnosis operation of the plant for the purpose of failure location.
- g) Support in flux tilting:
- Programmed on-line signal evaluation,
 - Comparison of the fission product signals and coolant temperatures at the fuel subassembly outlet with information from the data bank,
 - Recommendations for subsequent diagnostic operation, i.e., operation of individual control rods,
 - Information about the core zone in which the cladding tube failure has occurred, continued, if possible, until an individual position can be indicated.

The more reliable the result of failure location is, the less handling of fuel subassemblies will be required. This aspect should be taken into account above all in case of subassemblies with a high burnup. Less handling in fact means less probability of human errors or plant-specific equipment errors. On the other hand, quick location of the failure means a shorter time of non-availability of the plant. In this way, COCOSS increases within certain given limits both the safety and the availability of the plant.

2.6.3.2 Necessary Investments

When thinking of realizing COCOSS, the question of the information required, i.e., measuring values from the plant, is in the foreground. It must be stated here as an advantageous feature of COCOSS that all necessary sensors are already installed in the plant so that an expensive additional instrumentation can be dispensed with (Table 1):

Table 1: Plant Specific Input Information for COCOSS

Measuring Variable	Principle and Sensor, resp.	Remarks
Fission product concentration in the coolant	Delayed neutron detection at the main coolant piping or bypass pipings	Redundant existing for safety instrumentation
Concentration of gaseous fission products in the cover gas	Gamma spectroscopy with Ge-detector and precipitator	Existing as operation surveillance system
Cover gas pressure and flow at gamma spectrometer	Pressure gauge and flowmeter	Existing as instrumentation for operation
Measurement of reactor power	Ex-core neutron flux measurement	
Coolant flow through the core	Flowmeter	
Coolant inlet temperature	Thermocouples	
Coolant temperatures at the outlets of the fuel subassemblies	Thermocouples	
Positions of the control rods	Linear displacement transducers	

Except for possibly required isolation amplifiers, the requested signals are thus obtained without additional costs in a suitable quality and with sufficient availability. The acquisition of appropriate microprocessors with external devices is necessary.

2.6.4 Stepwise Development of COCOSS

For the reasons stated below COCOSS is being and will be further developed stepwise:

- Novelty of the problem and its treatment,
- Process of learning by the development team and COCOSS computer from one step to the next,
- Simultaneous elaboration of necessary criteria for decision making by in-pile experiments with open fuel [Hoffmann 82].

2.6.4.1 COCOSS I

The first essential and large step was the development of the LMFBR-specific computerized gamma spectrometer for evaluation of the cover gas signals [Hoffmann 80]. This was followed by the processing of further signals: DND, reactor power, other signals and parameters of the cover gas system. Daily, weekly or monthly plots are now available on request of the

- DND signals,
- Pressure corrected cover gas signals,
- Reactor power.

Computer printouts and spectrum diagrams in any form are completing this information (Fig. 3). This system in the COCOSS I version already operates in an interactive mode with the reactor, e.g.:

- automated setting of the collimator position at the gamma spectrometer;
- preselection of measuring time for the Ge-detector;
- record output when given limit values are overrated or underrated.

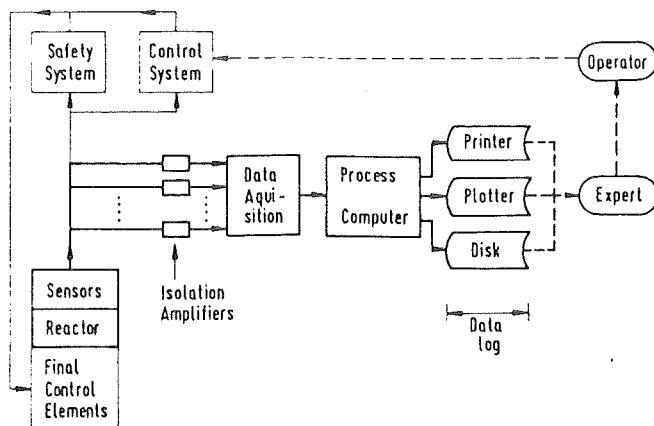


Fig. 3: Information flow sheet of COCOSS I

The following hardware is used to operate the RECOS (Reactor Core Observation Software) surveillance program:

A DEC computer PDP 11/34 with 128 K byte memory, two disk drives RL01, one line printer, one multi-channel analyzer with 4096 channels, one four-color plotter and one Canberra 6911 Datanim computer interface with eight counter/timer channels for the acquisition of measuring data and one device actuator for moving the collimator.

The first in-pile calibration tests with open UO₂ fuel are completed; calibration tests with metallic fuel are in preparation [Hoffmann 82].

At this stage COCOSS I

- has been capable of advising the expert,
- has been qualified to take over expert knowledge,
- has constituted the basis for starting further work.

2.6.4.2 COCOSS II

The following work has been started within the second step of development:

- a) Correlation of information from different systems stored by the computer.
- b) Simplified functional model of the reactor simulating e.g.
 - The dependence of fission product release on reactor power and on the position of the failed fuel subassembly,
 - The ratio of effective to geometrical size of the failure (k-factor) depending on reactor power, position and burnup of the subassembly.
- c) Stored expert knowledge about the time dependence of typical cladding failures.
- d) The adapted version of the computer code FICTION (Fission Product Signal Calculation) [Jacobi 82b]. This code calculates the free fuel surface of a cladding failure from the measured DND-signals and plant conditions.

In this way COCOSS II gets the simplified knowledge of an expert.

At this stage of completion, "Plant Model", "Fixed Plant Data" and "FICTION code and Data" must be added in Fig. 3 as additional software for COCOSS II. The output of information is still the same, COCOSS II being only an interim solution on the way to the final goal.

2.6.4.3 Cause-Consequence Trees

It is the established goal of COCOSS to largely substitute the expert at the final stage and to give to the operator the same recommendations as an expert does. This means that COCOSS must make logical on-line decisions, starting from

- very differing types of signals,
- different sequences in time of these signals,
- different plant conditions,
- a stored expert knowledge.

To solve this problem, "Cause-Consequence Trees" are used as in the disturbance analysis systems mentioned in the chapter on the State of the Art, which means signal flow diagrams with logical links, the items mentioned above being the input variables. Recommendations for given operations are derived from them.

The simplest case is the occurrence of a leaker, i.e., a fuel pin failure where only fission gases are released and no direct contact is as yet established between the fuel and the coolant so that, consequently, no DND-signal can be generated (Fig. 4).

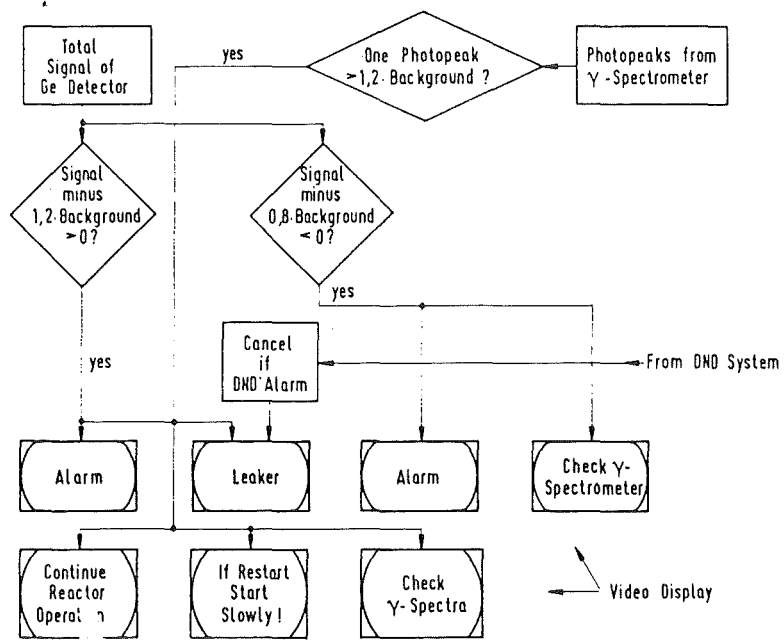


Fig. 4: Schematic cause-consequence tree for the simple case of a leaker

The cause-consequence tree is much more complex in case of a DND-failure. This is shown in a highly simplified representation in Fig. 5; colored graphical displays of the control rod positions and changes of coolant temperatures caused by them at the fuel subassembly outlet as well as continuous recording of the DND-signals undergoing permanent variations are just briefly mentioned in the text.

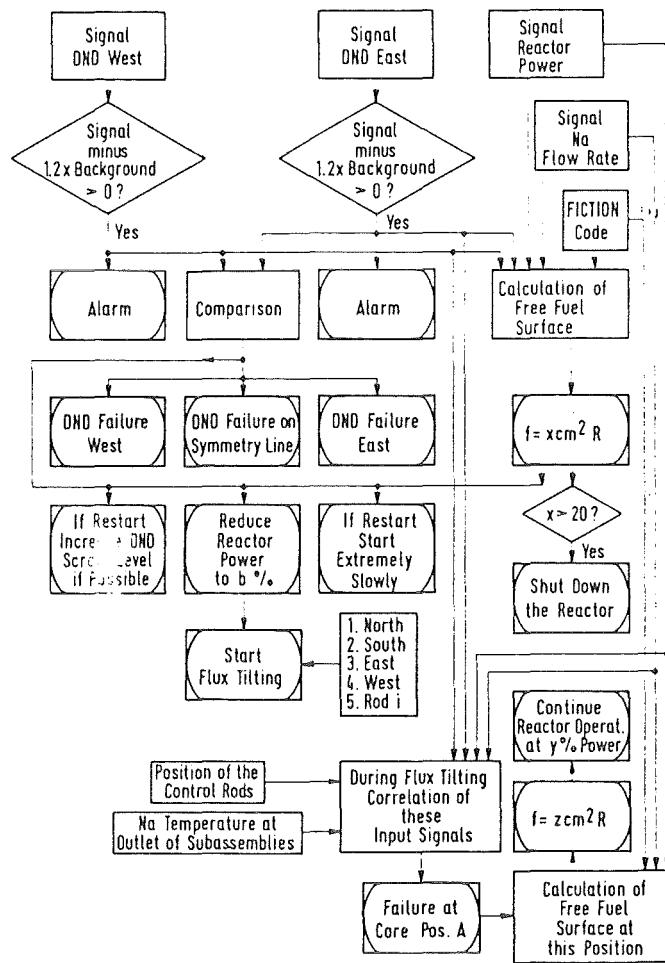


Fig. 5: Simplified cause-consequence tree of a DND-failure. Values are typically for KNK II

2.6.4.4 COCOSS III

To the extent not yet implemented in COCOSS II, COCOSS III now receives additional formalized expert knowledge on failed fuel detection and location in additional memories and computer codes. This transfer breaks down into three groups:

1. Active Signal Evaluation:

- Computation of the most probable free defective area, still independent of the fuel subassembly position,
- Diagnosis of the type of defect,
- In case of large DND-signals computation of power reduction,
- During flux tilting evaluation of the signals received,
- After completion of flux tilting:
 - computation of defect position,
 - computation of defective area for these positions,
 - computation of power reduction.

2. Recommendations to the Operator:

- Reactor shutdown or continuation of operation, possibly at reduced power,
- Instructions for a restart,
- Start flux tilting,
- Procedure during flux tilting,
- After indication of failure position:
 - recommendations concerning subsequent operation.

3. Disturbance Prediction

- Within a given error band the most probable subsequent development of the failure can be extrapolated from the sum of expert knowledge, using a graphical colored display.
- It can be estimated how long the reactor can still be operated at which power. Major criteria include: scram signal level and free defective area with possible consequences.

By this transfer of expert knowledge the structure represented in Fig. 6 is obtained for COCOSS III.

- In this version COCOSS III becomes an expert itself:
- It evaluates the signals from the plant,
 - It gives recommendations,
 - It makes disturbance prediction.

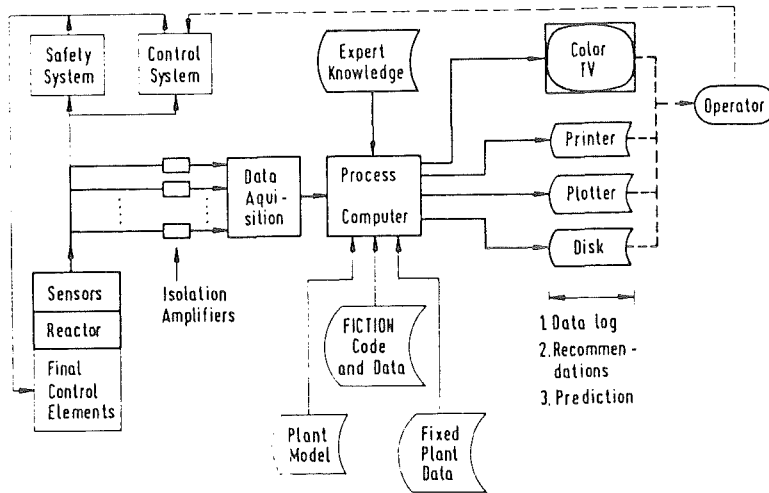


Fig. 6: Information flow sheet of COCOSS III

References

- [Bastl 82] W. Bastl: Rechnergestützte Operateurhilfen in Kernkraftwerken.
Jahrestagung Kerntechnik, Mannheim, 4-6. Mai 1982
Fachsitzung Informationsverarbeitung in Kernkraftwerken, Deutsches Atomforum e.V.
- [Heising 82] C.D. Heising: The Determination of Plant Status Abnormal Reactor Operating Conditions: Accident Sequence Identification. Nucl. Eng. Des. 71 (1982) 137
- [Long 80] A.B. Long: Technical Assessment of "Disturbance Analysis Systems.
Nucl. Safety, 21 (1980) 38
- [Jacobi 82] S. Jacobi, Editor: Fuel Failure Detection and Location in LMFBRs.
Proc. of Int. Atomic Energy Agency Specialists' Meeting, Karlsruhe, May 11-14, 1981, KfK 3203, June 1982
- [Jacobi 79] S. Jacobi, G. Schmitz: Delayed Neutron Signals from Failed Fuel and Bundles and their Relation to Safety and Operating Problems.
Int. Meeting on Fast Reactor Safety Technology, Aug. 19-23, 1979, Seattle, ANS, Vol. IV p. 2612
- [Jacobi 82a] S. Jacobi: The Delayed Neutron Detection Method for Cladding Tube Monitoring and Experiment Results.
Int. Topical Meeting on Irradiation Technology, Grenoble, Sept. 28-Oct. 1, 1982
- [Richard 82] H. Richard et al.: Experience of Failed Fuel Detection and Localization at KNK II.
In [Jacobi 82], p. 93

[Hoffmann 82]

G. Hoffmann, et al.: Open Fuel in KNK II for Investigating Cladding Failures and their Possible Consequences.
Int. Topical Meeting on Liquid Metal Fast Breeder Reactor Safety, July 19-23, 1982, Lyon

[Hoffmann 80]

G. Hoffmann, K.-D. Letz: On-line Gamma Spectroscopy Measuring Station for Cover Gas Monitoring at KNK II, KfK 2797, Febr. 1980

[Jacobi 82b]

S. Jacobi et al.: German Research and Development Program on Failed Fuel Detection and Location in LMFBRS. In [Jacobi 82], p. 246

2.7 Neutron noise analysis

The potential of neutron noise analysis for disturbance detection is well known and has been investigated in the frame of the R+D-work on cooling disturbance monitoring. One application is given in chapter 2 where the combination of temperature- and neutron noise is used for sensitive indirect flow rate measurements. Another application is the determination of coolant boiling. As real in-pile boiling experiments in an operating sodium-cooled reactor are rather difficult - especially from the licensing point of view - emphasis has been laid on boiling simulation experiments in our heavy water cooled research reactor FR2 and in theoretical investigations. Both have shown that boiling is detectable by neutron noise, but as the void-coefficient is zero on certain regions of the core of a Fast Breeder, these activities have been terminated. Furthermore, the potential of neutron noise analysis - correlated with the fuel element outlet temperature - has been demonstrated by the identification of vibrating fuel elements. But as that is not part of this study, this topic will not be considered here.

3. Integrated Approach

L. Gmeiner, U. Voges

Institut für Datenverarbeitung in der Technik

The last chapter summarizes different core surveillance techniques and methods for early detection of coolant disturbances and of failed fuel elements in an LMFBR.

The methods considered are mainly the same as in the overview diagram of chapter 1. The figures within the brackets refer to the chapters with extended descriptions:

- mean temperature supervision (TM, 2.1, 2.2)
- (indirect) flow (FI, 2.2)
- temperature noise (TN, 2.3)
- acoustic noise detection (AN, 2.4)
- reactivity noise (RN, 2.2, 2.4)
- delayed neutron detection (DN, 2.5)
- covergas monitoring (CM, 2.5)

Additionally the

- flux-tilting technique (FT, 2.6)

is reviewed, which is especially appropriate for the location of failed fuel elements.

Figure 3-1 describes the current situation for these individual core surveillance methods. The integration of these techniques is described in figure 3-2.

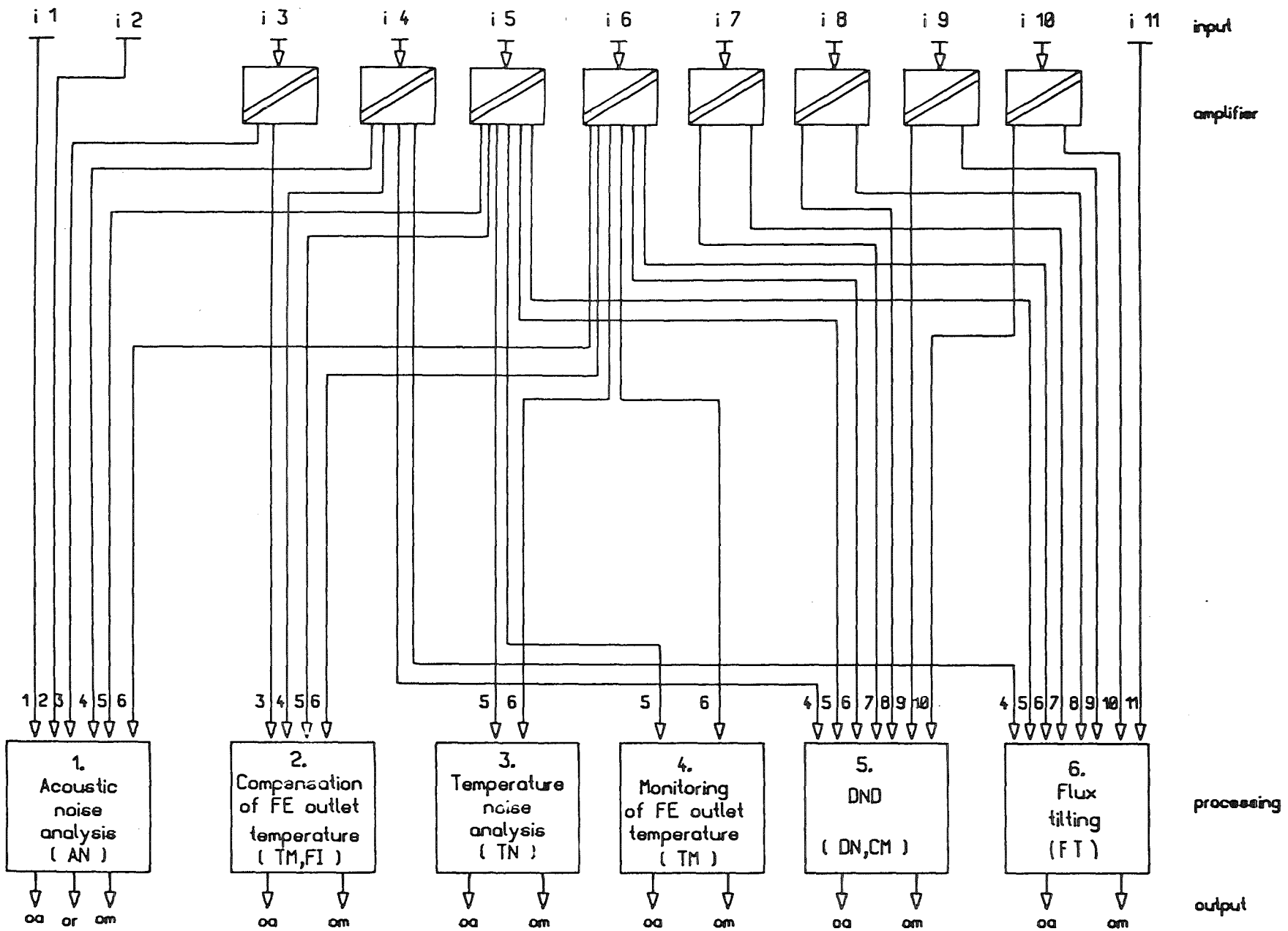


Fig.3-1: Existing Core Surveillance

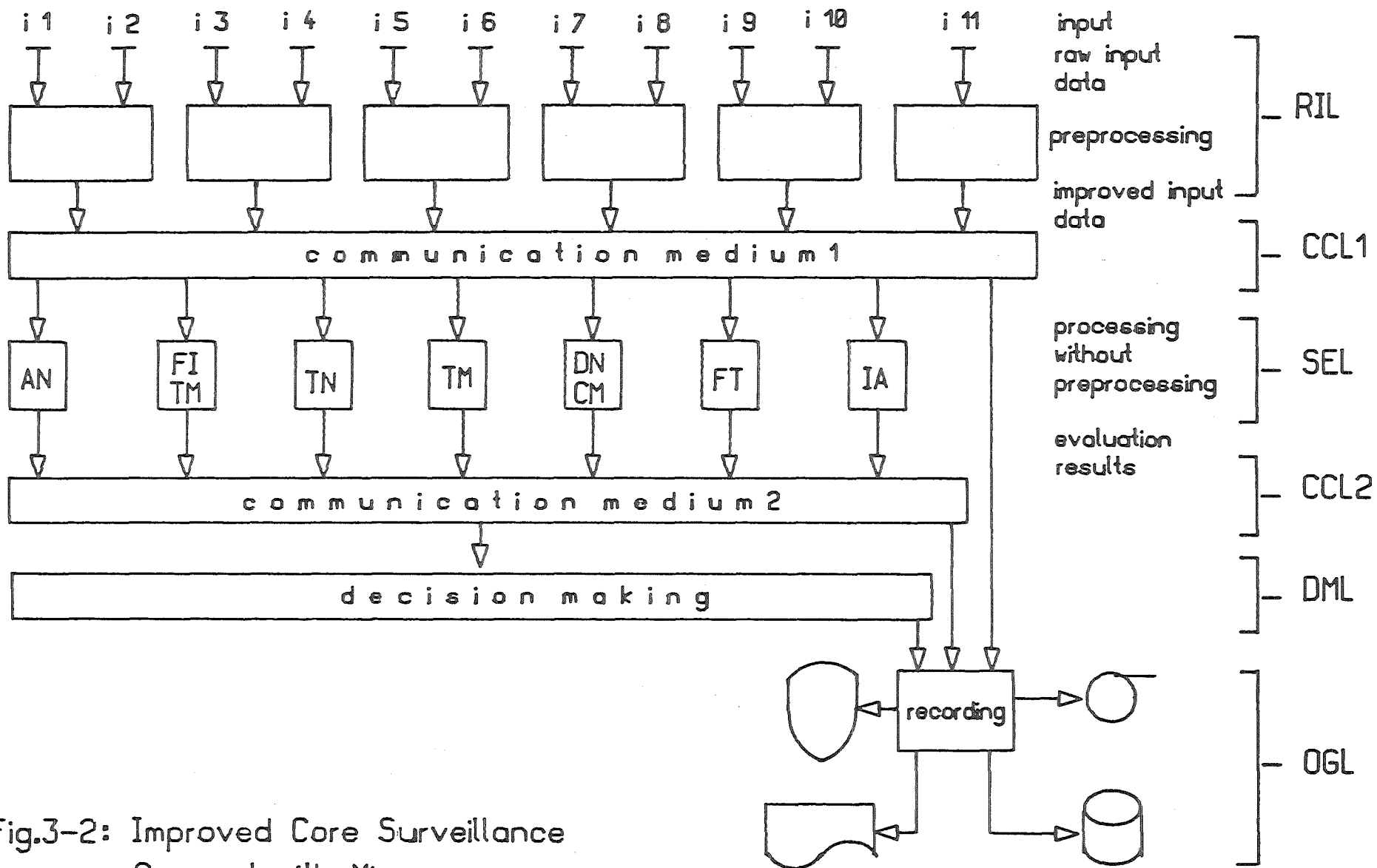


Fig.3-2: Improved Core Surveillance Concept with Microprocessors

Legend to Fig. 3-1 and Fig. 3-2

input:

input-id	meaning	number of data items	redundancy	sampling rate	measurement range
i1	acoustic noise	10	-	2/s	-10...+10V
i2	rotation speed of pumps	1	-	1/s	-10...+10V
i3	neutron flux	5-10	-	10/s	0...+10V
i4	primary flow rate	1 per inlet	3	1/s	0...+10V
i5	core inlet temperature	1 per inlet	-/3	1...10/s	0...+10V
i6	FE outlet temperature	1 per FE	-/3	1...10/s	0...+10V
i7	DND signal	2-4	-/3		
i8	reactor power	1-2	-		
i9	GeLi-system count rate	1-2	-		
i10	precipitator count rate	1-2	-		
i11	position of absorber rods	1 per absorber	-		

output:

- oa: output of alarm or scram
- or: output for data recording
- om: output of messages on printer or VDU

processing:

the processing includes:

- analog/digital conversion
- measurement preprocessing (adjustment, filtering, etc.)
- calculation of secondary signals
- actual processing
- output generation

The proposed integration concept is based on the assumption to use as far as possible existing capabilities of the freestanding surveillance methods. We can identify two main areas, where the integrated system differs from the original approach described in figure 3-1.

- 1) The area of measurement precalculation and signal conditioning.
- 2) The decision-making computers, located on top of our existing surveillance techniques.

The integrated approach has some evident advantages. Especially duplication of measurement effort can be avoided. As can be seen from figure 3-1 there exist some measurements which are used by different surveillance techniques.

The same argument, concerning duplication of effort, holds for the generated output, too. In an integrated system we need to have a only limited number of output units (e. g. plotters, printers, graphic devices, ...).

Besides these economical arguments we have some reliability arguments, too. Our philosophy is to combine and correlate the outputs of the described monitoring techniques, in order to get a more sensitive , condensed information. This kind of information allows quicker reaction in the 'early-warning' area and results, as a consequence of this, in higher reliability of control and safety decisions. As well we get improvements for plant availability.

Starting from these considerations we propose an integrated core surveillance system whose structure is shown in fig. 3-2. The complete system can be subdivided into six levels:

- reading and input level (RIL)
- common communication level 1 (CCL1)
- separate evaluation level (SEL)
- common communication level 2 (CCL2)
- decision making level (DML)
- output generation level (OGL)

In the reading and input level the raw, mainly analog, input data from the process (the reactor) are read and preprocessed. For each independent class of process signals there is a separate unit for

preprocessing. The preprocessing includes

- analog/digital conversion
- standard noise removal
- basic plausibility checks for data validity
- fault detection for the measurement instrumentation
- basic data operations.

The result of this level is a set of improved input data.

Via the common communication level 1 the data are transported to the next active level, the SEL. The structure of the CCL1 can be partially a point-to-point connection from a unit of RIL to a unit of SEL, e. g. if an input data is used for a single evaluation unit only, and partially a common bus by which several units of RIL and SEL are interconnected.

The separate evaluation level consists of independently working evaluation units. Each unit incorporates a different core surveillance method. Compared with the separate realisation of each method here the units receive already prevalidated input in digital form.

Again the single units of the SEL give their evaluation results via the CCL2 to the DML and the OGL. As is the case with the CCL1 the CCL2 can be organised partially by direct lines, partially by a common bus.

The decision making level contains the major extension of the integrated approach as compared with the separate independent realisations of the core surveillance methods. Here the evaluation results are analysed in comparison and correlated with each other. A simple example of such a correlated analysis is the following: two independent methods report a reactor state which is still in the 'normal' field, but close to the upper limits. For both methods individually this means only a low probability of disturbance. But for the correlated analysis this can be interpreted as a somewhat higher probability of a starting disturbance, and therefore some action is resulting.

The sophistication of the DML can have different grades. This depends very strongly on the correlation between the different core

surveillance methods which can be found through theory and experiments, and also on the effects the methods are detecting, and where the methods are located in the fault propagation diagram.

Different methods can be applied for the decision making, e. g.

- cause-consequence analysis
- fault tree evaluation
- pattern recognition
- procedure prompting
- expert systems.

Which of these methods will be used depends on the level of knowledge available.

Cause-consequence analysis and fault tree evaluation are closely related to the theory of the fault propagation diagram (compare fig. 1-1).

Pattern recognition is based as well on early test experience as well as on operating experience. Certain patterns - reactor states or state sequences in terms of input data and evaluation results - can be judged as possibly leading to a disturbance, others as being not dangerous.

Procedure prompting is related to an interaction with the operator: depending on the different evaluations some actions could be suggested to the operators.

The method of an expert system is partially including the other methods. Based on previously gained information and knowledge and predefined decision rules a reactor state evaluation is made and resulting information is given to the operators, may be with the request for certain actions.

The aim of these methods is to increase the capability and the knowledge of the integrated core surveillance system even during operation.

Finally, the output generation level is the last part processing the data. It is possible to realise here some data logging device which is

storing the data with high resolution (e. g. 1 data block per sec) for a short period of time (e. g. 10 to 30 min). In case of a disturbance or an accident this data is then available for post accident analysis etc. For long term logging (> 30 min) only a lower resolution is sufficient (> 1 data block per min).

In case some part of the system is operating in a closed loop fashion this can be achieved either by direct connection of the actuators with the respective evaluation unit or via the OGL.

The envisaged integrated core surveillance system has two major advantages as compared with the separated stand-alone core surveillance systems. First, the inputs of the different surveillance methods are partially identical. Therefore a common preprocessing is possible which can save some instrumentation costs and efforts, and also give the possibility to do some more sophisticated preprocessing. Second, the outputs of the single methods can be correlated. This increases the capability for early fault detection.

4. Concept of Global LMFBR Core Surveillance Procedure

A. Holick

INTERATOM

The "Global LMFBR Core Surveillance Procedure" (GCSP) is thought to be part of the Signal Processing Module of the overall protection system with artificial intelligence features. It is based upon recursive parameter- and state-estimation and provides all surveillance variables which are relevant to classifying core dynamics status to the decision making subsystems (diagnostic modules). The following data are made available by means of direct and indirect measurements:

Direct Measurements: outlet temperature for every fuel element, inlet temperature, flow-rate, neutron-density, reactivity, rod position.

Indirect Measurements: consist of the fast reacting core state with the components fuel temperature and smoothed average coolant temperature for every f. e., itemized reactivity contributions, in particular, the feedback reactivity and the effective control rod reactivity, and of the slowly varying core parameters such as heat transfer coefficients, coolant heat capacities, fraction of power and flow in every f. e., time constant and gain error of the thermocouples at the outlet, the estimates of the reactivity feedback coefficients and control rod parameters.

Error Signals: observation residuals (mean values) of the Kalman filters for estimating subassembly thermohydraulic states and the reactivity balance. The basic function of the error signals is to provide a measure of uncertainty on the surveillance variables to the diagnostic module.

An overall blockdiagram of the surveillance system is shown in Figure 1. The surveillance functions are subdivided into 2 categories:

- a) surveillance of fuel-element thermo-hydraulics associated with every fuel element,
- b) surveillance of reactivity contributions (balance meter) associated with the total core; it is anticipated, that the reactivity components can be partitioned such, that every fuel element has eventually its own balance meter.

Surveillance of Fuel-Element Thermo-Hydraulics

The concept of monitoring cooling abnormalities is shown in Figure 2 for one fuel element. It is thought to be applied to every fuel element which has a thermocouple at the outlet. The system architecture is modular and functionally failure tolerant. The underlying sampled data fuel element model (prediction model) has the following form:

$$(4-1) \quad \begin{aligned} x_{K+1} &= \phi x_K + \Gamma u_K + \Gamma w_K \\ Y_K &= M x_K + D u_K + v_K \end{aligned}$$

where

$$x^T = [\delta T_f, \delta T_c] \quad \text{state vector of dimension } n = 2$$

$$u^T = [\delta P, \delta T, \delta W] \quad \text{input vector (measured)}$$

$$y = \delta T_o \quad \text{output (measured)}$$

$$w \quad \text{vector of process noise}$$

$$v \quad \text{measurement noise}$$

The index denotes sampling time. Closed form expressions of the system matrices ϕ , Γ , M , D in terms of physical core parameters are given in /5/.

A "Kalman filter Modul" with constant weighting factors /1/, /5/, provides estimates of the fuel- and coolant-temperatures, and, hence, provides the basic surveillance function:

$$(4-2) \quad \hat{x}_{j+1}^{j+1} = \hat{x}_{j+1}^j + K \cdot (y_{j+1} - \hat{y}_{j+1}^j)$$

$$\hat{x}_{j+1}^j = \phi \hat{x}_j^j + \Gamma u_j$$

$$\hat{y}_{j+1}^j = M \hat{x}_{j+1}^j + D u_{j+1}$$

where

$$\hat{x}_j^i = (\delta T_f, \delta T_c)^T = \text{estimate of } x_j \text{ based on all measurements up to and including } y_i = y(t_i)$$

$$K^T = [k_1, k_2] \quad \text{gain vector with } k_i = \text{constant}$$

$$\hat{y}_j^j = \text{predicted observation based on the most recent estimate } \hat{x}_{j-1}^{j-1} \text{ and the measured input } u_j.$$

The simplicity of the constant gain Kalman filter is shown in /5/, p. 54.

The state estimates \hat{x} are now available for surveillance in addition to the measurements. The variables are compared with prespecified thresholds and/or with the corresponding estimates of other fuel elements in a subsequent comparator module not shown in the diagram.

The availability of the fuel temperature in addition to the coolant temperatures (etc.) offers diagnostic capabilities which are not at one's disposal in the case of conventional outlet temperature monitoring.

The condition of core cooling is, of course, not only characterized by temperatures. Knowledge of the fraction of flow in a fuel element, the fraction of power, the heat transfer coefficient and heat capacity of the coolant provide a significant early warning potential. These parameters are determined in the "Parameter Estimation Modules".

It is a feature of the selected methods that parameter estimation can be performed without explicit knowledge of the state estimates (separation task Section 4.2). In order to accomplish separation, the prediction model (4.1) is transformed to "output identifiable form" /5/, where the system matrices have the following structure:

$$(4-3) \quad \phi = \begin{bmatrix} 0 & I_p \\ \phi^1 & \phi^2 \end{bmatrix} \quad M = \begin{bmatrix} I_r & 0 \end{bmatrix}$$

Γ remains arbitrary

$p = n - r = 1$

$r = \text{dimension of the output vector} = 1$

Note that the selector matrix in this space becomes the unit matrix I_2 .

Now the coefficients of the prediction model can be expressed in terms of the measurements only /2/, /5/:

$$(4-4) \quad z = Z^T \cdot \Lambda + v$$

where the scalar z and the row matrix Z^T are functions of the measurements, Λ is the parameter vector to be estimated, and v is a noise term.

Equation (4-4) is in standard linear regression form and the parameter vector Λ can be determined by means of the conventional recursive least square method without matrix inversion. The theoretical effort associated with transformation to canonical form and with separation has obviously no other purpose than to reduce the task of on-line calibration of the Kalman filter to a standard least square problem.

The system matrices of the prediction model in output identifiable form are very simple functions of the parameters Λ_i . They are computed in a separate modul and are transferred to the Kalman filter upon request.

Such a request can be initiated by the observation residual of the Kalman filter. If its expectation exceeds a pre-specified threshold then the prediction model does not match the true situation and the system matrices need to be up-dated. In the case of failure in the parameter estimation modul or in the computation of the system matrices the Kalman filter can still operate, but the estimation error increases with the model mismatch.

The physical core parameters such as gap conductance (integral heat transfer coefficient), k , fraction of flow, κ_w , fraction of power, κ_p , and coolant heat capacity,

C_c , can be computed in a separate modul and in parallel since knowledge of these parameters is only needed for diagnostics and, therefore, only occassionally. Failure in this modul does not degrade the basic surveillanc function.

Reactivity Surveillanc (Figure 3)

The promise of high performance rests upon a prediction model with state independent coefficients and upon the capability to provide sufficiently detailed information upon core transients and parameter anomalies by means of on-line parameter and state estimation.

The objectives are somewhat different from those of the conventional reactivity balance:

- a) surveillanc is restricted to monitoring the time history of the reactivity feedback coefficients and rod worth. Thermohydraulic performance is monitored in a different surveillanc module.
- b) the reactivity balance signal is not the primary surveillanc variable, but initiates the parameter estimation procedure (calibration) if it exceeds a prespecified bound. Hence, it allows for reducing the number of calibrations needed. It does not classify system state into "normal" and "abnormal".

Most of the disadvantages of the conventional concept (Section 5.2) can be overcome by expressing the prediction formula in a space, where the physical reactivity contributions (characterized by the nearly constant coefficients β_i) can be determined

separately on-line. A feasible equation for the reactivity feedback is:

$$(4-5) \rho_{fd} = (\beta_D + \beta_A) \cdot \delta T_f + \beta_C \cdot \delta T_C + \beta_B \cdot (\delta T_{SO} - \delta T_{SI}) + \beta_G \cdot \delta T_I^* + \Delta$$

The state space is represented in (4-5) by the perturbations of

T_f	=	fuel temperature
T_C	=	coolant temperature
T_{SO}	=	temperature of the upper part of the fuel-element-can
T_{SI}	=	temperature of the lower part of the fuel-element-can
T_I^*	=	grid plate temperature

and the reactivity feedback effects are given by the product terms

$\beta_D \cdot \delta T_f$	=	Doppler reactivity
$\beta_A \cdot \delta T_f$	=	axial expansion reactivity
$\beta_C \cdot \delta T_C$	=	coolant temperature reactivity
$\beta_B \cdot \frac{\delta T_{SO} - \delta T_{SI}}{T_{SO} - T_{SI}}$	=	bowing reactivity
$\beta_G \cdot \delta T_I^*$	=	grid plate reactivity

Δ = sum of all reactivity feedback contributions which are not correlated with state perturbations; they are modelled as a linear function of time.

The control rod (bank) reactivity is described by

$$(4-6) \quad \rho_{CR} = \beta_{CR} \cdot (t - t_0) + \beta_{CR,0}$$

or

$$(4-7) \quad \rho_{CR} = \frac{d\rho_{CR}}{dh} \cdot \delta h + \beta_{CR,0}$$

where

$$(4-8) \quad \beta_{CR} = \frac{d\rho_{CR}}{dh} \cdot v_{CR} \quad v_{CR} = \text{rod speed}$$

$\beta_{CR,0}$ = control rod reactivity worth before the control action is initiated at $t = t_0$; it includes the effect of differential expansions prior to control action. Note that Δ in equation (4-5) and $\beta_{CR,0}$ cannot be separated, except if Δ is a function of time.

If information on the state can be provided for on-line, then we have a basis for estimating the coefficients β_i from reactivity measurements by means of the least square method:

$$\rho_{MEAS}^k = \sum_{i=1}^L m_i^k \beta_i + \epsilon^k$$

L = number of parameters

or, in matrix notation

$$(4-9) \quad S_{NEAS}^K = M^K \cdot \beta + \epsilon^K$$

where

$$(4-10) \quad M^K = [\delta T_f^K, \delta T_c^K, (\delta T_{SO}^K - \delta T_{SI}^K), \delta T_I^{*K}, 1, \delta h^K]$$

The index k denotes sampling time and ϵ^K is the random measurement error. The components of the observation gradient M^K are not directly measurable with the usual out-of-core instrumentation. These indirect measurements are provided by the fuel element thermohydraulic surveillance modules. Hence, the data vector M^K is available for reactivity monitoring as a by-product of core cooling surveillance.

The temperatures of the fuel-element-can and grid plate could be measured directly with thermocouples and the estimation procedure be adapted to such a more comfortable instrumentation. But it is assumed in this report, that these temperatures are coupled to the coolant temperatures at the inlet and outlet and that the time constants of the temperature transients of these structures are known. Hence, the perturbations δT_{SO} , δT_{SI} and δT_I can be computed approximately from δT_O and δT_I measurements via first order lags (simple observers).

The reactivity surveillance procedure performs three functions:

1. estimation of the slowly varying β_i -parameters (calibration) whenever needed. If there is no control action during calibration, then $\beta_{CR} = 0$ and the number of parameters to be estimated is equal $L = 5$. The

stationary control rod worth including differential expansion effects are represented by $\beta_{CR,0}$. The calibration procedure takes approximately $N \cdot \Delta t \approx 40$ seconds.

2. Continuous computation of itemized reactivity feedback effects in accordance with equation (4-5) based upon the most recent estimates of the β_i 's.
3. Continuous estimation of the control rod contribution by means of the relation (see section 4.6, method 1)

$$(4.11) \quad \hat{\rho}_{CR} = \rho_{MEAS} - \hat{\rho}_{fd}$$

Equation (4-11) provides a mean for compensating the effect of control actions upon the reactivity balance signal without reliance upon position measurements. The estimate (4-11) holds even for the time varying case as long as the feedback parameter estimates are correct. Otherwise the calibration procedure will be initiated by the diagnostics module and ρ_{CR} -estimation can continue with high accuracy after approximately 1 minute. Hence, reactivity feedback anomalies affect estimation accuracy only during the short time interval between anomaly occurrence and completion of parameter estimation.

Rod worth can, in principle, also be determined from position measurements by the equation (method 2, section 4.6)

$$(4-12) \quad \Delta h = C_{CR} \cdot (\rho_{CR} - \rho_{CR,0}) + \xi_{CR}$$

This method is susceptible to differential expansion effects and staggered control actions. But method 1 (section 4.6) provides a mean for frequently updating knowledge on $\beta_{CR,0}$ and C_{CR} .

It is shown in Chapter 5 with extensive simulation tests that recursive on-line least square estimation based upon the state space formulation (4-5), (4-11) and (4-12) can cope with the simultaneous occurrence of reactivity anomalies, rod movements and differential expansion effects. (Experience must still be gained in optimally combining the two methods of rod worth estimation for diagnostics.)

Reactivity anomalies are indicated if $|E \overline{\Delta \rho}|$ exceeds 0.5% . This small threshold is representative even during non-stationary operations. The cause of anomaly is identified by observing the time histories of the reactivity coefficients $\beta_i(t)$. Thresholds on the β_i -estimates may serve to automatize the surveillance function.

The parameter estimates, $\hat{\beta}_i$, together with the direct and indirect measurements provide an opportunity for computing the coefficients of the conventional reactivity prediction model (see Appendix A4.5). The converse does not hold.

Figure 3 shows a block diagram of the reactivity balance meter. The direct and indirect measurements are processed in the "Preprocessing Module" where the local measurements associated with fuel elements are combined to give average values for the total core and where the perturbations of structure temperatures (grid plate and fuel-element-can) are predicted from coolant temperature measurements. Details of this module are shown in figure 4.

The surveillance functions are performed in the

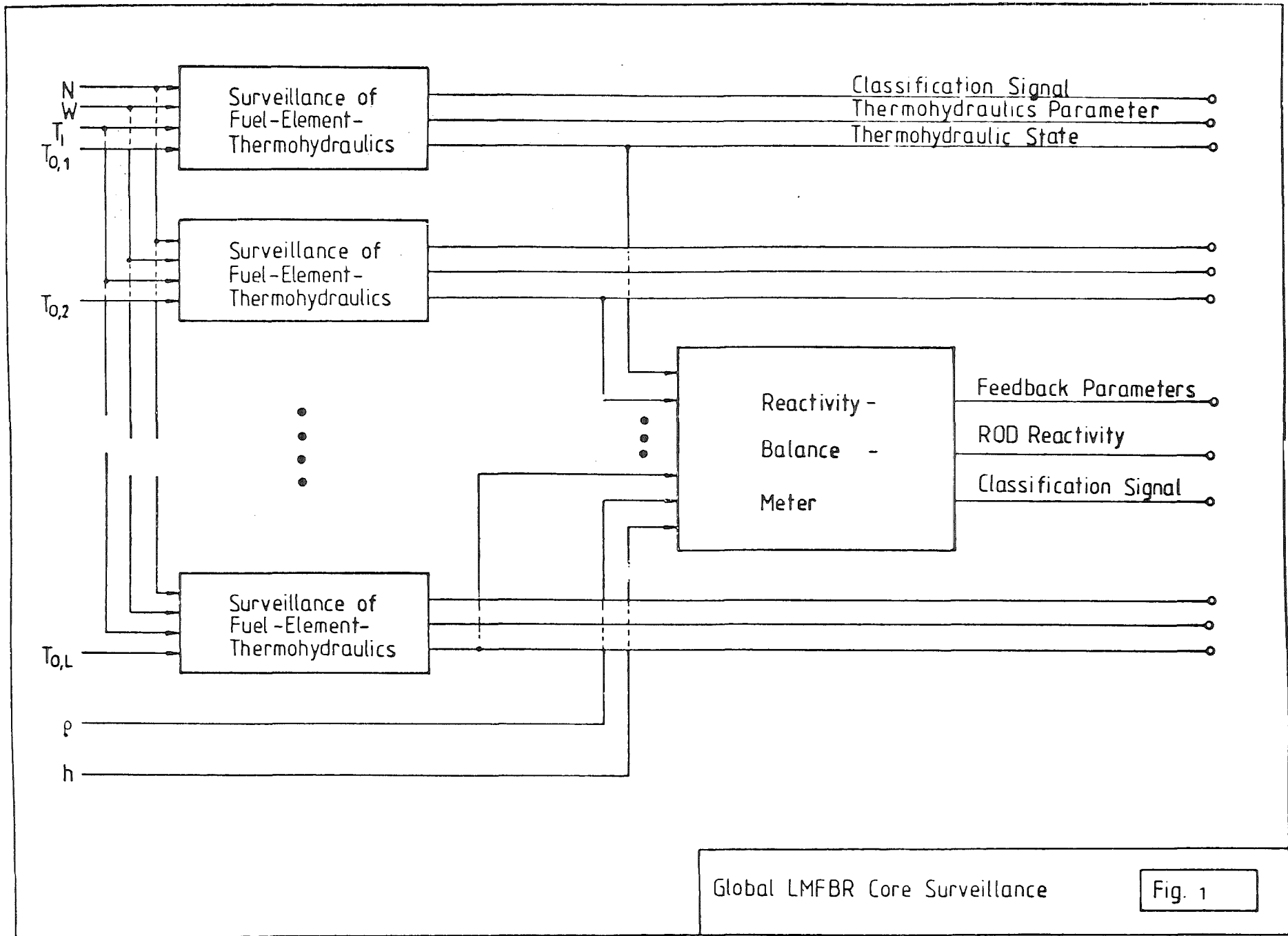
- . reactivity balance module,
- . parameter estimation module,
- . diagnostic - with subsequent calibration control module.

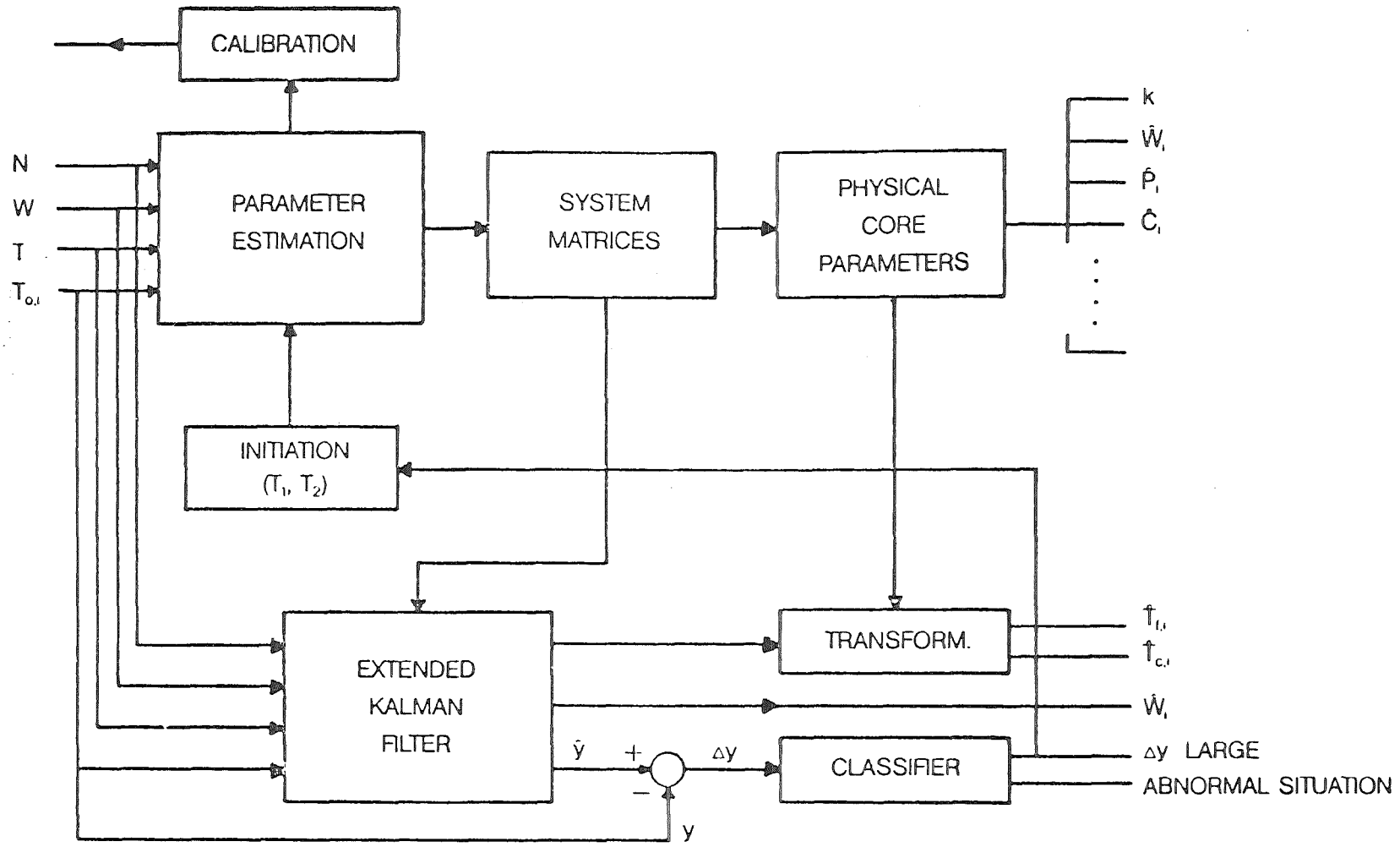
The reactivity balance module provides estimates of the various feedback terms (transient and stationary) based upon the most recent parameter estimates. It also computes control rod transient contributions and, of course, the overall reactivity balance. The latter surveillance variable is led through a digital filter in order to reduce noise. It indicates slow anomalies (time constant is 3 seconds, at present). All the other outputs of this module describe the transient state.

The continuously available information on transient state is fed into the diagnostic module where the decision is made whether or not calibration has to be initiated or alarm should be given.

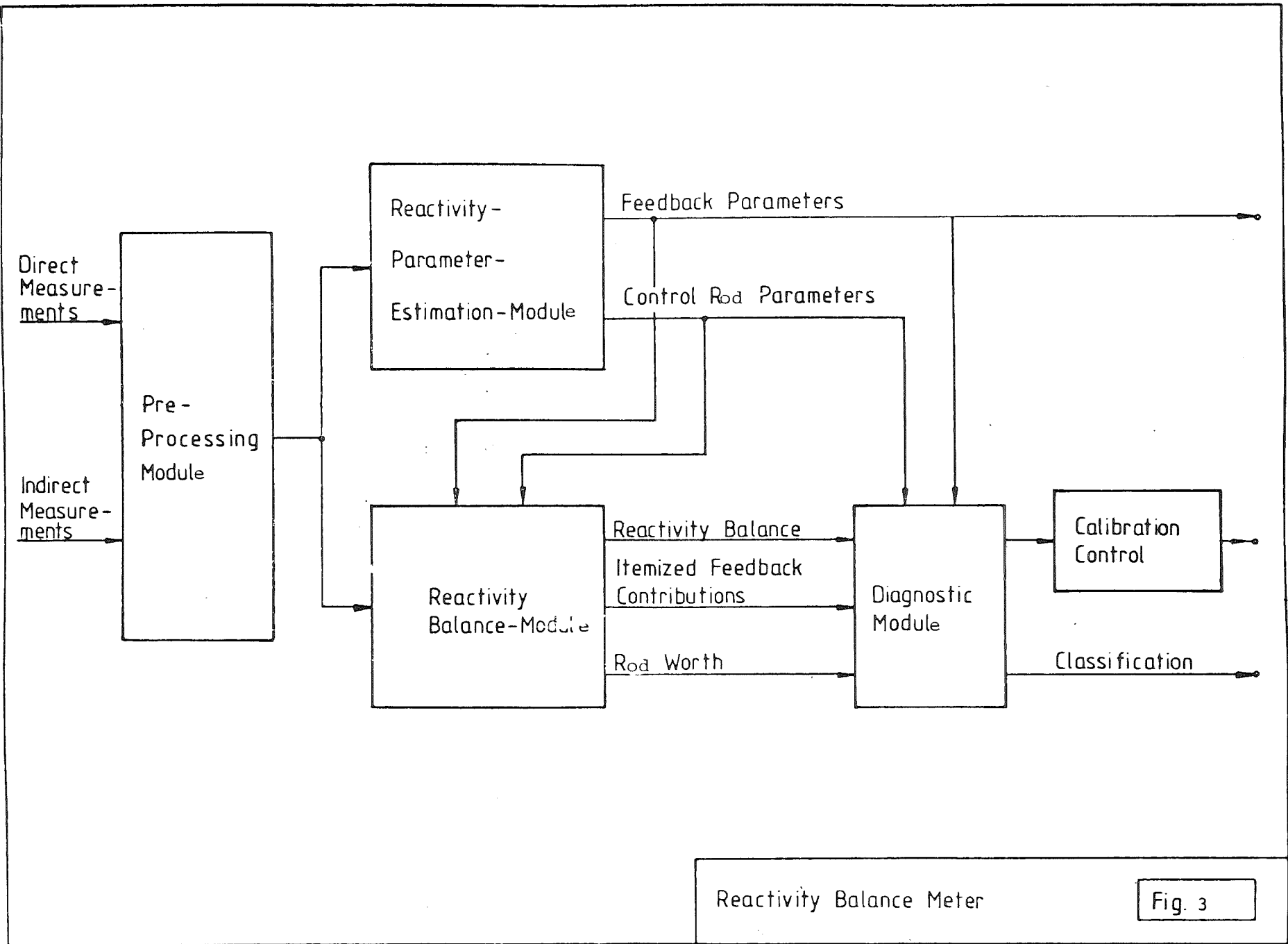
The parameter estimation module computes estimates of the reactivity parameters, β_i , based upon a set of N measurement samples (N is usually equal to 200). The number of parameters to be estimated in a particular calibration process is optional, i. e., may range from 1 to 6. The appropriate input disturbance will be selected by the calibration control module.

Calibration is required for both surveillance functions - the fuel element thermohydraulics and reactivity surveillance. Calibration success (which is equivalent to "complete observability" of the prediction model parameters) is assured by exciting the core externally with small input perturbations in the neighbourhood of the nominal state over a time interval of less than 2 minutes. The required plant disturbance should be judged in comparison with the effort needed to calibrate, for instance, the conventional reactivity balance meter and should be traded off against the gain in noise insensitivity (no special instrumentation is required for retaining the process noise properties). The input disturbance can be automatized and does not place more constraints on plant operation than automatic control.



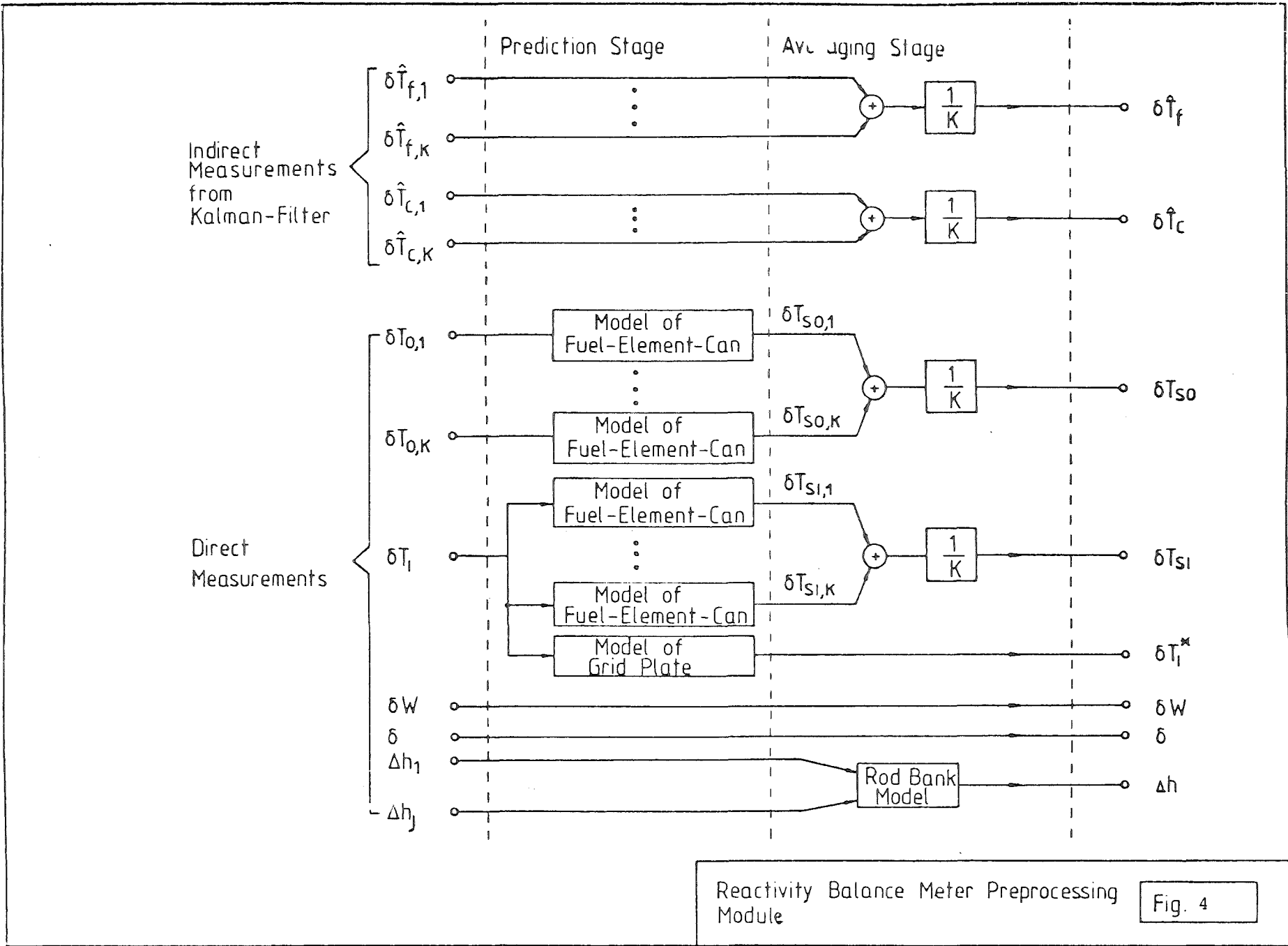


SURVEILLANCE OF FUEL ELEMENT THERMOHYDRAULICS



Reactivity Balance Meter

Fig. 3



4.1 Prediction Model for Parameter- and State-Estimation

In state-estimation with a Kalman filter or observer the estimate, \hat{x} , is computed from the measurement vector, y , with an algorithm of the form

$$\dot{\hat{x}} = A \cdot \hat{x} + Bu + K(t) \cdot (y - C\hat{x})$$

where the measurements are linear combinations of the state components

$$y = Cx$$

The matrices A, B and C represent our knowledge from the process (prediction model) in the neighbourhood of the nominal state (moving equilibrium) and are determined or up-dated via parameter estimation (system identification).

Model accuracy is in proportion to the accuracy of the standard out-of-core instrumentation and is kept within a range commonly found in noise analysis in context with transfer function estimation. It should be kept in mind, that the parameters of the prediction model will be up-dated on-line from measurements.

The thermohydraulic behaviour of one fuel element (index j) is described by the equations:

$$(4-13) \quad \begin{aligned} \dot{T}_{fj} &= \frac{\alpha_{pj}}{C_{fj}} - \frac{k_j}{C_{fj}} \cdot (T_{fj} - T_{cj}) \\ \dot{T}_{cj} &= \frac{k_j}{C_{cj}} (T_{fj} - T_{cj}) - \frac{2 C_{pj} \alpha_{wj} W}{C_{cj}} (T_{cj} - T_i) \end{aligned}$$

where

T_f = fuel temperature

T_c = coolant temperature

T_o = outlet temperature

C_f = heat capacity of fuel

C_c = heat capacity of coolant

h = specific heat of coolant

k = heat transfer coefficient between fuel and coolant

W = primary flow

P = core power

κ_{wj} = fraction of flow in fuel element j

κ_{pj} = fraction of power in fuel element j

The reactivity prediction model is expressed in terms of coefficients, which are independent of the thermo-hydraulic core state:

$$(4-14) \quad \rho = \rho_{fd} + \rho_{CR}$$

$$(4-15) \quad \rho_{fd} = (\beta_D + \beta_A) \cdot \delta T_f + \beta_C \delta T_c + \beta_B (\delta T_{so} - \delta T_{sr}) + \beta_G \delta T_f^* + \Delta$$

It is shown in Appendix A4.5 that the coefficients of the conventional reactivity model depend upon core state (i.e. fuel temperature), thermohydraulic parameters and the above β_i 's. In Appendix A4.6, a non-stationary version of the conventional reactivity feedback model is derived for comparison.

The external reactivity contribution (control rod) is assumed to be a linear function of time or position:

$$(4-16) \quad \rho_{CR} = \beta_{CR} \cdot (t - t_0) + \beta_{CR,0} \quad \text{for } v_{CR} \neq 0$$

or

$$(4-17) \quad \rho_{CR} = \beta_{CR}^* \cdot \delta h + \beta_{CR,0}^* \quad \text{for } \delta h \neq 0$$

and

$$\rho_{CR} = \beta_{CR,0} \quad \text{or} \quad \beta_{CR,0}^*$$

otherwise, where

- β_D = Doppler coefficient
- β_A = axial expansion coefficient
- β_C = coolant temperature coefficient
- β_B = bowing coefficient
- β_G = gridplate coefficient
- β_{CR}^* = rod-worth per unit position variation

and

- T_I = grid plate temperature
- T_{SO}, T_{SI} = temperatures of the fuel-element-can at the upper and lower end
- h = bank position

The constant term $\beta_{CR,0}$ can be separated from the bias term Δ in (4-15) only, if Δ is a function of time. Otherwise, reactivity feedback model errors and differential expansions are not separable.

The Doppler- and axial expansion coefficients are state-dependent; the latter is assumed to be coupled with fuel temperature only, since the cladding temperature is not available yet. The bowing effect is taken to be dependent upon the temperature gradient in the fuel-element-can being zero at 100 % nominal power. The can temperatures are assumed to behave like first order lags:

$$\begin{aligned}
 \dot{T}_{soj} &= \frac{1}{\tau_{soj}} \cdot (T_{oj} - T_{soj}) \\
 (4-18) \quad T_{szj} &= \frac{1}{\tau_{szj}} \cdot (T_I - T_{szj}) \\
 \tau_s &= \frac{C_s}{\alpha_{sc}} = \frac{M_s C_{ps}}{\alpha_{sc}}
 \end{aligned}$$

Similar for the grid plate temperature

$$\begin{aligned}
 (4-19) \quad T_I^k &= \frac{1}{\tau_I} \cdot (T_I - T_I^k) \\
 \tau_I &\approx 30 \text{ sec.}
 \end{aligned}$$

The discrete version of the thermohydraulic state equations has the structure (ideal thermocouple at the fuel element outlet)

$$\begin{aligned}
 (4-20) \quad x^{k+1} &= \phi \cdot x^k + T \cdot u^k \\
 y^k &= M \cdot x^k + D \cdot u^k
 \end{aligned}$$

where ϕ is the state transition matrix, Γ is the input matrix, and

$$x = \begin{bmatrix} \delta T_f \\ \delta T_c \end{bmatrix} \quad \gamma = \delta T_{oi}$$

$$u = \begin{bmatrix} \delta P \\ \delta T_f \\ \delta W \end{bmatrix}$$

Explicit expressions for ϕ and Γ in terms of the physical core parameters are given in /5/ and

$$M = \begin{bmatrix} 0 & 2 \end{bmatrix}, \quad D = \begin{bmatrix} 0 & -1 & 0 \end{bmatrix}$$

The expression for Γ holds whenever the input u can be assumed constant during the sampling interval $[0, t_s]$:

$$x(t) = \phi(t, 0) \cdot x^0 + \int_0^t \phi(t, \tau) \cdot B \cdot u(\tau) \cdot d\tau$$

$$= \phi(t, 0) \cdot x^0 + \int_0^t \phi(t, \tau) \cdot B \cdot u^0 \cdot d\tau$$

$$\Gamma \triangleq \int_0^t \phi(t, \tau) \cdot d\tau \cdot B$$

Non-Ideal Thermocouple

The measured and actual temperatures are not identical because of the low-pass characteristics of the thermocouple. It is modelled in terms of a first order lag:

$$(4-21) \quad \dot{T}_{oj}^* = \frac{1}{\tau_{Mj}} \cdot (\alpha_{Mj} \cdot T_{oj} - T_{oj}^*)$$

where

τ_{Mj} = time constant

α_{Mj} = gain factor, representing the radial mixing process at the outlet of neighbouring fuel elements

In discrete form:

$$(4-22) \quad \xi^{K+1} = \varphi \cdot \xi^K + \gamma \cdot \gamma^K$$
$$\gamma^{*K} = \xi^K \quad = \text{measured outlet temperature}$$

where

$$\varphi(t, t_0) = e^{-(t-t_0)/\tau_{Mj}}$$

$$\gamma(t, t_0) = \alpha_M \cdot (1 - \varphi)$$

Noise in the Observational Equations

It is assumed that the measured variables y and u are corrupted by additive Gaussian process and measurement noise:

$$(4-23) \quad y = \bar{y} + \eta_M + \eta_P = y^* + \eta_M$$

$$(4-24) \quad u_i = \bar{u}_i + \xi_{M,i} + \xi_{P,i} = u_i^* + \xi_{M,i}$$

The measurement noise is white with mean zero and the variances

$$(4-25) \quad E[\eta_M^2] = R \qquad E[\xi_{M,i}^2] = Q_i$$

The process noise of the inputs is treated as a natural disturbance of the core and it is measured. The random errors of the inputs are, therefore, only due to the measurement errors $\xi_{M,i}$. The process noise of the output is assumed to be dominated by the system response to the input process noise.

4.2 Analytical Separation of Parameter- and State- Estimation

In order to separate the parameter estimation task from state estimation, it is necessary to relate the elements of the system matrices directly to the measurements of the output, y , and input, u . It is accomplished by eliminating the state vector x in the thermohydraulic state equations associated with the fuel elements:

$$(4-26) \quad \begin{aligned} x^{k+1} &= \phi \cdot x^k + \Gamma u^k \\ y^k &= M \cdot x^k + D u^k \end{aligned}$$

where the index denotes sampling time, the transition matrix ϕ and the input matrix Γ are given in /5/ as explicit functions of the physical core parameters and the sampling interval, and the observation gradients are given by

$$M = [0 \quad 2] \quad , \quad D = [0 \quad -1 \quad 0]$$

for the case with ideal thermocouples.

System (4-26) is transformed to output identifiable form in order to accommodate elimination of x :

$$(4-27) \quad x = P \cdot \bar{x}$$

$$(4-28) \quad P = \frac{1}{2 \cdot \phi_{21}} \begin{bmatrix} -\phi_{22} & 1 \\ \phi_{21} & 0 \end{bmatrix}, \quad \phi_{ij} = \text{elements of } \phi$$

and

$$(4-29) \quad \begin{aligned} \bar{x}^{k+1} &= \bar{\phi} \cdot \bar{x}^k + \bar{\Gamma} \cdot u^k \\ y^k &= \bar{M} \cdot \bar{x}^k + \bar{D} \cdot u^k \end{aligned}$$

where

$$\bar{\Phi} = \begin{pmatrix} 0 & 1 \\ \bar{\Phi}_{21} & \bar{\Phi}_{22} \end{pmatrix} \quad \bar{M} = \begin{bmatrix} 1 & 0 \end{bmatrix}$$

$$\bar{D} = D$$

It follows from (4-27) and (4-26) that

$$(4-30) \quad y^K = \bar{x}_1^K - u_2^K$$

$$y^{K+1} = \bar{x}_2^K + (\bar{\gamma}_{11} u_1^K + \bar{\gamma}_{12} u_2^K + \bar{\gamma}_{13} u_3^K) - u_2^{K+1}$$

The lower index denotes the element of the vectors \bar{x} , u and of the input matrix $\bar{\Gamma}$. The state vector \bar{x} at time t_K can be expressed, therefore, in terms of the measurements y and u :

$$(4-31) \quad \bar{x}^K = \begin{pmatrix} y^K \\ y^{K+1} \end{pmatrix} - \begin{pmatrix} 0 & -1 & 0 \\ \bar{\gamma}_{11} & \bar{\gamma}_{12} & \bar{\gamma}_{13} \end{pmatrix} \begin{pmatrix} u_1^K \\ u_2^K \\ u_3^K \end{pmatrix} - \begin{pmatrix} 0 & 0 & 0 \\ 0 & -1 & 0 \end{pmatrix} \begin{pmatrix} u_1^{K+1} \\ u_2^{K+1} \\ u_3^{K+1} \end{pmatrix}$$

Inserting (4-31) into (4-30) gives the "observational equations":

$$(4-32) \quad z^{K+2} = \sum_{i=0}^{T,K} z_i^{T,K} \cdot \Lambda + v^{K+2} \quad K = 1, 2, \dots, N$$

where

$$z \triangleq y + u_2$$

$$\sum_{i=0}^{T,K} z_i^{T,K} = \begin{bmatrix} z^K & z^{K+1} & u_1^K & u_2^K & u_3^K & u_1^{K+1} & u_2^{K+1} & u_3^{K+1} \end{bmatrix}$$

$$\begin{aligned}
 \Lambda^T &= [\lambda_1, \lambda_2, \dots, \lambda_8] \\
 \lambda_1 &= \bar{\Phi}_{21} & \lambda_2 &= \bar{\Phi}_{22} \\
 (4-33) \quad \lambda_3 &= \bar{y}_{21} - \bar{\Phi}_{22} \cdot \bar{y}_{11} & \lambda_4 &= \bar{y}_{22} - \bar{\Phi}_{22} \cdot \bar{y}_{12} \\
 \lambda_5 &= \bar{y}_{23} - \bar{\Phi}_{22} \cdot \bar{y}_{13} & \lambda_6 &= \bar{y}_{41} \\
 \lambda_7 &= \bar{y}_{12} & \lambda_8 &= \bar{y}_{13}
 \end{aligned}$$

Note that the second column of $\bar{\Gamma}$ can be expressed in terms of the third column:

$$\begin{aligned}
 (4-34) \quad \bar{y}_{12} &= \alpha \bar{y}_{13} \\
 \bar{y}_{22} &= \alpha \bar{y}_{23} \\
 \alpha &= -2 \cdot \frac{W}{T_0 - T_1}
 \end{aligned}$$

Hence, the number of parameters can be reduced from 8 to 6 and disturbance of the input $u_2 = \delta T_I$ is not needed in order to determine the system matrices from the measurements. It is sufficient to disturb $u_1 = \delta P$ and $u_3 = \delta W$.

The observational equations, (4-32) are in standard linear regression form and can be solved for the parameter vector Λ by means of the recursive least square procedure.

The transformed system matrices, $\bar{\phi}$, $\bar{\Gamma}$, are related to the original system matrices as follows:

$$\begin{aligned}
 \bar{\phi}_{21} &= \phi_{12} \cdot \phi_{21} - \phi_{11} \cdot \phi_{22} \\
 \bar{\phi}_{22} &= \phi_{11} + \phi_{22} \\
 (4-35) \quad \bar{\Gamma}_{11} &= 2 \cdot \Gamma_{21}, \quad \bar{\Gamma}_{12} = 2 \cdot \Gamma_{22}, \quad \bar{\Gamma}_{13} = 2 \cdot \Gamma_{23} \\
 \bar{\Gamma}_{21} &= 2 \cdot (\phi_{21} \Gamma_{11} + \phi_{22} \Gamma_{21}) \\
 \bar{\Gamma}_{22} &= 2 \cdot (\phi_{21} \Gamma_{12} + \phi_{22} \Gamma_{22}) \\
 \bar{\Gamma}_{23} &= 2 \cdot (\phi_{21} \Gamma_{13} + \phi_{22} \Gamma_{23})
 \end{aligned}$$

The ϕ and Γ matrices are given in /5/ as explicit functions of the physical core parameters.

Observability Problem and Calibration Control

Estimability of the thermohydraulic and of the reactivity parameters (i.e.: the capability of determining these parameters from the direct and indirect measurements) can be quantified in terms of the convergence properties of the estimation error covariance matrices, P^j . If the normalized covariance matrix is diagonally dominant, then the considerations can be restricted to the diagonal elements, P_{ii} , of P^j . The i^{th} component of the parameter vector Λ can be estimated from the data, if P_{ii}^j decreases sufficiently rapid with j (the number of measurement samples) - it is said to be "observable". The converse holds also. If P_{ii}^j does not converge sufficiently rapid, then the data do not contain information on the parameter Λ_i - it is not observable.

Observability Analysis of the Thermohydraulic Parameters

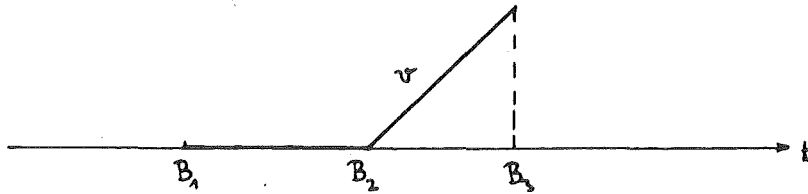
The structure of the estimation algorithms (see section 4.2 and reference /5/) already guarantees "observability" with respect to the thermohydraulic model parameters. Hence, the amount of information contained in the measurements on these parameters solely depends upon the particular time functions we are able to choose for the input disturbances.

The core-inputs (control rod position, flow rate and, possibly, inlet temperature) must be changed in such a manner, that the transient behaviour of the measurements is affected by all the parameters to be estimated. Limiting factors are the speeds by which the control

rods and the flow rate can be changed. The disturbance amplitude can be kept small. Its effect on core power does not need to exceed $\pm 2\%$ of the nominal value.

An experimental procedure has been adopted for determining a proper disturbance function. The covariance matrix of estimation error will be computed as a function of time, i. e. of the number of measurements processed for a particular sample disturbance function. If all the diagonal elements converge sufficiently rapid with increasing number of measurements, then the system is completely observable. Otherwise, the free parameters of the disturbance function must be varied until convergence is achieved.

Because of the constraints on rod movements and flow-rate perturbations, a "random walk type disturbance" has been picked, where a period of constant input is followed by a period of constant change, and s. f..



The total random function will be made up of a sequence of these random walk elements, where the time differences $(B_2 - B_1)$, $(B_3 - B_2)$ and the velocity signs are uniformly distributed random variables. The standard deviations of these random variables need to be varied between successive computer runs, until the system is completely observable.

Then, a "disturbance profile" is found which guarantees the convergence of the parameter estimation procedure for the particular core-design.

In the case of KNK-II, the speed of the control bank is ± 0.5 mm/s and the flow-rate can be varied with ± 0.2 kg/s². Excitation of the inlet-temperature is not required for the estimation of the thermohydraulic parameters. The corresponding parameters are redundant and can be expressed by the others:

$$\Gamma_{22} = \frac{W}{T_2 - T_c} \cdot \Gamma_{23}$$

$$\Gamma_{42} = \frac{W}{T_2 - T_c} \cdot \Gamma_{43}$$

It is difficult in practice, at present, to disturb bank position and flow-rate simultaneously. Excitation of only one core-input implies, that not all Λ -parameters can be estimated. It will be shown in section 6.3 that

$$\lambda_1, \lambda_2, \lambda_3, \lambda_6$$

are observable, if the bank position is disturbed and

$$\lambda_1, \lambda_2, \lambda_5, \lambda_8$$

are observable otherwise. Since we have 5 physical core parameters

$$k, x_p, x_w, C_c, C_f$$

we need to select 4 parameters with the highest diagnostic value, i. e.:

$$k, x_p, x_w, C_f$$

and relate them to the λ_i -estimates.

If C_c cannot be computed from the geometry and the a-priori knowledge of specific heats and the densities, then bank position and flow-rate have to be disturbed simultaneously.

Extension of the observability analysis to the case with non-ideal thermocouples is considered in section 6.3, where also experimental results are shown.

Observability of Reactivity Parameters

It follows from the equations (4-14), (4-15), (4-16) and (4-17), that the observation gradient is defined as follows:

$$M = \begin{bmatrix} \delta T_f^1, & \delta T_c^1, & (\delta T_{SO}^1 - \delta T_{SI}^1), & \delta T_I^{N1}, & 1 \\ \delta T_f^2, & \delta T_c^2, & (\delta T_{SO}^2 - \delta T_{SI}^2), & \delta T_I^{N2}, & 1 \\ \vdots & & & & \vdots \\ \delta T_f^N, & \delta T_c^N, & (\delta T_{SO}^N - \delta T_{SI}^N), & \delta T_I^{NN}, & 1 \end{bmatrix}$$

The index denotes sampling time. Complete observability requires, that the columns of M are linearly independent (which is equivalent to requiring convergence of the estimation error statistics) and, hence, that $T_f, T_c, T_{SO}, T_{SI}, T_I^N$ become sufficiently disturbed.

In this report, the observability test for the reactivity parameters is based on the disturbance of primary flow and/or coolant inlet temperature. The latter is not easy to implement at the plant, but required for estimating the grid plate coefficient. If this coefficient can be neglected or can assumed to be known, then the bank position can replace the inlet temperature in providing sufficient core disturbance. A further restriction placed upon the observability test was to employ elementary disturbance functions such as 2 consecutive steps with opposite sign rather than binary random sequences or random walk type disturbance. Table 1, 2, 3 and 4 show the normalized standard deviations of the estimation errors for various types of core input disturbances.

The index j of σ_j in the tables refers to the reactivity coefficients:

$j = 1$	\dots	$\beta_D + \beta_A$
$j = 2$		β_C
$j = 3$		β_B
$j = 4$		β_B
$j = 5$		$\beta_{CR,0}$

Step-like disturbance of flow and inlet temperature (Table 1) produces data which contain information on the Doppler, axial expansion and on the rod worth parameter $\beta_{CR,0}$. But the temperature gradient in the fuel element can does not deviate sufficiently from its nominal value. Hence, the bowing effect is negligible and the bowing coefficient β_B is not observable. The diagonal element P_{33} was set, therefore, equal to a very small initial value pretending to know β_B very well. Grid plate reactivity contributes very little to the reactivity balance in comparison with Doppler etc. and varies only slowly with time as a consequence of the large grid plate time constant ($\tau_G \cong 30$ seconds). Hence, the fourth column of M is nearly proportional to the 5th column for this type of input disturbance. Convergence of P_{44} is poor.

Convergence of P_{44} can be improved either by removing the other reactivity components from the estimation procedure (setting the corresponding $P_{ii}(0)$ equal to a small value after an estimate has been obtained) or by modifying

the inlet temperature disturbance profile. Table 2 shows the effect of taking P_{11} , P_{22} and P_{33} equal to $0.1 \text{ E-}05$. Convergence can be improved further by increasing the frequency contents of the disturbance function. Picking, for instance, a binary random sequence with a switching interval distributed uniformly between 0 and 30 seconds (equal to the time constant of the grid plate), the convergence becomes very good (see Table 3).

The bowing effect can contribute to the reactivity balance only, if the temperature difference between upper and lower part of the fuel element can deviates sufficiently from the nominal value. It can be estimated, therefore, separately without degrading the overall estimation accuracy. It seems necessary, however, to determine the differential expansion term simultaneously with the bowing coefficient. Table 4 shows the result for a ramp-like disturbance of the flow. The corresponding maximum power disturbance is 1 %.

Some precaution is required after set point change. New nominal values have to be introduced for the estimates of T_f , T_c and T_I^* so that the entries of the observation gradient M are not dominated by the set point change.

It is concluded that every coefficient of the reactivity prediction model can be estimated on-line requiring only small disturbances of the core inputs W and T_I over a short time interval in the order of 1 minute. It is permissible to subdivide the set of coefficients into the 3 subsets:

1. $\beta_D + \beta_A$, β_C , $\beta_{CR,0}$
2. β_B , $\beta_{CR,0}$
3. β_G , $\beta_{CR,0}$

and to estimate each subset separately with the appropriate input disturbance. The observability analysis will be complemented by rod position disturbances in a subsequent paper in context with experiments.

Table 1:

Convergence for Flow and Inlet Temperature Disturbances

Number of Samples	Normalized Standard Deviation of Estimation Errors				
	σ_1	σ_2	$\sigma_3^{*)}$	σ_4	σ_5
0	1	1	1	1	1
100	0.0648	0.167	1	0.987	0.152
200	0.054	0.138	1	0.965	0.095

*) bowing reactivity coefficient known initially

Table 2:

Convergence for Inlet Temperature Disturbance

Number of Samples	Normalized Standard Deviation of Estimation Errors				
	$\sigma_1^{*)}$	$\sigma_2^{*)}$	$\sigma_3^{*)}$	σ_4	σ_5
0	1	1	1	1	
100	1	1	1	0.908	0.126
200	1	1	1	0.612	0.0592

*) Doppler, coolant temperature and bowing coefficients are known initially

Table 3:

Convergence for Inlet Temperature Disturbance with Binary Random Sequence

Number of Samples	Normalized Standard Deviation of Estimation Error				
	$\sigma_1^{*)}$	$\sigma_2^{*)}$	$\sigma_3^{*)}$	σ_4	σ_5
0	1	1	1	1	1
80	1	1	1	0.648	0.242
400	1	1	1	0.106	0.096
500	1	1	1	0.106	0.092

*) Doppler, coolant temperature and bowing coefficients are known initially

Table 4:

Convergence for Ramp-like Disturbance of Flow

Number of Samples	Normalized Standard Deviation of Estimation Error				
	$\sigma_1^{*)}$	$\sigma_2^{*)}$	σ_3	$\sigma_4^{*)}$	σ_5
0	1	1	1	1	1
100	1	1	0.30	1	0.15
200	1	1	0.09	1	0.12

*) Doppler, coolant temperature and grid plate coefficients are known initially

Table 5: Core Input Disturbances for Estimation of Reactivity Coefficients

Surveillance Variable	Disturbance of Core Input			Maximum Power Perturbation
	Primary Flow	Inlet Temperature	Rod Position	
$\beta_D + \beta_A$	<p>A graph showing a step function for Primary Flow. The vertical axis is labeled '%' and has values 0.0 and 2.5. The horizontal axis is labeled 'sec' and has values 5, 20, and 40. The function is at 0.0% until 5 seconds, then jumps to 2.5% and remains constant until 20 seconds, then returns to 0.0%.</p>	<p>A graph showing a step function for Inlet Temperature. The vertical axis is labeled '°K' and has values 0.0 and 2.5. The horizontal axis is labeled 'sec' and has values 5, 20, and 40. The function is at 0.0°K until 5 seconds, then jumps to 2.5°K and remains constant until 20 seconds, then returns to 0.0°K.</p>	-	5 %
β_C	as for $(\beta_D + \beta_A)$	as for $(\beta_D + \beta_A)$	-	5 %
β_G	-	as for $(\beta_D + \beta_A)$	-	2.5 %
β_B	Quasi-stationary flow ramp during the calibration interval	-	-	1 %
β_{CRO}	as for $(\beta_D + \beta_A)$	as for $(\beta_D + \beta_A)$	-	5 %
β_{CR}	-	-	ramp-like disturbance, see section 5.3, example 2	3 %

4.4 Estimation of Thermohydraulic Core Parameters

The estimation procedure consists, in general, of the following major steps:

- . initiation of the calibration period, during which the core inputs are excited in accordance with the results of section 4.3;
- . estimation of the Λ -parameters based on the observational equations derived in section 4.2:

$$(4-36) \quad z^{k+2} = \sum^{k,T} \Lambda + V^{k+2}, \quad k = 1, 2, \dots, N$$

$$V^{k+2} = -v^{k+2} + v^k \cdot \Lambda_1 + v^{k+1} \cdot \Lambda_2 + \sum_{M1}^k \Lambda_3 + \sum_{M2}^k \Lambda_4 + \sum_{M3}^k \Lambda_5 + \sum_{M4}^{k+1} \Lambda_6 + \sum_{M2}^{k+1} \Lambda_7 + \sum_{M3}^{k+1} \Lambda_8$$

$$v^k = \gamma_M^k + \sum_{M}^5 \quad (\text{see section 4.1})$$

- . iterative computation of the physical core parameters, $k, \kappa_p, \kappa_w, C_c, C_f$ from the Λ -estimates by means of the Newton-Raphson method after the estimation procedure has been completed (has converged).

The overdetermined system of equations (4-36) is solved for Λ with the recursive least square procedure of Appendix A4.4. Parameter estimation with the standard least square method is advantageous because of its simplicity and low computational requirements. But a

basic disadvantage lies in the bias error which accumulates as a consequence of noisy entries in the coefficient matrix Z and the noise term V^{K+2} in (4-36). Solving (4-36) gives

$$\begin{aligned}
 \mathcal{L} &= (Z^T Z)^{-1} Z^T z = (Z^T Z)^{-1} Z^T (Z \mathcal{L} + V) \\
 &= \mathcal{L} + N \cdot P_N \cdot \frac{1}{N} Z^T V \\
 (4-37) \quad \hat{\mathcal{L}} &= \mathcal{L} + b
 \end{aligned}$$

The bias term, b , depends upon the covariance matrix of estimation error, P_N , and the product $Z^T V$. It is shown in Appendix A4.3, that

$$(4-38) \quad \frac{1}{N} Z^T V = \psi \cdot \mathcal{L}$$

where the elements of ψ are given by the measurement noise variances R and Q_i . Inserting (4-38) into (4-37) gives

$$\hat{\mathcal{L}} = \mathcal{L} + N P_N \psi \mathcal{L}$$

or

$$(4-39) \quad \mathcal{L} = (I + N P_N \psi)^{-1} \hat{\mathcal{L}}$$

The inverse in (4-39) can be circumvented by observing that

$$(4-40) \quad \psi \cdot \mathcal{L} = \begin{bmatrix} \psi^{11} & \vdots & \psi^{21,T} \\ \vdots & \ddots & \vdots \\ \psi^{21} & \vdots & \psi^{22} \end{bmatrix} \begin{bmatrix} \mathcal{L}^1 \\ \vdots \\ \mathcal{L}^2 \end{bmatrix} = \begin{bmatrix} \psi^{11} \cdot \mathcal{L}^1 \\ \vdots \\ 0 \end{bmatrix}$$

where

$$\lambda^{\wedge} = [\lambda_1, \lambda_2]^T$$

and

$$(4-41) \quad \psi^{11} = \begin{bmatrix} -(R+Q_2) & 0 \\ 0 & -(R+Q_2) \end{bmatrix}$$

Hence

$$\hat{\lambda} = \lambda + N \cdot \left[\begin{array}{c|c} P^{11} & P^{21,T} \\ \hline P^{21} & P^{22} \end{array} \right] \cdot \left[\begin{array}{c} \psi^{11} \lambda^1 \\ \hline 0 \end{array} \right]$$

$$(4-42) \quad \begin{bmatrix} \hat{\lambda}^1 \\ \hat{\lambda}^2 \end{bmatrix} = \begin{bmatrix} \lambda^1 \\ \lambda^2 \end{bmatrix} + N \cdot \begin{bmatrix} P^{11} \psi^{11} \lambda^1 \\ P^{21} \psi^{11} \lambda^1 \end{bmatrix}$$

and the unbiased estimates become:

$$(4-43) \quad \begin{aligned} \lambda^1 &= (I + N \cdot P^{11} \cdot \psi^{11})^{-1} \cdot \hat{\lambda}^1 \\ \lambda^2 &= \hat{\lambda}^2 - N \cdot P^{21} \psi^{11} \lambda^1 \end{aligned}$$

This method for unbiaseding the least square estimate is due to E.V. Bohn and M.K. de Beer /3/ and has the advantage not to burden the least square computations and not to affect the convergence properties of the sequential estimation procedure. Bias compensation can be carried out in parallel and after the calibration process has been terminated, i.e.: when the unbiased estimates are needed.

A variety of other compensation methods are also available. But it did not seem worthwhile to find the best possible procedure, since data prefiltering (see Chapter 6) reduces the statistical errors in z and Z and, hence, causes this type of bias to become negligible against other sources of systematic estimation errors.

The computation of the physical core parameters from the Λ -parameter estimates is, in general, only possible by solving the following nonlinear equation system iteratively by means of the Newton-Raphson procedure:

$$\Lambda = \Lambda(\bar{\phi}, \bar{\Gamma})$$

where

$\bar{\phi}$ and $\bar{\Gamma}$ are functions of ϕ and Γ , which, in turn, are functions of the core parameters

$$\phi = \phi(k, \kappa_p, \kappa_w, C_c, C_f)$$

$$\Gamma = \Gamma(k, \kappa_p, \kappa_w, C_c, C_f)$$

If only single parameters (for instance κ_w) are to be determined, then very simple equations are available, as it will be illustrated next with the fraction of flow, κ_w :

If the sampling interval is sufficiently small, then

$$\Lambda_6 \approx -4 \Delta t \frac{\kappa_w \cdot (T_c - T_I)}{M}$$

where

Δt = sampling interval

T_c = coolant temperature (nominal value prior to calibration)

T_I = inlet temperature (nominal value prior to calibration)

M = coolant mass in the fuel element (nominal value prior to calibration)

Variation in κ_w can be expressed in terms of the variation in Λ_6 :

$$\frac{\delta \hat{\kappa}_{wi}}{\kappa_{wio}} = \frac{\Lambda_{6i}}{\Lambda_{6i0}} - 1 \quad \text{the index zero denotes nominal value or the previous calibration result}$$

None of the other physical core parameters need to be known beforehand in order to determine $\delta \hat{\kappa}_w$ from Λ_6 . They are embedded in $\hat{\Lambda}_1 \dots \hat{\Lambda}_5$ and can be computed as desired.

Another simple example is the fraction of power generated in a particular fuel element:

$$\frac{\delta \kappa_p}{\kappa_{p0}} = \frac{P_i}{P_{i0}} - 1$$

$$\frac{P_i}{P_{i0}} = \left(1 - \frac{\delta \hat{\kappa}_w}{\kappa_{w0}} \right) \cdot \frac{\bar{T}_{oi} - T_I}{T_{oi0} - T_{co}}$$

\bar{T}_{oi} = smoothed value of the outlet temperature measurement prior to calibration

The error in $\delta \hat{\kappa}_p / \kappa_{p,0}$ will be slightly higher than in $\delta \hat{\kappa}_w / \kappa_{w,0}$ because of the residual smoothing error in $\delta \bar{T}_{o,i}$. Similar relations are available for k and C_c .

4.5 Estimation of Thermohydraulic Core State

The core state represents the transient behaviour of the core and is made up of the fuel temperature for every fuel element which has a thermocouple at its outlet and of the corresponding coolant temperatures (averaged over the fuel element). If non-ideal thermocouples have to be considered, then the state vector is augmented by the fuel element outlet temperatures, which are also not directly measurable because of the thermocouple time constants and of the radial mixing process in the upper mixing chambre.

Decoupling of the state equations based upon physical reasoning allows for state vector partitioning. Every fuel element can be modelled separately. The only radial coupling occurs at the core-outlet and can be considered in terms of the thermocouple gain factor introduced in section 4.1.

The fuel temperatures are sensitive measures of cooling disturbances. Phase differences between fuel- and coolant temperatures in a particular subassembly provide additional information about the origin of a local power/cooling mismatch. Furthermore, knowledge of fuel temperature is needed for compensating set-point dependent effects on the reactivity balance (see section 4.6).

A means for computing the state components on-line from the measurements of the out-of-core instrumentation is the Kalman filter. Its most simple version with a constant gain matrix suffices for estimating subassembly state

$$x = (\delta T_f, \delta T_c)^T \dots\dots \text{ideal thermocouple}$$

or

$$x = (\delta T_f, \delta T_c, \delta T_o)^T \dots\dots \text{non-ideal thermocouple}$$

and has the structure:

$$\hat{x}_{j+1}^{j+1} = \hat{x}_{j+1}^j + K \cdot (y_{j+1} - \hat{y}_{j+1})$$

$$\hat{x}_{j+1}^j = \phi \hat{x}_j^j + \Gamma \cdot u_j$$

$$\hat{y}_{j+1} = M \hat{x}_{j+1}^j + D \cdot u_{j+1}$$

where

$$\hat{x}_j^i = \text{estimate of } x \text{ for sampling time } t_j \text{ based upon all measurements up to and including } y_i = y(t_i)$$

$$K = \text{constant filter gain vector}$$

Filter convergence is continuously monitored in terms of the observation residual:

$$\Delta y_j = y_j - \hat{y}_j$$

If its expectation exceeds a prespecified threshold, then the prediction model does not match the true situation and the system matrices ϕ and Γ need to be up-dated. In case of failure in the parameter estimation modul, the Kalman filter can still operate, but with degraded performance.

If it is desirable to estimate the coolant flow in particular fuel elements continuously and without having to disturb the system externally, then the "Augmented Kalman filter" provides a solution. The prediction model is derived in Appendix A4.2 and has the structure:

$$(4-44) \quad x_{K+1} = \phi^* x_K + \Gamma^* u_K$$

where

$$x = [x_1 \ x_2 \ x_3]^T = \text{augmented subassembly state}$$

$$x_1 = \delta T_f, \quad x_2 = \delta T_c, \quad x_3 = \delta \kappa_w$$

$$\kappa_w = \text{fraction of flow in subassembly}$$

$$\phi^* = \begin{bmatrix} \phi & \vdots & \Theta \\ \hline 0 & \vdots & 1 \end{bmatrix} \quad \Gamma^* = \begin{bmatrix} \Gamma \\ \hline 0 \end{bmatrix}$$

The filter gain matrix can not be computed here from the stationary solution of the Riccati equation, since the 3. state equation in (4-44) is not corrupted by input-noise; hence, the corresponding gain element would tend to zero with increasing number of measurements processed - the Kalman filter is known to diverge in this case.

In order to avoid divergence, a limited memory filter is implemented, where the weighting matrix becomes reset to its initial value after a certain number of measurement samples have been processed.

4.6 On-line Estimation of Reactivity Parameters and Reactivity Contributions

It has been shown in the sections 4 and 4.1, that the reactivity parameters can be linearly related to the reactivity measurements:

$$\rho_{\text{MEAS}}^K = M^K \cdot \beta + \epsilon^K$$

where

$$M^K = \left[\delta T_f^K, \delta T_c^K, (\delta T_{\text{SO}}^K - \delta T_{\text{SI}}^K), \delta T_I^K, \delta h, 1 \right]$$

and

$$\beta = \left[(\beta_D + \beta_A), \beta_C, \beta_B, \beta_G, \beta_{\text{CR}}, \beta_{\text{CR},0} \right]$$

The index k denotes sampling time and ϵ^K is the random measurement error. It has also been shown, that the data vector M^K is available for reactivity surveillance as a by-product of fuel-element cooling surveillance.

The considerations in the sections 4.3 and 4.6 may seem redundant at a first glance. But convergence of P does not always imply success in estimating the parameters from the data (bias problem). Conversely, if bias in the estimates does not match the expectation, then it may be difficult sometimes to determine the cause without the results of section 4.3.

Table 5 shows a set of elementary disturbance profiles, which suffices to estimate all reactivity feedback parameters including the grid plate coefficient. If the latter is not required, then bank position can replace the inlet temperature disturbance in Table 5

and flow disturbance is only needed for estimating the bowing coefficient β_B . No sufficient effort has been expended yet to investigate the minimal disturbance amplitudes required. This task will be taken up again in context with experiments. It suffices for the time being to recognize, that plant operation will only be disturbed occasionally by a small power perturbation (see Table 5) of less than 2 minutes duration. It is proposed to automatize the calibration process and to develop a microcomputer based calibration control module which initiates, terminates and checks the input disturbances.

If the set point is changed more than 5 %, then the dependency of the Doppler and axial expansion coefficients upon fuel temperature must be taken into account by one of the following methods:

- . estimation of A_D , B_D rather than β_D , where

$$\beta_D = \frac{1}{T_f} \cdot \left(A_D + \frac{B_D}{\sqrt{T_f}} \right)$$

- . estimation of β_D rather than A_D and B_D , but calibration after every large set point change. The reactivity balance signal serves as an anomaly indicator and initiates parameter estimation automatically.
- . prediction of $\beta_D + \beta_A$ as a function of T_f between calibrations. The following prediction formula permits to waive calibration after regular set point changes. It is included into the balance meter:

$$\frac{\beta_D + \beta_A}{\beta_{D0} + \beta_{A0}} = \frac{\frac{1}{T_f} \cdot \left(A_D + \frac{B_D}{\sqrt{T_f}} \right) + (g_0 + g_1 \cdot (T_f - 273.))}{\frac{1}{T_{f0}} \cdot \left(A_D + \frac{B_D}{\sqrt{T_{f0}}} \right) + (g_0 + g_1 \cdot (T_{f0} - 273.))}$$

where

$$A_D = - 0.03334,$$

$$B_D = + 0.60359$$

$$g_0 = - 1.15056 \cdot 10^{-5}$$

$$g_1 = - 9.8136 \cdot 10^{-9}$$

T_f = fuel temperature in °K

The index 0 refers to the most recent estimate. The range of the average fuel temperature of the KNK-core is shown in Figure 5 as a function of set-point. The corresponding Doppler and axial expansion coefficients are shown in Figure 6. Whatever error is made in taking a crude average over the total core, this error will not vary as a consequence of small perturbations of the core state. We observe the following variations over the power range:

$$\beta_D \dots + 7 \%$$

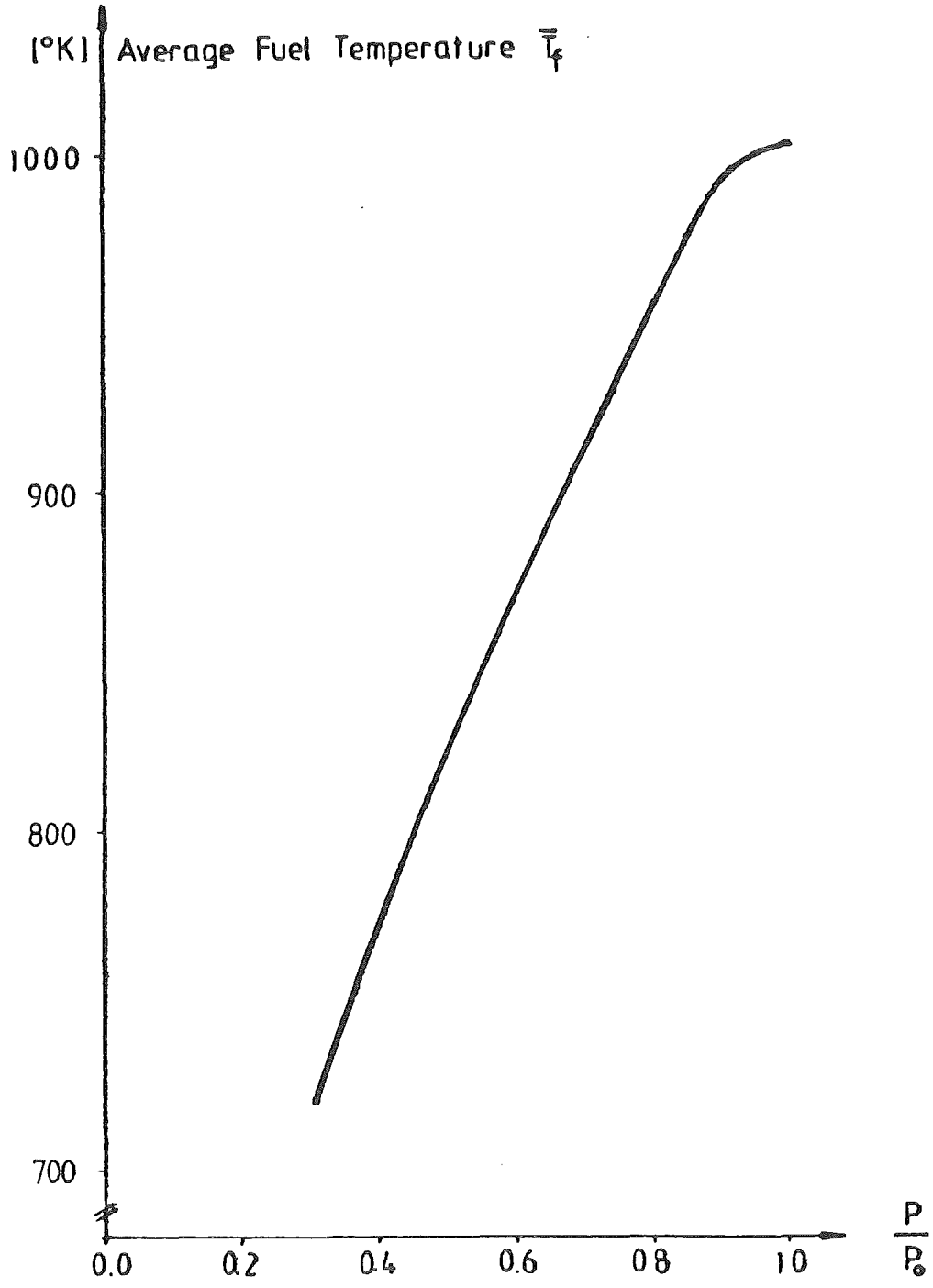
$$\beta_A \dots - 18 \%$$

The burn-up effect on the reactivity coefficients is in the same order of magnitude:

days of full power operation	0	255	365
$\frac{\delta\beta_D}{\beta_D} \quad / \quad \% \quad /$	0	4	- 1
$\frac{\delta\beta_A}{\beta_A} \quad / \quad \% \quad /$	0	- 15	-24
$\frac{\delta\beta_B}{\beta_B} \quad / \quad \% \quad /$	0	12	17

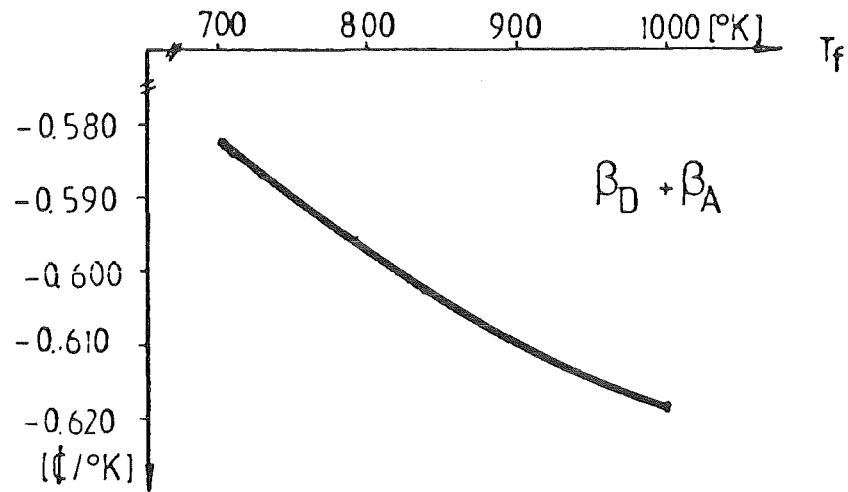
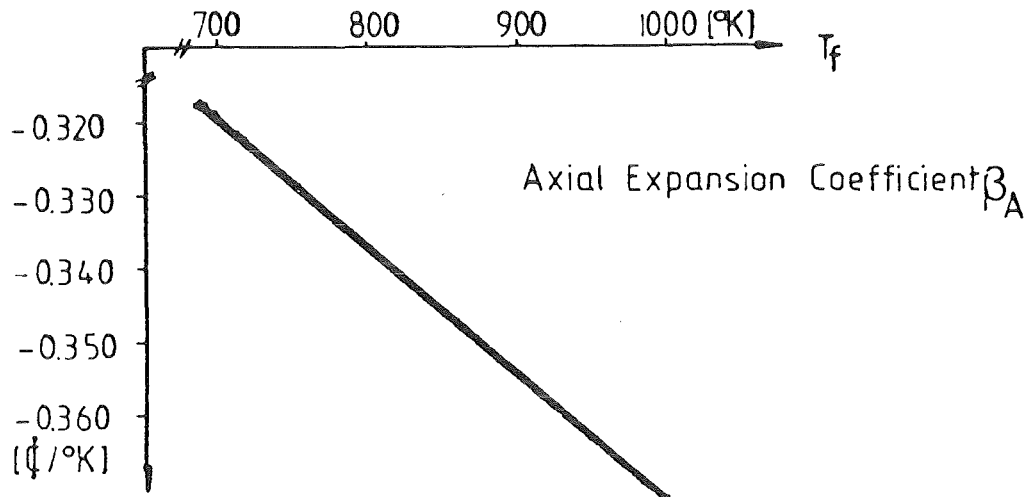
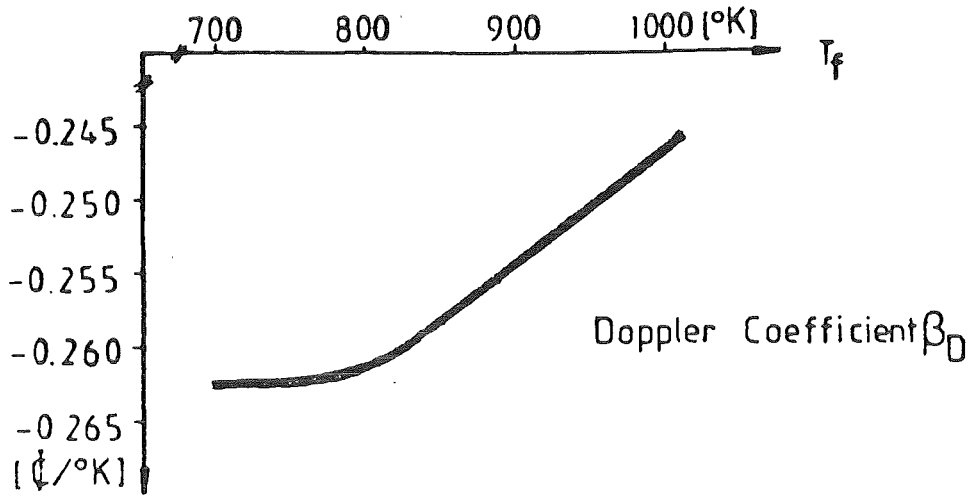
Hence, the estimation accuracy obtained with the simple disturbance patterns of Table 5 obviously suffices to track the burn-up effects and the effect of set-point variations. The estimation accuracy is expected to become higher, if a disturbance function with a higher frequency contents can be chosen, i.e.: random walk type and if bank position is disturbed rather than inlet temperature.

Partitioning of the reactivity model is in progress and will eventually allow to detect small changes of the reactivity coefficients for every fuel element.



AVERAGE FUEL TEMPERATURE AS A
FUNCTION OF SET-POINT

Fig 5



TEMPERATURE DEPENDENCE OF DOPPLER- AND AXIAL EXPANSION COEFFICIENT

Fig. 6

On-Line Estimation of Control Rod Reactivity Worth

At a first glance, it seems simple to measure rod position and to deduce the corresponding rod worth from a predetermined characteristic relating position with reactivity. Rod drop experiments performed every six month could provide, for instance, the calibration curve. Such a measurement system has been implemented at the KNK-II plant with ± 0.05 mm quantization error. Total position range is 600 mm corresponding to approximately 24 % reactivity.

Tests have shown, that the average rod movements due to control actions fall within the position quantization error (less 0.005 mm). Furthermore, differential expansion effects, where worth changes occur without position changes, cannot be detected by the position measurements. Individual rod position errors relative to the bank position are difficult to assess, etc.

The problems associated with rod worth estimation from position measurements can be overcome by using the facts that $\rho_{CR} = \rho_{MEASURED} - \rho_{fd}$ and that ρ_{fd} is estimated continuously in the balance meter.

Three complementary methods are available for determining rod worth with the reactivity balance meter (users options):

Method 1: The estimate of rod reactivity is the difference between measured total reactivity and estimated feedback reactivity:

$$\hat{\rho}_{CR} = \rho_{MEASURED} - \hat{\rho}_{fd}$$

where

$$\hat{\rho}_{fd} = \sum_{i=1}^4 \hat{\beta}_i \delta x_i \quad (\text{see section 4})$$

and where the $\hat{\beta}_i$ are the results of the most recent calibration. The estimate of ρ_{CR} is erroneous if the feedback coefficients have changed meanwhile. But the error will be small, since the β_i 's are not expected to vary much in comparison with rod reactivity contribution. An error can be present only during the small time interval between anomaly occurrence and subsequent on-line calibration.

It is noted that the expectation of the reactivity balance, $E[\Delta\rho]$, is zero as a consequence of the above equations and has little value as a surveillance variable. It will only indicate those discrepancies between $\rho_{MEASURED}$ and $\hat{\rho}_{fd} + \hat{\rho}_{CR}$ which are suppressed by the digital smoothing filter the estimate ρ_{CR} is passed through in order to reduce noise. Hence, $E[\Delta\rho]$ will only indicate transient anomalies which are present in $\rho_{MEASURED}$ or $\hat{\rho}_{fd}$ but not in $\hat{\rho}_{CR}$.

Anomalies would be detected in the diagnostic module by examining the itemized reactivity contributions rather than the reactivity balance, and by examining the parameter estimates, $\hat{\beta}_i$, after calibration.

Method 2: Position measurements are related to rod worth by the equation

$$\Delta h_{CR} = C_{CR} \cdot (\rho_{CR} - \rho_{CR,0}) + \xi_{CR}$$

The coefficient C_{CR} can be determined on-line with method 1 during set point change or rod movement, if no perturbation of feedback coefficients β_i has been indicated by the diagnostic module. Otherwise calibration of the β_i has to be repeated. Note that estimation of feedback coefficients and rod worth can be combined, if equation (4-17) instead of (4-16) is inserted into the observational equation.

The reactivity balance, Δg , may indicate here anomalies in ρ_{fd} and ρ_{CR} . But its diagnostic value is still seriously degraded by the opportunity of mutual compensations between anomalies. The diagnostic information lies in the itemized reactivity contributions and in the parameter estimates.

Method 3: $\rho_{CR} = \beta_{CR} \cdot (t - t_0) + \beta_{CR,0}$ where

β_{CR} and $\beta_{CR,0}$ are elements of the parameter vector ($L = 6$). If no rod movement occurs during calibration then $\beta_{CR} = 0$.

4.7 Diagnostics

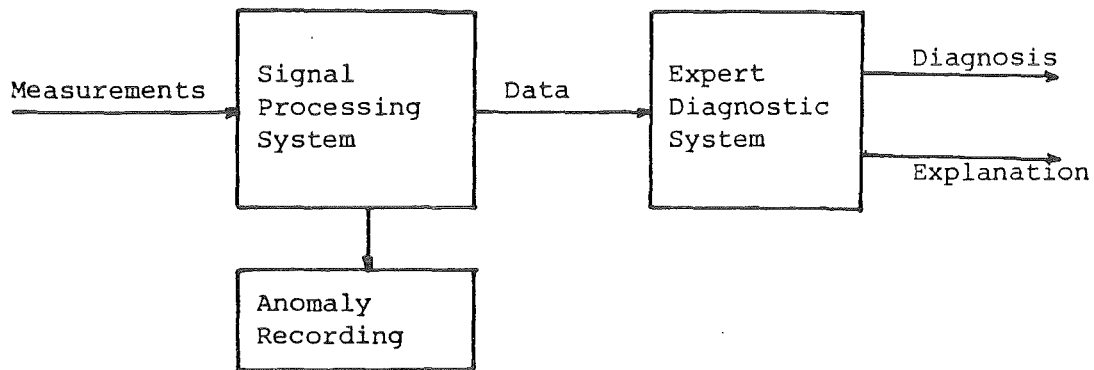
The diagnostic concept is beyond the study objectives and will, therefore, only be sketched briefly. It seems important to show the diagnostic potential inherent in parameter- and state estimation, to indicate the need for automizing the diagnostic process and to establish some connection to "artificial intelligence" / 13 /, / 14 /.

The "Global Core Surveillance Algorithms" are part of the Signal Processing System (Figure 7). The results of processing measured data are provided to the Expert Diagnostic System / 13 / where a pre-diagnosis is made. Every surveillance variable is classified

normal uncertain abnormal

dependent upon its value relative to a threshold and also dependent upon the classification of selected co-states. Then, during the next sampling interval, the prediagnosis will be evaluated by the knowledge based Expert System and a diagnosis will be made based on all the information available at this time. The built-in capability of learning by experience and deciding on the validity of the decision rules are important features / 13 /.

Figure 7:
Core Surveillance and Diagnosis



The Signal Processing System (= Global Core Surveillance) provides the following data to the Diagnostic-System at every sampling point:

Measurements: outlet temperature for every f. e., inlet temperature, flow-rate, neutron density, rod position (bank position), etc.

Core State: fuel temperature and smoothed average coolant temperature for every f. e., itemized reactivity contributions, in particular, the feedback reactivity and the effective control rod reactivity.

Core Parameters: heat transfer coefficient, coolant heat capacity, fraction of power and flow in every f. e., time constant and gain error of the thermo-couples at the outlet, the estimates of the reactivity feedback coefficients and control rod parameters.

Error Signals: observation residuals (mean values) of the Kalman filters for estimating subassembly thermohydraulic states and the reactivity balance. The basic function of the error signals is to provide a measure of uncertainty on the surveillance variables to the diagnostic modules.

The diagnostic potential can be improved by partitioning the reactivity model so that every fuel element has its own reactivity balance meter.

The large number of surveillance variables makes it already very desirable to automate a significant portion of the diagnostic process. But if one adds the even longer list of failure-states and logic operations which are necessary to clearly identify anomalies, then automation becomes mandatory.

Next, some of the features of the Global Surveillance Concept are summarized, which reduce the effort needed in the diagnostic module:

Estimation of Fuel Temperature

Fuel temperature is a very sensitive and relatively noiseless indicator of cooling anomalies. The availability of both, fuel and coolant temperatures provide information about the cause of anomalies. The amplitude ratio and the phase angle between $\delta\hat{T}_f$ and $\delta\hat{T}_c$ are dependent upon whether the origin of the perturbation lies in the fuel element power or in the coolant flow.

Gas Bubble Problem. Gas bubbles in the coolant do not only affect the reactivity measurement, but also the flow rate, heat transfer coefficient and heat capacity of the coolant; hence, gas bubbles influence both, the measured as well as the predicted reactivity leaving the balance $\Delta\rho$ unchanged.

Estimation of Feedback Reactivity Coefficients.

The time history of the feedback reactivity coefficients provides information on the combined effects of burn-up, conversion/breeding and poisoning. Prediction models would be required in order to separate these very low frequency components.

Estimation of Rod Reactivity Coefficients. Since both, β_{CR} and $\beta_{CR,0}$ are estimated, differential expansion effects can be diagnosed and the rod/bank characteristics will be available without costly calibration experiments.

Itemized Reactivity Contributions. Since feedback reactivity and control rod reactivity are both available as a function of time, the effect of normal control actions on reactivity can be easily distinguished from other types of reactivity perturbations. There is no need for special compensation devices in order to avoid false alarm.

Utilization of the Observation Residuals. Large expected values (time averages) of the observation residuals of the Kalman filter and the balance meter indicate systematic errors either in the measurements or in the prediction models. Bias in the ρ -measurement can be diagnosed by testing the consistency of ρ - and n -measurements assuming, that simultaneous occurrence of

biases is unlikely. Bias in the T_{Oj} -measurements can, for instance, be tested by comparing outlet temperatures of different fuel elements with equal flow and power.

Having established the presence of model errors, a calibration control sequence plus parameter estimation is to be initiated. The updated model parameters enter the Diagnostic System, if the corresponding observation residuals are now unbiased. Otherwise, the calibration procedure is repeated. If a second parameter estimation has not been successful either, then a model deficiency of unknown cause will be deduced and the corresponding observation residual will be classified "abnormal".

How the classification of the observation residuals, Δy , enters the pre-diagnosis will be shown with a simple example.

Example: If the fuel temperature disturbance, δT_{fj} , exceeds the threshold ϵ_{fj} longer than Δt_j and if Δy_j is "normal" or "uncertain", then the fuel temperature disturbance is classified abnormal. But if Δy is "abnormal", then the large fuel temperature disturbance is classified "uncertain".

Appendix A4.1: Compensation of Very Short Parameter Perturbations (Slug Flow)

Slug flow through a fuel element is characterized by a very short local perturbation of the heat transfer coefficient, flow rate and heat capacity (mass) in accordance with slug size and coolant velocity. It is certainly not possible to adjust the prediction model coefficients of the Kalman filter to these core parameter variations within fractions of a second. Hence, the state estimates will be erroneous (see Chapter 5) and the observation residual will be substantially different from zero during the time interval of filter distuning.

Consider the definition of observation residual:

$$(A4.1-1) \quad \Delta y_j \triangleq y_j - M \cdot \hat{x}_j^{j-1} - D u_j$$

or

$$(A4.1-2) \quad \Delta y_j = y_j + u_{2j} - 2 \cdot \left(\phi_{21} \cdot \delta \hat{T}_{f,j-1}^{j-1} + \phi_{22} \cdot \delta \hat{T}_{c,j-1}^{j-1} \right) \\ - 2 \cdot \left(\gamma_{21} u_{1j-1} + \gamma_{22} u_{2j-1} + \gamma_{23} u_{3j-1} \right)$$

Solving equation (A4.1-2) for $\delta \hat{T}_{f,j-1}^{j-1}$ and setting $\Delta y_j = 0$ gives the corrected fuel temperature estimate:

$$(A4.1-3) \quad \delta \hat{T}_{f,j-1}^{j-1} = \frac{1}{\phi_{21}} \cdot \left(\frac{1}{2} (y_j + u_{2j}) - (\gamma_{21} u_{1j-1} + \gamma_{22} u_{2j-1} + \gamma_{23} u_{3j-1}) \right. \\ \left. - \phi_{22} \delta \hat{T}_{c,j-1}^{j-1} \right)$$

The right hand side of equation (A4.1-3) depends upon measurements only, since $\hat{T}_c = 0.5 (T_o + T_I)$. The implementation of equation (A4.1-3) is shown in figure 8.

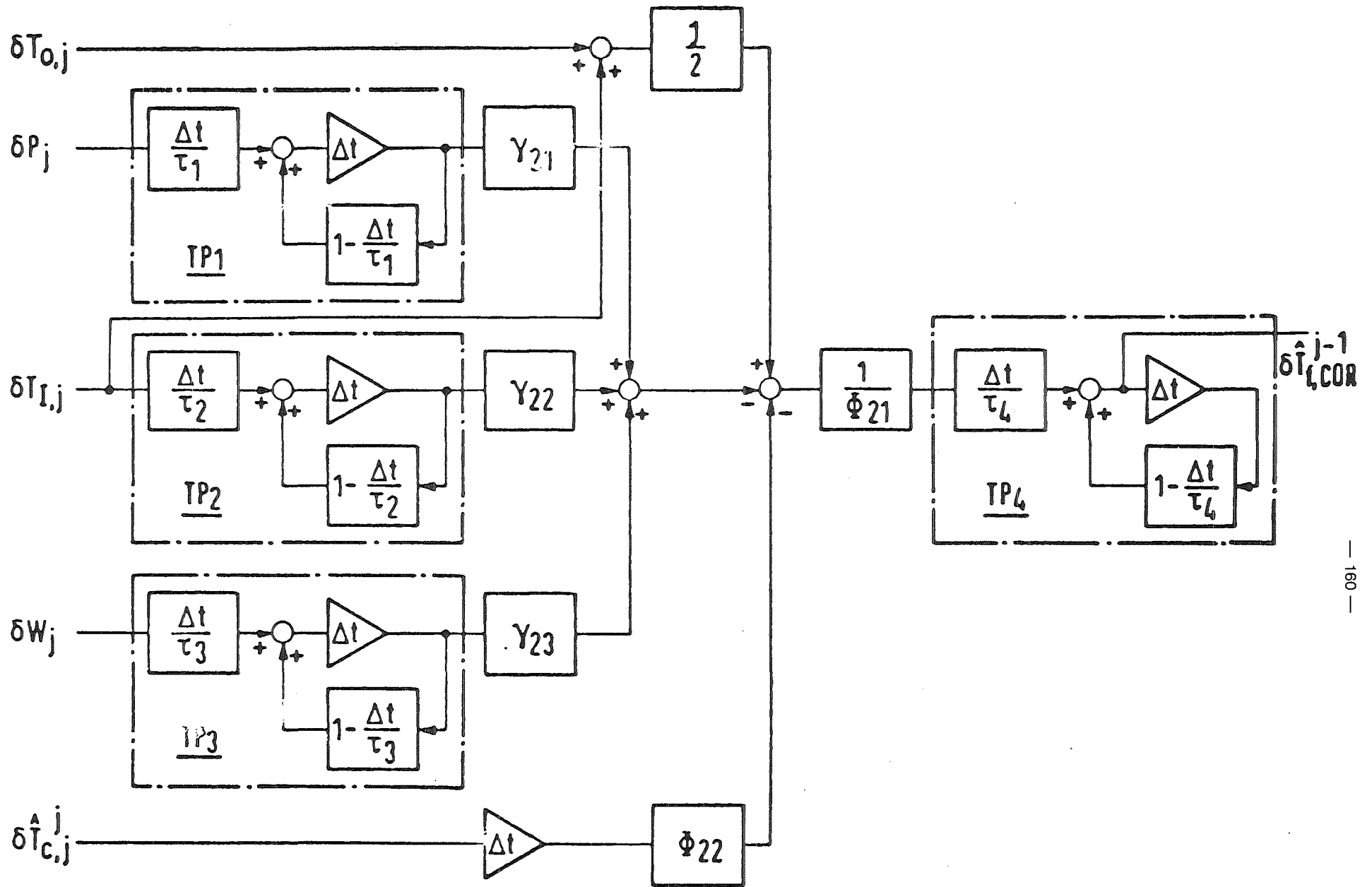


Figure 8 Compensation Device for Correcting the Fuel Temperature in Case of Slug Flow

Appendix A4.2 Augmented Kalman-Filter

Parameter estimation with the Augmented Kalman-filter is very attractive for continuously monitoring slow parameter variations, since it does not require the system inputs to be disturbed externally. Good experience has been made with estimating the flow parameter, α_w in addition to fuel and coolant temperature. The corresponding process equations will be given in the sequel.

Linearization of the equations (8) in Chapter III of reference / 5 / and subsequent discretization gives:

$$(A4.2-1) \quad x_{k+1} = \phi x_k + \Theta \xi_k + \Gamma u_k$$

$$(A4.2-2) \quad \xi_{k+1} = \xi_k$$

where

$$x^T = [\delta T_f, \delta T_c]$$

$$\xi = \delta \alpha_w$$

$$u^T = [\delta P, \delta T_s, \delta W]$$

ϕ, Γ are given in Chapter III of / 5 /

and

$$(A4.2-3) \quad \Theta^T = [\theta_1, \theta_2]$$

$$(A4.2-4) \quad \theta_1 = g \cdot L_1$$

$$\theta_2 = g \cdot L_2$$

$$(A4.2-5) \quad g = - \frac{2hW \cdot (\tau_1 - \tau_2)}{C_c}$$

$$L_1 = \frac{1}{\tau_1} \cdot \left[\frac{1}{s_1 s_2} - \frac{1}{s_1 \cdot (s_2 - s_1)} e^{s_1 \Delta t} + \frac{1}{s_2 \cdot (s_2 - s_1)} e^{s_2 \Delta t} \right]$$

$$L_2 = \frac{1}{\tau_2} \cdot \left[\frac{1}{s_1 s_2} - \frac{1 + \tau_1 s_1}{s_1 \cdot (s_2 - s_1)} e^{s_1 \Delta t} + \frac{1 + \tau_1 s_2}{s_2 \cdot (s_2 - s_1)} e^{s_2 \Delta t} \right]$$

Δt = sampling interval

s_1, s_2, τ_1 are given in /5/ in terms of the physical parameters.

The basic Kalman filter for estimating x operates in canonical space. The transformation between the output identifiable form and the original process equations is very simple and should not be made more complex by increasing state dimension. The Augmented Kalman filter is expressed, therefore, in a "mixed space" as follows:

$$(A4.2-6) \quad x = P \cdot \bar{x} \quad \bar{x} = \text{state vector canonical space}$$

$$P = V^{-1} \quad V = \text{observability matrix (observability index i equal 2)}$$

Applying transformation (A4.2-6) to the process (A4.2-1) gives

$$(A4.2-7) \quad \bar{x}_{k+1} = \bar{\Phi} \cdot \bar{x}_k + \bar{\Theta} \cdot \xi_k + \bar{\Gamma} \cdot u_k$$

$$\xi_{k+1} = \xi_k = \delta x_w$$

where

$$(A4.2-8) \quad \begin{aligned} \bar{\Phi} &= \bar{P}^{-1} \Phi P, & \bar{\Theta} &= \bar{P}^{-1} \Theta \\ \bar{\Gamma} &= \bar{P}^{-1} \Gamma \end{aligned}$$

and

$$(A4.2-9) \quad \bar{P}^{-1} = \begin{bmatrix} 0 & 2 \\ 2\phi_{21} & 2\phi_{22} \end{bmatrix} \quad \phi_{i,j} \text{ are elements of } \phi$$

Note that the third state component, $\xi = \delta\kappa_w$, remains unaffected by the transformation. It is obvious that the augmented transformation P^*

$$(A4.2-10) \quad P^* = \begin{bmatrix} P & 0 \\ 0 & 1 \end{bmatrix}$$

is non-singular, if P is non-singular. The equations (A4.2-7) can be combined in terms of the "augmented state vector \bar{x}^* ":

$$(A4.2-11) \quad \bar{x}_{k+1}^* = \bar{\Phi}^* \bar{x}_k^* + \bar{\Gamma}^* u_k$$

where

$$\begin{aligned} \bar{x}^{*T} &= [\bar{x}^T, \xi] \\ \bar{\Phi}^* &= \begin{bmatrix} \bar{\Phi} & \bar{\Theta} \\ 0 & 1 \end{bmatrix} & \bar{\Gamma}^* &= \begin{bmatrix} \bar{\Gamma} \\ 0 \end{bmatrix} \end{aligned}$$

Equation (A4.2-11) is the basis for the Augmented Kalman filter.

Appendix A4.3: Bias Errors in Least Square Estimation

The left hand side of equation (4-38) in itemized form becomes:

$$\frac{1}{N} \sum V^T =$$

$$= \sum_{k=1}^N \left[\begin{aligned} & v^k v^{k+2} - v^k v^k \lambda_1 - v^k v^{k+1} \lambda_2 - v^k \sum_{M1}^k \lambda_3 - v^k \sum_{M2}^k \lambda_4 - v^k \sum_{M3}^k \lambda_5 \\ & \quad - v^k \sum_{M1}^{k+1} \lambda_6 - v^k \sum_{M2}^{k+1} \lambda_7 - v^k \sum_{M3}^{k+1} \lambda_8 \\ & v^{k+1} v^{k+2} - v^{k+1} v^k \lambda_1 - v^{k+1} v^{k+1} \lambda_2 - v^{k+1} \sum_{M1}^k \lambda_3 - v^{k+1} \sum_{M2}^k \lambda_4 - v^{k+1} \sum_{M3}^k \lambda_5 \\ & \quad - v^{k+1} \sum_{M1}^{k+1} \lambda_6 - v^{k+1} \sum_{M2}^{k+1} \lambda_7 - v^{k+1} \sum_{M3}^{k+1} \lambda_8 \\ & \sum_{M1}^k v^{k+2} - \sum_{M1}^k v^k \lambda_1 - \sum_{M1}^k v^{k+1} \lambda_2 - \sum_{M1}^k \sum_{M1}^k \lambda_3 - \sum_{M1}^k \sum_{M2}^k \lambda_4 - \sum_{M1}^k \sum_{M3}^k \lambda_5 \\ & \quad - \sum_{M1}^k \sum_{M1}^{k+1} \lambda_6 - \sum_{M1}^k \sum_{M2}^{k+1} \lambda_7 - \sum_{M1}^k \sum_{M3}^{k+1} \lambda_8 \\ & \sum_{M2}^k v^{k+2} - \sum_{M2}^k v^k \lambda_1 - \sum_{M2}^k v^{k+1} \lambda_2 - \sum_{M2}^k \sum_{M1}^k \lambda_3 - \sum_{M2}^k \sum_{M2}^k \lambda_4 - \sum_{M2}^k \sum_{M3}^k \lambda_5 \\ & \quad - \sum_{M2}^k \sum_{M1}^{k+1} \lambda_6 - \sum_{M2}^k \sum_{M2}^{k+1} \lambda_7 - \sum_{M2}^k \sum_{M3}^{k+1} \lambda_8 \\ & \sum_{M3}^k v^{k+2} - \sum_{M3}^k v^k \lambda_1 - \sum_{M3}^k v^{k+1} \lambda_2 - \sum_{M3}^k \sum_{M1}^k \lambda_3 - \sum_{M3}^k \sum_{M2}^k \lambda_4 - \sum_{M3}^k \sum_{M3}^k \lambda_5 \\ & \quad - \sum_{M3}^k \sum_{M1}^{k+1} \lambda_6 - \sum_{M3}^k \sum_{M2}^{k+1} \lambda_7 - \sum_{M3}^k \sum_{M3}^{k+1} \lambda_8 \\ & \sum_{M1}^{k+1} v^{k+2} - \sum_{M1}^{k+1} v^k \lambda_1 - \sum_{M1}^{k+1} v^{k+1} \lambda_2 - \sum_{M1}^{k+1} \sum_{M1}^k \lambda_3 - \sum_{M1}^{k+1} \sum_{M2}^k \lambda_4 - \sum_{M1}^{k+1} \sum_{M3}^k \lambda_5 \\ & \quad - \sum_{M1}^{k+1} \sum_{M1}^{k+1} \lambda_6 - \sum_{M1}^{k+1} \sum_{M2}^{k+1} \lambda_7 - \sum_{M1}^{k+1} \sum_{M3}^{k+1} \lambda_8 \end{aligned} \right]$$

$$\left[\begin{aligned}
 \sum_{M_2}^{K+1, K+2} v^k &= \sum_{M_2}^{K+1, K} \lambda_1 - \sum_{M_2}^{K+1, K+1} \lambda_2 - \sum_{M_2}^{K+1, K} \lambda_3 - \sum_{M_2}^{K+2, K} \lambda_4 - \sum_{M_2}^{K+2, K} \lambda_5 \\
 &\quad - \sum_{M_2}^{K+1, K+1} \lambda_6 - \sum_{M_2}^{K+1, K+1} \lambda_7 - \sum_{M_2}^{K+1, K+1} \lambda_8 \\
 \sum_{M_3}^{K+1, K+2} v^k &= \sum_{M_3}^{K+1, K} \lambda_1 - \sum_{M_3}^{K+1, K+1} \lambda_2 - \sum_{M_3}^{K+1, K} \lambda_3 - \sum_{M_3}^{K+1, K} \lambda_4 - \sum_{M_3}^{K+1, K} \lambda_5 \\
 &\quad - \sum_{M_3}^{K+1, K+1} \lambda_6 - \sum_{M_3}^{K+1, K+1} \lambda_7 - \sum_{M_3}^{K+1, K+1} \lambda_8
 \end{aligned} \right]$$

where $v^k = \eta^k + \sum_{M_2}^k$. Neglecting correlation of the measurement errors with respect to time and defining

$$\frac{1}{N} \sum_{k=1}^N \eta^k \eta^k = R$$

$$\frac{1}{N} \sum_{k=1}^N \sum_{M_i}^k \sum_{M_i}^k = Q_i$$

most of the above terms become zero.

$$\begin{aligned}
 \frac{1}{N} Z^T V &= - (R + Q_2) \lambda_1 - Q_2 \lambda_4 \\
 &\quad - (R + Q_2) \lambda_2 - Q_2 \lambda_7 \\
 &\quad - Q_1 \lambda_3 \qquad \qquad \qquad - Q_1 \lambda_6 \\
 &\quad - Q_2 \lambda_1 - Q_2 \lambda_4 \qquad \qquad - Q_2 \lambda_2 - Q_2 \lambda_7 \\
 &\quad - Q_3 \lambda_5 \qquad \qquad \qquad \qquad - Q_3 \lambda_8
 \end{aligned}$$

or

$$\left(\begin{array}{cc|cccccc} -(R+Q_2) & 0 & 0 & -Q_2 & 0 & 0 & 0 & 0 \\ 0 & -(R+Q_2) & 0 & 0 & 0 & 0 & -Q_2 & 0 \\ \hline 0 & 0 & -Q_1 & 0 & 0 & 0 & 0 & 0 \\ -Q_2 & 0 & 0 & -Q_2 & 0 & 0 & 0 & 0 \\ 0 & 0 & 0 & 0 & -Q_3 & 0 & 0 & 0 \\ 0 & 0 & 0 & 0 & 0 & -Q_1 & 0 & 0 \\ 0 & -Q_2 & 0 & 0 & 0 & 0 & -Q_2 & 0 \\ 0 & 0 & 0 & 0 & 0 & 0 & 0 & -Q_3 \end{array} \right) \begin{array}{l} \lambda_1 \\ \lambda_2 \\ \lambda_3 \\ \lambda_4 \\ \lambda_5 \\ \lambda_6 \\ \lambda_7 \\ \lambda_8 \end{array}$$

or

$$\frac{1}{N} Z^T V = \psi \cdot \lambda = \begin{pmatrix} \psi^{11} & \psi^{12} \\ \psi^{21} & \psi^{22} \end{pmatrix} \cdot \lambda$$

Appendix A4.4: Recursive Least Square and Kalman filter algorithms

Least Square Approach

The observational equations are

$$y^k = M^k \cdot \lambda + \eta^k$$

where

$$M = [m_1, m_2, \dots, m_L]$$

$$\lambda = [\lambda_1, \lambda_2, \dots, \lambda_L]$$

η = process plus measurement noise

L = number of parameters to be estimated

and k denotes sampling time. Estimates of the parameter vector λ are computed with the following recursive algorithms:

$$\hat{\lambda}^k = \hat{\lambda}^{k-1} + W^k \cdot (y^k - M^k \cdot \hat{\lambda}^{k-1})$$

$$W^k = P^{k-1} M^{kT} \cdot (M^k P^{k-1} M^{kT} + 1)^{-1}$$

$$P^k = P^{k-1} - P^{k-1} M^{kT} \cdot (M^k P^{k-1} M^{kT} + 1)^{-1} M^k P^{k-1}$$

The term $M^k P^{k-1} M^{kT}$ is a scalar and, hence, no matrix inversion is needed. Two users options are provided in the program to start the recursive algorithms:

Option 1: P^0 and $\hat{\Lambda}^0$ are input variables;

Option 2: P^0 and $\hat{\Lambda}^0$ are computed recursively from the data vector M^k for $k = L$
(minimum norm case)

$$C^k = (I - Q^{-1+k}) \cdot M^k, \quad Q^0 = 0$$

$$\beta^k = \frac{1}{C^{kT} \cdot C^k}$$

$$Q^k = Q^{k-1} + \beta^k C^k C^{kT}$$

$$g^k = \beta^k C^{kT}$$

$$R^k = (I - M^k g^k)^T \cdot R^{k-1} \cdot (I - M^k g^k) + g^{kT} \cdot g^k$$

$$\hat{\Lambda}^k = \hat{\Lambda}^{k-1} + g^{kT} \cdot (\beta^k - \hat{\Lambda}^{k-1,T} \cdot M^k)$$

$$R^0 = \hat{\Lambda}^0 = 0$$

Kalman filter

Process: $x^{k+1} = \phi x^k + \Gamma u^k$

$$y^k = M x^k + D u^k$$

Filter: $\hat{x}_{k+1}^{k+1} = \hat{x}_{k+1}^k + K_{k+1} \cdot (y_{k+1} - M \hat{x}_{k+1}^k - D u^{k+1})$

$$K_{k+1} = P_{k+1}^k M^T \cdot (M P_{k+1}^k M + R)^{-1}$$

Riccati-Equation for the Estimation Error Covariance Matrix:

$$P_{k+1}^k = \Phi P_k^k \Phi^T + \Gamma Q_k \Gamma^T$$

$$P_k^k = P_k^{k-1} - K_k M P_k^{k-1}$$

where

x^k = state vector at sampling time t_k

\hat{x}_j^j = estimate of state vector at time t_j based upon all measurements up to and including y_i

R = covariance matrix of measurement noise

Q = covariance matrix of process noise

Appendix A4.5

Conventional Reactivity Feedback Coefficients; Stationary Case

In order to derive the feedback coefficients β_P , β_T and β_W as explicit functions of core state, we start with a reactivity prediction model which is characterized by the fact that its coefficients are state independent.

A suitable model is:

$$(A4.5-1) \quad \rho_{fd} = \sum_j \left(\beta_{D,j} \delta T_{fj} + \beta_{C,j} \delta T_{Cj} + \beta_{A,j} \delta T_{fj} + \beta_{B,j} (\delta T_{S0} - \delta T_{SI})_j \right) + \beta_G \delta T_I^*$$

The state perturbations $(\delta T_{fj}, \delta T_{Cj}, \delta T_{S0j}, \delta T_{SIj})$ are solutions of the discrete state equations:

$$(A4.5-2) \quad \begin{pmatrix} \delta T_{fj}^k \\ \delta T_{Cj}^k \end{pmatrix} = \begin{pmatrix} \phi_{11j} & \phi_{12j} \\ \phi_{21j} & \phi_{22j} \end{pmatrix} \cdot \begin{pmatrix} \delta T_{fj}^{k-1} \\ \delta T_{Cj}^{k-1} \end{pmatrix} + \begin{pmatrix} \Gamma_{1j} & \Gamma_{12j} & \Gamma_{13j} \\ \Gamma_{2j} & \Gamma_{2j} & \Gamma_{23j} \end{pmatrix} \cdot \begin{pmatrix} \delta P^k \\ \delta T_I^k \\ \delta W^k \end{pmatrix}$$

The index j denotes the fuel element and the index k denotes sampling time. The stationary solution of (A4.5-2) for unit step inputs becomes

$$(A4.5-3) \quad \begin{pmatrix} \delta T_{fj} \\ \delta T_{Cj} \end{pmatrix} = \begin{pmatrix} g_{11j} & g_{12j} & g_{13j} \\ g_{21j} & g_{2j} & g_{23j} \end{pmatrix} \cdot \begin{pmatrix} \delta P_0 \\ \delta T_{I0} \\ \delta W_0 \end{pmatrix} = (I - \Phi)^{-1} \cdot \Gamma \cdot \begin{pmatrix} \delta P_0 \\ \delta T_{I0} \\ \delta W_0 \end{pmatrix}$$

$$\delta T_{I0}^* = \delta T_{I0}$$

$$\delta T_{SIj} = \delta T_{I0}$$

$$\delta T_{S0j} = \delta T_{0j} = 2 \delta T_{Cj} - \delta T_{I0}$$

Inserting (A4.5-3) into (A4.5-1) and collecting terms gives:

$$\begin{aligned} \beta_P &= \sum_j \left((\beta_{Dj} + \beta_{Aj}) g_{4j} + \beta_{Cj} g_{21j} + 2\beta_{Bj} g_{21j} \right) \\ \beta_W &= \sum_j \left((\beta_{Dj} + \beta_{Aj}) g_{13j} + \beta_{Cj} g_{23j} + 2\beta_{Bj} g_{23j} \right) \\ \beta_T &= \sum_j \left((\beta_{Dj} + \beta_{Aj}) g_{12j} + \beta_{Cj} g_{22j} - 2\beta_{Bj} + 2\beta_{Bj} g_{22j} \right) + \beta_G \end{aligned}$$

Suppose (for sensitivity analysis only) that all fuel elements are alike; then $g_{1,m,j} = g_{1,m}$ for all j and

$$\begin{aligned} \beta_P &= g_{41} \cdot \sum_j (\beta_{Dj} + \beta_{Aj}) + g_{21} \cdot \sum_j \beta_{Cj} + 2g_{21} \cdot \sum_j \beta_{Bj} \\ \beta_W &= g_{13} \cdot \sum_j (\beta_{Dj} + \beta_{Aj}) + g_{23} \cdot \sum_j \beta_{Cj} + 2g_{23} \cdot \sum_j \beta_{Bj} \\ \beta_T &= g_{12} \cdot \sum_j (\beta_{Dj} + \beta_{Aj}) + g_{22} \cdot \sum_j (\beta_{Cj} + 2\beta_{Bj}) - 2 \cdot \sum_j \beta_{Bj} + \beta_G \end{aligned}$$

or

$$\begin{aligned} \beta_P &= g_{41} \cdot (\beta_D + \beta_A) + g_{21} \beta_C + 2g_{21} \beta_B \\ \beta_W &= g_{13} \cdot (\beta_D + \beta_A) + g_{23} \beta_C + 2g_{23} \beta_B \\ \beta_T &= g_{12} \cdot (\beta_D + \beta_A) + g_{22} (\beta_C + 2\beta_B) - 2\beta_B + \beta_G \end{aligned} \tag{A4.5-4}$$

where the definition of the "global coefficients" is obvious.

Next, the model coefficients g_{ij} are expressed in terms of physical core parameters. Carrying out the matrix manipulations in (A4.5-3) gives:

$$(A4.5-5) \quad \begin{aligned} g_{11} &= \frac{A_{12} B_{21} - A_{22} B_{11}}{A_{11} A_{22} - A_{12} A_{21}} & g_{12} &= \frac{A_{12} B_{22} - A_{22} B_{12}}{A_{11} A_{22} - A_{12} A_{21}} & g_{13} &= \frac{A_{12} B_{23} - A_{22} B_{13}}{A_{11} A_{22} - A_{12} A_{21}} \\ g_{21} &= \frac{A_{21} B_{11} - A_{11} B_{21}}{A_{11} A_{22} - A_{12} A_{21}} & g_{22} &= \frac{A_{21} B_{12} - A_{11} B_{22}}{A_{11} A_{22} - A_{12} A_{21}} & g_{23} &= \frac{A_{21} B_{13} - A_{11} B_{23}}{A_{11} A_{22} - A_{12} A_{21}} \end{aligned}$$

where, for sufficiently small sampling interval, Δt ,

$$\phi_{ii} \cong 1 + A_{ii} \cdot \Delta t, \quad i = 1, 2$$

$$\phi_{ij} \cong A_{ij} \cdot \Delta t, \quad i \neq j$$

$$\Gamma_{ij} \cong B_{ij} \cdot \Delta t$$

and / 5 /

$$(A4.5-6) \quad \begin{aligned} A_{11} &= -\frac{K}{C_F}, & A_{12} &= \frac{K}{C_F} \\ A_{21} &= \frac{K}{C_C}, & A_{22} &= -\frac{K + 2C_p \alpha_w W}{C_C} \\ B_{11} &= \frac{\alpha_p}{C_F}, & B_{12} &= 0, & B_{13} &= 0 \\ B_{21} &= 0, & B_{22} &= \frac{2C_p \alpha_w W}{C_C}, & B_{23} &= -\frac{2C_p \alpha_w (T_C - T_F)}{C_C} \end{aligned}$$

Inserting (A4.5-6) into (A4.5-5) gives:

$$(A4.5-7) \quad \begin{aligned} g_{11} &= \frac{x_p \cdot (k + 2c_p x_w W)}{2c_p k x_w W} & g_{12} &= 1 & g_{13} &= \frac{T_i - T_c}{W} \\ g_{21} &= \frac{k x_p}{2c_p k x_w W} & g_{22} &= 1 & g_{23} &= g_{13} \end{aligned}$$

and

$$(A4.5-8) \quad \begin{aligned} \beta_p &= \frac{x_p}{2c_p k x_w W} [(\beta_D + \beta_A) \cdot (k + 2c_p x_w W) + (\beta_C + 2\beta_B) k] \\ \beta_w &= \frac{T_i - T_c}{W} [\beta_D + \beta_A + \beta_C + 2\beta_B] \\ \beta_T &= \beta_D + \beta_A + \beta_C + \beta_G \end{aligned}$$

Appendix A4.6

Non-stationary Version of the Conventional Reactivity Balance

It is of interest to assess in which manner the equations (A4.5-8) change if the core state is not restricted to remain stationary. In order to simplify the algebra only 4 reactivity feedback coefficients will be considered (namely β_D , β_A , β_C and β_G).

It is necessary to eliminate the core state in (A4.5-1) without being able to rely on the stationary relation (A4.5-3). In order to express the state in terms of the measurements P , T_I and W the state equations are transformed into canonical space (output identifiable form) where the desired non-stationary replacement of (A4.5-3) can be obtained.

The state equations in the original physical space are:

$$(A4.6-1) \quad \begin{aligned} x^{k+1} &= \phi \cdot x^k + \Gamma \cdot u^k \\ y^k &= M \cdot x^k + D \cdot u^k \end{aligned}$$

the transformed equations become:

$$(A4.6-2) \quad \begin{aligned} \bar{x}^{k+1} &= \bar{\phi} \cdot \bar{x}^k + \bar{\Gamma} \cdot u^k \\ y^k &= \bar{M} \cdot \bar{x}^k + \bar{D} \cdot u^k \end{aligned}$$

where

$$(A4.6-3) \quad \begin{aligned} x^k &= P \bar{x}^k, & \bar{\phi} &= P^{-1} \phi P, & \bar{\Gamma} &= P^{-1} \Gamma \\ \bar{M} &= M P, & \bar{D} &= D \end{aligned}$$

and

$$(A4.6-4) \quad P = \begin{pmatrix} -\frac{\phi_{22}}{2\phi_{21}} & \frac{1}{2\phi_{21}} \\ \frac{1}{2} & 0 \end{pmatrix} = [P_{ij}]$$

After some simple manipulations, we obtain:

$$\begin{pmatrix} \bar{x}_1^k \\ \bar{x}_2^k \end{pmatrix} = \begin{pmatrix} y^k \\ y^{k+1} \end{pmatrix} - \begin{pmatrix} 0 & d_1 & 0 \\ \bar{y}_{11} & \bar{y}_{12} & \bar{y}_{13} \end{pmatrix} \cdot \begin{pmatrix} \delta P^k \\ \delta T_z^k \\ \delta W^k \end{pmatrix} - \begin{pmatrix} 0 & 0 & 0 \\ 0 & d_1 & 0 \end{pmatrix} \cdot \begin{pmatrix} \delta P^{k+1} \\ \delta T_z^{k+1} \\ \delta W^{k+1} \end{pmatrix}$$

$$y^k = \delta T_0^k \quad = \text{core outlet temperature}$$

or, in the original space

$$(A4.6-5) \quad \begin{pmatrix} x_1^k \\ x_2^k \end{pmatrix} = \begin{pmatrix} P_{11} \delta T_0^k + P_{12} \delta T_0^{k+1} \\ P_{21} \delta T_0^k + P_{22} \delta T_0^{k+1} \end{pmatrix}$$

$$- \begin{pmatrix} P_{12} \bar{y}_{11} \delta P^k + (P_{12} \bar{y}_{12} + P_{21} d_1) \delta T_z^k + P_{12} \bar{y}_{13} \delta W^k \\ P_{22} \bar{y}_{11} \delta P^k + (P_{22} \bar{y}_{12} + P_{21} d_1) \delta T_z^k + P_{22} \bar{y}_{13} \delta W^k \end{pmatrix}$$

$$- \begin{pmatrix} P_{12} d_1 \delta T_z^{k+1} \\ P_{22} d_1 \delta T_z^{k+1} \end{pmatrix}$$

Inserting (A4.6-5) into (A4.5-1) gives:

$$\begin{aligned} S_{fd}^k &= -(\beta_D + \beta_A) P_{12} \bar{y}_{11} \delta P^k - (\beta_D + \beta_A) P_{12} \bar{y}_{13} \delta W^k \\ &\quad - [(\beta_D + \beta_A) \cdot (P_{12} \bar{y}_{12} - P_{11}) + \beta_C P_{21}] \cdot \delta T_I^k \\ &\quad + (\beta_D + \beta_A) \cdot P_{12} \cdot \delta T_I^{k+1} + \beta_G \delta T_I^{*k} \\ &\quad + [(\beta_D + \beta_A) P_{11} + \beta_C P_{21}] \delta T_0^k + (\beta_D + \beta_A) P_{12} \delta T_0^{k+1} \end{aligned}$$

or, since $P_{12} \bar{y}_{11} = 0$,

$$\begin{aligned} (A4.6-6) \quad S_{fd}^k &= -(\beta_D + \beta_A) P_{12} \bar{y}_{13} \delta W^k \\ &\quad - [(\beta_D + \beta_A) \cdot (P_{12} \bar{y}_{12} - P_{11}) + \beta_C P_{21}] \delta T_I^k + (\beta_D + \beta_A) P_{12} \delta T_I^{k+1} + \beta_G \delta T_I^{*k} \\ &\quad + [(\beta_D + \beta_A) P_{11} + \beta_C P_{21}] \cdot \delta T_0^k + (\beta_D + \beta_A) P_{12} \delta T_0^{k+1} \end{aligned}$$

Equation (A4.6-6) represents the reactivity feedback term in the balance equation for the non-stationary case. Note that it reduces to (A4.5-8) for stationary conditions, except for the bowing term which has been left out for convenience.

The coefficients in (A4.6-6) are functions of the thermohydraulic core parameters and can, in principle, be computed from the results obtained in the thermohydraulic surveillance module. Hence, the coefficients could be made easily available on-line for any set-point.

Appendix A4.7: Literature

- / 1 / A. H. Jazwinski
 "Stochastic Process and Filtering Theory"
 Academic Press, New York and London, 1970
- / 2 / M. A. Budin
 "Parameter Identification and State Es-
 timation for Linear Systems"
 Dissertation, Stanford University
 Aeronautical Engineering, 1970
- / 3 / E. V. Bohn, M. K. de Beer
 "Consistent Parameter Estimation in Multi-
 Input Multi-Output Discrete Systems"
 Automatica, Vol. 13, pp. 301 - 305
- / 4 / E. V. Bohn, H. Zuercher
 "Implementation of Optimum Estimation
 Algorithms of High-Performance Micro-
 processors"
 IEEE Trans. on Ind. Electronics and Contr.
 Instr., Vol. IECI-25, No. 4, November 1978
 pp. 334-339
- / 5 / A. Holick
 "Study on Micro-Processor Application to
 Accident Detection, Prevention and Process
 Control of Liquid Metal Cooled Fast Reactors"
 Final Report, Commission of the European
 Communities, Contract-No. 598-79-9 ECI D
 August 1980, Chapter III

- / 6 / A. Holick
"Surveillance Concept for LMFBR-Core-Cooling"
ITB 70.01821.7, November 1981
- / 7 / A. Holick
"Algebraic Bias Error Compensation in Recursive Least Square Algorithms"
ITB 70.01845.1, January 1982
- / 8 / A. Holick
"Mikrorechnergestützte Überwachung von Kühlungsstörungen im Core Schneller Brüter"
Fachtagung der Fachgruppe Reaktorphysik
10./11. März 1982, Offenbach, FRG
published in Atomkernenergie/Kerntechnik,
Bd. 41 (1982), Lfg. 3, p. 191
- / 9 / J. C. Gauthier, A. Gouriou, R. Jullian, L. Maire
"Comparateur de Réactivité"
IAEA-SM-244/28, pp. 429 - 446, Sept. 1979
- / 10 / J. C. Gauthier
"Reactivity Balance Meter: Feedback Effects Measurements at Phénix"
NEACRP Annual Meeting, Idaho, 22/24 Sept. 1980
- / 11 / J. C. Gauthier
Personal communications
Nov. 1981

/ 12 / R. A. Harris

Personal communications, October 1979

/ 13 / G. Le Guillow, J. P. Parcy, C. Berlin
"Application of Artificial Intelligence
to the Detection and Diagnosis of Core
Faults in Fast Reactors"

International Symposium on Nuclear Power
Plant Control and Instrumentation,
Munich, FRG, 11 - 15 October 1982

/ 14 / M. B. Abbott, J. J. de Nordwall, B. Swets
"On Applications of Artificial Intelligence
to the Control and Safety Problems of
Nuclear Power Plants", Final Report,
CEC sponsored study on A.I.

5. Performance Tests by Means of Simulation

A. Holick
INTERATOM

The performance of the GCSP has been tested by means of simulation, i.e. the measurements which are provided normally by the out-of-core instrumentation have been computed with the model of section 4.1 plus the neutron point kinetics equations with 6 groups of delayed neutrons:

$$\dot{n} = \frac{\rho - \beta}{\ell} \cdot n + \sum_{i=1}^6 \lambda_i C_i$$
$$\dot{C}_i = -\lambda_i C_i + \frac{\beta_i}{\ell} n \quad i = 1, \dots, 6$$

The physics of the model is rather crude, but contains all effects which need to be estimated on-line. It is practical to choose a continuous copy of the discrete prediction model of section 4.1. The results of parameter and state estimation can be checked easily with this reference and errors can be attributed to the cause. The model must hold only for first order perturbations about slowly moving set-points between 30 % and 110 % of nominal power.

The total core is subdivided into 1 fuel element and the remainder in order to simulate the local as well as the global effects.

The performance of the thermohydraulic surveillance modules is shown in section 5.1, while section 5.2 contains the results of the reactivity surveillance tests.

5.1 Performance of Core Cooling Surveillance

Emphasized are anomalies such as slug-flow, partial blockage with simultaneous perturbation of the radial power distribution, and on-line calibration by means of parameter estimation (rather than blindfolded removal of slowly developing bias).

Sensitive Monitoring of Subassembly Cooling by Determining Fuel Temperature in Addition to the Coolant Temperatures

The noise problem is significantly reduced by both, the smoothing effect of the Kalman filter and the time constant of the fuel with respect to temperature transients.

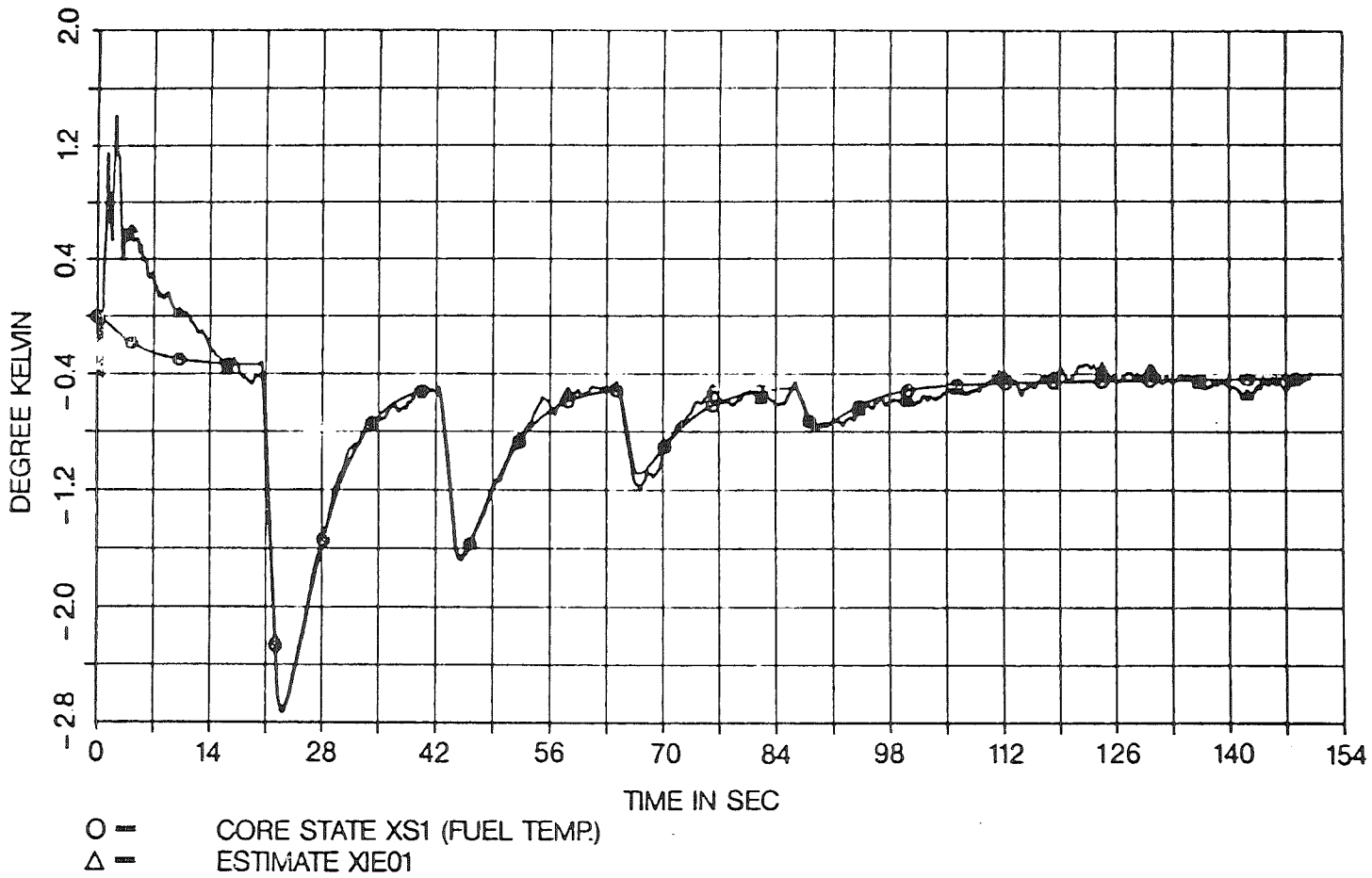
The effect of a sequence of flow disturbances with decreasing amplitudes is shown in Figure 9. The disturbance impulses of 2 seconds length have an amplitude of 2 %, 1 %, 0.5 % and 0.25 % of the nominal flow rate. Even the very small fourth impulse shows a recognizable effect upon fuel temperature.

Parameter Estimation

The core inputs were disturbed with binary random sequences in addition to the simulated process noise.

Disturbance amplitudes were in the order of 2 % of the nominal values. The measurement noise (responsible for the bias) has the following standard deviations:

$$\begin{aligned}\sigma(T) &= 0.1 \text{ [}^{\circ}\text{C]} \\ \sigma(W) &= 1.5 \text{ [kg/s]} \\ \sigma(P) &= 3 \cdot 10^{+3} \text{ [W]}\end{aligned}$$



**CORE SURVEILLANCE KNK-II
FLOW-DISTURBANCE
IN FUEL-ELEMENT**

Figure 9

Table 6 shows the estimates after 200 measurement samples have been processed. No significant changes occur if the number of measurements is increased up to 600. The algebraic compensation procedure is applied only once, i. e. after all measurements have been processed. The bias errors can be reduced from almost 100 % down to approximately 1 %.

The fraction of the bias errors which is caused by the input measurement noise can also be reduced by pre-filtering. This is no problem in the case of step disturbances. If random disturbances are required, then a trade-off opportunity exists between the frequency contents of the disturbances (pulse length), sampling interval and the critical frequency of the pre-filter (see section 6.2).

Computation of the system matrices ϕ and Γ from the parameters is rather simple. The error in the elements of the system matrices is in the order of 1 %. These updated matrices are supplied to the Kalman filter and guarantee the basic surveillance function.

The physical core parameters can be computed from the Λ -parameters in various ways. If all parameters are required simultaneously a Newton-Raphson procedure provides the result. The maximum error is approximately 20 % (at present) despite the small errors in Λ . If only single parameters are to be monitored then very simple equations are available (see section 4.4) and the estimation error reduces down to approximately 1 %.

Table 6: Accuracy of Parameter Estimation

	λ_1	λ_2	λ_3	λ_4	λ_5	λ_6
Exact Values	-0.4269	1.4061	$0.48126 \cdot 10^{-2}$	0.3608	$0.638 \cdot 10^{-2}$	-0.3782
L. S. Estimates (Biased)	-0.3492	1.2371	$0.9126 \cdot 10^{-2}$	0.2971	$0.3442 \cdot 10^{-2}$	-0.3780
Unbiased Estimates	-0.4329	1.4177	$0.4821 \cdot 10^{-2}$	0.3641	$0.639 \cdot 10^{-2}$	-0.3774
Error ^{*)}	1.4 %	0.8 %	0.17 %	0.9 %	0.16 %	0.2 %

^{*)} Difference between the exact values and the unbiased estimates (performance measure of bias-compensation)

3.4 Detection and Identification of Slug Flow
 (see Appendix A4.1)

A sequence of 4 slugs of decreasing axial length has been tested by means of simulation (Figure 10). The axial length and corresponding reactivity effects of the test bubbles (gas) are summarized in table 7. Note that the test bubbles No. 3 and 4 are not detectable with the reactimeter.

The corresponding fuel element outlet temperature is shown in Figure 10. Slug No. 3 and 4 are already close to the noise level. But even if the bubbles are sufficiently large to cause a recognizable outlet temperature perturbation (slug No. 1 and 2), the nature of this perturbation remains dubious.

Table 7: Effect of Test Slugs in 1 Fuel Element on Reactivity (KNK-II)

Slug No.	1	2	3	4
Slug Length (fraction of active core length)	0.40	0.20	0.10	0.05
Reactivity Contribution (%)	2.8	1.4	0.7	0.35

The average fuel temperature in the fuel element affected (figure 11) is a sensitive indicator of such short cooling disturbances. Even the test bubbles No. 3 and 4 produce fuel temperature perturbations which are quite distinct from the noise.

The availability of both, fuel and coolant temperatures provide an opportunity for analysing the cause of anomalies. The amplitude ratio and the phase angle between $\delta\hat{T}_F$ and $\delta\hat{T}_C$ are dependent upon whether the origin of the perturbation lies in the fuel element power or in the coolant flow. Comparison of the Figures 9 and 11 illustrates this diagnostic potential.

In Figure 9 only the mass flow is disturbed. All the other core parameters (k, κ_p, C_c) remain constant. The reactivity feedback effect causes negative power perturbations which dominate the effect of cooling disturbances on fuel element temperature. Fuel and coolant temperature perturbations are of opposite sign.

Slug flow causes not only flow perturbations but also perturbations of the heat transfer between fuel and coolant and of the heat capacity (mass of coolant). Figure 11 shows that the disturbed heat transfer between fuel and coolant dominates the power perturbations caused by the reactivity feedback effects. The fuel temperature disturbance has positive sign.

Continuous Monitoring of Subassembly Flow

If continuous monitoring of κ_w is desirable without having to disturb the system externally, the "Augmented Kalman filter" provides a solution (see section 4.6). Fig. 13 shows continuous tracking of a κ_w -ramp of $1 \cdot 10^{-3} / 1/s$ /. In order to maintain the estimation accuracy demonstrated in Figure 13 it is necessary that all the other core parameters (k, κ_p, C_c) remain constant. Otherwise the observation residual of the Kalman filter will tend to deviate from zero indicating increasing estimation error in κ_w and a new calibration (parameter estimation) must be initiated.

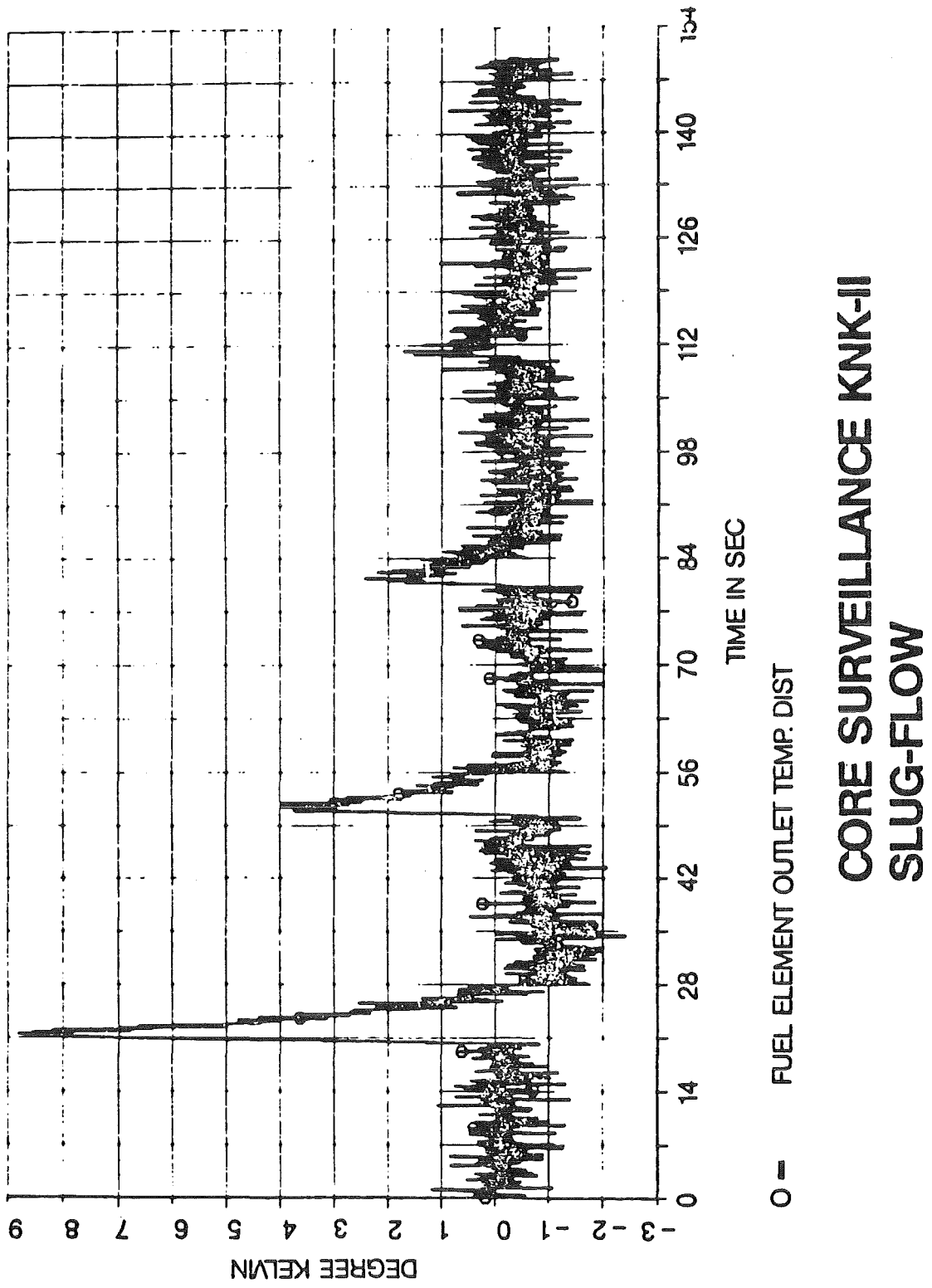
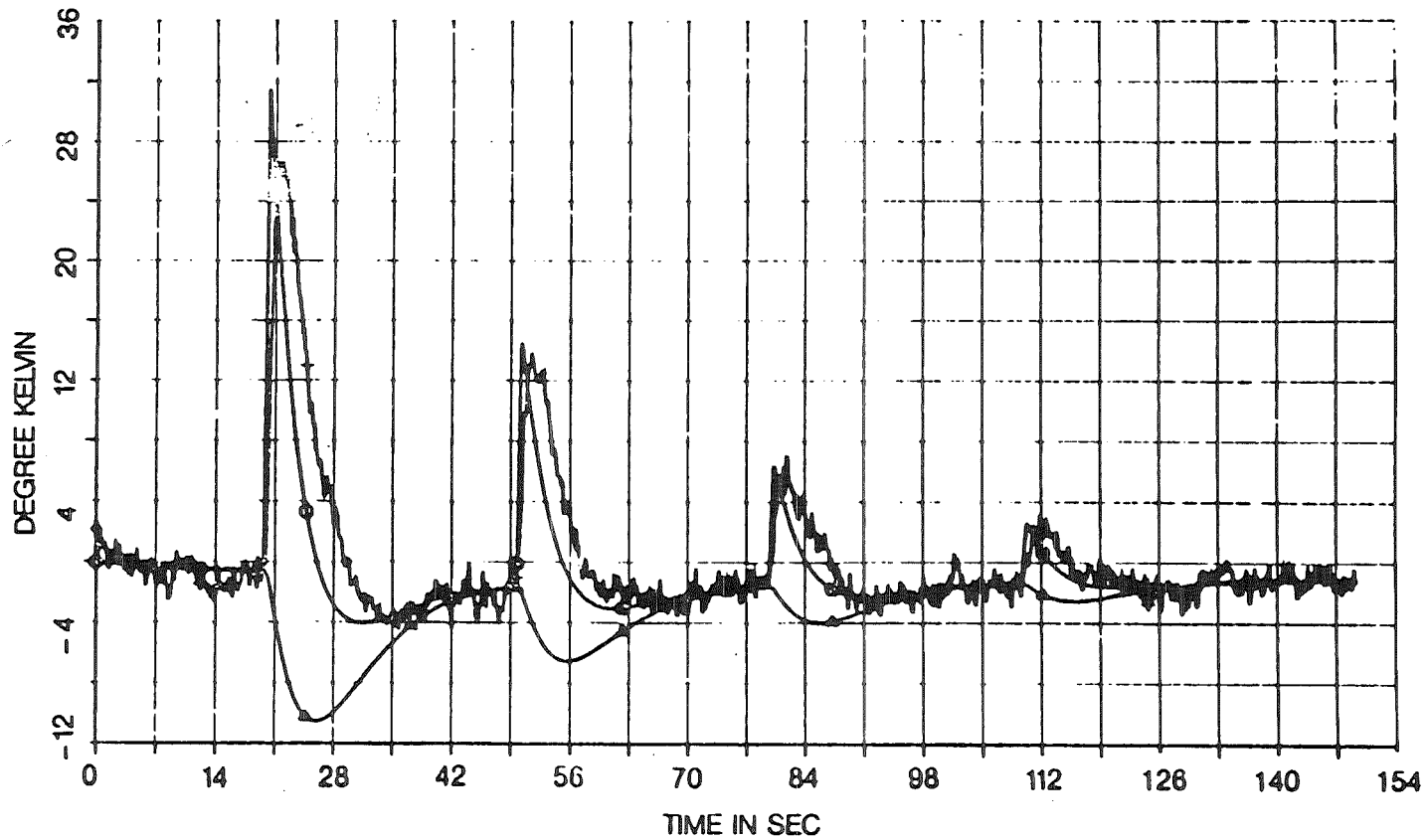


Figure 10



O | CORE STATE XS1 (FUEL TEMP.)
 Δ | ESTIMATE XIE01
 + | CORRECTED FUEL TEMP. ESTIMATE

CORE SURVEILLANCE KNK-II
SLUG-FLOW
SAMPLING INTERVAL = 0.025

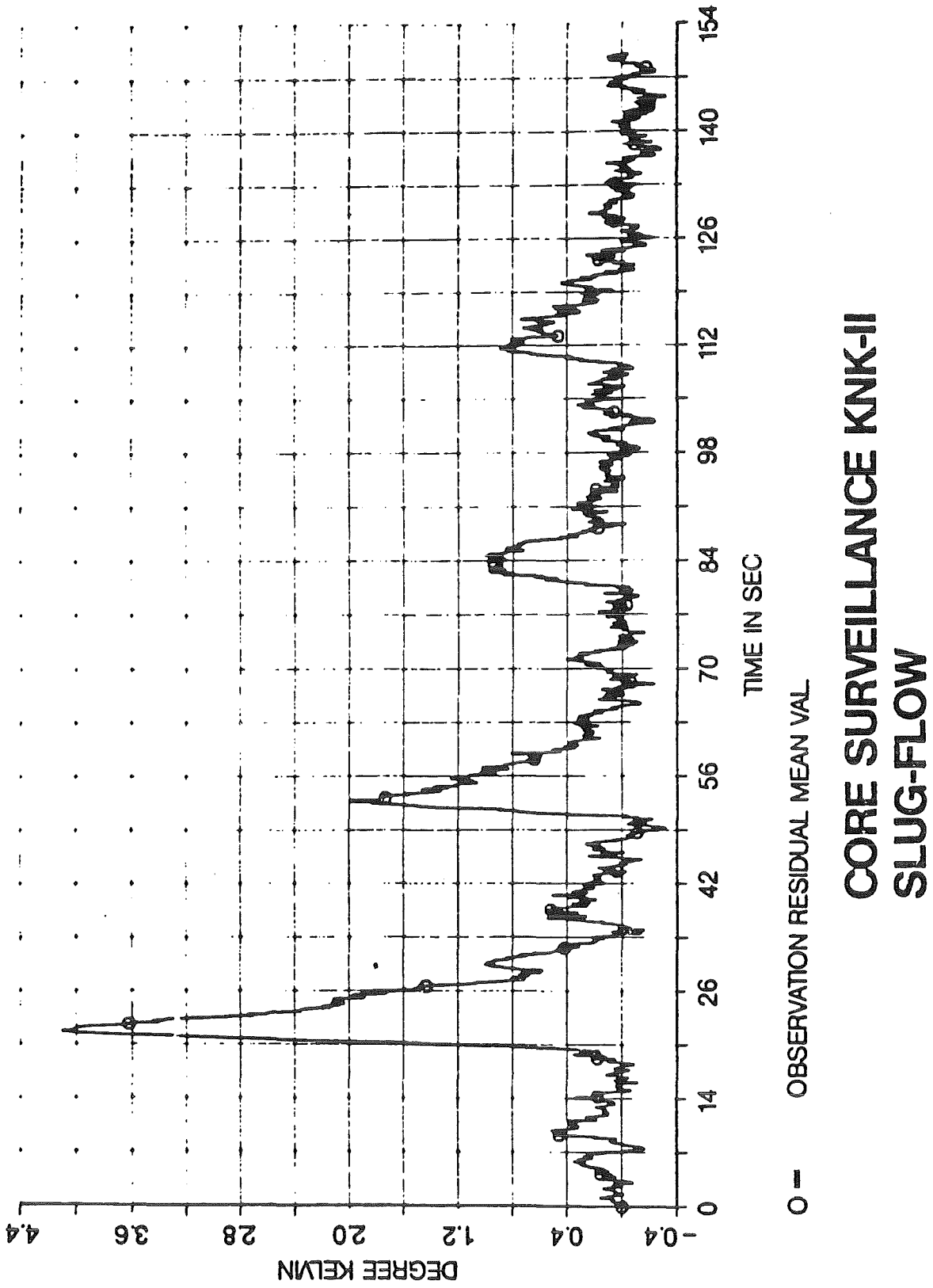
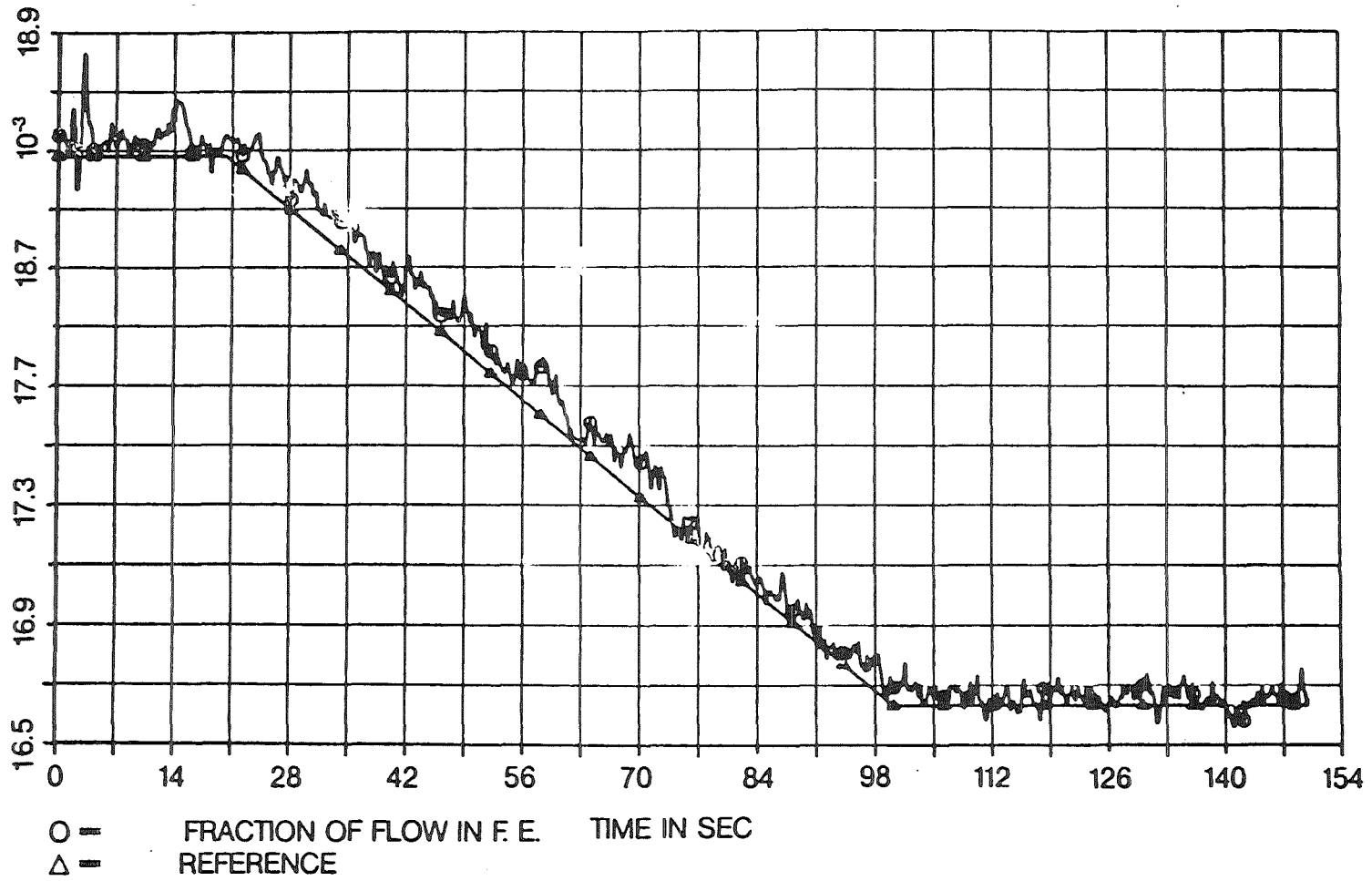


Figure 12



CORE SURVEILLANCE KNK-II PARTIAL BLOCKAGE IN FUEL-EL

5.2 Performance of Reactivity Surveillance

Performance of the reactivity surveillance procedure is tested in this section in terms of selected examples and with some emphasis on nonstationary operation.

On-Line Estimation of Reactivity Feedback Coefficients

Table 5 shows a set of elementary disturbance profiles, which suffices to estimate all reactivity feedback parameters including the grid plate coefficient. If the latter is not required, then bank position can replace the inlet temperature disturbance in Table 5 and flow disturbance is only needed for estimating the bowing coefficient β_B . No sufficient effort has been expended yet to investigate the minimal disturbance amplitudes required. This task will be taken up again in context with experiments. It suffices for the time being to recognize, that plant operation will only be disturbed occasionally by a small power perturbation (see Table 5) of less than 2 minutes duration. It is proposed to automatize the calibration process and to develop a microcomputer based calibration control module which initiates, terminates and checks the input disturbances.

The accuracy achieved with the disturbance set of Table 5 is in the order of 3 %, if more than one parameter have to be estimated simultaneously (differential expansion effects included). If, for instance, only the Doppler plus axial expansion coefficients are needed, then the estimation error is less than 1 % after 200 measurement samples.

Estimation of Control Rod Worth

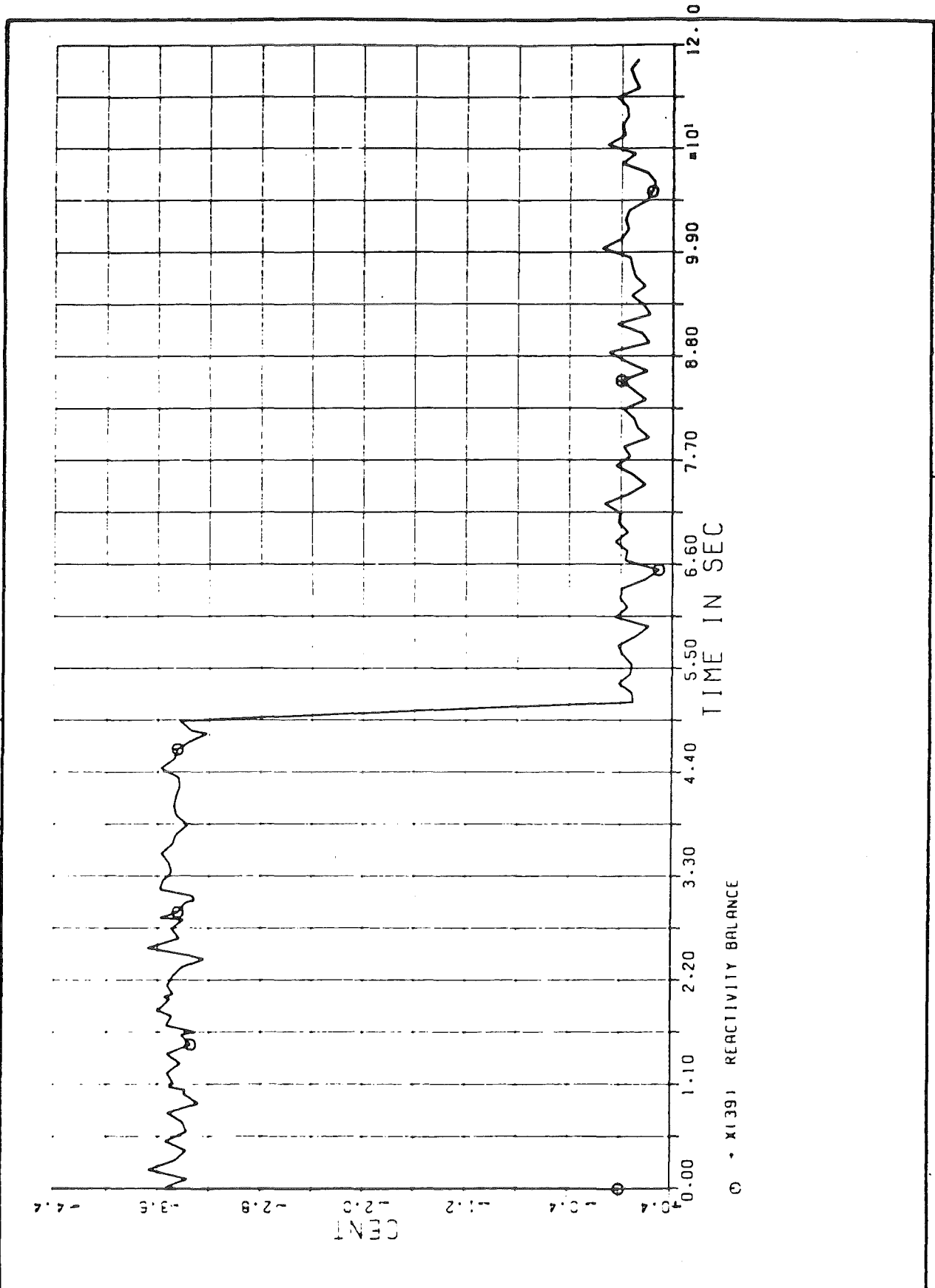
Example 1: Differential expansion at time zero results in a constant external reactivity contribution of $\rho_{CR,0} = 0.2 \cdot 10^{-3} = 3.48 \phi$

The reactivity balance (Figure 14) shows the bias of the rod worth estimate with method 2. The calibration procedure is initiated arbitrarily at $t = 10$ seconds. Updated estimates of the β -parameters are available after 40 seconds (200 measurement samples). The bias in $E \overline{\Delta \rho}$ disappears and the remaining random fluctuations are in the order of $\pm 0.2 \phi$.

Rod worth estimates based upon method 1 and 2, respectively, are shown in the figures 15 and 16. Method 1 gives the correct solution, while method 2 cannot get a grasp at the differential expansion effect.

Since the rod worth estimate with method 1 coincides with Δ_0 , it may be assumed that the feedback coefficients of the prediction model are correct and, hence, calibration would not be required.

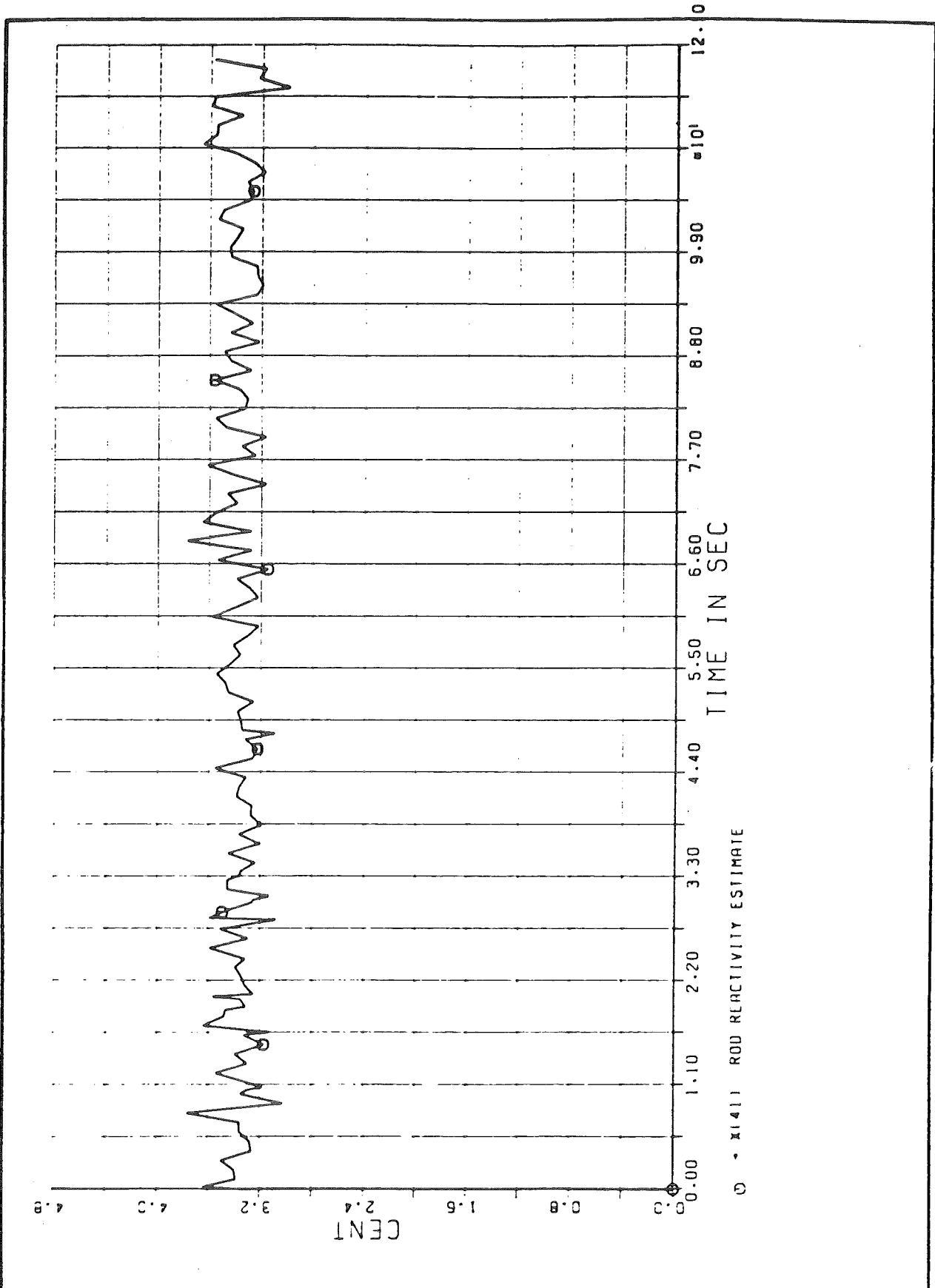
INTERATOM



REACTIVITY BALANCE KNK-II
DIFFERENTIAL EXPANSION
CALIBRATION BETWEEN 10-50 SEC

FIG. 14

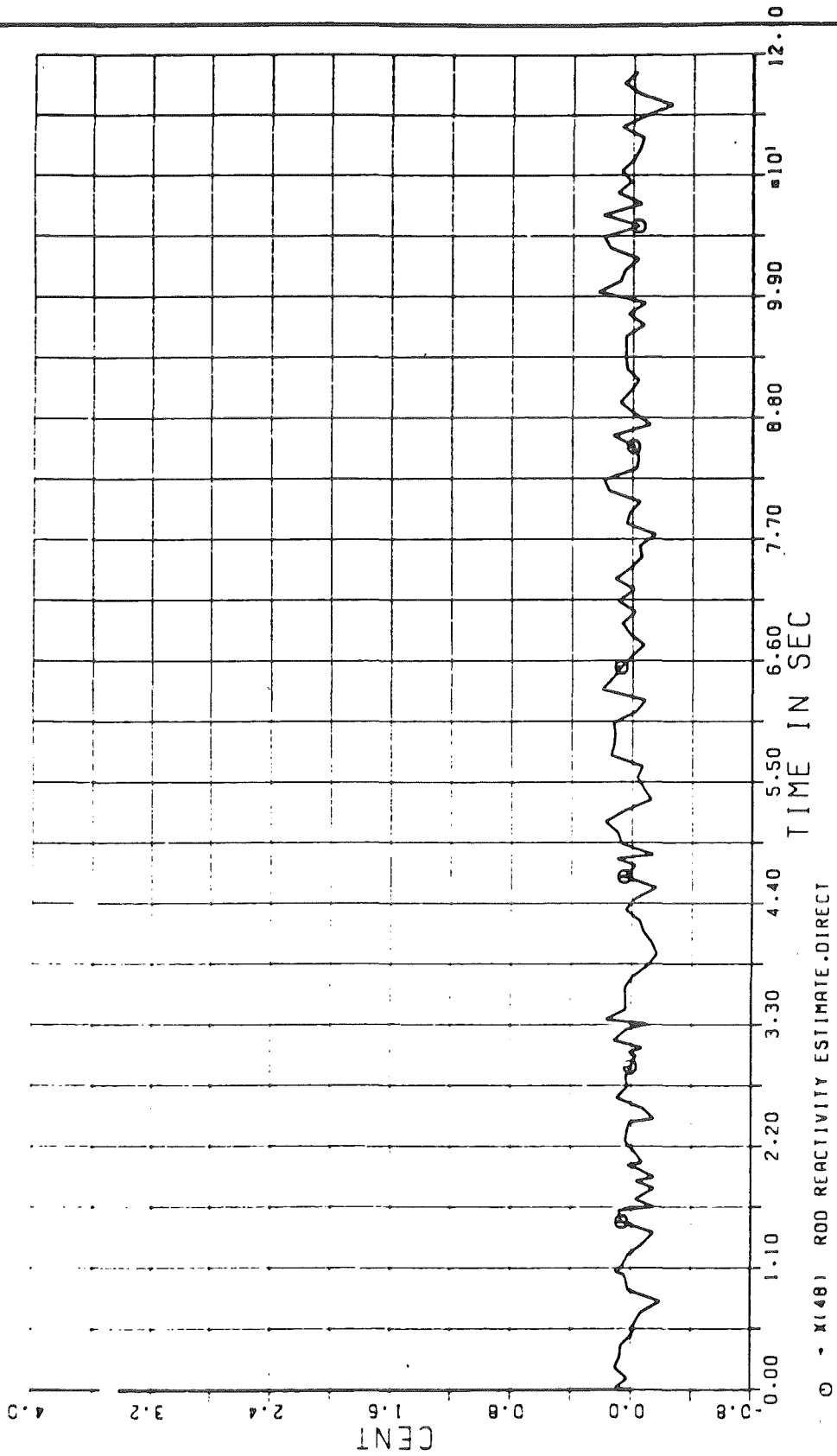
INTERATOM



REACTIVITY BALANCE KNK-II,
DIFFERENTIAL EXPANSION
CALIBRATION BETWEEN 10-50 SEC

FIG. 15

INTERATOM



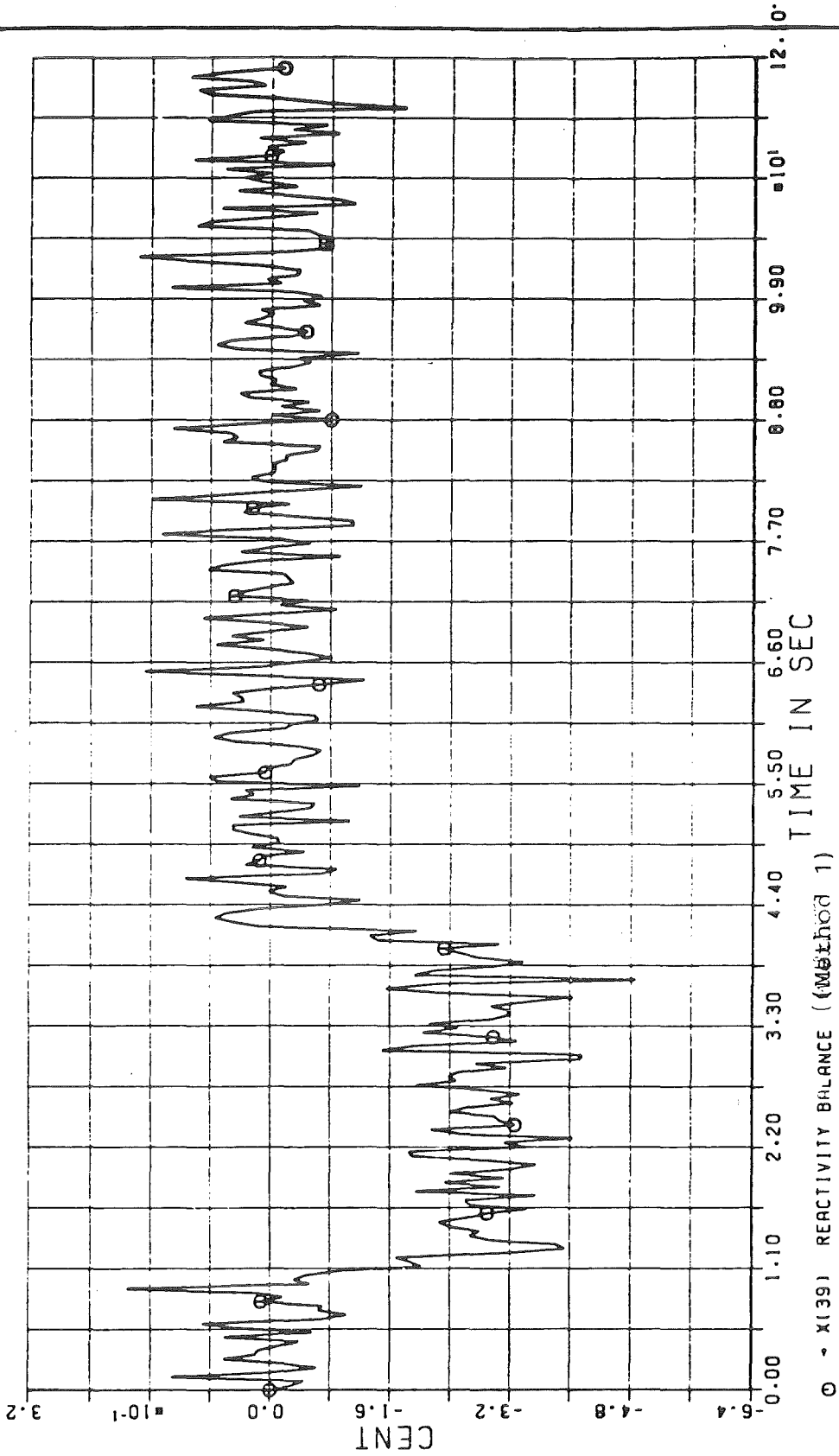
REACTIVITY BALANCE KNK-II
DIFFERENTIAL EXPANSION
CALIBRATION BETWEEN 10-50 SEC

FIG. 16

Example 2: Ramp-like rod movement between 10 and 40 seconds; maximum rod contribution is - 17.4 ϕ . No calibration.

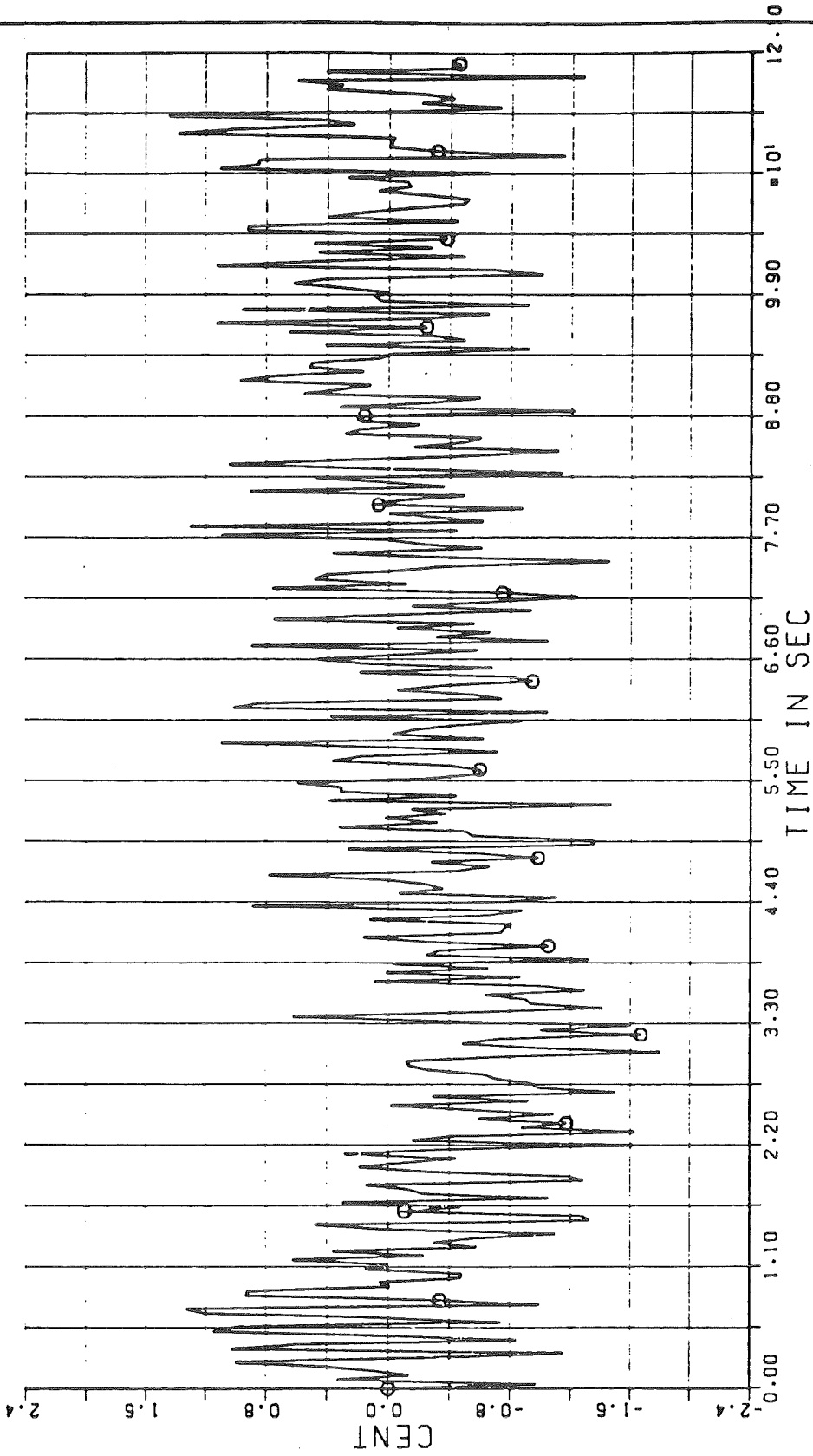
The reactivity measurement and the corresponding neutron density (noiseless) are shown in the figures 18 and 19. The estimated rod worth in figure 20 illustrates the accuracy of method 1 since no feedback coefficient errors are indicated by the reactivity balance of method 2. The itemized feedback reactivity estimates do not announce any anomaly either. Therefore, the rod reactivity estimate of figure 20 is an acceptable estimate of the actual rod contribution. Method 2 gives the same result for $\hat{\rho}_{CR}$, because no differential expansion has occurred by assumption. Note that the rod speed profile (rod motion may be staggered) has no effect on estimation accuracy and that position measurements are not required.

INTERATOM



COMPENSATION OF CONTROL ACTION
IN THE REACTIVITY BALANCE SIG.
ROD RAMP BETWEEN 10-40 SEC.

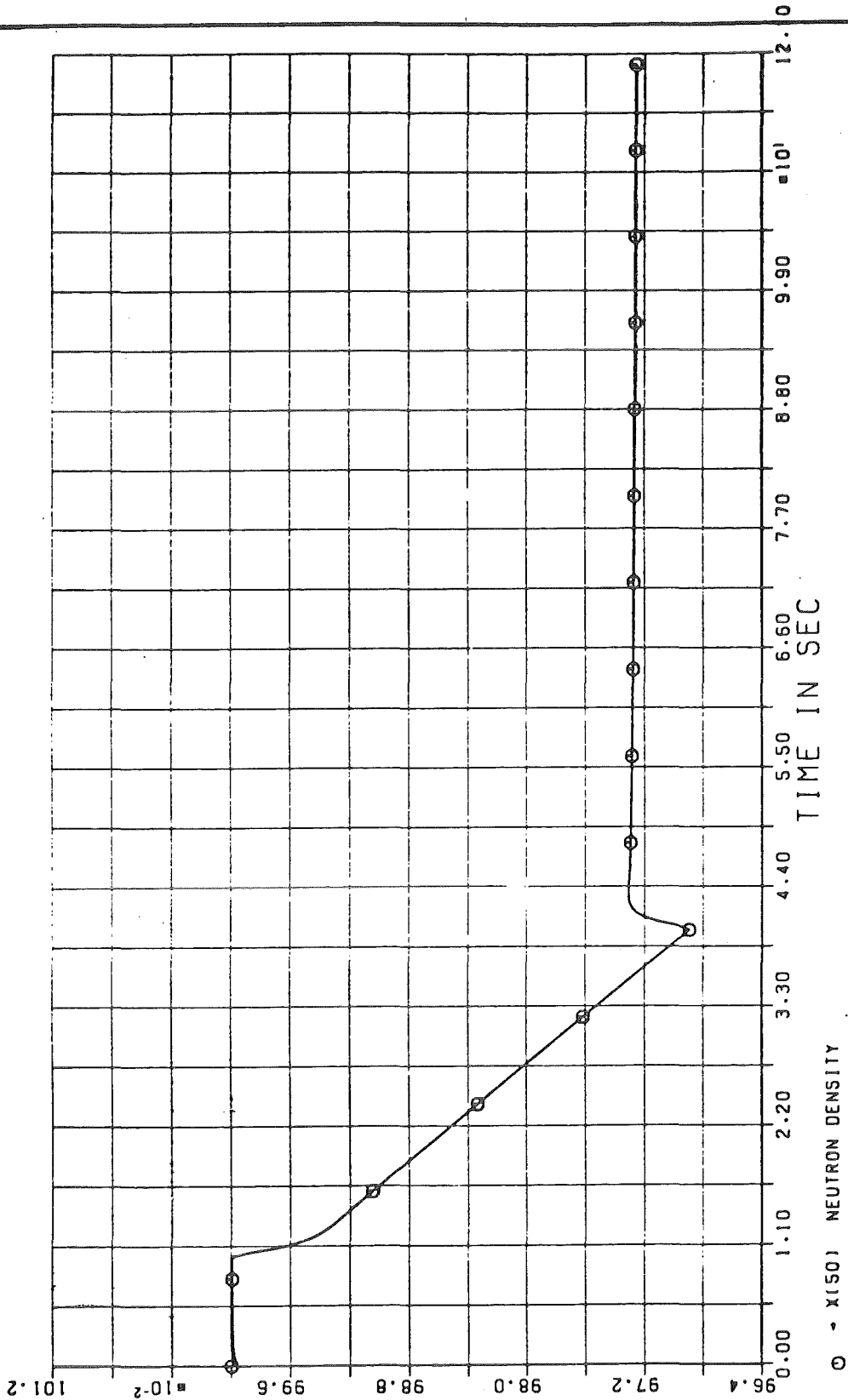
FIG. 17



COMPENSATION OF CONTROL ACTION
IN THE REACTIVITY BALANCE SIG.
ROD RAMP BETWEEN 10-40 SEC.

FIG. 18

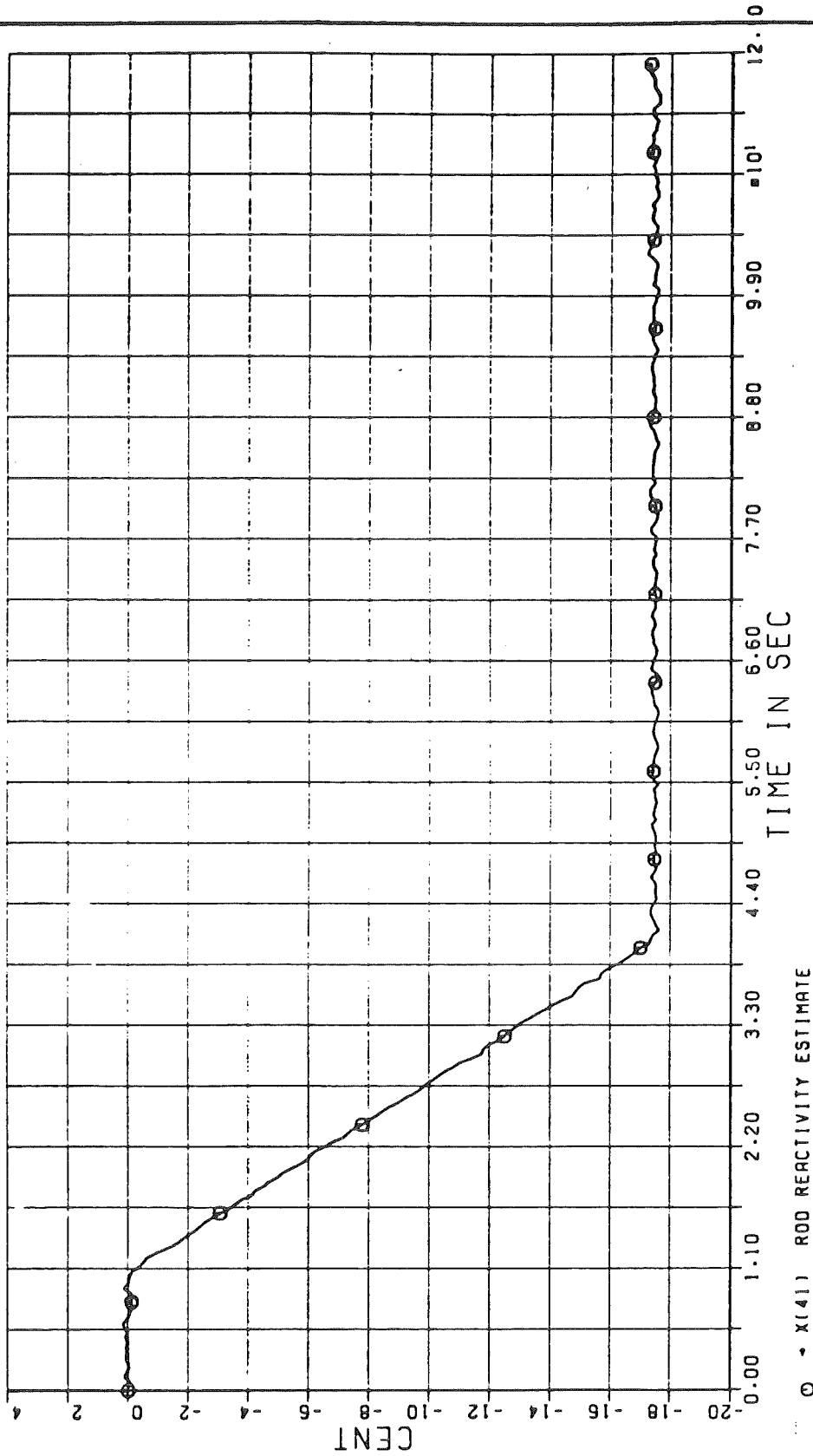
INTERATOM



COMPENSATION OF CONTROL ACTION
IN THE REACTIVITY BALANCE SIG.
ROD RAMP BETWEEN 10-40 SEC.

FIG. 19

INTERATOM



○ - X(41) ROD REACTIVITY ESTIMATE

COMPENSATION OF CONTROL ACTION
IN THE REACTIVITY BALANCE SIG.
ROD RAMP BETWEEN 10-40 SEC.

FIG 20

Reactivity Surveillance during Non-Stationary Operations

The essential result of this section is that the surveillance sensitivity or diagnostic potential is not degraded during set point changes. The time dependent control rod contributions can be determined with high accuracy even in the presence of differential expansion effects. No special compensation device is needed to eliminate the effect of rod movements on the reactivity balance.

The same holds for flow disturbance or inlet temperature disturbance. The predicted feedback reactivity (4-15) will always (in the absence of anomalies) be very near to the actual value, since the fuel temperature and structure temperatures are available via "indirect measurements".

In a first test example, the set point is reduced from 100 % to approximately 80 % of nominal power ramp-like between 10 and 130 seconds (figure 21). The maneuver is repeated with opposite sign between 250 and 370 seconds. The reactimeter outputs are shown in the figures 22 to 28. The reactivity balance signal (method 1, figure 22) is slightly biased during the periods of rod movement as a consequence of smoothing $\hat{\rho}_{CR}$:

$$\Delta\rho = \rho_{MEASURED} - \sum_{i=1}^5 \hat{\beta}_i \delta x_i$$

$$\hat{\beta}_5 = \hat{\rho}_{CR} \dots \text{smoothed}$$

For method 1 (section 4.6)

$$\hat{\rho}_{CR} = \rho_{MEASURED} - \sum_{i=1}^4 \hat{\beta}_i \delta X_i$$

and needs to be smoothed mainly because of the noise in $\rho_{MEASURED}$. For method 2 (figure 23)

$$\hat{\rho}_{CR} = \frac{\Delta h_{CR}}{C_{CR}} + \rho_{CR,0}$$

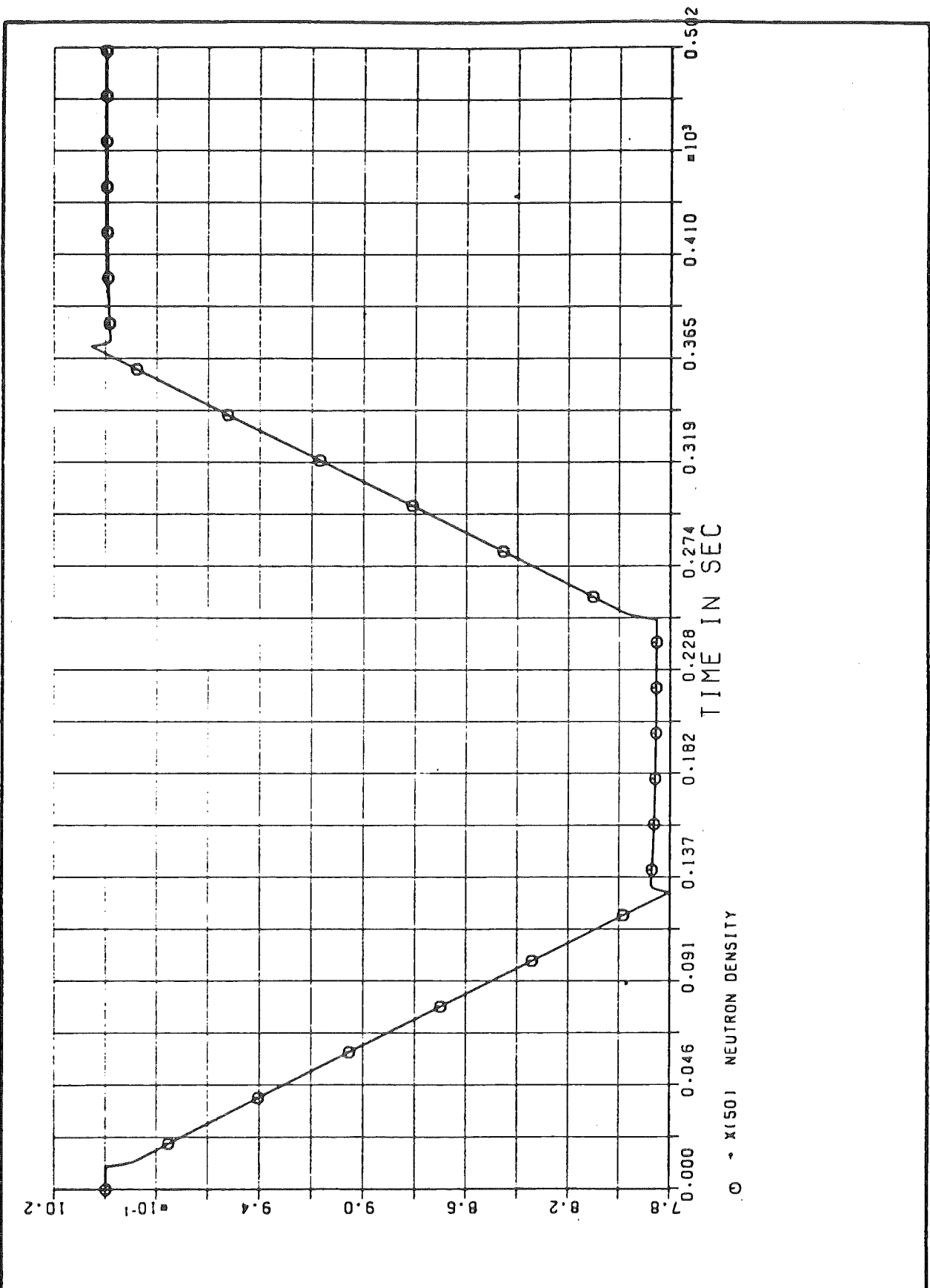
and is filtered in order to reduce the noise in the position measurements. The bias in $\Delta \rho$ can be made arbitrarily small by taking a sufficiently small time constant for the digital filters and accepting larger random noise in the estimate of rod worth.

The corresponding reactivity measurement (figure 24) shows a low frequency bias of $+ 3 \phi$ and random noise with a standard deviation of 0.6ϕ .

The nearly perfekt tuning (figure 23) of the balance meter during set point changes stems from the accurate rod worth estimation (figure 25), from the availability of the reactivity feedback parameter estimates and from the "indirect measurement" of fuel temperature (figure 28).

The only substantial feedback term is the Doppler reactivity (figure 26). Its time dependency is caused by the fuel temperature perturbation (figure 28). Coolant temperature feedback adds only a few cents to the reactivity balance (figure 27). Bowing and grid plate reactivity are negligible in this case.

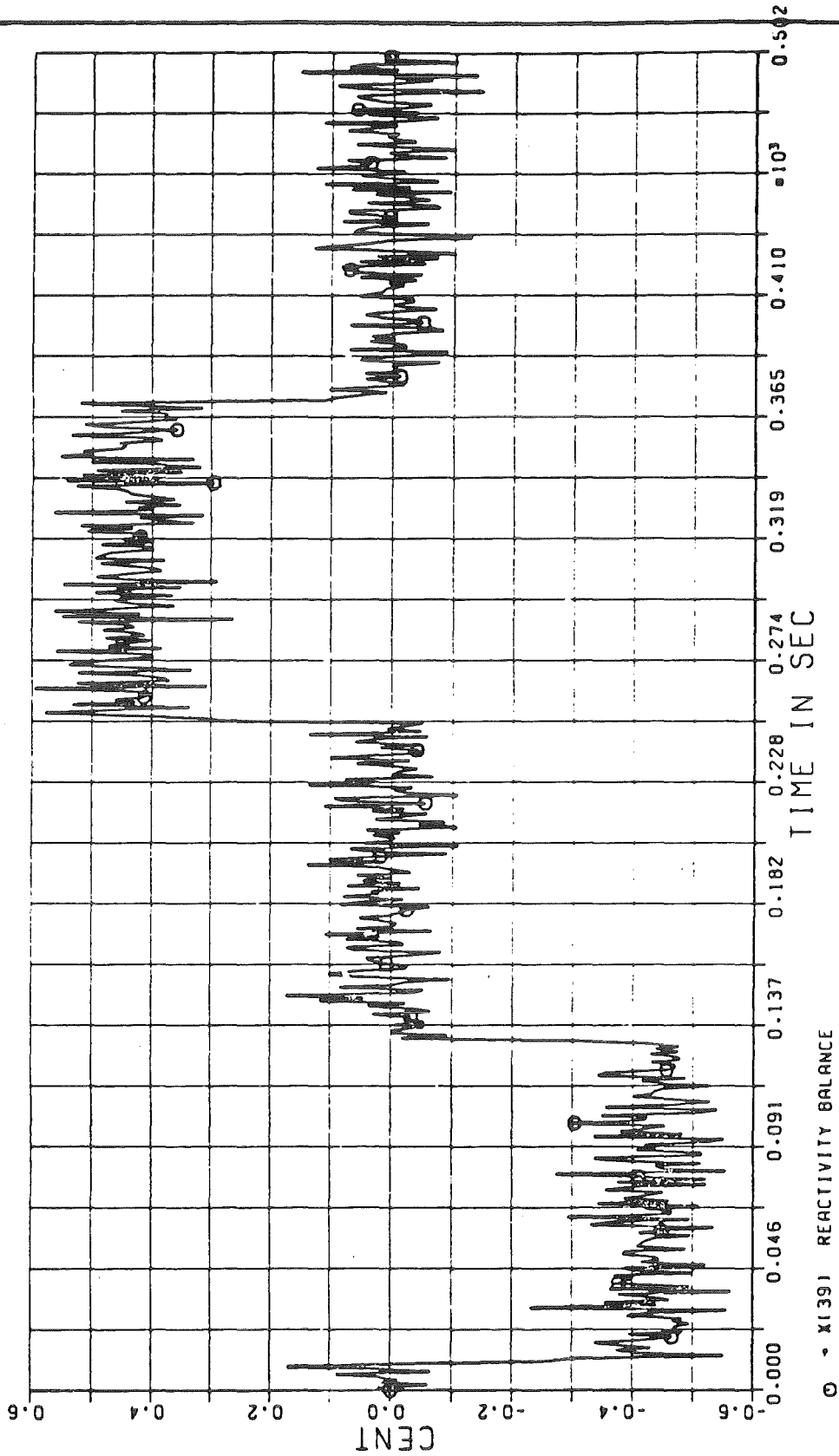
INTERATOM



SET POINT CHANGE
COMPENSATION OF CONTROL ACTION
IN THE REACTIVITY BALANCE SIG.

FIG. 21

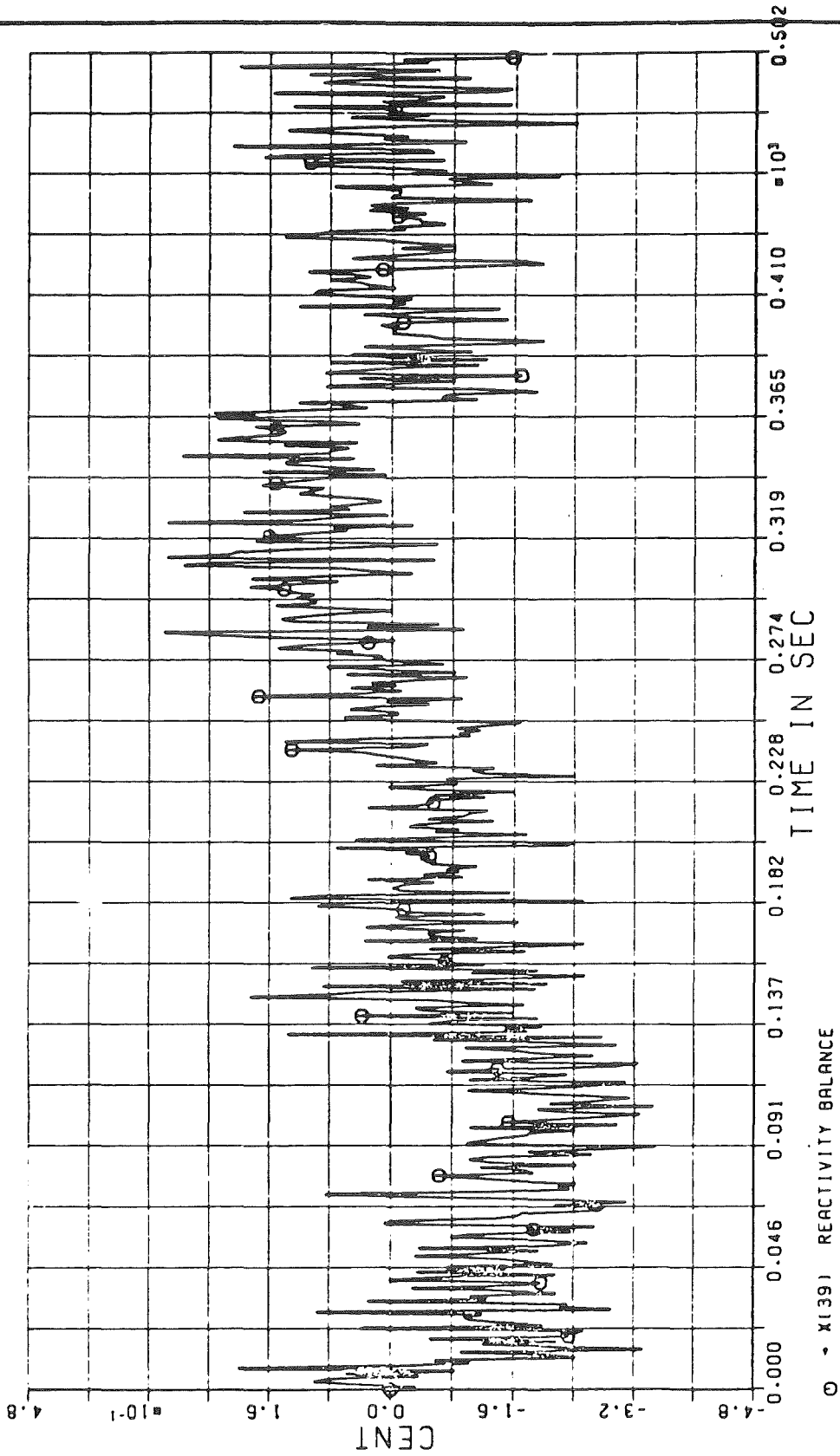
INTERATOM



SET POINT CHANGE
COMPENSATION OF CONTROL ACTION
IN THE REACTIVITY BALANCE SIG.

FIG. 22

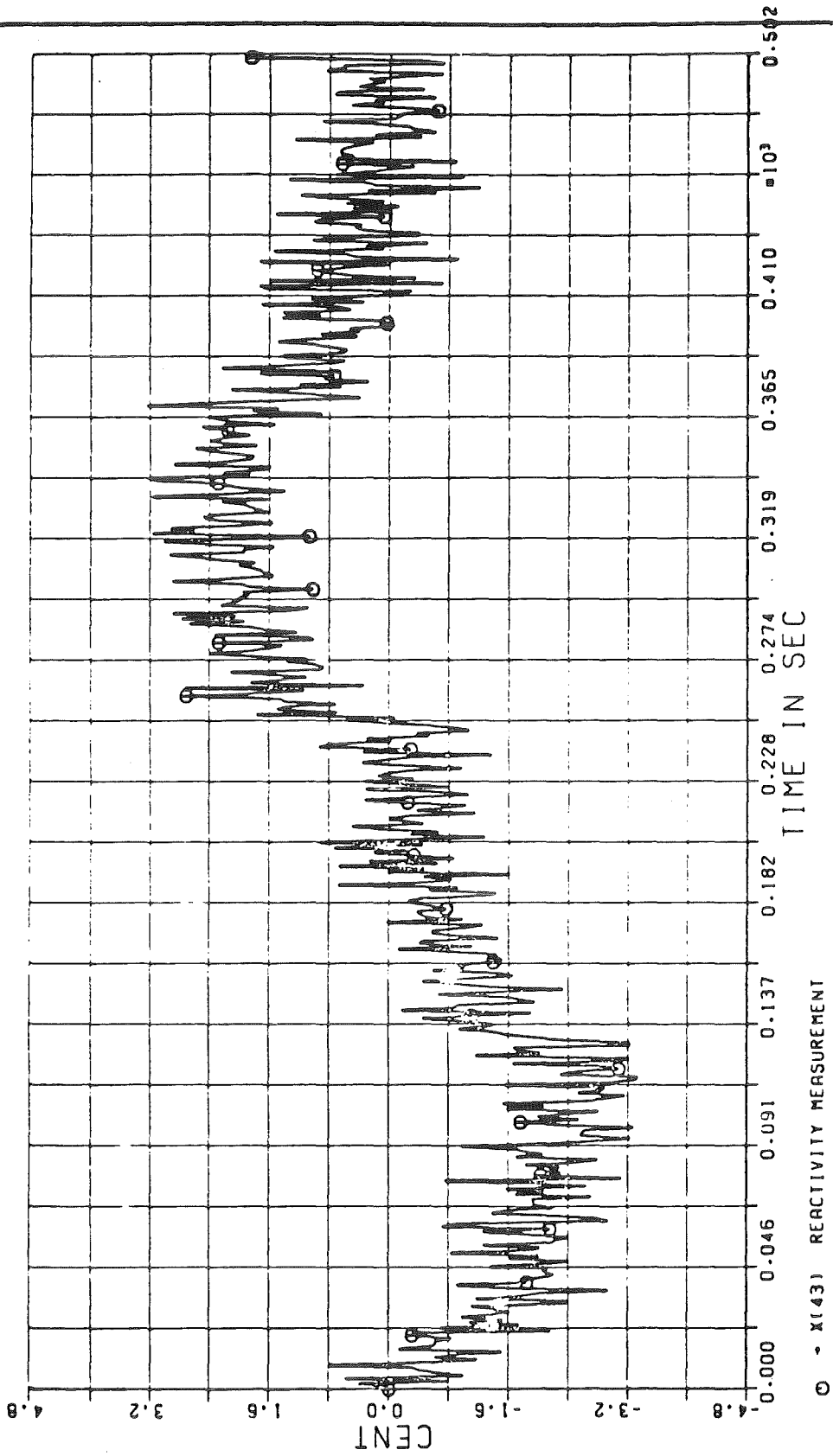
INTERATOM



SET POINT CHANGE
COMPENSATION OF CONTROL ACTION
IN THE REACTIVITY BALANCE SIG.

FIG. 23

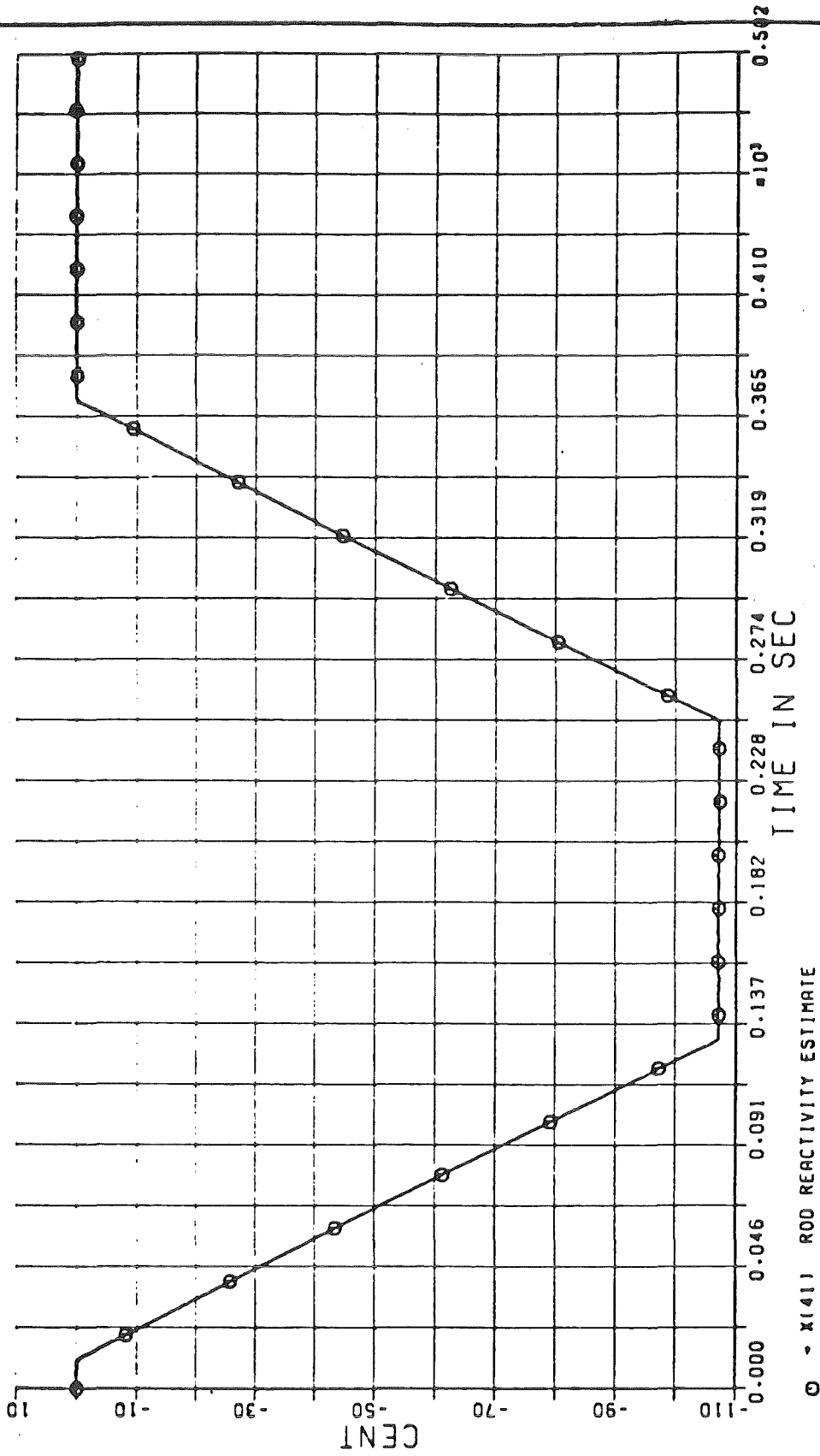
INTERATOM



SET POINT CHANGE
COMPENSATION OF CONTROL ACTION
IN THE REACTIVITY BALANCE SIG.

FIG. 24

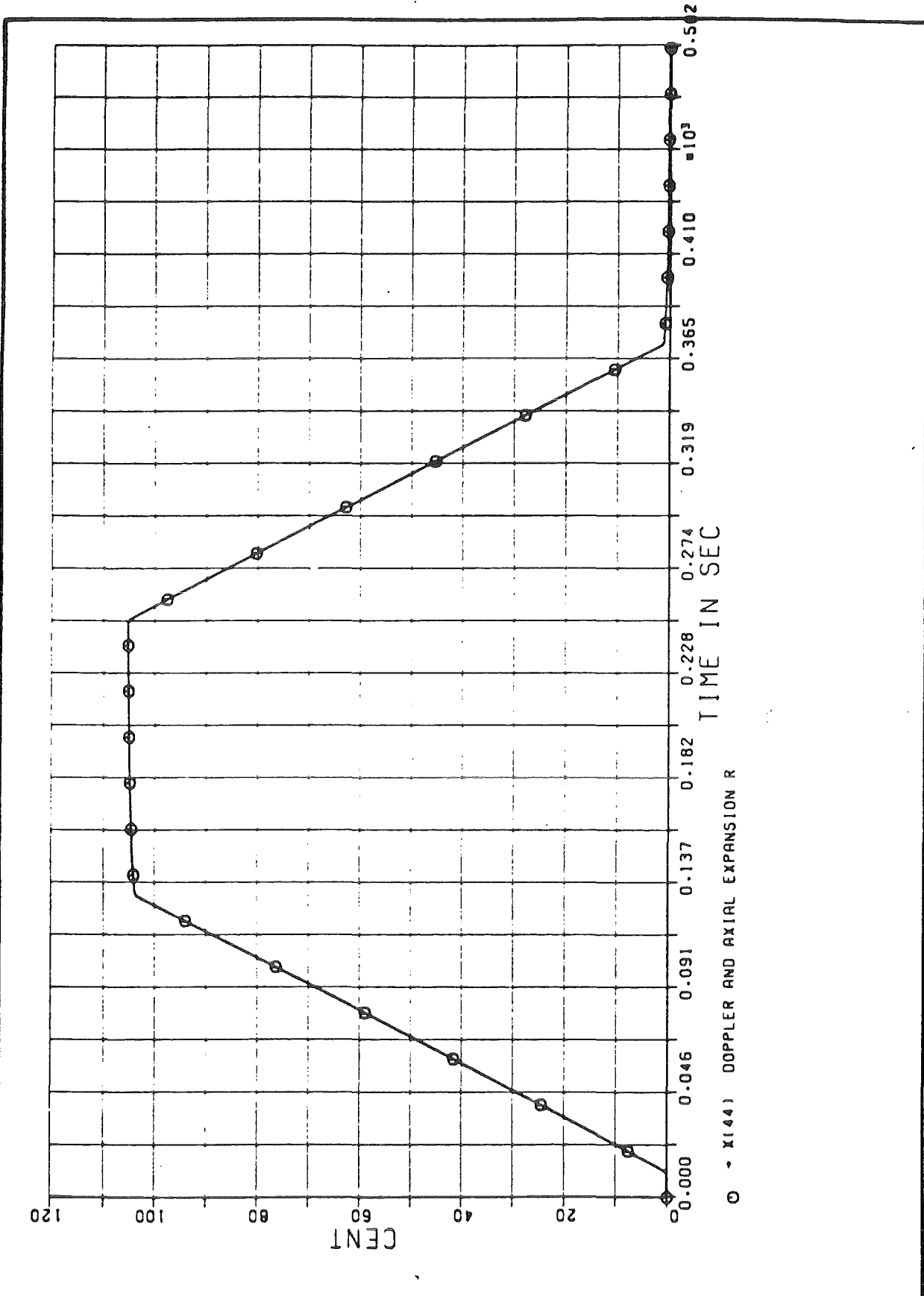
INTERATOM



SET POINT CHANGE
COMPENSATION OF CONTROL ACTION
IN THE REACTIVITY BALANCE SIG.

FIG. 25

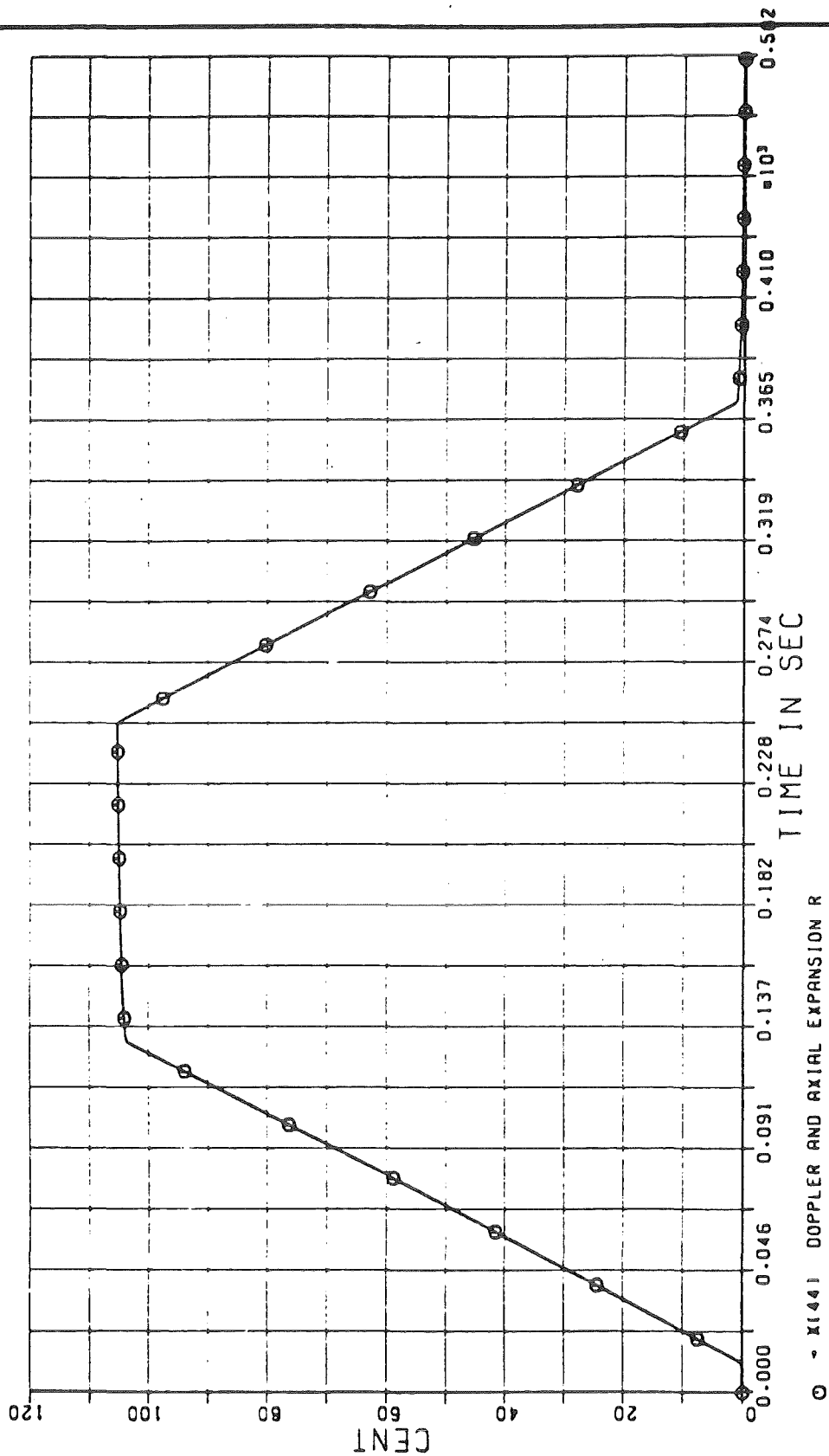
INTERATOM



SET POINT CHANGE
COMPENSATION OF CONTROL ACTION
IN THE REACTIVITY BALANCE SIG.

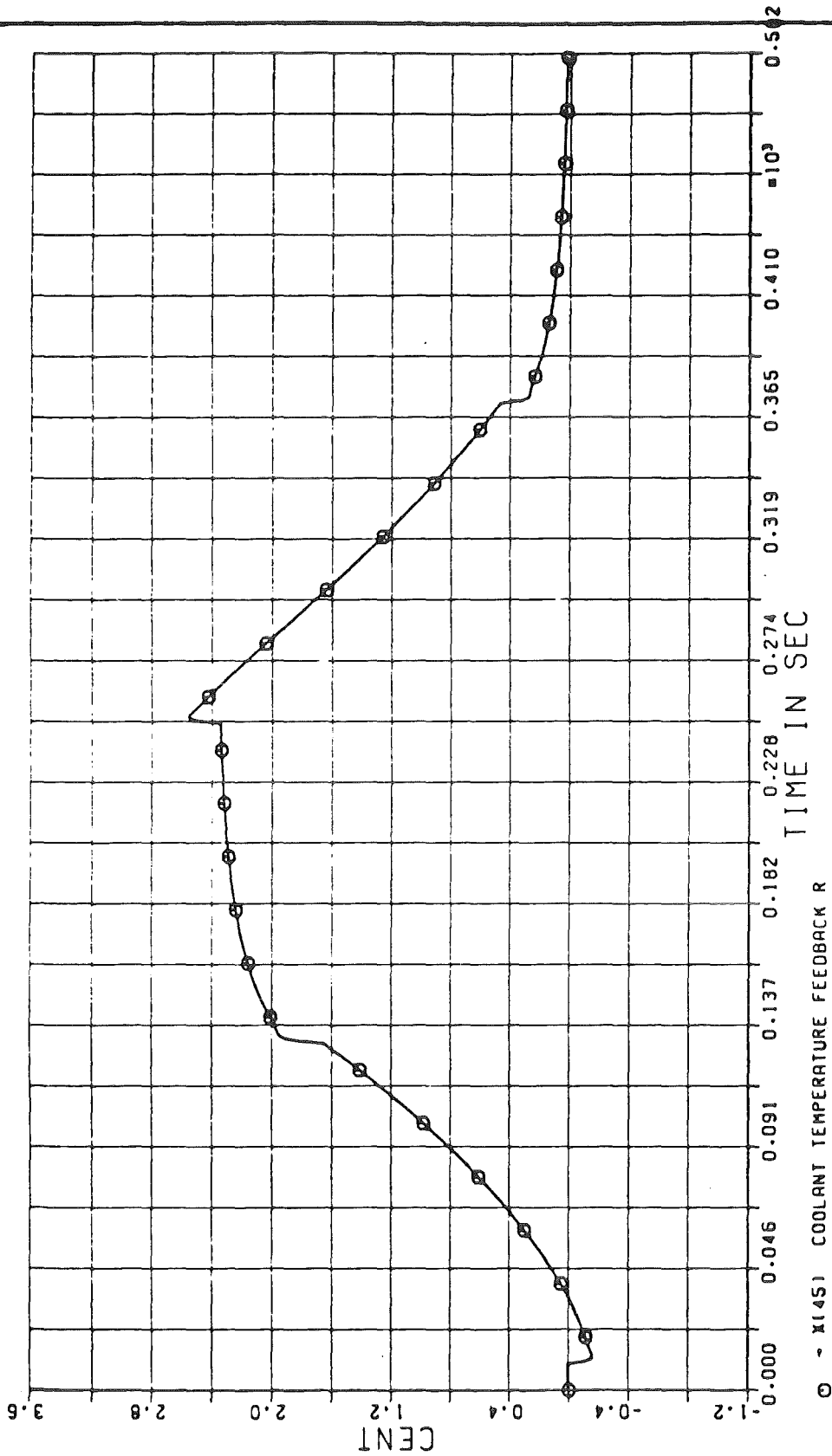
FIG. 26

INTERATOM



SET POINT CHANGE
COMPENSATION OF CONTROL ACTION
IN THE REACTIVITY BALANCE SIG.

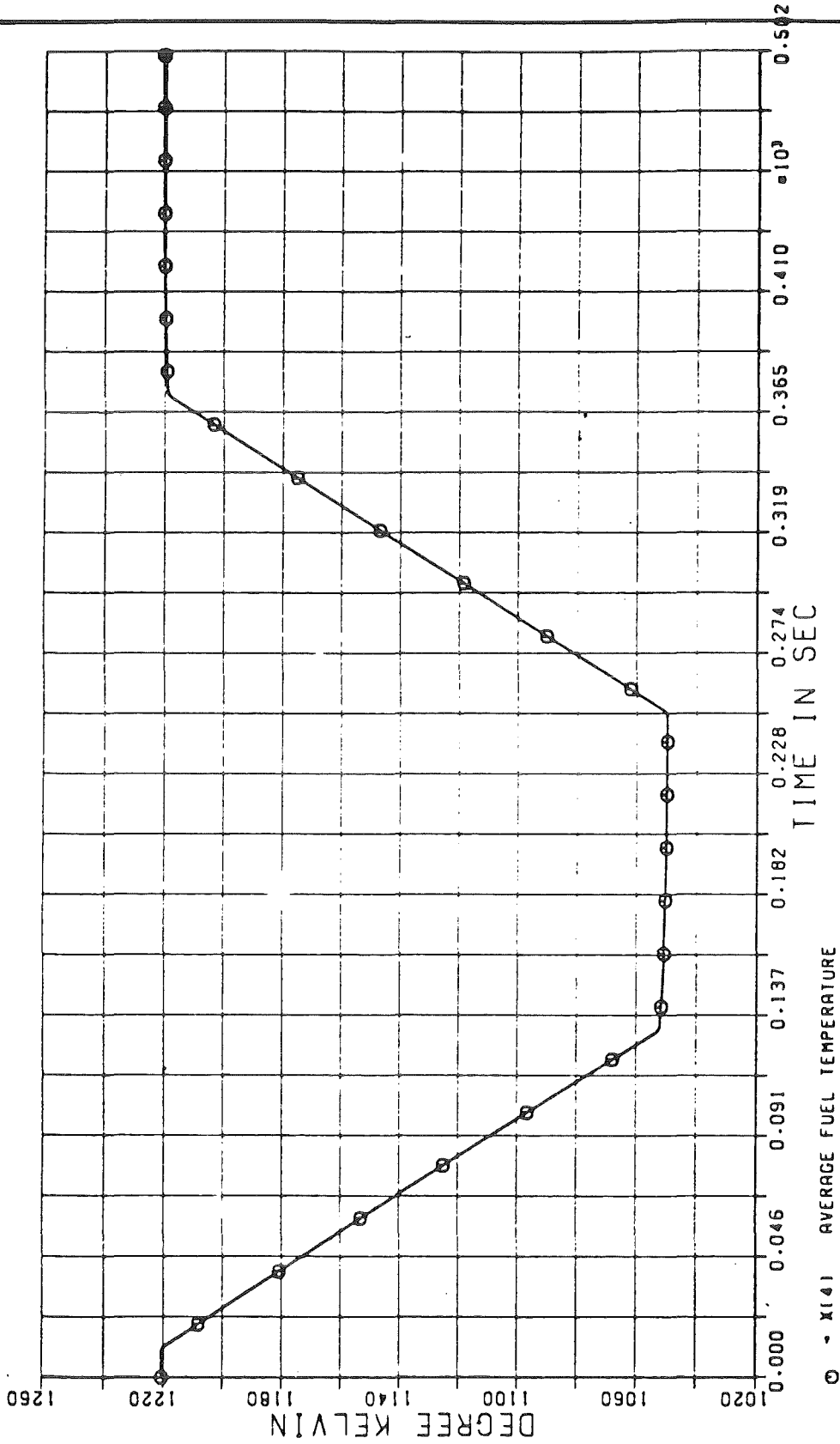
FIG. 26



SET POINT CHANGE
COMPENSATION OF CONTROL ACTION
IN THE REACTIVITY BALANCE SIG.

FIG. 27

INTERATOM



SET POINT CHANGE
COMPENSATION OF CONTROL ACTION
IN THE REACTIVITY BALANCE SIG.

FIG. 28

The figures 29 to 35 show a set-point change plus a perturbation of β_D by a factor 1.5 for $t \approx 50$ seconds (or equivalently, a perturbation of β_A by a factor 1.25). Disturbance of β_i is taken stepwise for convenience. Table 8 illustrates the number ranges which have to be recognized by the monitoring device. The β_D - and β_A -values of the (simulated) core depend upon T_f , while the estimated parameters of the balance meter are taken to be constant.

The reactivity measurement (figure 29) reacts to the stepwise change of $(\beta_D + \beta_A)$ with a short peak similar to the neutron density in figure 30. Power is only reduced to $0.813 P_0$ instead of $0.787 P_0$ by the maneuver as a consequence of the larger inherent negative feedback. The fuel temperature is also affected in both, the speed of change and the stationary value ($= 1070$ instead of 1050 °C).

Of course the Doppler and axial expansion reactivity (figure 32) show the effect of the parameter perturbation; but it turns out to be smaller than expected because the δT_f -values are smaller than in the normal case.'

The reactivity balance (figure 33) indicates the abnormal change of $(\beta_D + \beta_A)$ with a nearly stepwise increase of the $\Delta \rho$ -signal at $t = 50$ seconds, which increases then further as a consequence of the set-point change with an incorrect β_D . An anomaly

is clearly indicated and calibration can be initiated after the desired set-point has been reached (calibration during set-point change will be described in a subsequent paper). The anomaly signal $\Delta\phi$ again becomes zero approximately after the initial set-point is reached, since δT_f is zero at nominal power.

Rod reactivity estimates with method 1 and 2 are shown in the figures 34 and 35. As expected, the curve obtained with method 1 is erroneous after the parameter anomaly has occurred, while the estimate obtained from processing position measurements (figure 35) has no bias. But even the large parameter error considered in this example only causes an almost negligible rod worth error with method 1, which disappears after calibration.

The actual diagnostic value lies in the parameter estimates attainable with the balance meter. Calibration can either be initiated by the irregularities observed or may be called for after every set-point change automatically.

Some of the outputs of the reactivity balance meter for this test case are shown in the figures 36 to 40.

The reactivity measurement in figure 36 has several more peaks because of the input disturbances during the calibration interval (140 - 180 seconds). The effect of these disturbances on fuel temperature is shown in figure 37. All reactivity feedback estimates are also affected, of course, by the input disturbances.

Figure 38 shows the dominant feedback contribution. The final value of $\rho_D + \beta_A$ is negative instead of zero because of the incorrect initial value at the beginning of the second half of the power maneuver.

The reactivity balance clearly indicates the abnormal situation (figure 39). It does not show any transient during the calibration period, where core inputs are disturbed and becomes zero again after calibration has been completed.

Next, the sensitivity of the balance meter is tested by keeping the Doppler and axial expansion coefficients constant in the prediction model of the balance meter (i. e.: independent of the fuel temperature). Otherwise, we repeat the set-point change plus stepwise perturbation of β_D for the plant as described in the previous example (figures 36 to 39). Figure 40 shows the effect of such a discrepancy between prediction model and reference. The reactivity balance increases from 0 to $-4 \text{ } \phi$ during the set-point change from 80 % back to 100 % of nominal power. It would again trigger the calibration procedure and the bias would be removed. The new values of the parameter estimates would reflect the dependence on fuel temperature.

Continuous updating of $\beta_D + \beta_A$ as described in section 4.6 removes this bias automatically and helps to avoid unnecessary calibration.

Table 8:

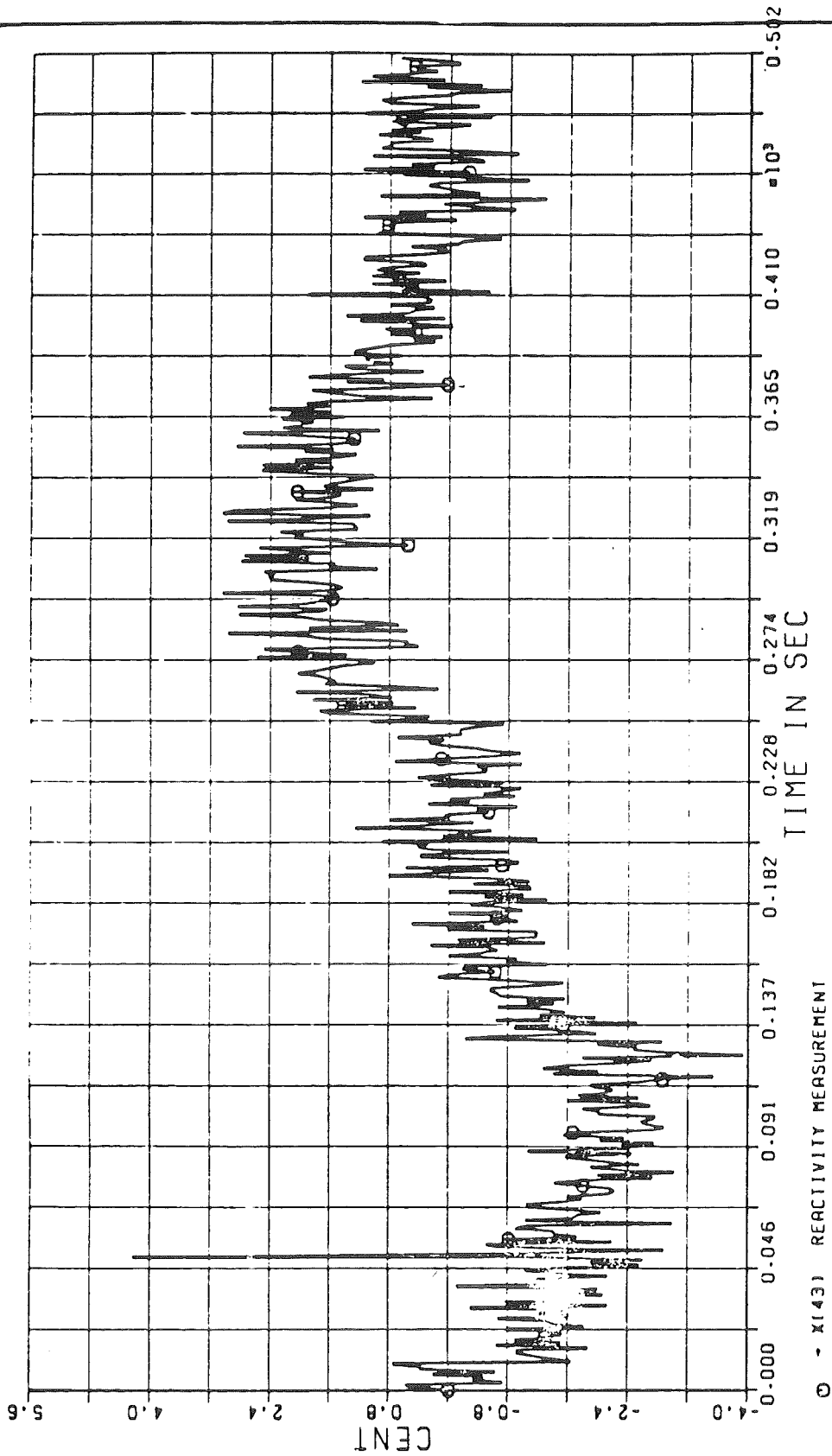
Examples of Doppler and Axial Expansion Coefficients
with and without Anomaly

Set Point	No Anomaly	With Anomaly	
	$f(T_f)$	$f(T_f)$	constant
100 %	- 0.616	- 0.719	- 0.719
80 %	- 0.602	- 0.694	- 0.719

The table entries refer to the sum of the Doppler and axial expansion coefficients; itemized nominal values are:

$$\beta_D = - 0.20 \text{ } \phi / ^\circ\text{K}, \quad \beta_A = - 0.41 \text{ } \phi / ^\circ\text{K}$$

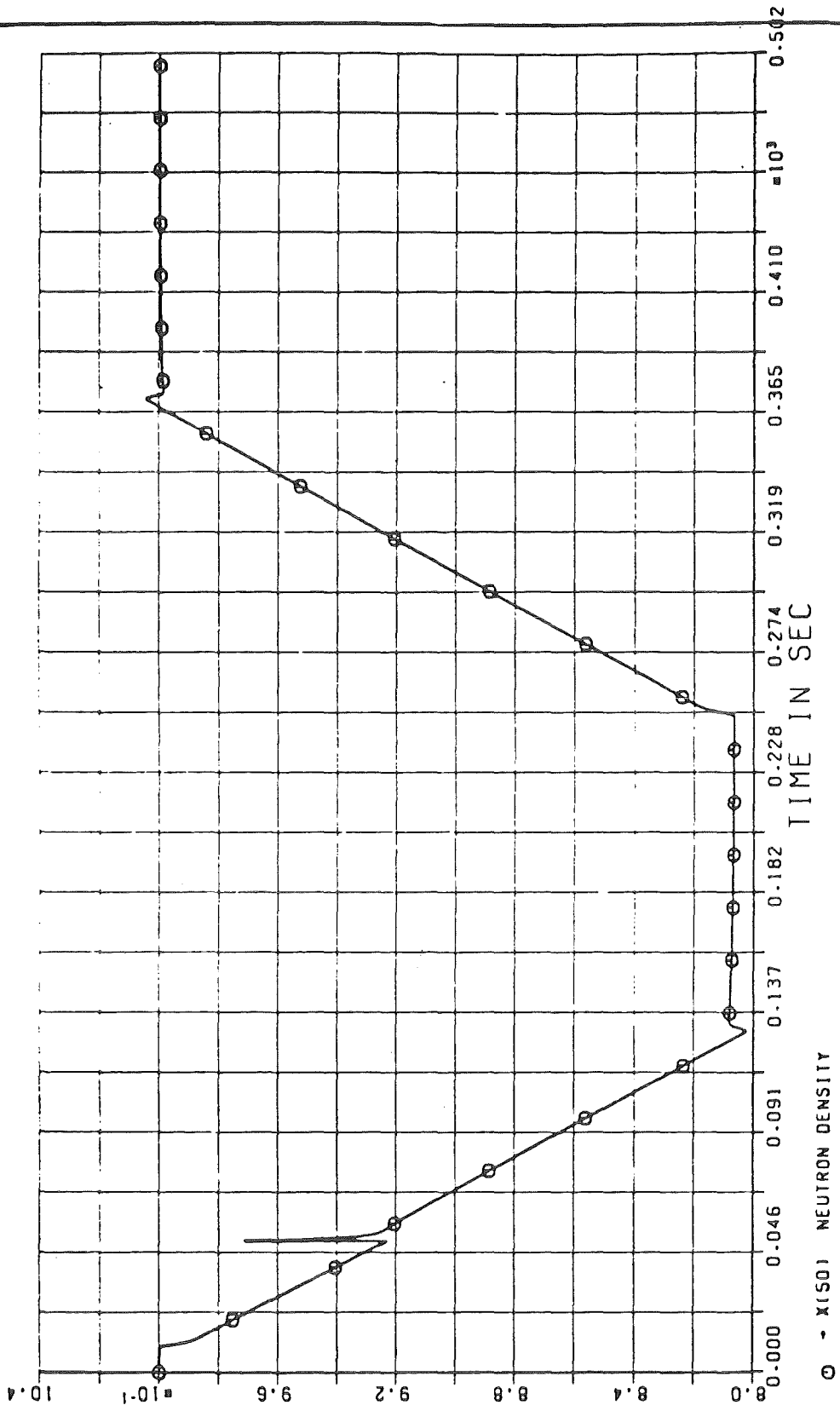
UNIVERSITY OF MICHIGAN



SET POINT CHANGE AND
PERTURBATION OF DOPPLER COEFF.
ROD POSITION MEASUREMENTS

FIG. 29

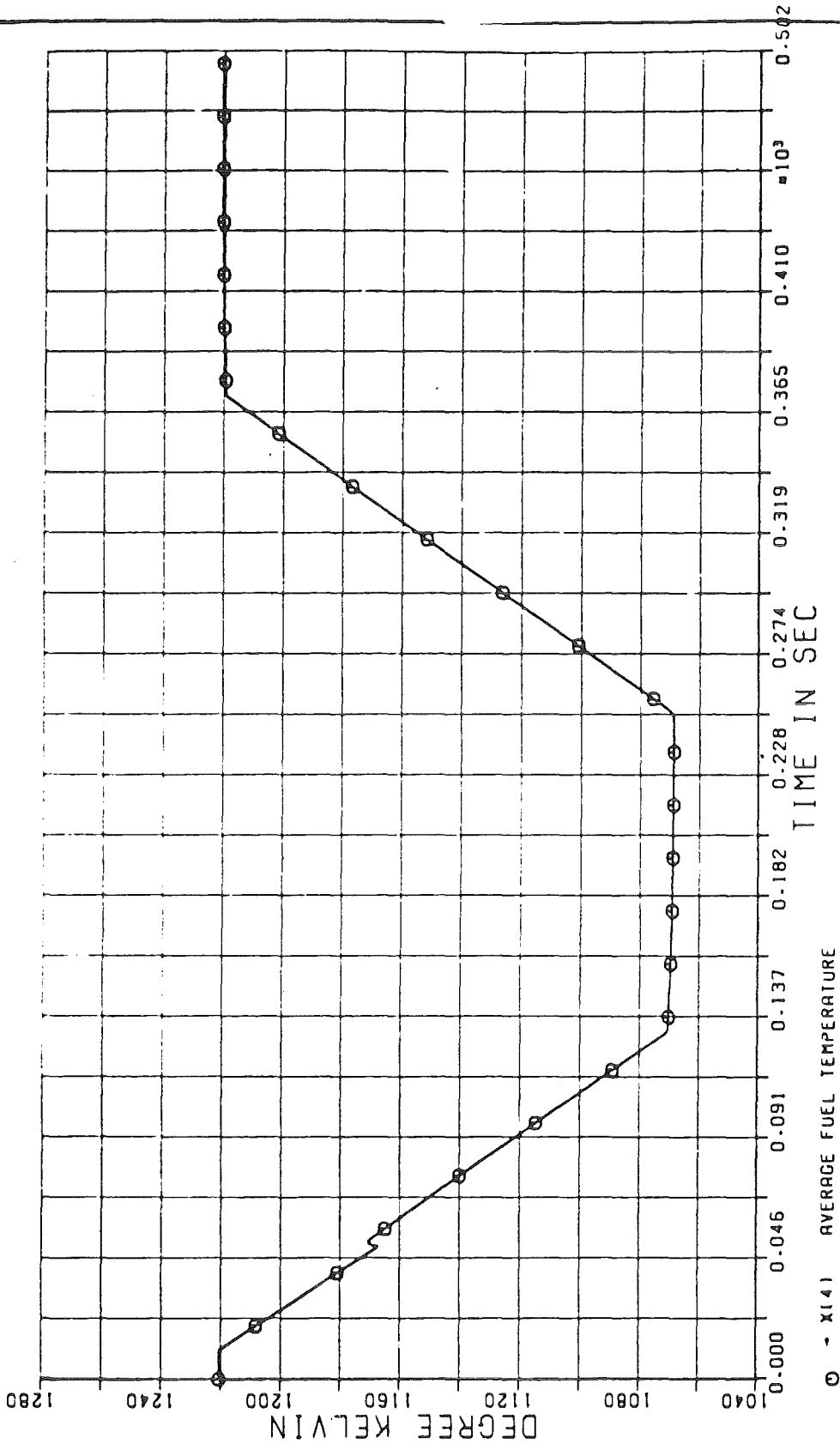
INTERATOM



SET POINT CHANGE AND
PERTURBATION OF DOPPLER COEFF.
ROD POSITION MEASUREMENTS

FIG. 30

INTERATOM

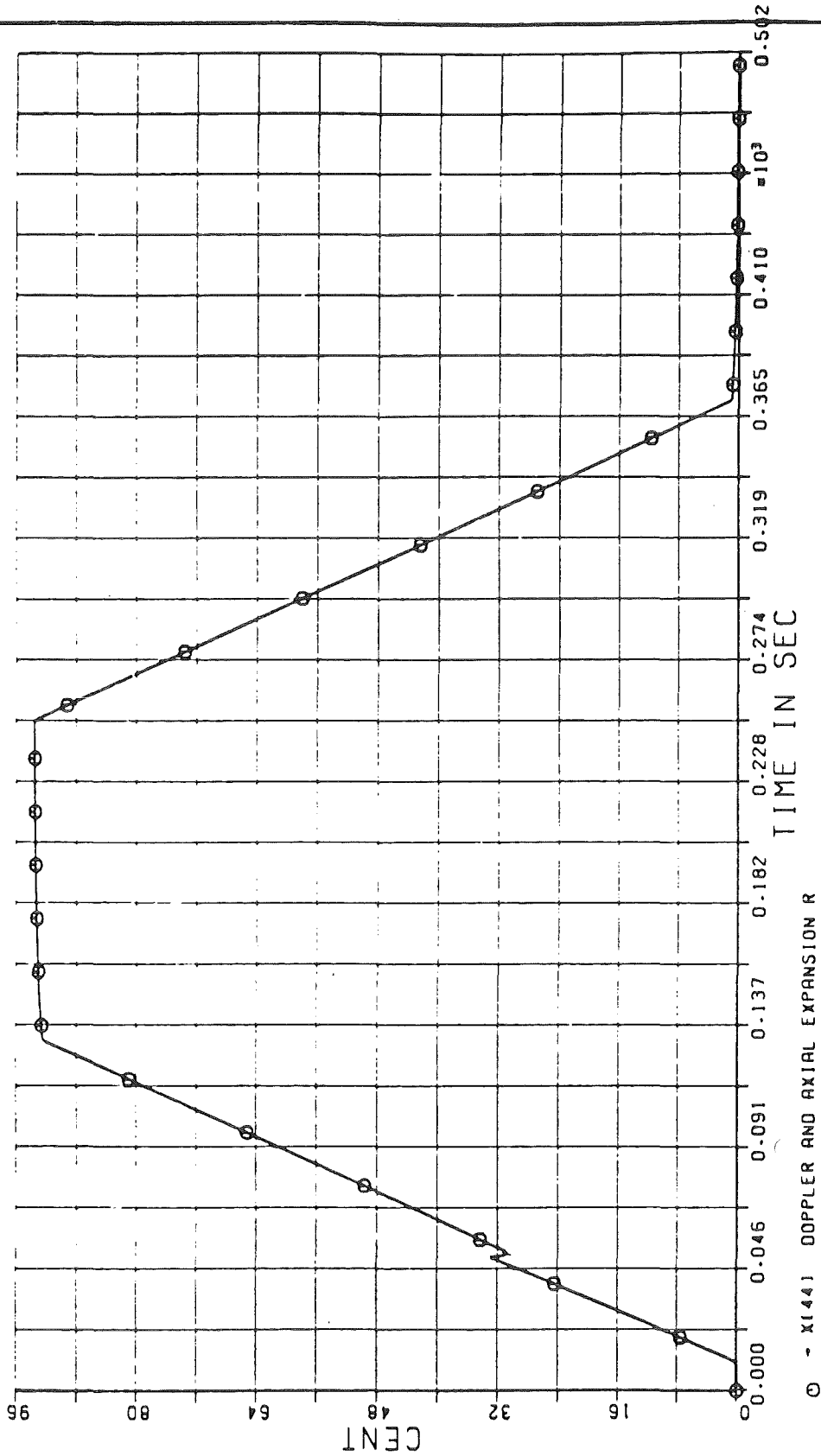


○ - X(4) AVERAGE FUEL TEMPERATURE

SET POINT CHANGE AND
PERTURBATION OF DOPPLER COEFF.
ROD POSITION MEASUREMENTS

FIG. 31

INTERATOM

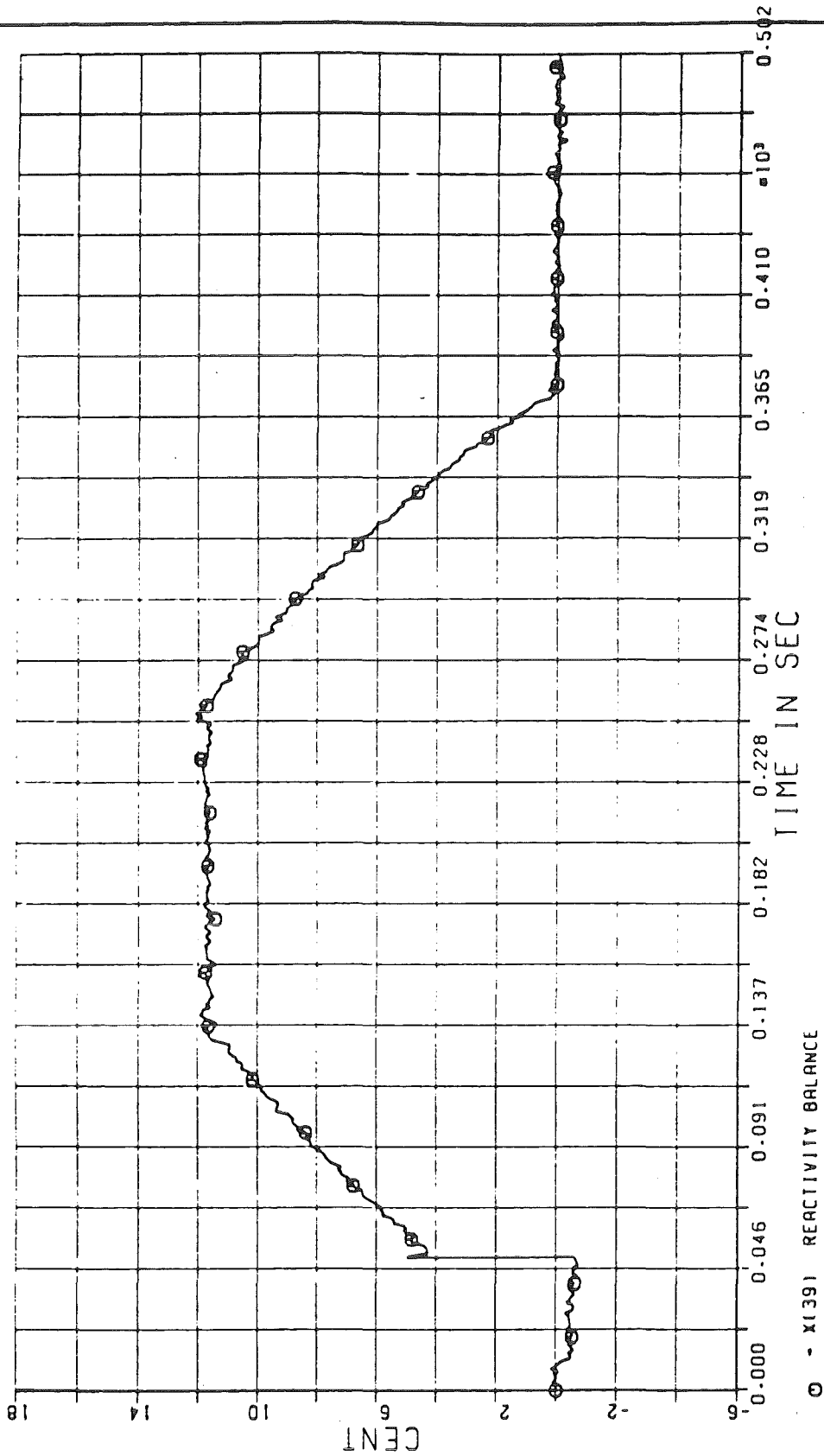


○ - X(144) DOPPLER AND AXIAL EXPANSION R

SET POINT CHANGE AND
PERTURBATION OF DOPPLER COEFF.
ROD POSITION MEASUREMENTS

FIG. 32

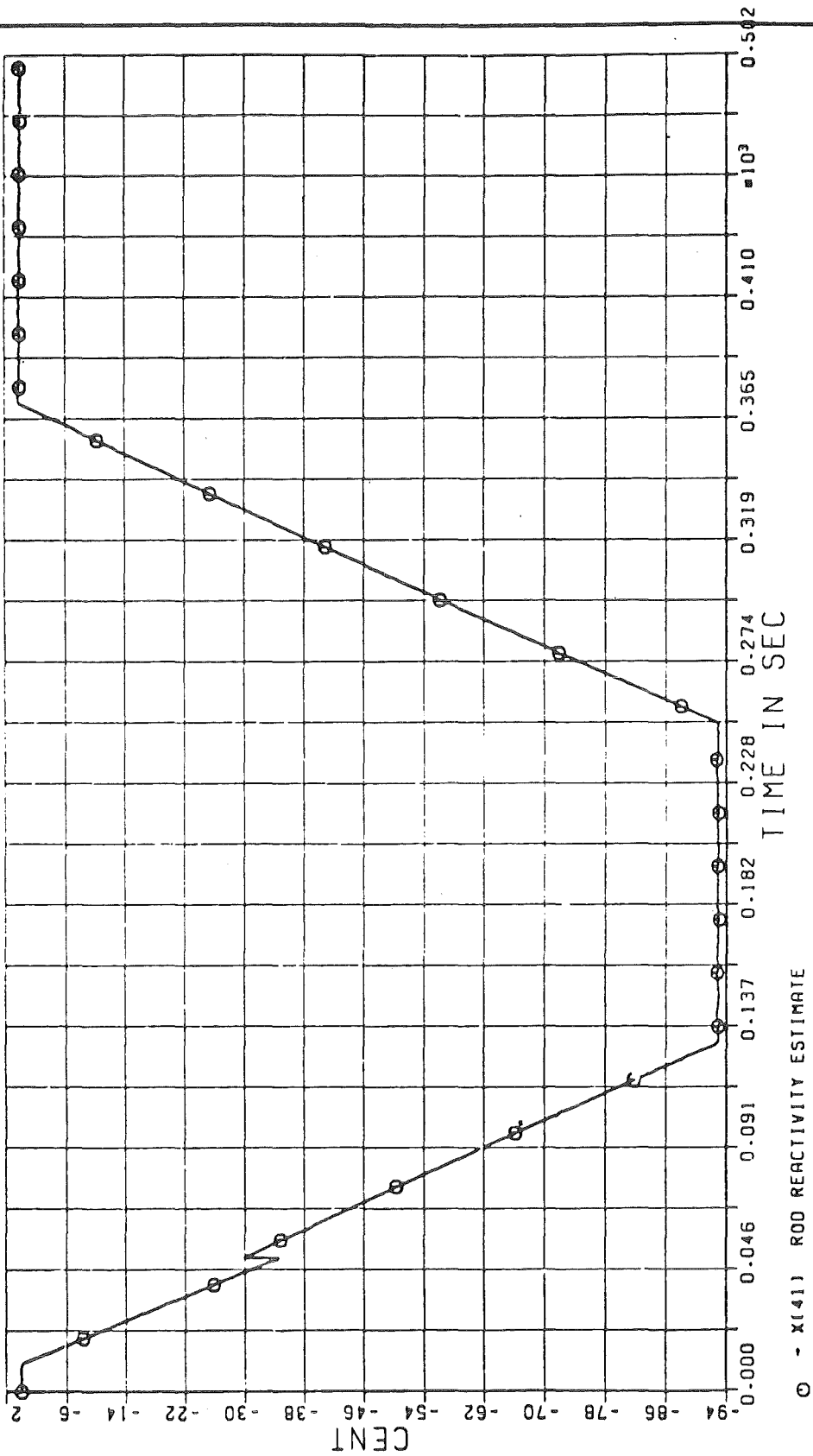
INTERATOM



SET POINT CHANGE AND
PERTURBATION OF DOPPLER COEFF.
ROD POSITION MEASUREMENTS

FIG. 33

INTERATOM

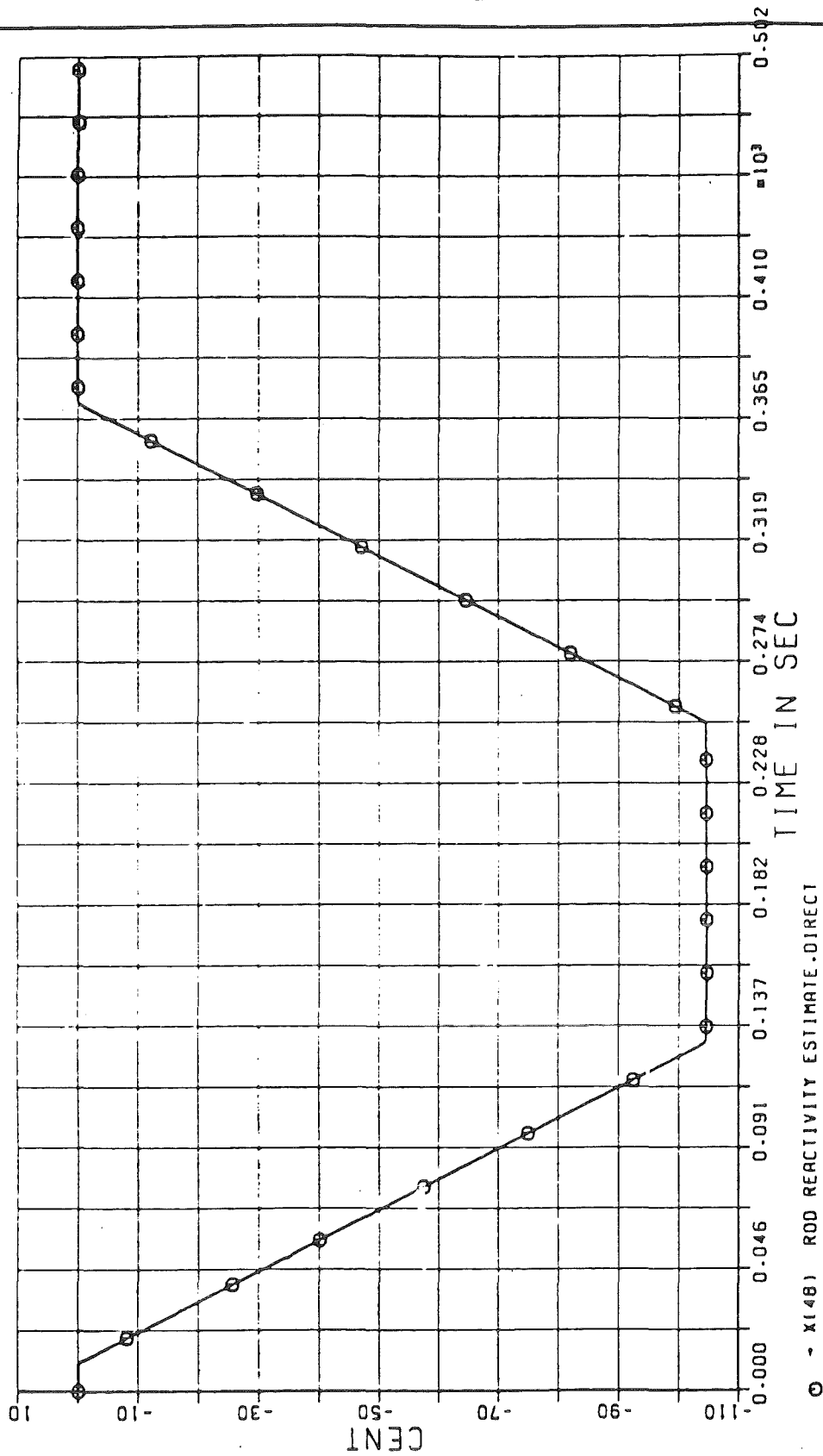


○ - X(141) ROD REACTIVITY ESTIMATE

SET POINT CHANGE AND
PERTURBATION OF DOPPLER COEFF.
ROD POSITION MEASUREMENTS

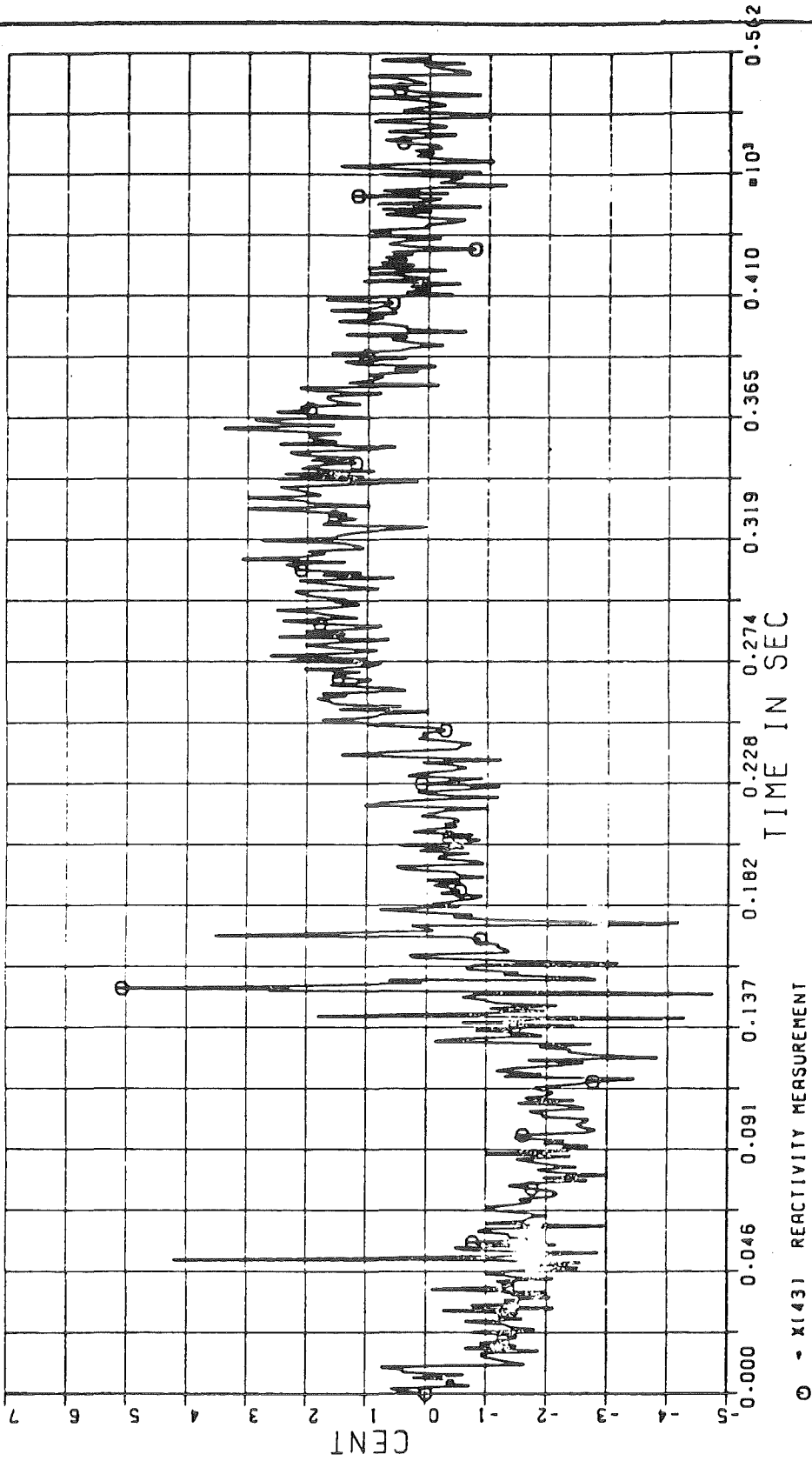
FIG 34

INTERATOM



SET POINT CHANGE AND
PERTURBATION OF DOPPLER COEFF.
ROD POSITION MEASUREMENTS

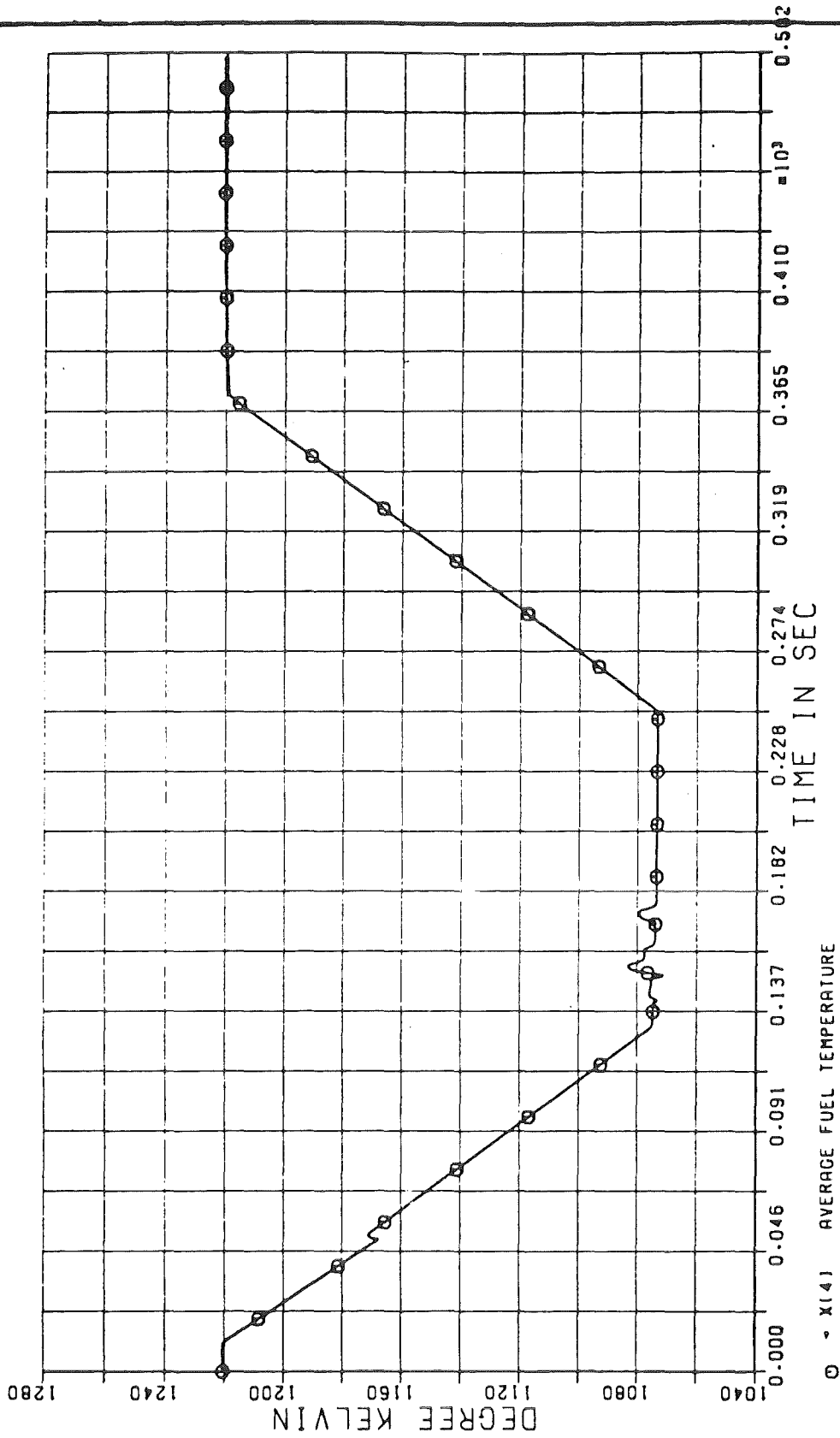
FIG. 35



DOPPLER-AND AXIAL EXPANSION
COEF. INDEPENDENT OF FUEL T.
CALIBRATION BETWEEN 140-180 S

FIG 36

INTERATOM

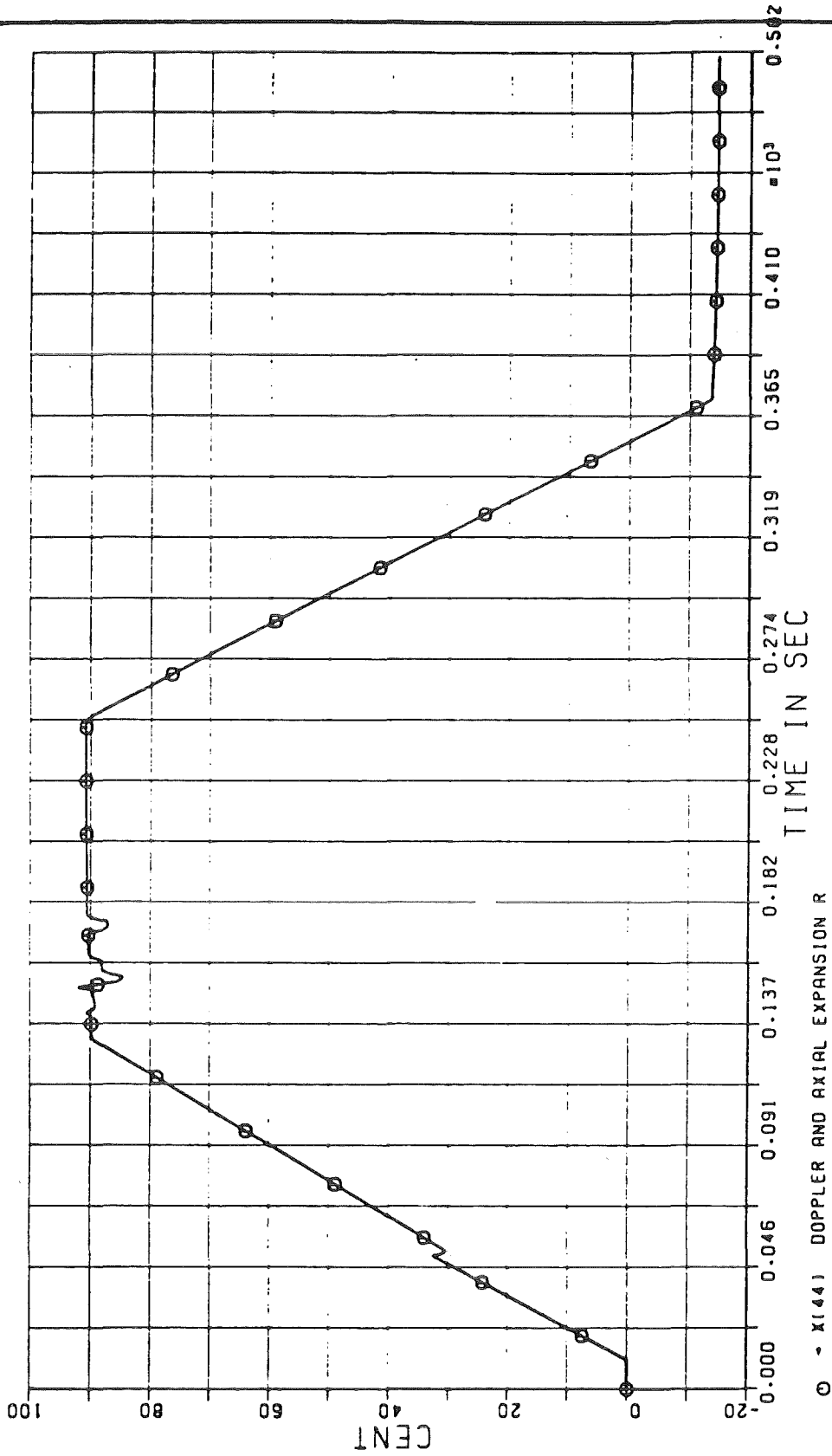


○ - X(14) AVERAGE FUEL TEMPERATURE

DOPPLER-AND AXIAL EXPANSION
COEF. INDEPENDENT OF FUEL T.
CALIBRATION BETWEEN 140-180 S

FIG. 37

INTERATOM

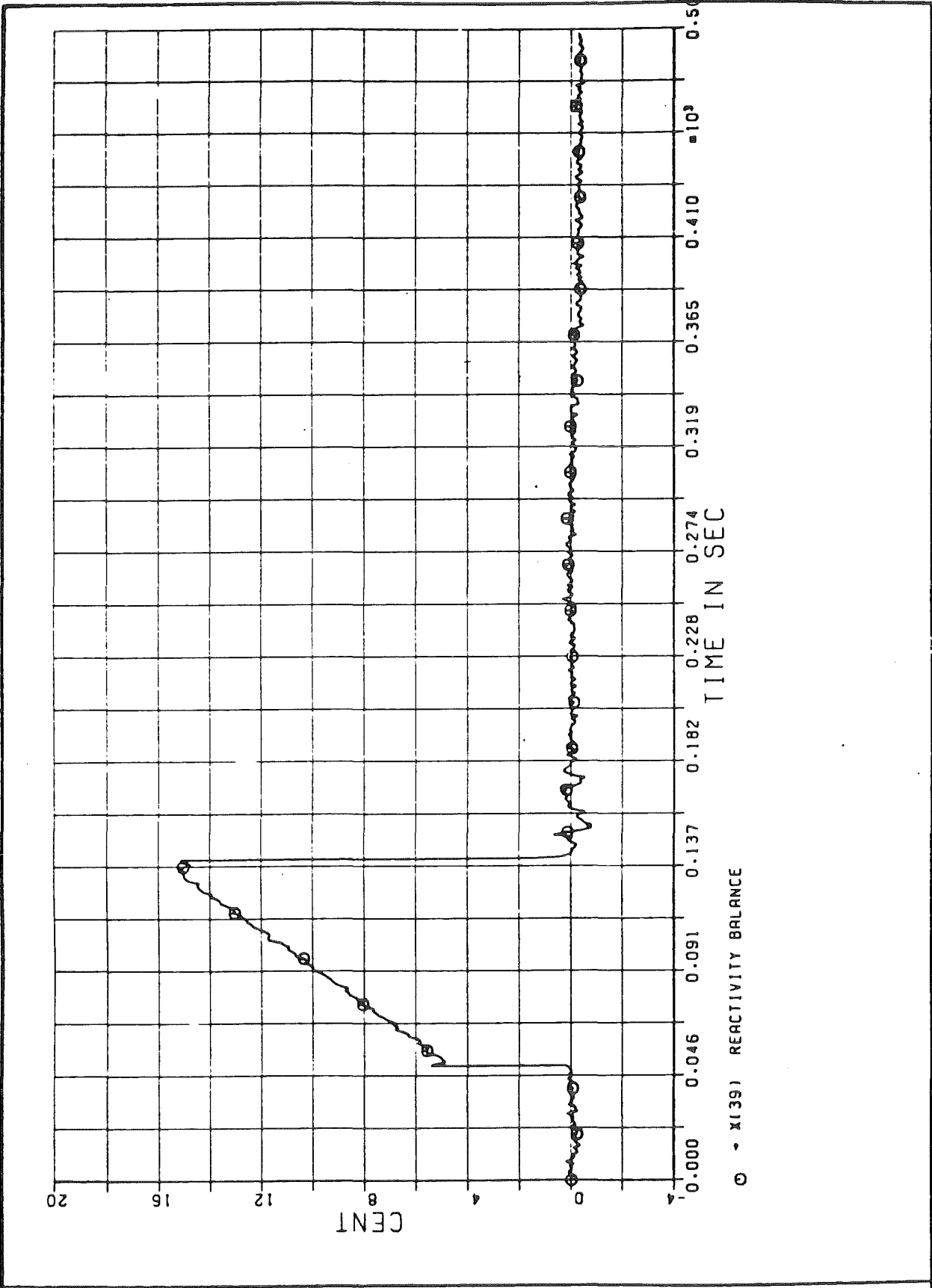


○ - X(144) DOPPLER AND AXIAL EXPANSION R

DOPPLER-AND AXIAL EXPANSION
COEF. INDEPENDENT OF FUEL T.
CALIBRATION BETWEEN 140-180 S

FIG. 38

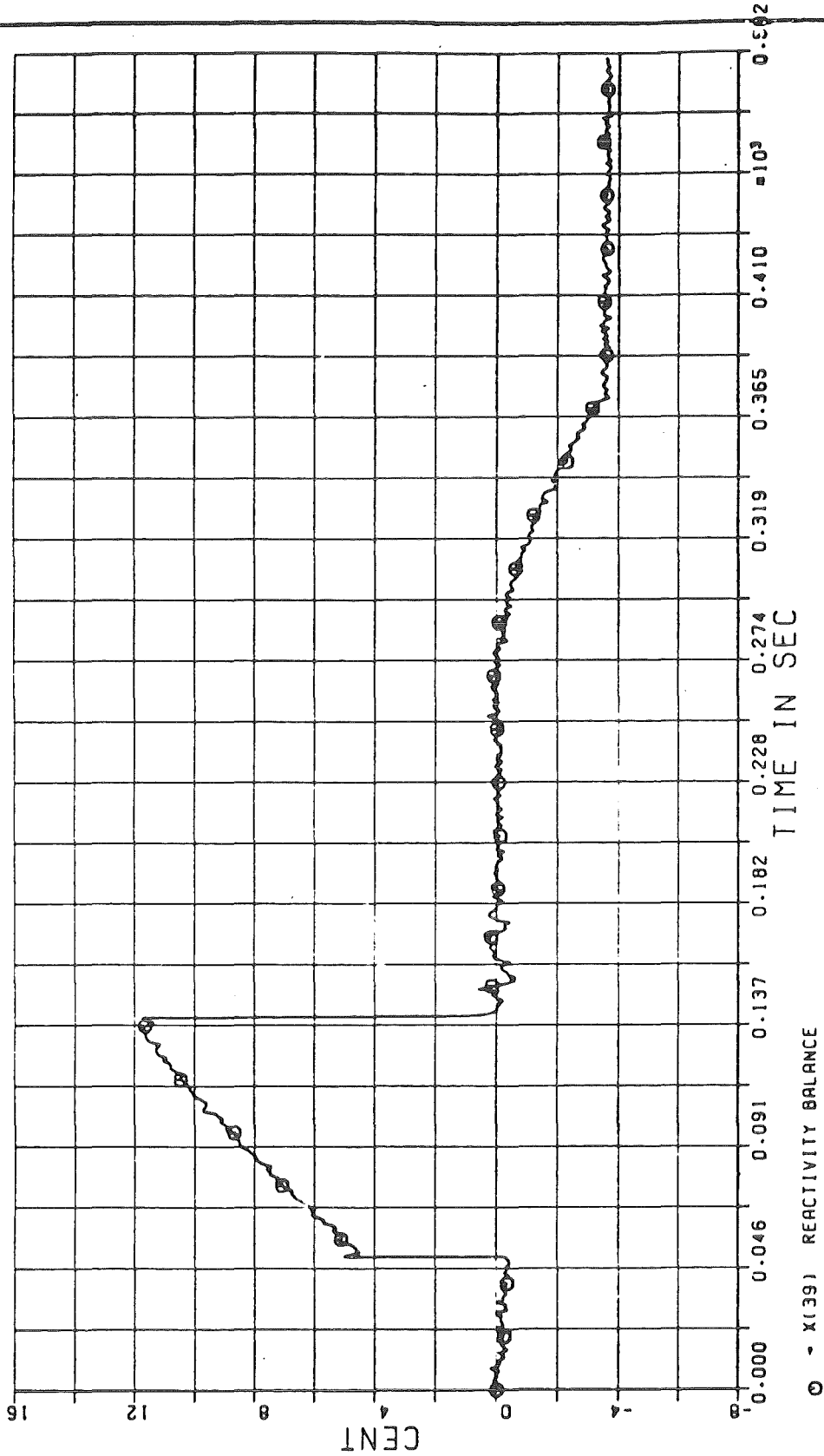
INTERATOM



DOPPLER AND AXIAL EXPANSION
COEF. INDEPENDENT OF FUEL T.
CALIBRATION BETWEEN 140-180 S.

FIG. 39

INTERATOM



SET POINT CHANGE AND
PERTURBATION OF DOPPLER COEFF.
CALIBRATION BETWEEN 140-180 S

FIG. 40

6. Preliminary Verification with KNK-II Experiments

A. Holick
INTERATOM

Experimental verification of the "Global Core Surveillance Procedure" (GCSP) has been started with off-line analysis of data from the KNK-II plant. Bank position was disturbed in the experiment by a sequence of alternating constant and ramplike function over a total of a few minutes. The resulting power perturbations did not exceed $\pm 2 \%$ of the nominal power.

The major problem areas were:

- 1 Quantization error in the measurements; due to the analog-to-digital conversion; its significance increases, if core excitation is kept small so that plant operation does not become recognizably disturbed by the calibration experiments. Smoothing with cubic SPLINE-functions suffices to compensate the effect on parameter estimation accuracy, if the signal to quantization - noise ratio is sufficiently large. If the power perturbations (at present) become smaller than $\pm 2 \%$ or temperature perturbations smaller than $\pm 3 \text{ }^\circ\text{K}$, then the smoothing approach becomes unsound and the conversion circuit has to be modified slightly by restricting the conversion range to amplitude perturbations.
- 2 Bias in the neutron density measurements; the bias can be identified with the on-line core simulator and can easily be removed before the parameter estimates start to drift.
- 3 Lack of observability; the only cause is insufficient excitation of the core input (i. e.: bank position) and can be avoided by just modifying the bank position disturbance function in accordance with an observability analysis prior to the experiment.

- 4 Large sampling interval; it causes a model error in the prediction function of the parameter estimation module. Its effect on estimation accuracy can be nearly eliminated by means of an interpolation scheme, which is based upon an on-line core simulator. Modification of the measurement sampling procedure is, of course, still desirable, but not cogent.

It is concluded from this analysis, that disturbance of one core input, namely the bank position, suffices to estimate the following thermohydraulic core parameters:

- . fraction of flow and power in any fuel-element,
- . heat transfer coefficient between fuel and coolant,
- . time constant of the thermo-couple at the fuel element outlet,
- . gain factor of the above thermo-couple (= factor of radial mixing at the core outlet).

Approximately 200 measurement samples are required at a rate of 1 (or better less) per second. Convergence of the procedure can be improved, if bank position and flow rate can be disturbed simultaneously.

It is recommended to continue the off-line verification process with an improved disturbance profile for the bank position and, possibly, with a reduced quantization error.

6.1 Description of the Experiment

The experiment is characterized by disturbing the core-inputs (rod position or primary flow) with a sequence of alternating constant and ramplike functions over a period of several minutes. The set-point corresponds to 50 % of nominal power and the maximum power perturbations do not exceed approximately ± 2 %. The corresponding state perturbations are shown in figure 41 and 42. In a third experiment, the flow was varied ramplike (figure 43).

The following measurements have been recorded:

Measurement	Unit	
bank position	mm	h
reactivity	ρ	ρ
neutron flux	%	n
primary flow, loop 1	m ³ /h	W _{V1}
primary flow, loop 2	m ³ /h	W _{V2}
inlet temperature, loop 1	°C	T _{I1}
inlet temperature, loop 2	°C	T _{I2}
outlet temperature, central element	°C	T _{Oi}

The primary mass flow is computed from the measured volumetric flows in the two coolant loops with the following formulas:

$$W_P = W_{P1} + W_{P2}$$

$$W_{Pi} = g(T_c) \cdot W_{Vi} \quad i = 1, 2$$

$$g(T_c) = 9492.0 - 0.223 T_c - 1.75 \cdot 10^{-5} T_c^2$$

The inlet temperature is the weighted average of the two measured loop temperatures:

$$T_I = \frac{1}{W_P} (W_{P1} \cdot T_{I1} + W_{P2} \cdot T_{I2})$$

The flow-rate and inlet temperature perturbations of the figures 41 and 42 are negligible. The information on the parameters is contained solely in the outlet and neutron density measurements. The perturbation amplitudes of experiment 2 and 3 are rather small and, hence, the quantization error which is due to the analog-to-digital conversion becomes the dominant error source. The curves from experiment 1 are much less affected by this error because of the larger perturbation amplitude. But it is still a serious problem and will be treated in section 6.2.

The quantization error is caused by discretizing the measurements and storing the result in a buffer register. The word length allows for approximately 2000 discrete

amplitude steps. If, for instance, a temperature of 600 °C is discretized, then the quantization error is in the order of 0.3 °C and dominates the relative measurement error. An error reduction can easily be achieved by discretizing the perturbation amplitude rather than the total quantity. Since parameter estimation requires only temperature perturbations of, at most, ± 7 °C, the quantization error can be reduced to 0.0035 °C and would be negligible.

Another error source stems from the thermo couple time constant and the fact, that the temperatures are measured at some distance from the fuel element outlet and, especially, from the core inlet.

This bias error in the outlet temperature measurements is modeled in terms of the time constant and the gain factor of a first order lag. Both unknown parameters are estimated on-line together with the other core parameters.

The time constant, τ_{IM} , of the inlet temperature measurements is especially large (in the order of 15 seconds) and requires special attention. It can be estimated separately from the inlet temperature measurements with the same method employed in this study to determine the core parameters. It will be sketched, therefore, only briefly for later reference:

The state components at the location of the measurement are

$$\begin{aligned}x_1 &= \text{actual temperature perturbation} \\ &= T_{IA} - T_{IAO} = \text{unknown}\end{aligned}$$

$$x_2 = \text{measured temperature perturbation}$$

and the state equations read

$$\begin{aligned} x^{k+1} &= \phi \cdot x^k \\ y^k &= C \cdot x^k \end{aligned}$$

where

$$\begin{aligned} x^T &= [x_1 \quad x_2] \\ \phi &= \begin{bmatrix} 1 & 0 \\ \phi_{21} & \phi_{22} \end{bmatrix} & C &= [0 \quad 1] \\ \phi_{21} &= 1 - \phi_{22} & \phi_{22} &= e^{-\frac{(t-t_0)}{\tau_{2M}}} \end{aligned}$$

The unknown transition matrix element, ϕ_{22} , can be directly related to the measurements with the equation

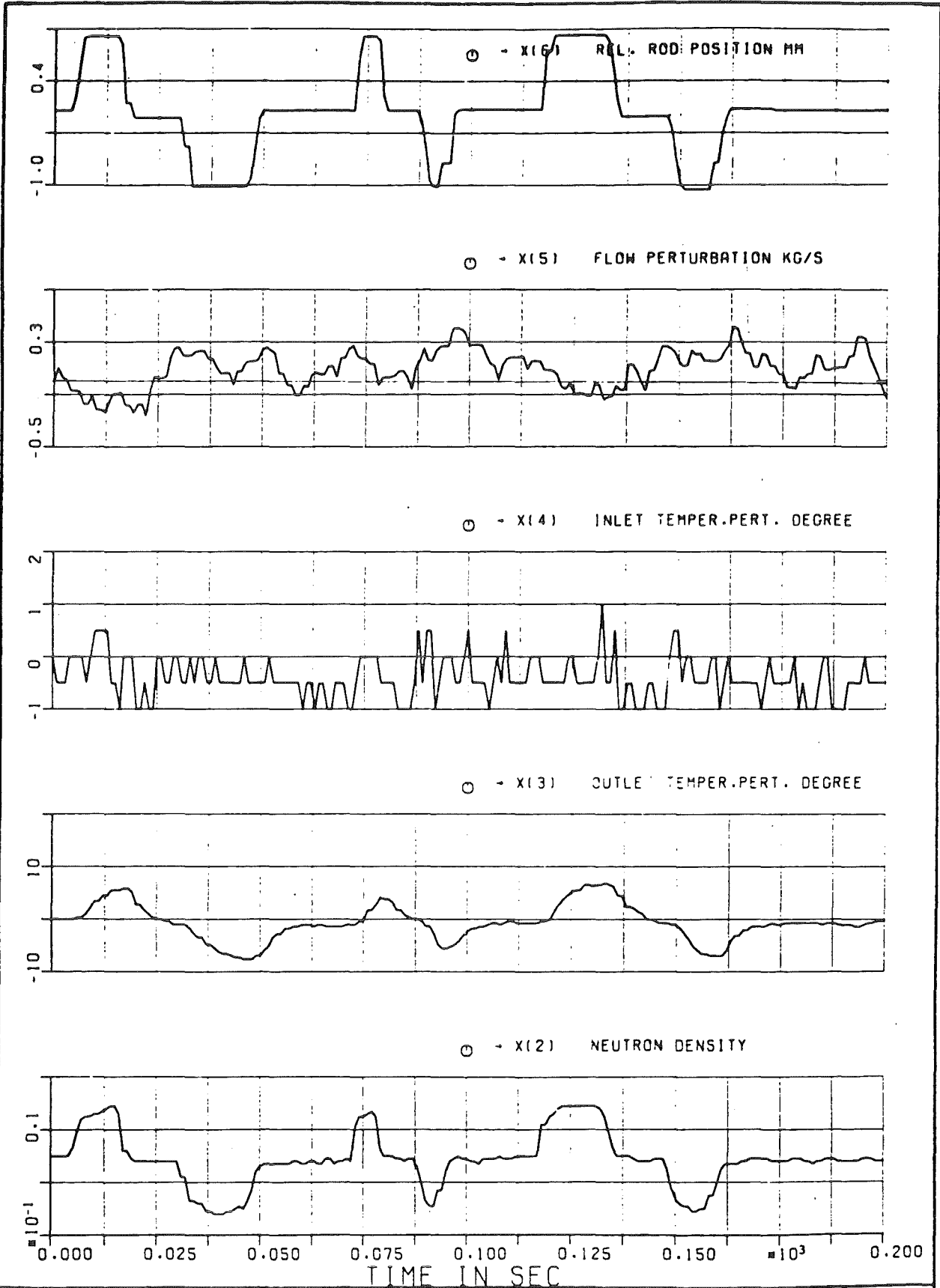
$$y^{k+2} - y^{k+1} = \phi_{22} \cdot (y^{k+1} - y^k)$$

and, hence, can be estimated during any transient phase, if subsequent measurement samples differ sufficiently, i. e.: $y^{k+1} - y^k \neq 0$. The actual inlet temperature at the location of the measurement is found with a simple observer.

The transport time between location of measurement and core inlet is in the order of 35 seconds for the 50 % set-point and can be computed from the geometry and the known flow rate.

The corresponding coolant volume is 5.34 m^3 , the coolant density is approximately 873 kg/m^3 and the primary flow is 133.6 kg/s .

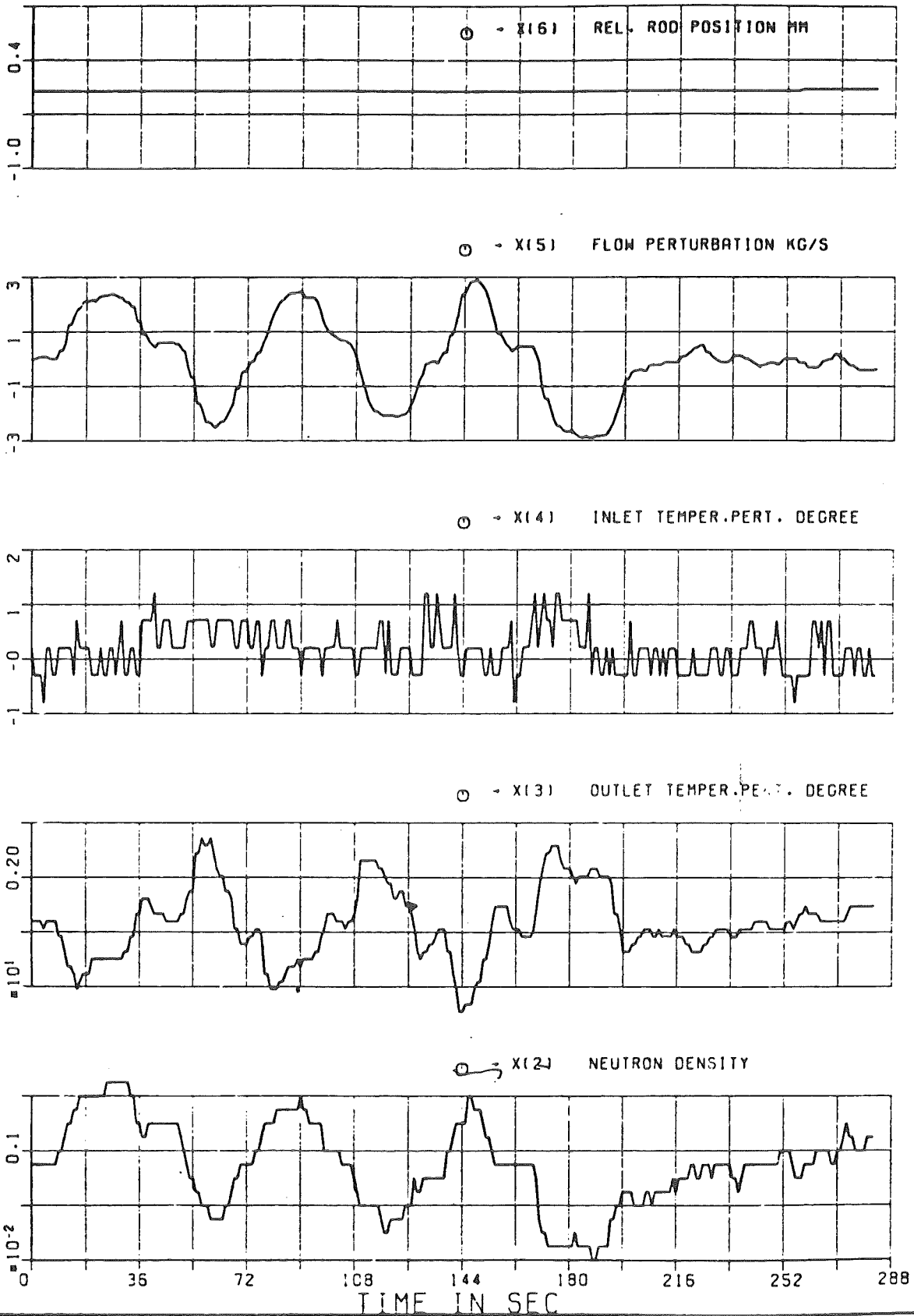
The sampling interval is 1 second and becomes a problem in processing neutron density measurements (see section 6.4.



SURVEILLANCE EXPERIMENTS KNK-II
CONTROL ROD POSITION DISTURBANCE
CASE 3

FIG. 41

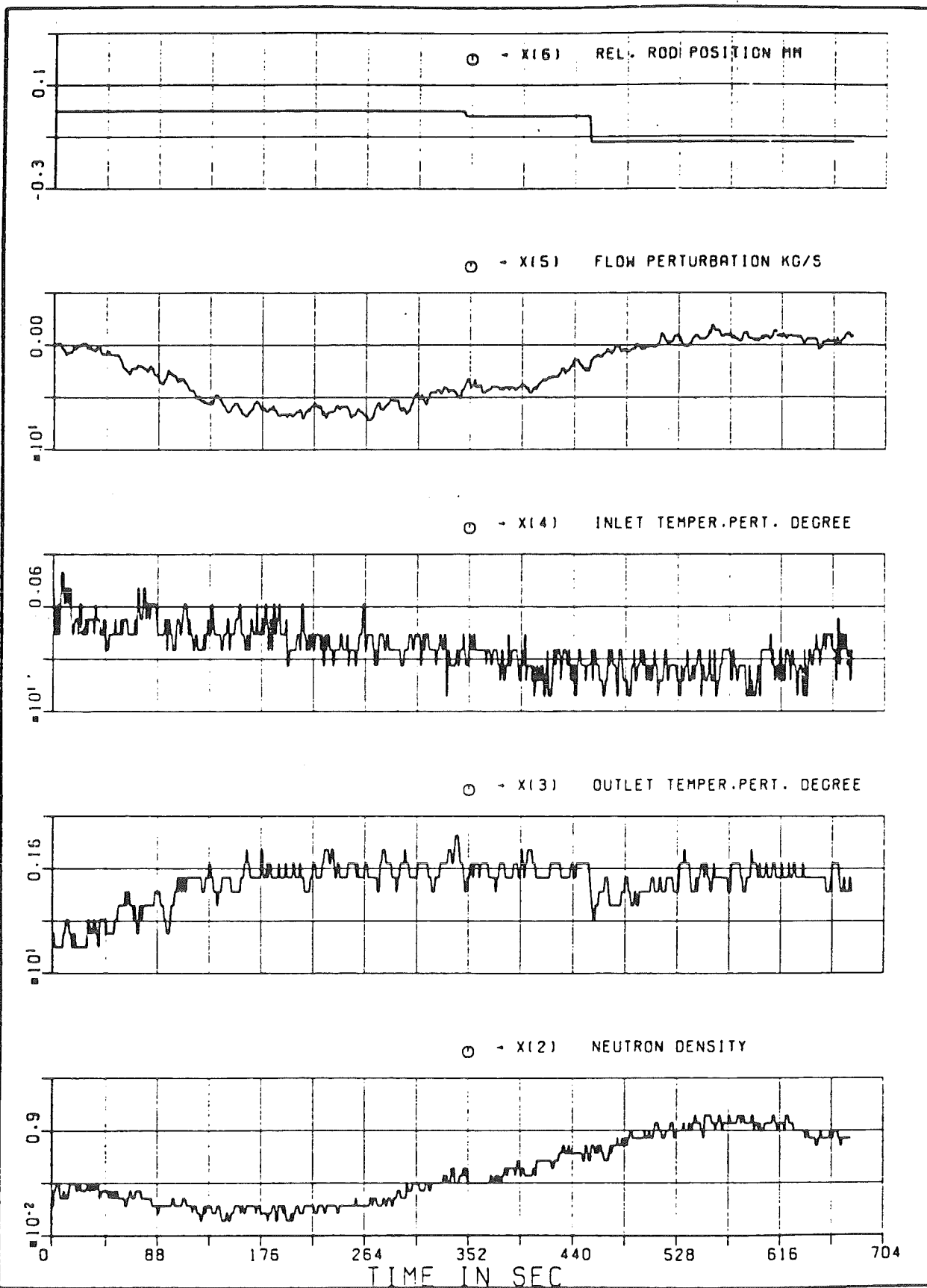
INTERATOM



INTERATOM

SURVEILLANCE EXPERIMENTS KNK-II
PRIMARY FLOW DISTURBANCE
CASE 6

FIG. 42



SURVEILLANCE EXPERIMENTS KNK-II
PRIMARY FLOW RAMP
CASE 5

FIG. 43

INTERATOM

6.2 Preprocessing of Data

There are the following two error sources, which must be eliminated/reduced in the measurements before they enter the parameter estimation module:

Quantization Error

The effect of the discretizing scheme on the measurements of temperature and neutron density for the bank position disturbance is shown in the figures 44 to 47. It is a typical quantization error and can be removed to a large extent by smoothing with SPLINE-functions. The curves will be approximated with a set of 3rd order polynomials between the measurements and, furthermore, the measurements will be smoothed. Smoothing could be improved further, by weighing the measurements in accordance with their deviation from the moving average (user's option of the subroutine), but this feature has not been explored.

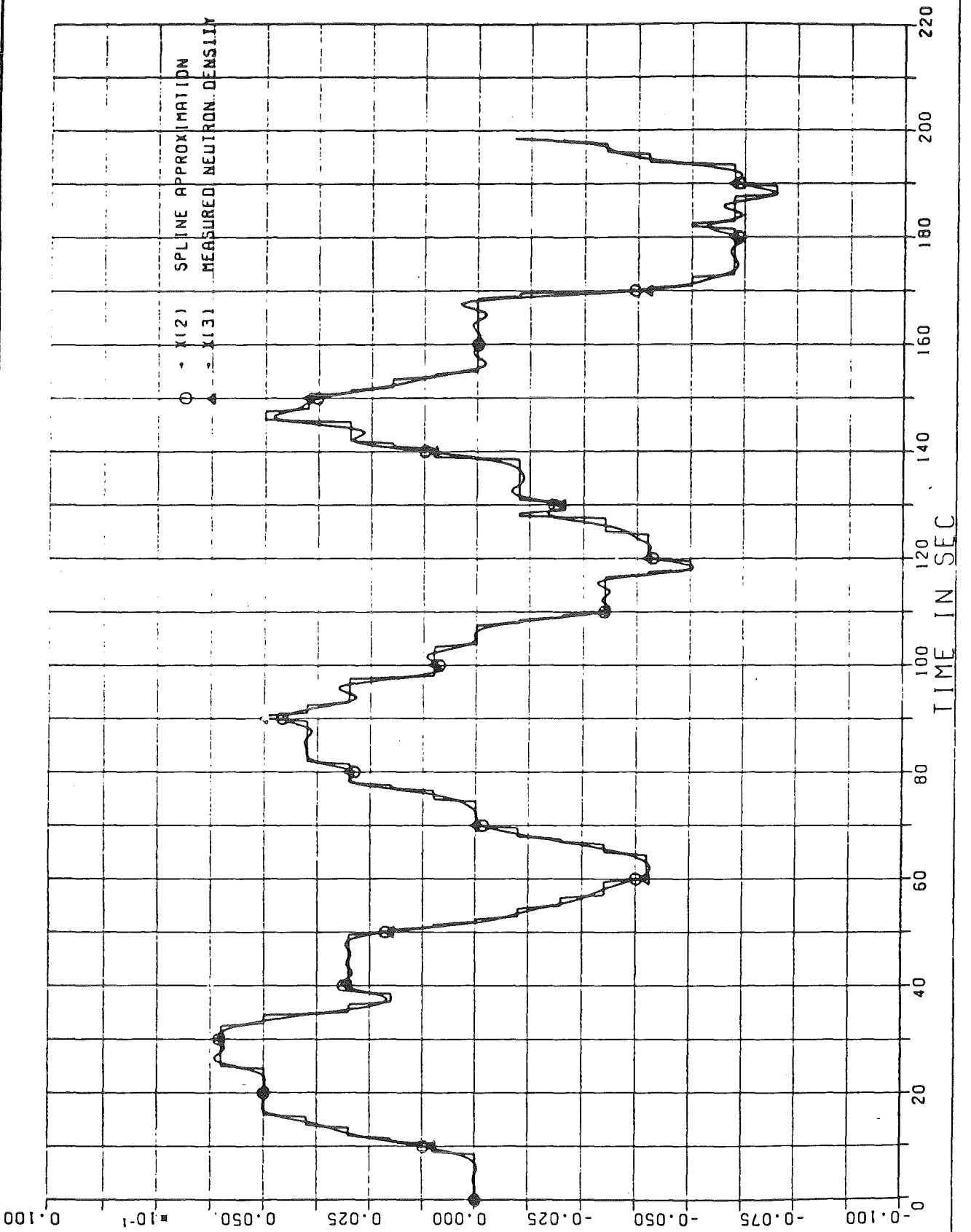
If the disturbance amplitudes become smaller, then the quantization error becomes dominant (see figure 42) and smoothing will not be a legitimate mean anymore for compensating the analog-to-digital conversion errors. The flow disturbance of section 6.1 (figure 42 and 43) is such a case and will, therefore, not be treated in this report.

Bias in the Neutron Density Measurements

The neutron density measurements

$$\delta n(t) = n(t) - n_0$$

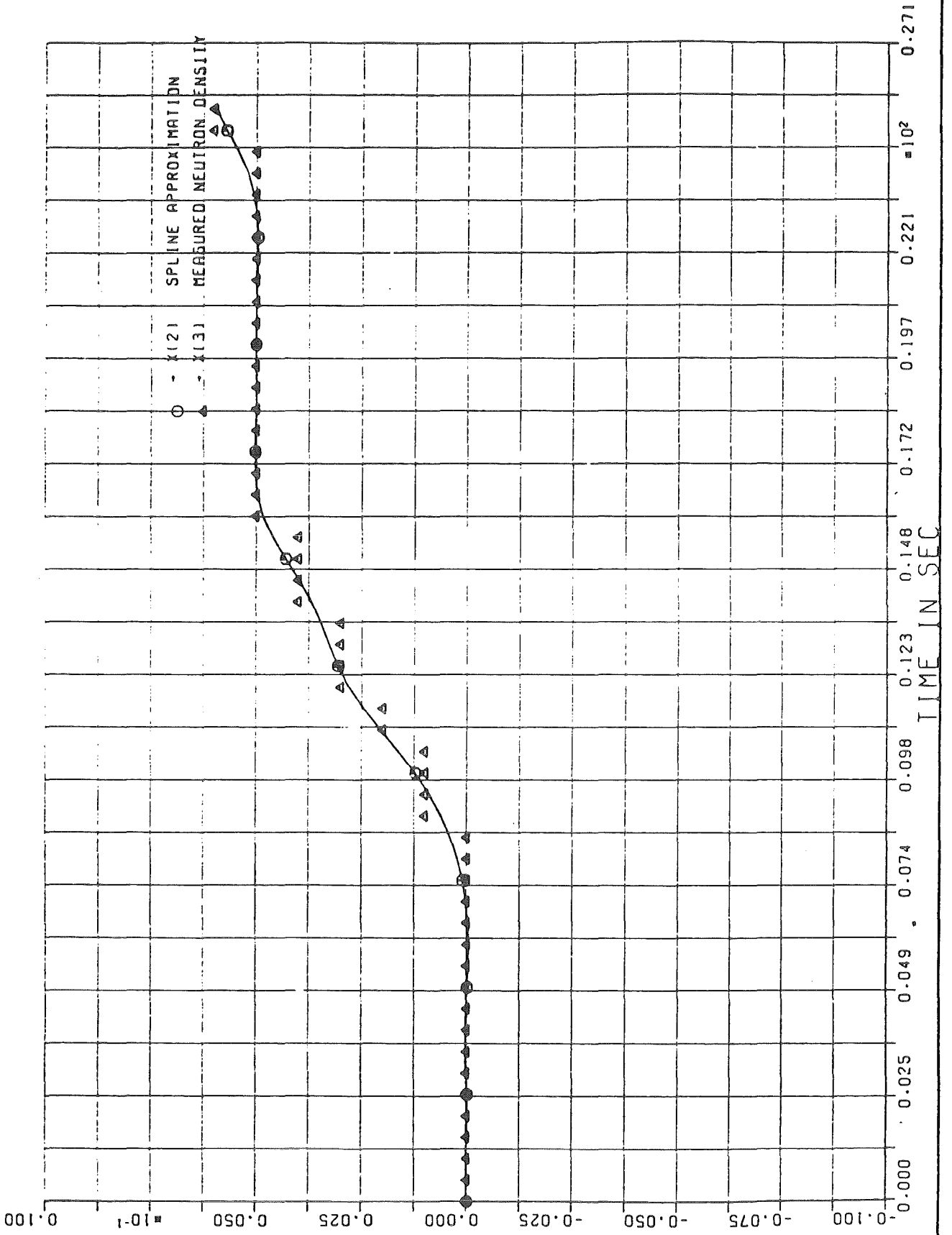
can be biased either because of instrument calibration errors or because of an erroneous nominal value n_0 .



CORRECTION OF QUANTIZATION ERRORS
INTERPOLATION AND SMOOTHING
WITH SPLINE POLYNOMIALS

FIG. 44

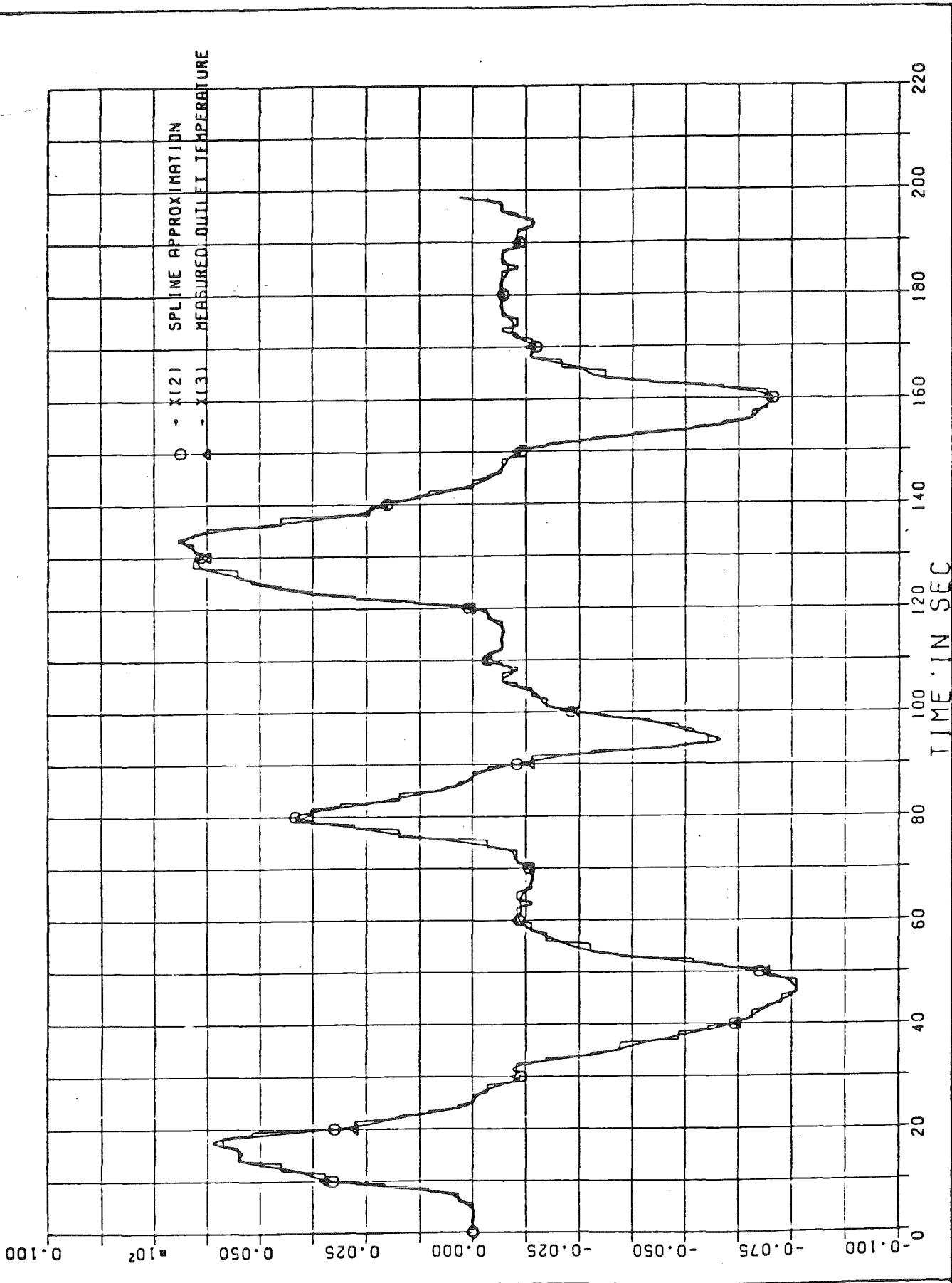
UNIVERSITÄT



CORRECTION OF QUANTIZATION ERRORS
INTERPOLATION AND SMOOTHING
WITH SPLINE POLYNOMIALS

FIG. 45

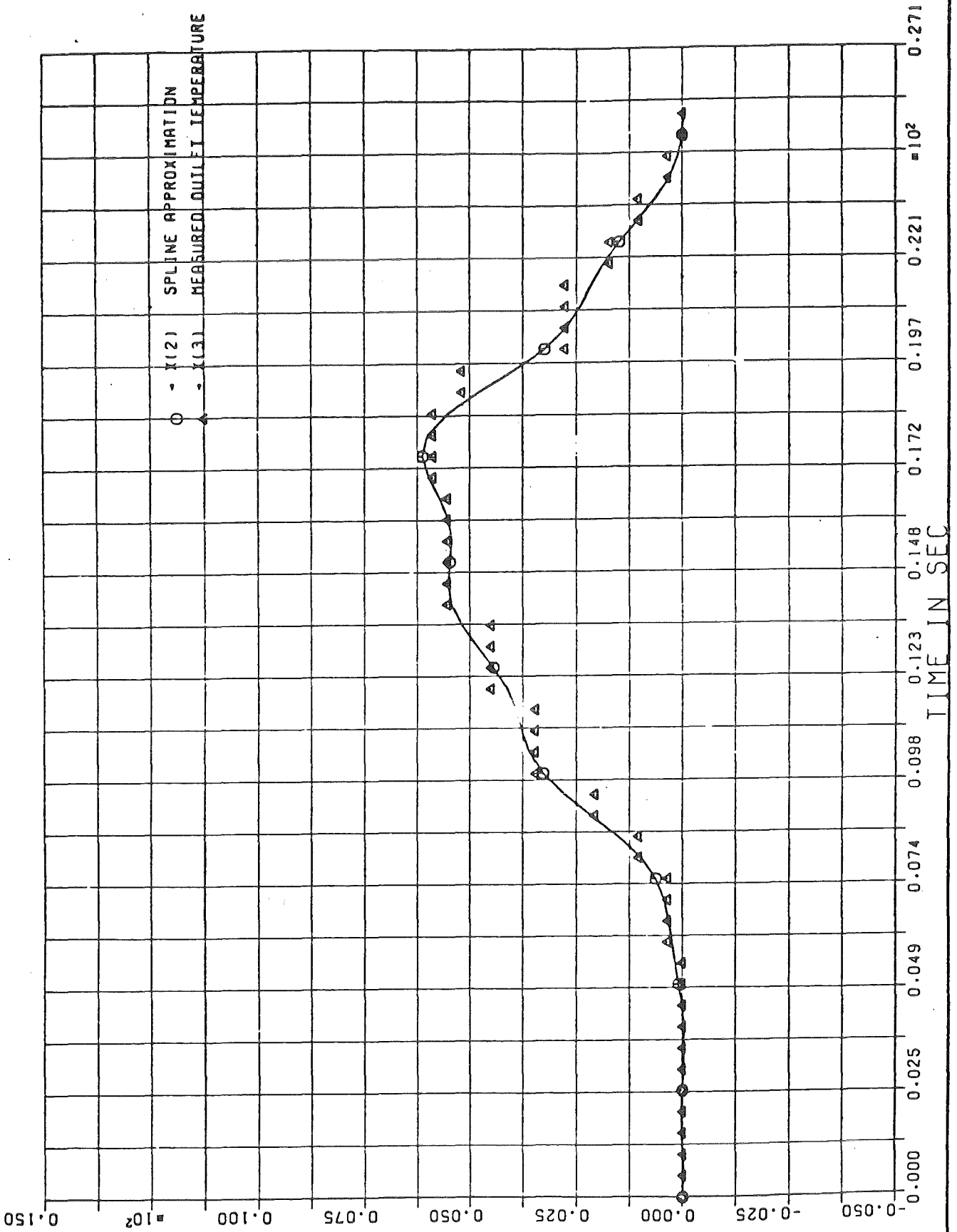
INTERATOM



CORRECTION OF QUANTIZATION ERRORS
INTERPOLATION AND SMOOTHING
WITH SPLINE POLYNOMIALS

FIG. 46

UNIVERSITY OF MICHIGAN



CORRECTION OF QUANTIZATION ERRORS
INTERPOLATION AND SMOOTHING
WITH SPLINE POLYNOMIALS

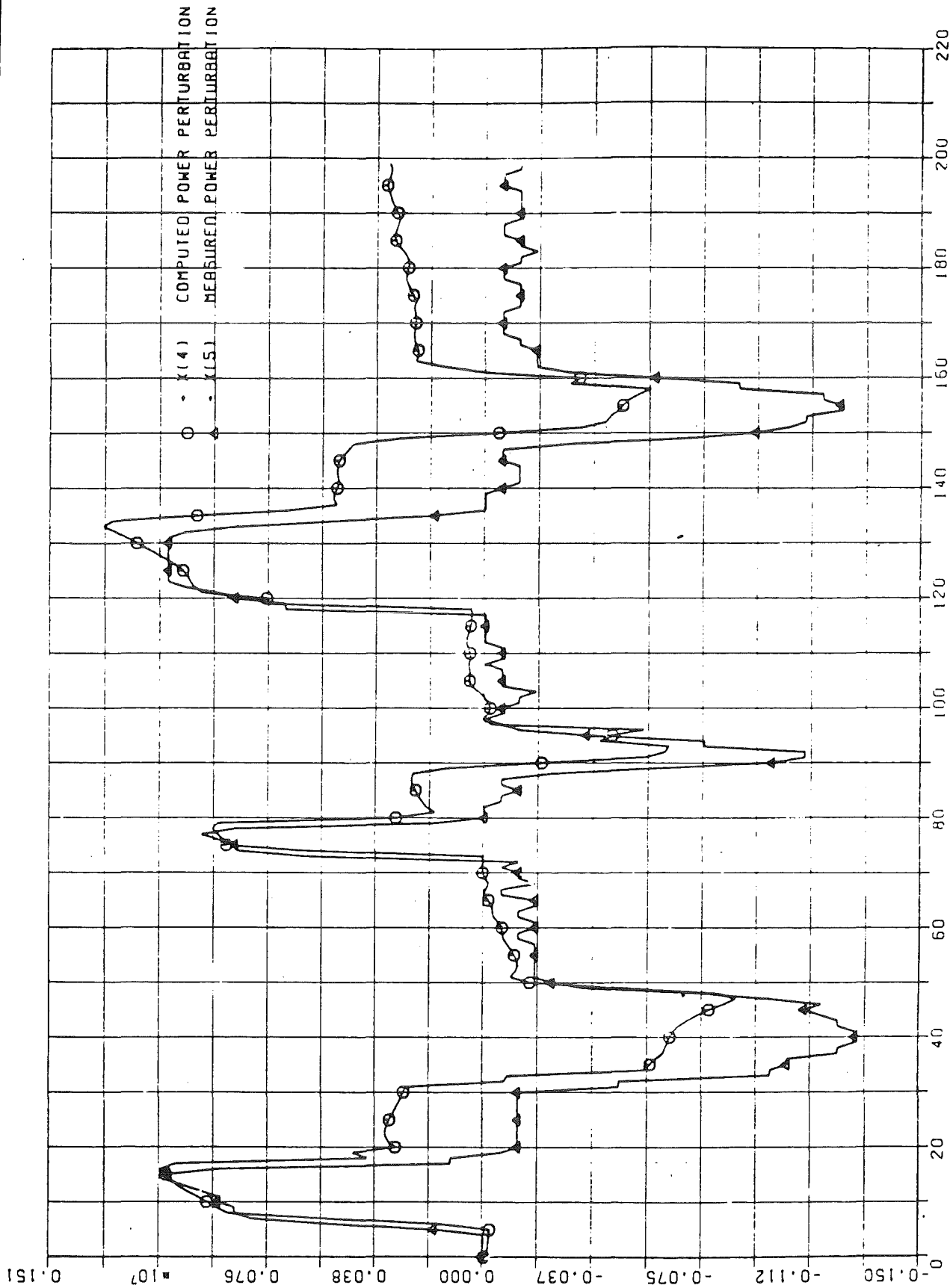
FIG. 47

INTEGRATION

The prediction model in the estimator reacts to this input error with a drift in fuel and coolant temperatures, which cause an erroneous contribution to the reactivity balance and, therefore, a drift in the computed power perturbation. The net effect is a drift in the parameter estimates.

Figure 48 shows the measured and computed power perturbation, whereby the latter was obtained with the core simulator. Input to the simulator is the measured power perturbation (open-loop mode). The drift can be removed by subtracting a constant quantity $U10$ from $\hat{n}(t)$. A first trial with $U10 = 0.116 \cdot 10^6$ led to overcompensation (figure 49). The second trial with $U10 = 0.043 \cdot 10^6$ was already successful in completely removing the drift.

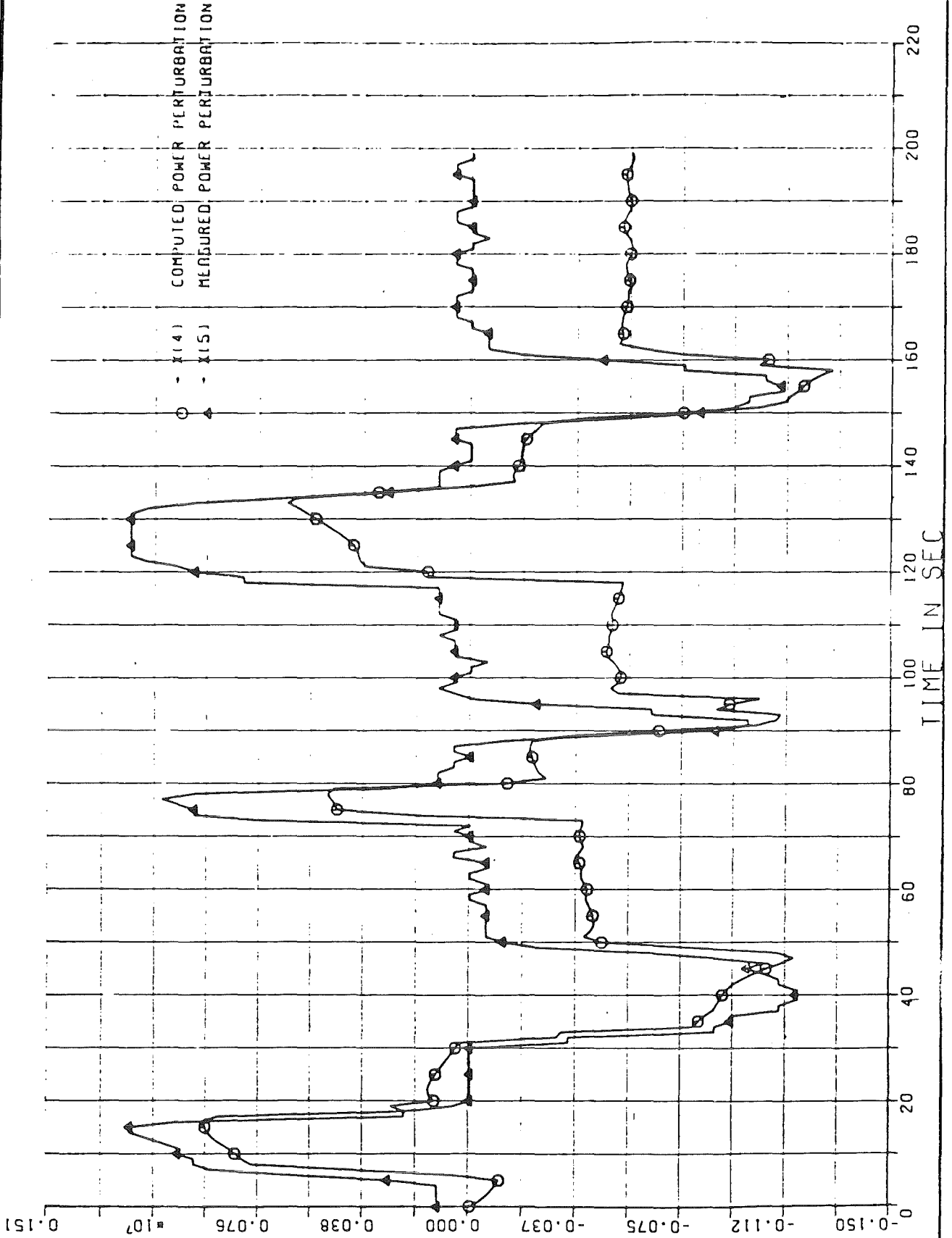
Hence, it turns out, that the on-line simulator is a sensitive instrument for determining bias errors in the neutron density measurements during stationary operation. It will suffice for off-line data analysis.



TEST OF PREDICTION MODEL ACCURACY
MEASUREMENTS NOT SMOOTHED U10 = 0
open Loop

FIG. 48

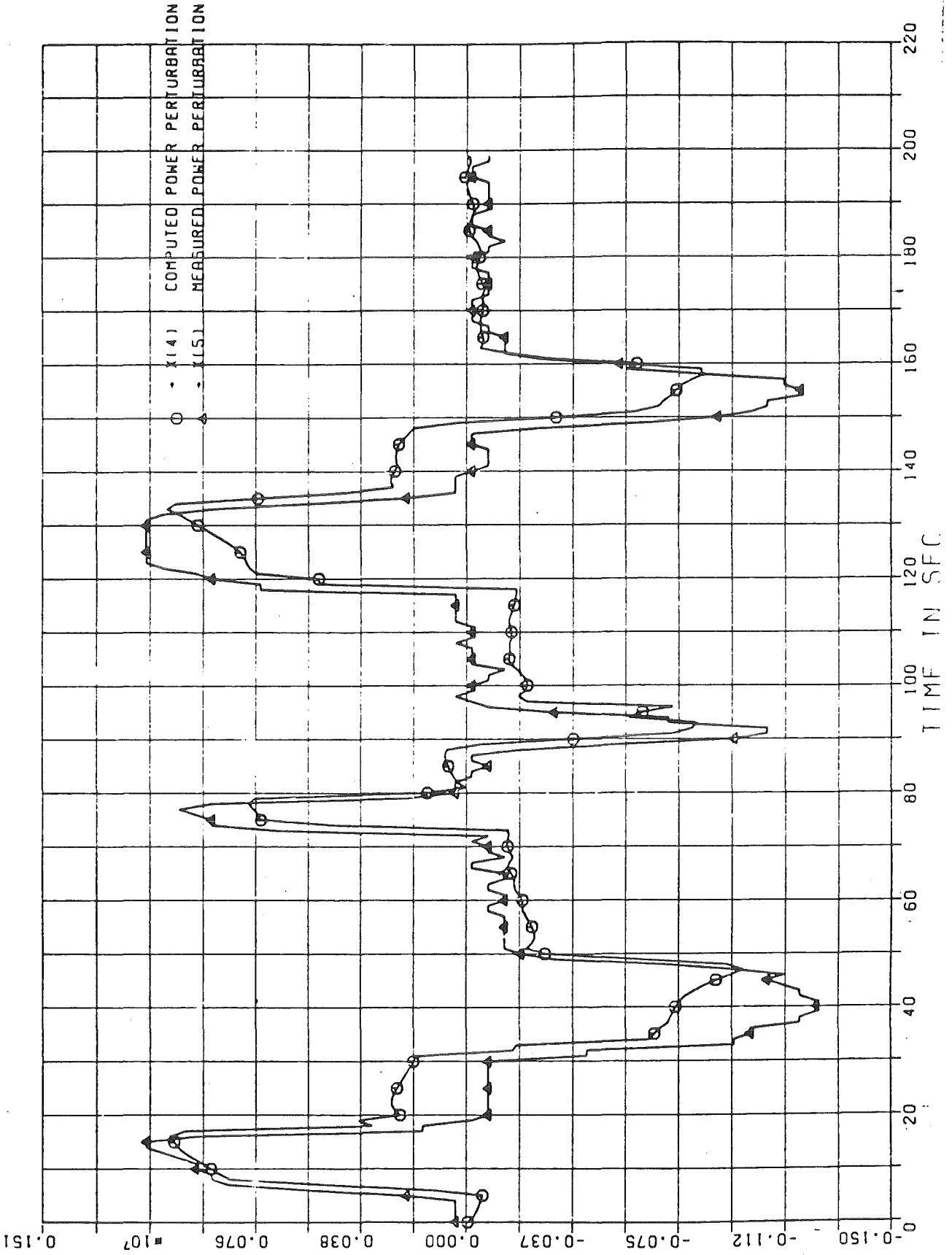
INTERATOM



TEST OF PREDICTION MODEL ACCURACY
MEASUREMENTS NOT SMOOTHED
OPEN LOOP, U(1) UNBIASED WITH $U_{10} = -0.116 \cdot 10^6$

FIG. 49

INTERATOM



TEST OF PREDICTION MODEL ACCURACY
MEASUREMENTS NOT SMOOTHED
OPEN LOOP, U(1) UNBIASED WITH $U_{10} = -0.043 \cdot 10^6$

FIG. 50

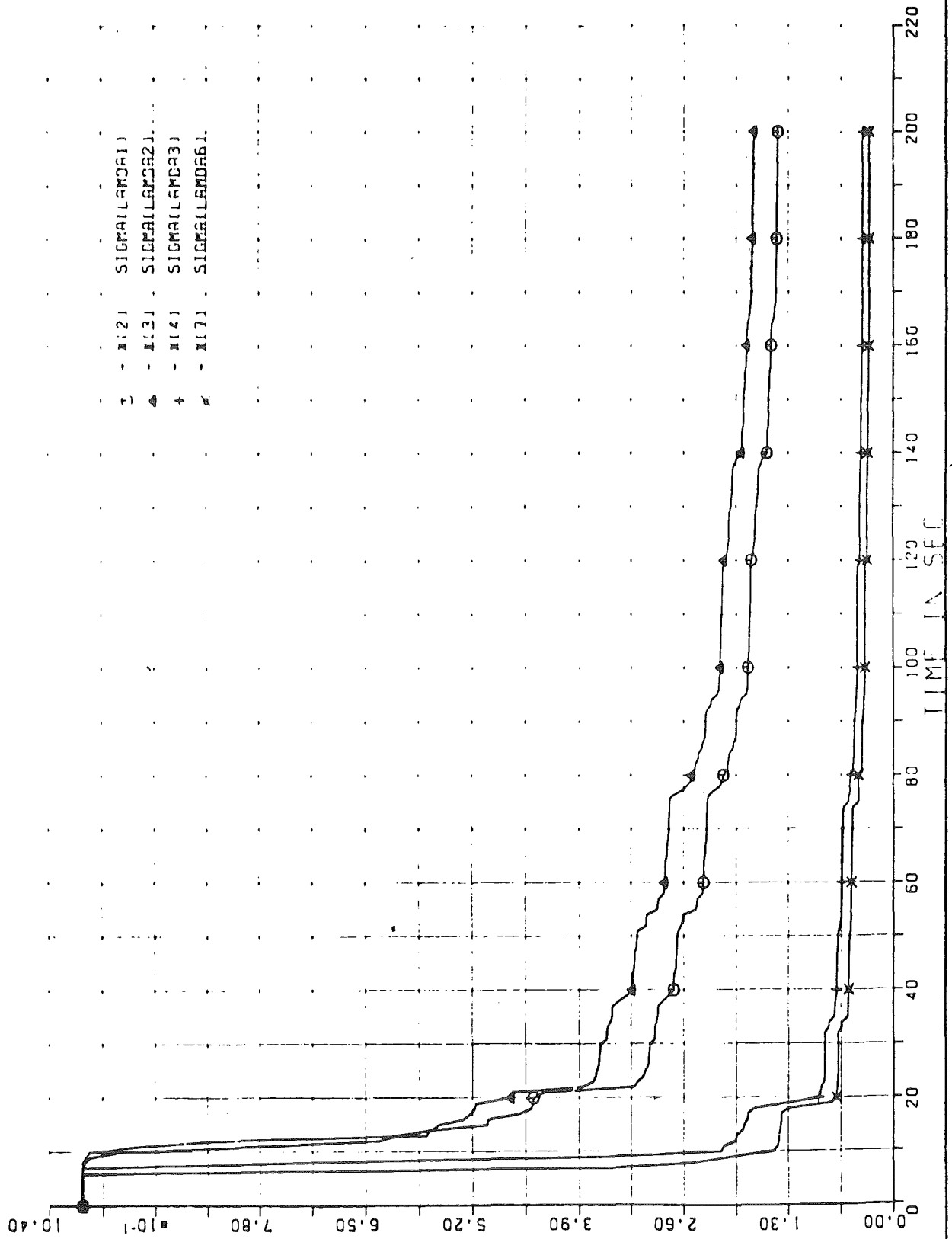
6.3 Observability Analysis

The normalized estimation error standard deviations obtained with the bank position disturbance profile actually used in this experiment (see figure 41) are shown in figure 51. The estimates of Λ_3 and Λ_6 (or Λ_4^* and Λ_7^*) converge very well, while the estimates of Λ_1 and Λ_2 (or Λ_1^* , Λ_2^* , Λ_3^*) are on the borderline to unobservability and, hence, will be biased.

In order to check what success can be expected from modifying the disturbance function, the test was repeated with simulated measurements.

If the same disturbance function is used as in the experiment, then observability becomes worth because of the missing power-noise (figure 52). If the random walk type function of figure 53 is employed, then observability becomes satisfactory (figure 55). It can be improved further, if bank position and flow-rate are disturbed simultaneously. Added power-noise will also improve convergence.

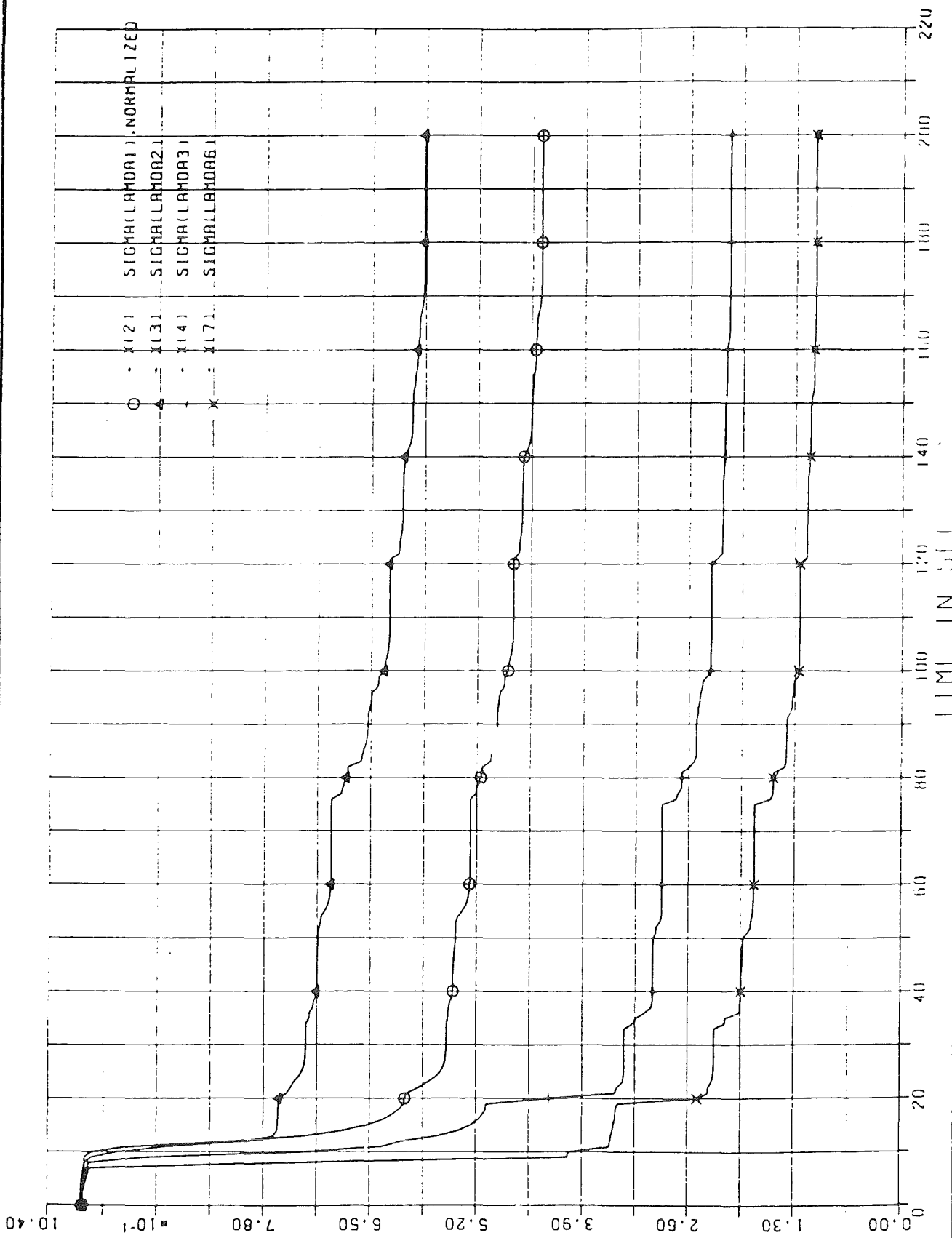
The observability test with flow-disturbance is shown in the figures 56 to 58 with simulated measurements. The actual measurements contain too large a quantization error (see section 6.1).



OBSERVABILITY TEST KNK II CORE
DISTURBANCE OF ROD POSITION
NORMALIZED STANDARD DEVIATIONS OF EST.E.

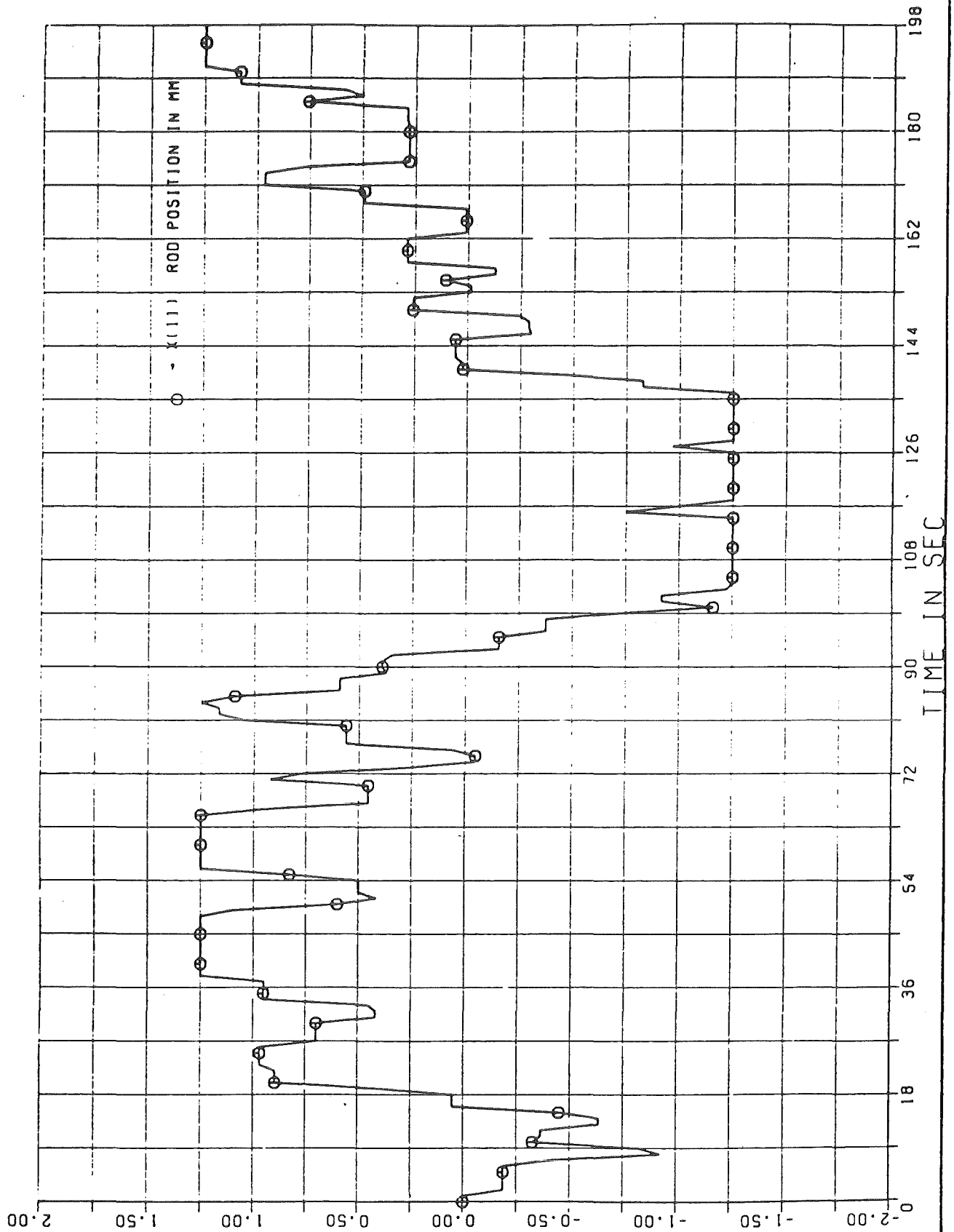
FIG. 51

INJUBKRAUWUM



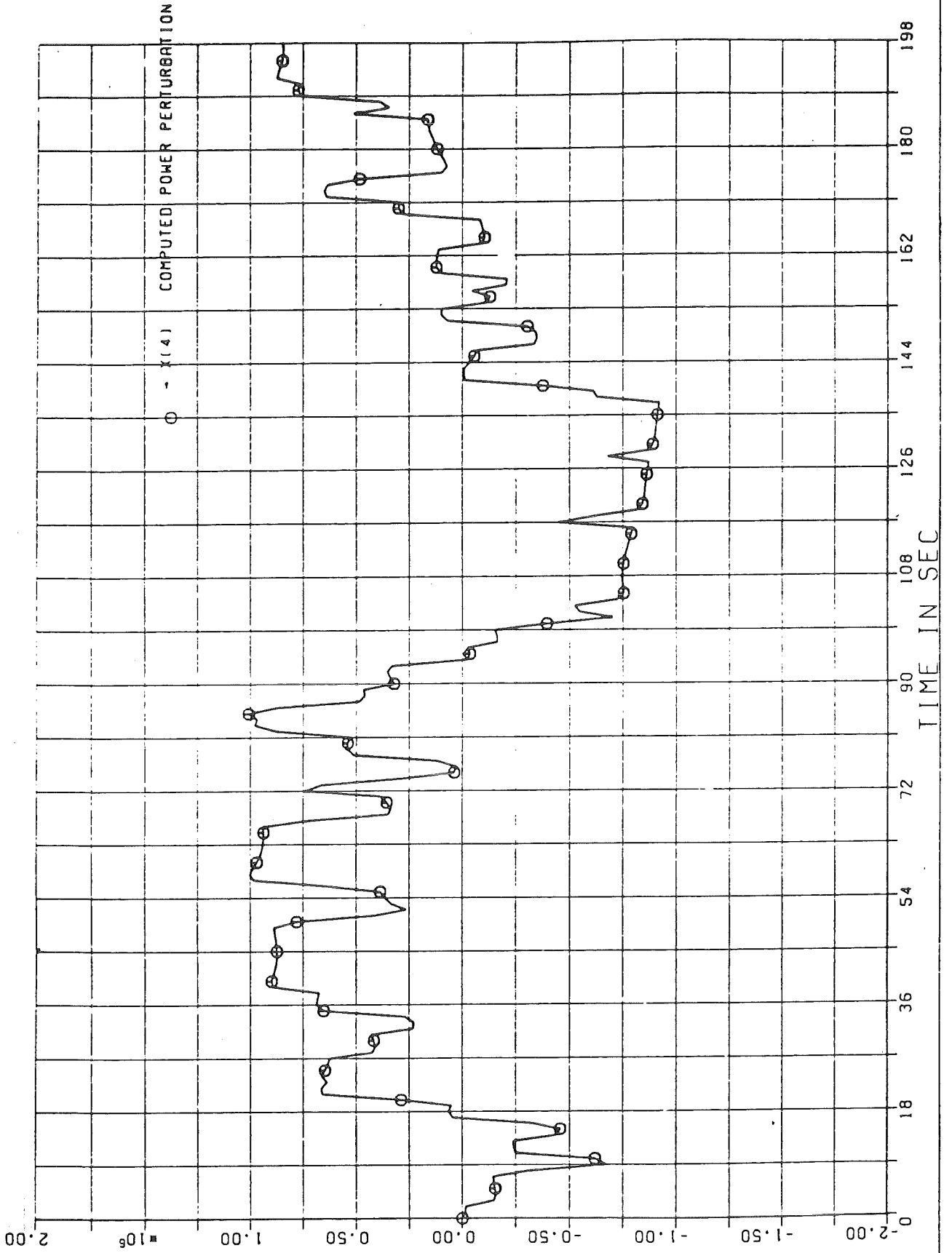
OBSERVABILITY TEST KNK II CORE
MEASUREMENTS SIMULATED
REGULAR ROD DISTURBANCE

FIG. 52



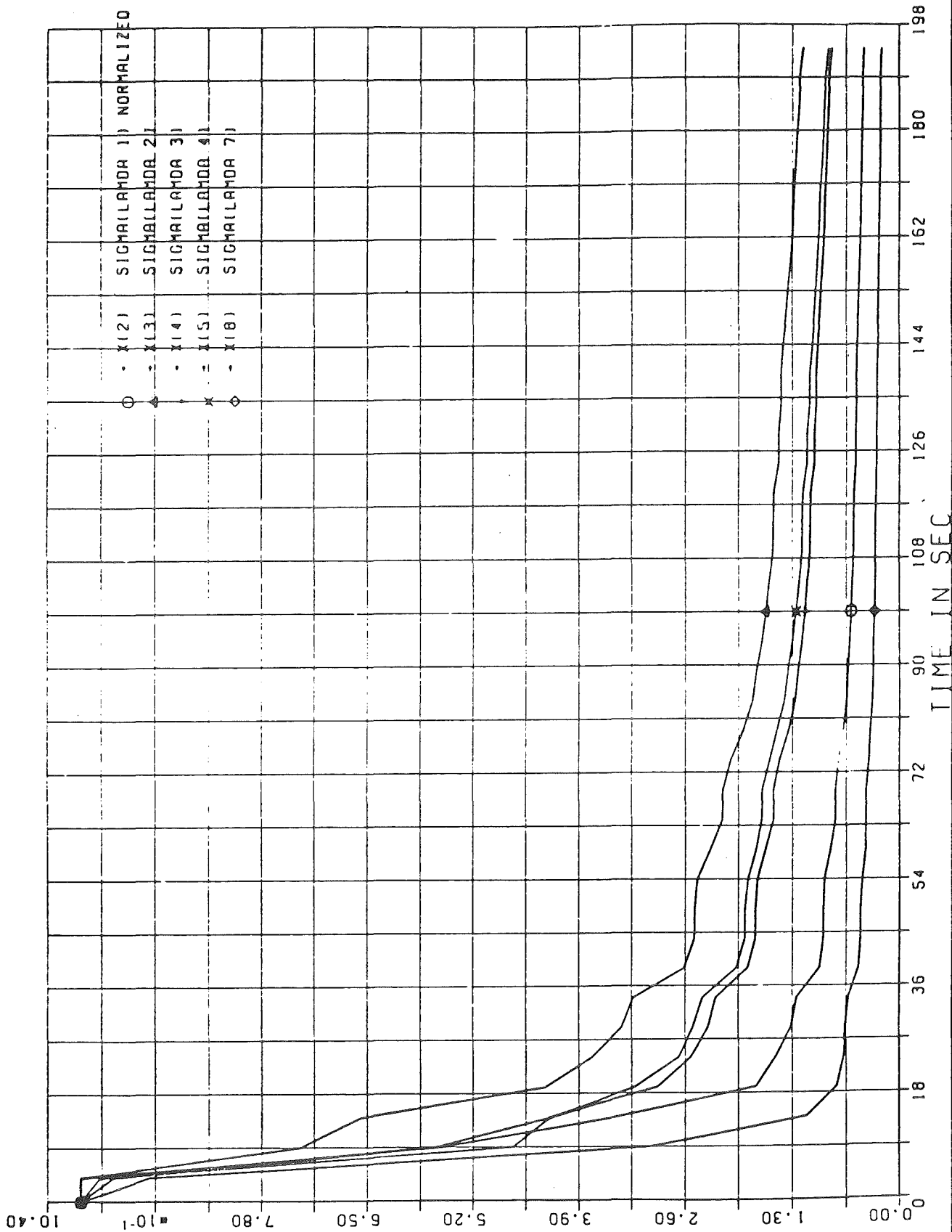
OBSERVABILITY TEST KNK II CORE
SIMULATED MEASUREMENTS
ROD DISTURBANCE BY RANDOM WALK

FIG. 53



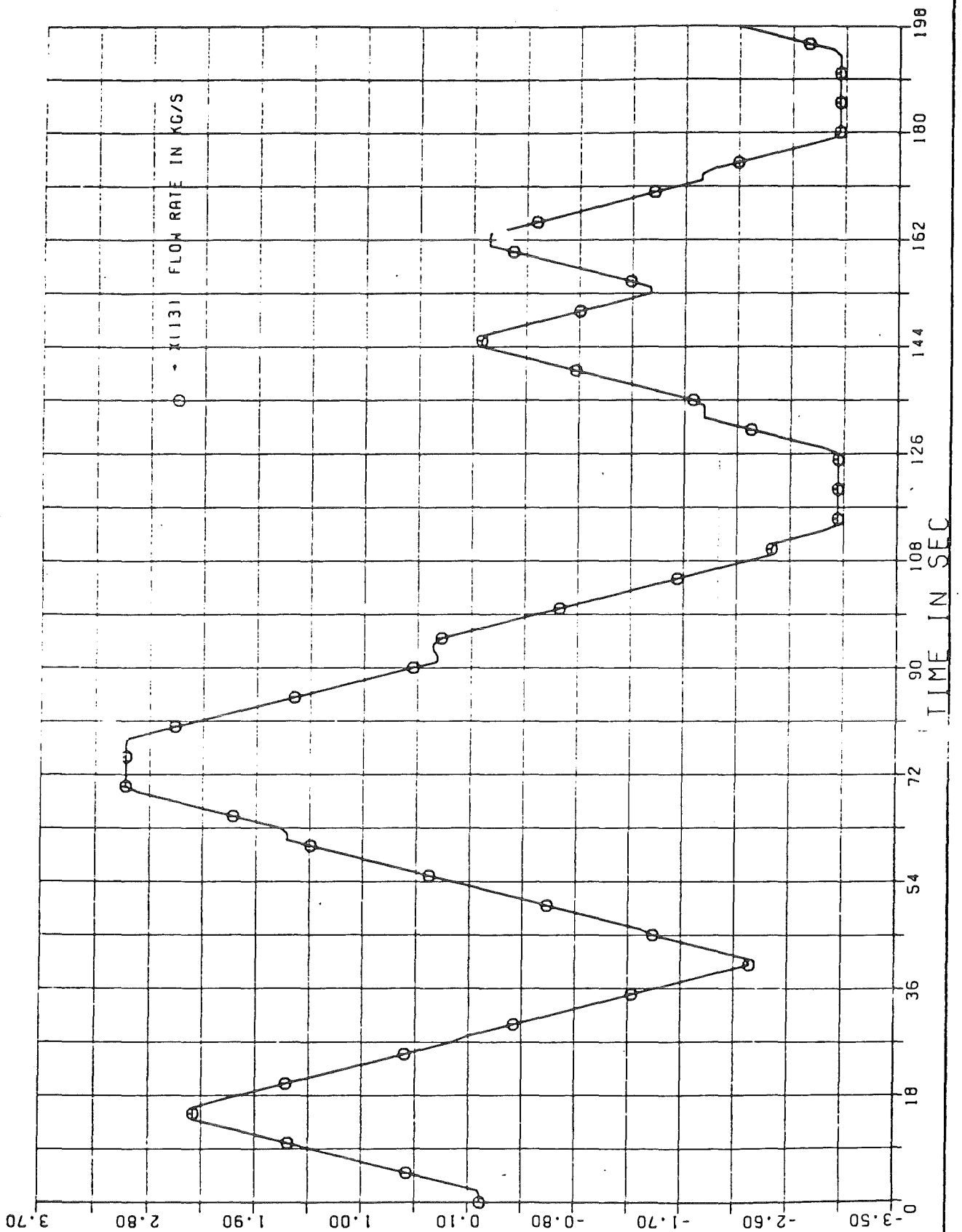
OBSERVABILITY TEST KNK II CORE
SIMULATED MEASUREMENTS
ROD DISTURBANCE BY RANDOM WALK

FIG. 54



OBSERVABILITY TEST KNK II CORE
MEASUREMENTS SIMULATED
ROD DISTURBANCE BY RANDOM WALK

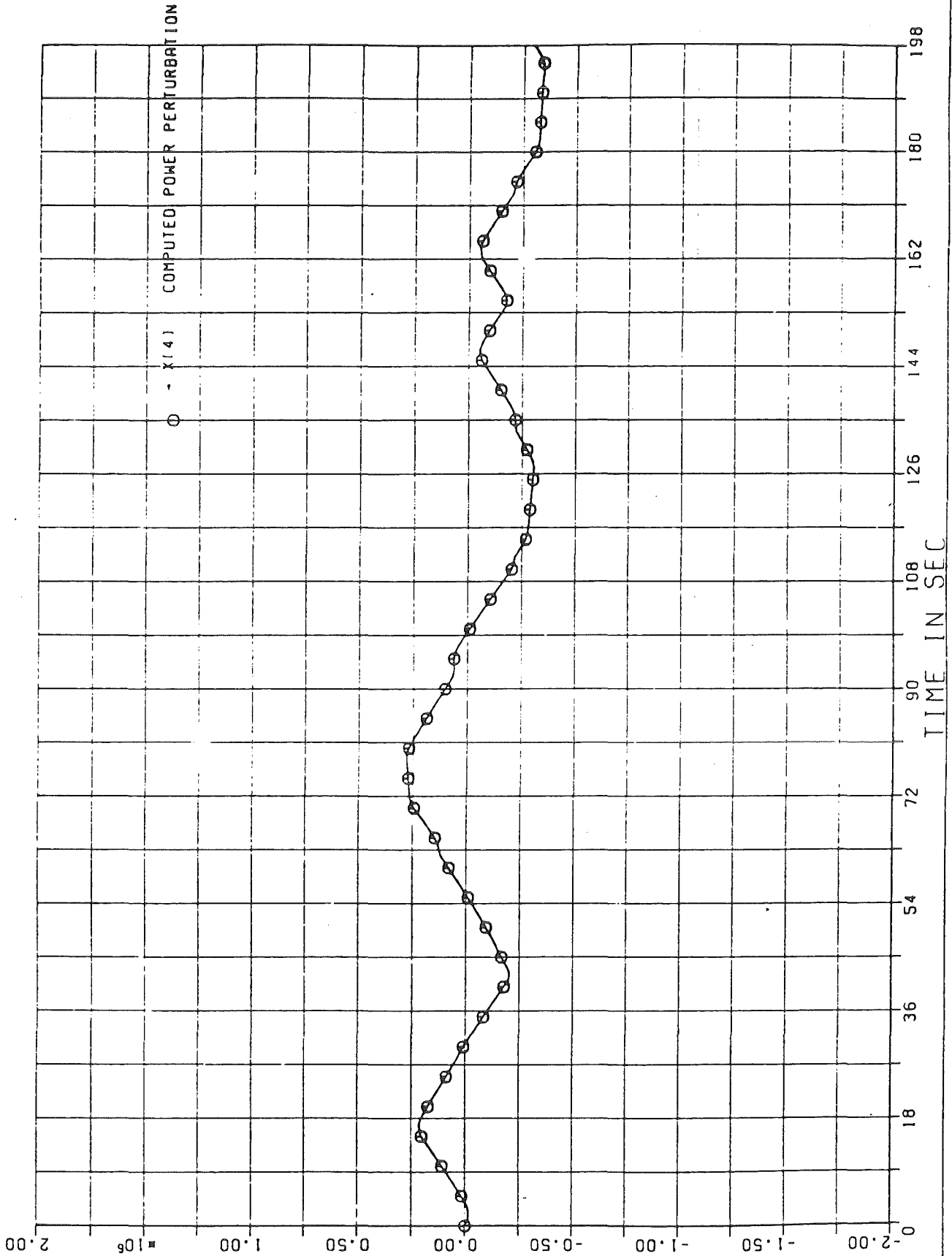
FIG. 55



OBSERVABILITY TEST KNK II CORE
SIMULATED MEASUREMENTS
FLOW RATE DISTURBANCE BY RANDOM WALK

FIG. 56

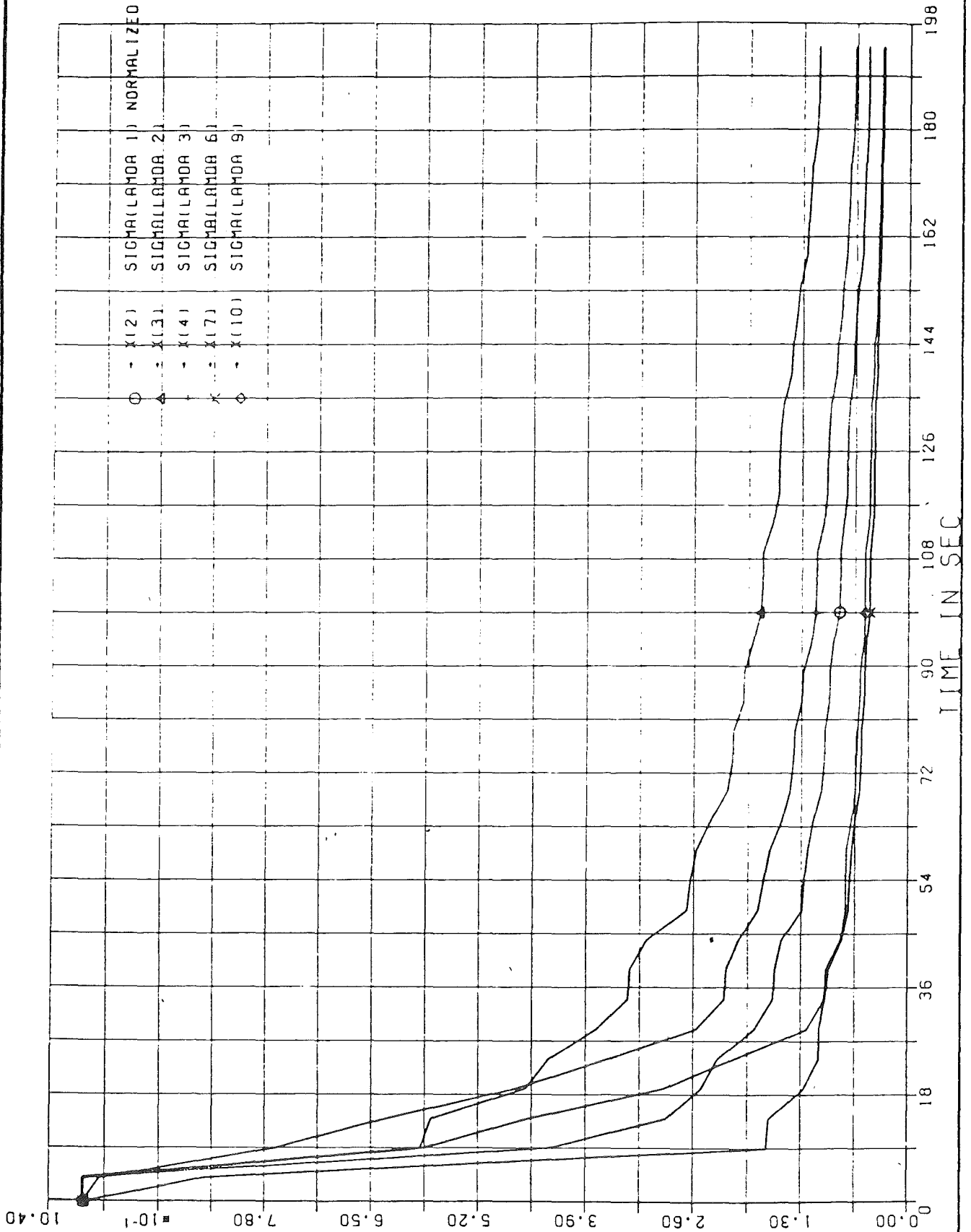
UNTERATOM



OBSERVABILITY TEST KMK-II CORE
SIMULATED MEASUREMENTS
FLOW RATE DISTURBANCE BY RANDOM WALK

FIG. 57

INTERATOM



OBSERVABILITY TEST KNK II CORE
MEASUREMENTS SIMULATED
FLOW RATE DISTURBANCE BY RANDOM WALK

FIG. 58

INTERATOM

6.4 Parameter Estimation

The off-line data analysis has revealed a variety of error sources. The bias in the measurements, especially in the neutron density measurements, is removed straight forwardly with a "diagnostic simulator". Quantization errors can be smoothed by applying SPLINE-functions, at least, if the signal-to-quantization noise ratio does not become too small. In this section, it is left to deal with the large sampling interval, and with insufficient input excitation.

At the outset, the parameter estimation procedure has been tested with simulated measurements. The model in the simulator and in the parameter estimation module were identical (zero order hold in both).

The parameter estimates were found to coincide with the true values within the first 3 digits after the decimal point already after 20 measurement samples.

Example: With the physical core parameter values

$$\begin{aligned} \kappa_p &= 0,048672, & \kappa_w &= 0,042328, & h &= 1270 \\ C_w &= 10185, & C_f &= 6144, & k &= 8000 \end{aligned}$$

we obtain the following Λ^* -parameters for a sampling interval of 1 second.

$$\begin{array}{lll} \Lambda_1^* &= 0,018353 & \Lambda_2^* &= - 0.3839 & \Lambda_3^* &= 1.1896 \\ \Lambda_4^* &= 0,290146 \cdot 10^{-6} & \Lambda_5^* &= - 0.1611 & \Lambda_6^* &= 0.11166 \\ \Lambda_7^* &= 0.9020 \cdot 10^{-6} & \Lambda_8^* &= 0.262477 & \Lambda_9^* &= - 0.37492 \\ \Lambda_{10}^* &= 0 & \Lambda_{11}^* &= - 0.3934 & \Lambda_{12}^* &= 0 \end{array}$$

Sensitivity Considerations

Since C_f and C_c cannot be estimated in this experiment, it is of interest to investigate the sensitivity of the Λ -parameters to errors in C_f and C_c . Furthermore, the Newton-Raphson procedure for computing the physical parameter estimates from the $\hat{\Lambda}_i$ sometimes has no solution because of a variety of reasons. Sensitivity considerations can be helpful in identifying the principle error source.

The following formulas relate the Λ_i -parameters with the physical core-parameters for a sufficiently small sampling interval (the relations between the Λ - and Λ^* -parameters are given in Appendix A6.3):

$$\Lambda_1 = -1 + \Delta t \cdot \left(\frac{k}{C_f} + \frac{k + 2h x_w W}{C_c} \right) - \frac{\Delta t^2}{C_f C_c} 2 h k x_w W$$

$$\Lambda_2 = 2 - \Delta t \cdot \left(\frac{k}{C_f} + \frac{k + 2h x_w W}{C_c} \right)$$

$$\Lambda_3 = 2 \frac{\Delta t^2}{C_f C_c} \cdot k \cdot x_p$$

$$\Lambda_6 = 0.$$

The equations become already erroneous for moderate sampling intervals and are useful, for instance, if reduction of the actual sampling interval by means of interpolation between measured data is acceptable. Otherwise, the sensitivity analysis is to be based upon the transition matrix formulation of Appendix A6.3.

Table 9 to 12 show the effect of variations in C_f , C_c und k on Λ_1 , Λ_2 , Λ_3 and Λ_6 for a 1 second sampling interval. Fuel element power and flow have been taken constant for simplicity. Some of the relations are shown graphically in figure 59.

Table 9: Sensitivity of Λ_1 With Respect to Variations in k, C_f, C_c ; Sampling Interval 1 Second

Parameters		Λ_1				
k	C_f	$C_c = 2000$	4000	6000	8000	9000
10000	11000	- 0.206.10 ⁻⁵	- 0.00091	- 0.0069	- 0.0192	- 0.0269
10000	7000	- 0.123.10 ⁻⁵	- 0.000542	- 0.00413	- 0.0114	- 0.0159
8000	11000	- 0.672.10 ⁻⁵	- 0.00180	- 0.0116	- 0.0295	- 0.04026
8000	7000	- 0.4435.10 ⁻⁵	- 0.00119	- 0.00767	- 0.0195	- 0.0266
8000	3000	- 0.0966.10 ⁻⁵	- 0.00026	- 0.00167	- 0.00424	- 0.00579
4000	11000	- 7.143.10 ⁻⁵	- 0.00705	- 0.0326	- 0.0699	- 0.0903
4000	7000	- 5.803.10 ⁻⁵	- 0.0057	- 0.0265	- 0.0569	- 0.0734
4000	3000	- 2.709.10 ⁻⁵	- 0.00267	- 0.0123	- 0.0265	- 0.0343
1000	11000	- 42.05.10 ⁻⁵	- 0.0196	- 0.0705	- 0.134	- 0.165
1000	7000	- 39.92.10 ⁻⁵	- 0.0186	- 0.0669	- 0.127	- 0.157
1000	3000	- 33.00.10 ⁻⁵	- 0.0154	- 0.0553	- 0.105	- 0.1299

Table 10: Sensitivity of Λ_2 With Respect to Variations in k , C_f , C_c ; Sampling Interval 1 Second

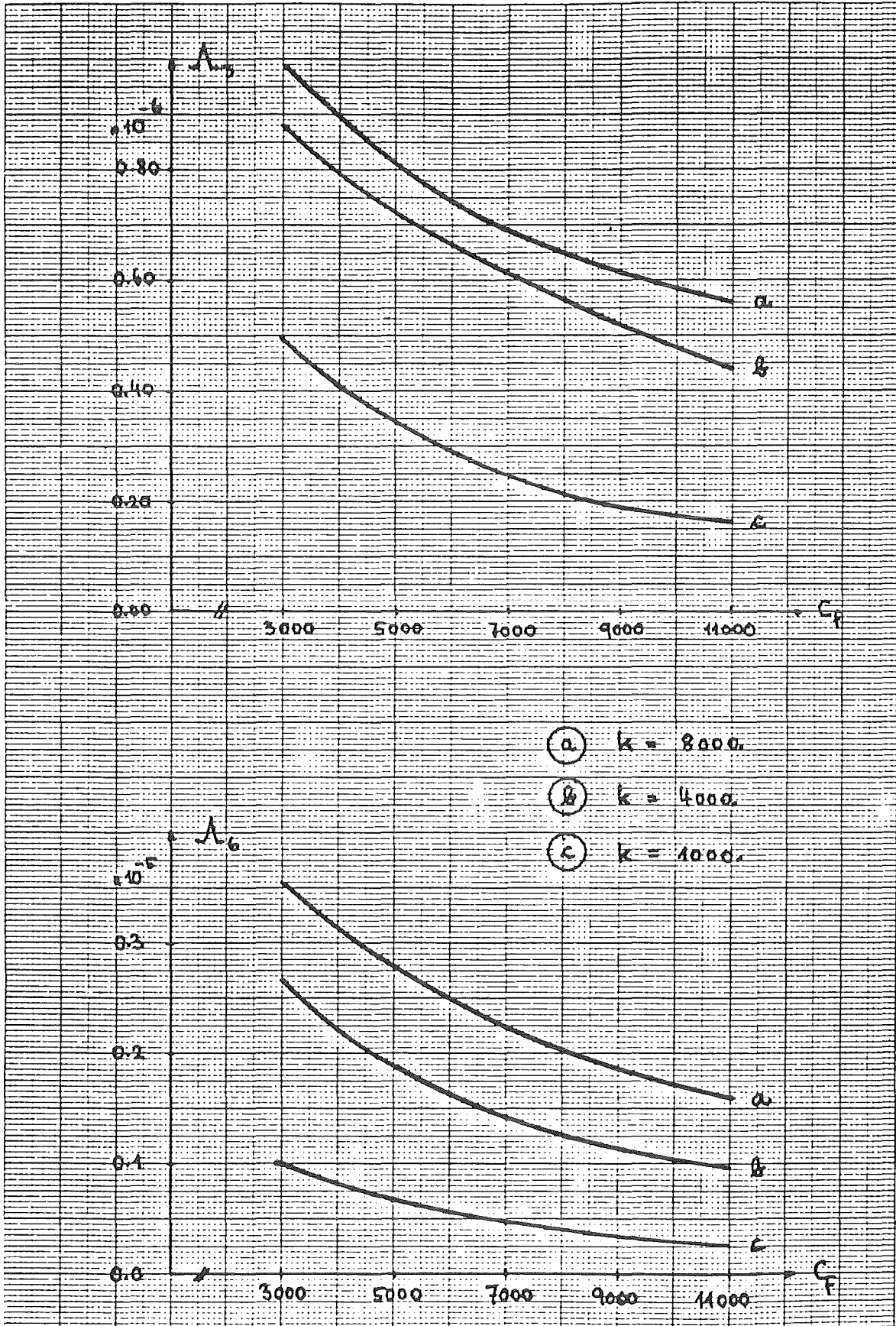
Parameters		Λ_2				
k	C_f	$C_c = 2000$	4000	6000	8000	9000
10000	11000	0.595	0.6065	0.627	0.657	0.674
10000	7000	0.449	0.469	0.497	0.531	0.550
8000	11000	0.6338	0.644	0.667	0.701	0.721
8000	7000	0.493	0.510	0.5377	0.575	0.5957
8000	3000	0.210	0.249	0.2956	0.347	0.372
4000	11000	0.7656	0.7656	0.801	0.8826	0.880
4000	7000	0.6437	0.6568	0.693	0.744	0.771
4000	3000	0.365	0.388	0.430	0.483	0.511
1000	11000	0.919	0.940	0.995	1.064	1.099
1000	7000	0.876	0.897	0.952	1.020	1.055
1000	3000	0.733	0.755	0.8098	0.878	0.9123

Table 11: Sensitivity of Λ_3 With Respect to Variations in k, C_f, C_c ; Sampling Interval 1 Second

Parameters		Λ_3				
k	C_f	$C_c = 2000$ $*10^{-6}$	4000 $*10^{-6}$	6000 $*10^{-6}$	8000 $*10^{-6}$	9000 $*10^{-6}$
10000	11000	0.174	0.339	0.467	0.548	0.573
10000	7000	0.203	0.396	0.545	0.638	0.667
8000	11000	0.178	0.347	0.473	0.546	0.567
8000	7000	0.216	0.424	0.577	0.666	0.692
8000	3000	0.207	0.421	0.581	0.673	0.699
4000	11000	0.160	0.306	0.397	0.438	0.446
4000	7000	0.216	0.416	0.541	0.599	0.611
4000	3000	0.293	0.583	0.770	0.859	0.878
1000	11000	0.069	0.125	0.153	0.160	0.161
1000	7000	0.104	0.189	0.231	0.243	0.244
1000	3000	0.208	0.383	0.470	0.497	0.498

Table 12: Sensitivity of Λ_6 With Respect to Variations in k, C_f, C_c ; Sampling Interval 1 Second

Parameters		Λ_6				
k	C_f	$C_c = 2000$	4000	6000	8000	9000
10000	11000	$0.257 \cdot 10^{-5}$	$0.233 \cdot 10^{-5}$	$0.211 \cdot 10^{-5}$	$0.191 \cdot 10^{-5}$	$0.182 \cdot 10^{-5}$
10000	7000	0.353	0.320	0.289	0.261	0.249
8000	11000	0.230	0.208	0.186	0.168	0.159
8000	7000	0.321	0.290	0.261	0.234	0.222
8000	3000	0.541	0.467	0.420	0.378	0.359
4000	11000	0.150	0.133	0.117	0.1035	$0.0977 \cdot 10^{-5}$
4000	7000	0.220	0.194	0.172	0.152	0.144
4000	3000	0.400	0.358	0.318	0.282	0.267
1000	11000	0.0482	0.0414	0.0356	0.031	$0.029 \cdot 10^{-5}$
1000	7000	0.0742	0.0638	0.0549	0.0477	0.0447
1000	3000	0.160	0.138	0.1194	0.1041	0.0975



PARAMETER SENSITIVITY

Fig. 59

The sampling interval appears to have a significant effect on sensitivity. The parameter Λ_3 , for instance, would be expected to decrease linearly with k . But with a sampling interval of 1 second, the Λ_3 -variation is reduced by a factor of 10.

Elimination of Bias due to a Large Sampling Interval

The data flow at nuclear power plants with a centralized process computer system (KNK, RAPSODIE, PHENIX) is characterized by a large sampling interval due to multiplexing. In processing sampled data for parameter estimation, the inputs and outputs are related with a discrete plant model. The inputs to the prediction model are taken constant during the sampling interval (zero order hold). In the case of slowly varying inputs (like the inlet-temperature), the zero order hold assumption does not present any problem. But it causes substantial model errors for the neutron density (or power) input and, hence, causes bias errors in the parameter estimates if the sampling interval is large.

Figure 63 illustrates the situation for the 1 second sampling interval of the experiment. Attempts to reduce the error by means of a first order hold circuit succeeded only partially because of the too large sampling interval and will not be discussed.

A quite satisfactory remedy is to reduce the time interval between the actual measurements by means of interpolation and to compute in-between measurements with the on-line core simulator.

The core simulator (for the purpose of interpolation) consists of the fuel element and reactivity models, and of a neutron kinetic model with 6 groups of delayed neutrons. Some care is required in exchanging results between the discrete thermohydraulic model (state transition formulation) and the neutron kinetic model (prompt jump approximation and Euler integration). The following timing has been implemented in the program in order to assure numerical stability:

$$x^{j+1} = \phi \cdot x^j + \Gamma \cdot u^j$$

ϕ, Γ = system matrices for the sampling interval
 $\Delta t = \Delta t / I_{AF}$, where

Δt = measurement sampling interval

I_{AF} = number of interpolation nodes to be placed
 between measurement samples

ρ^j = $\rho(x^j)$

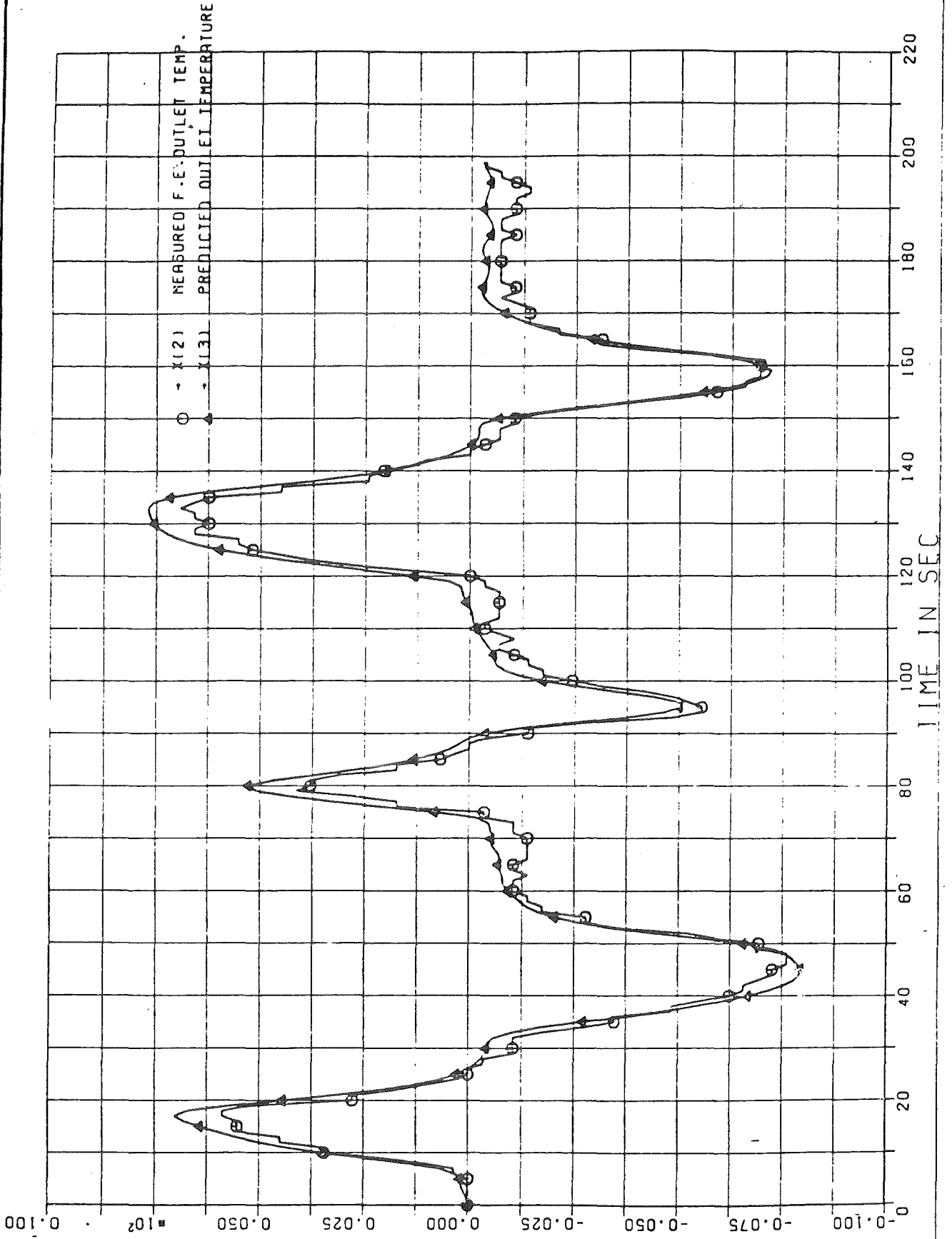
C^{j+1} = $g(C^{j+1}, \rho^j)$

If $j = I_{AF}$, then

n^{j+1} = neutron density at t_{K+1}

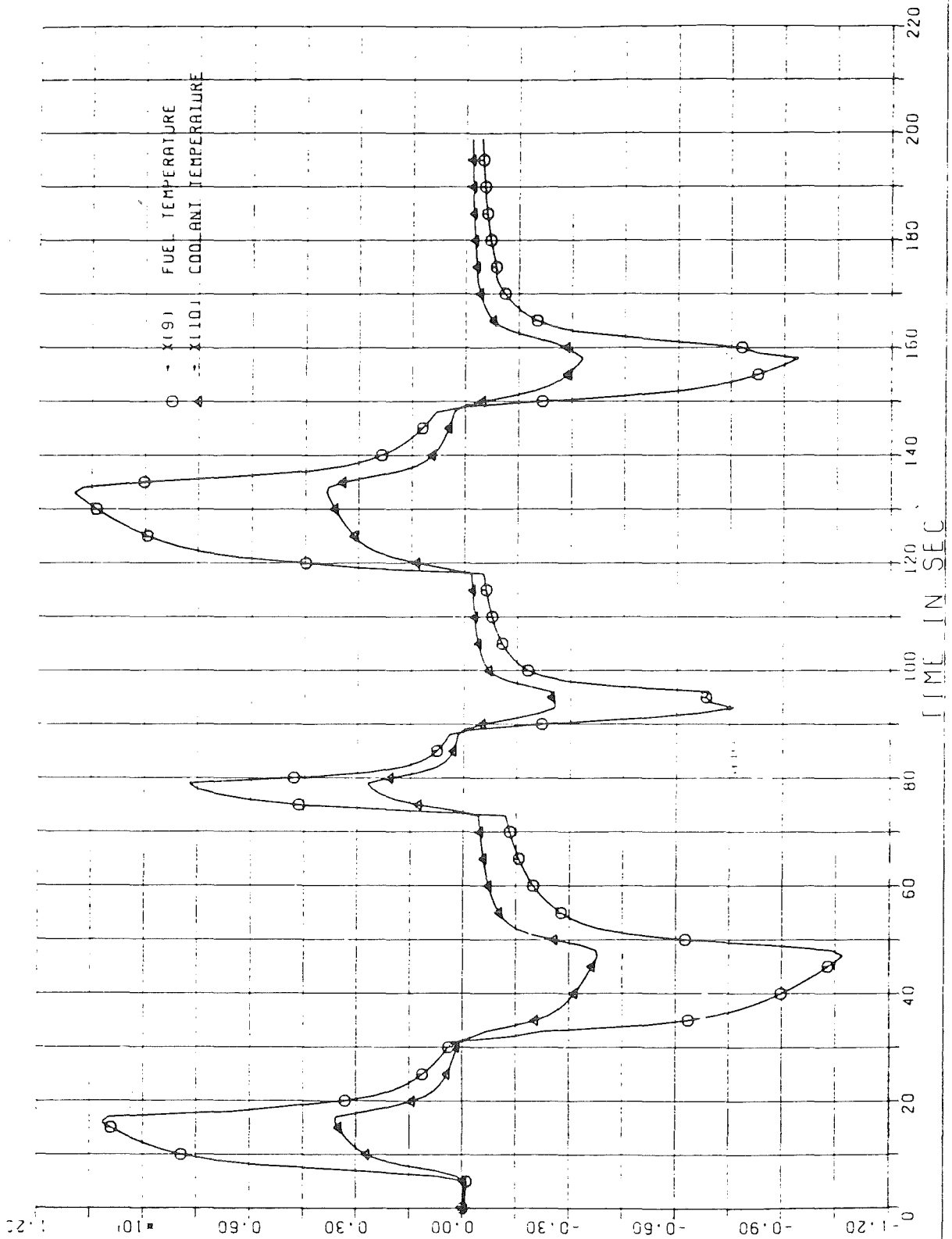
x^{j+1} = state at t_{j+1}

Figure 60 shows the measured and simulated fuel element outlet temperatures. The agreement is very good, especially if the model simplicity is taken into account. Note, that the model must hold only between two measurement samples (i. e. for 1 second). The figures 61 and 62 illustrate the availability of state components without the need for state estimation - these curves are outputs of the on-line simulator.



TEST OF PREDICTION MODEL ACCURACY
MEASUREMENTS NOT SMOOTHED
OPEN LOOP .U(1) UNBIASED WITH $U10 = -0.043 \cdot 10^6$

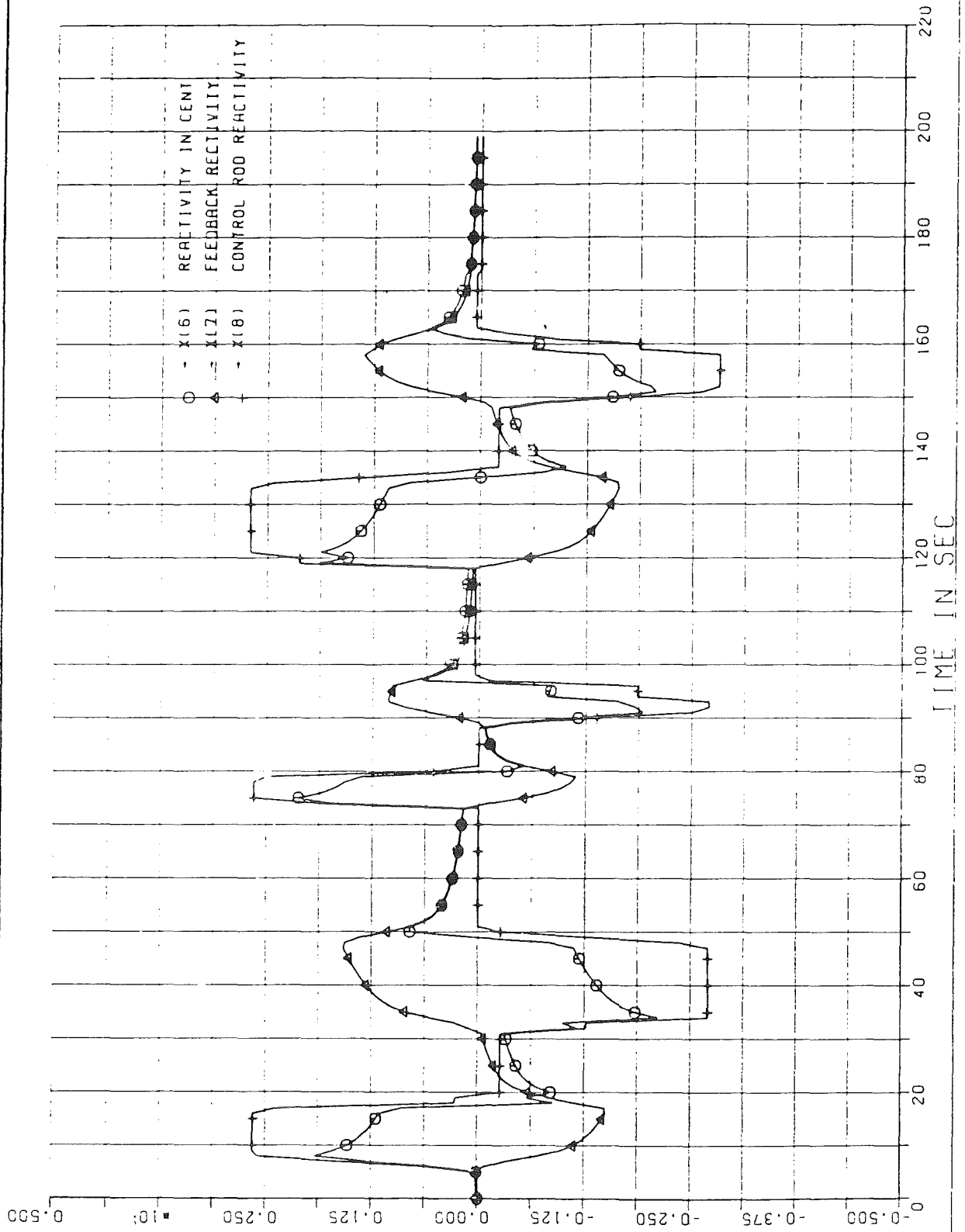
FIG. 60



TEST OF PREDICTION MODEL ACCURACY
CLOSED LOOP, $U(1) = U(2) = 0$.

FIG. 61

INTERATOM



TEST OF PREDICTION MODEL ACCURACY
 CLOSED LOOP, $U(1) = U(2) = 0$.

FIG. 62

In order to maximize the accuracy of interpolation, the simulated measurement curve, y_s , which may slightly deviate from the actual curve, will be scaled such that $y_s(t_{K+1}) = y^{K+1}$. Note that the model must only hold between the measured sample values (y^K, y^{K+1}) .

The success of interpolation in reducing the estimation error is shown in figure 64, where the mean square observation residual is employed as the performance criterion. The criterion value, J , decreases approximately quadratically with the sampling interval. A reasonable choice seems $\Delta t = 0.005$ to 0.10 seconds.

It is obvious, that errors in the measurements (y^K, y^{K+1}) affect all interpolation results. Hence, the substitution of simulated measurements is only feasible, if y^K and y^{K+1} can be made sufficiently accurate by means of smoothing. The SPLINE-function approximation (see section 6.2) turned out to perform satisfactorily.

Parameter Estimation with Limited Observability

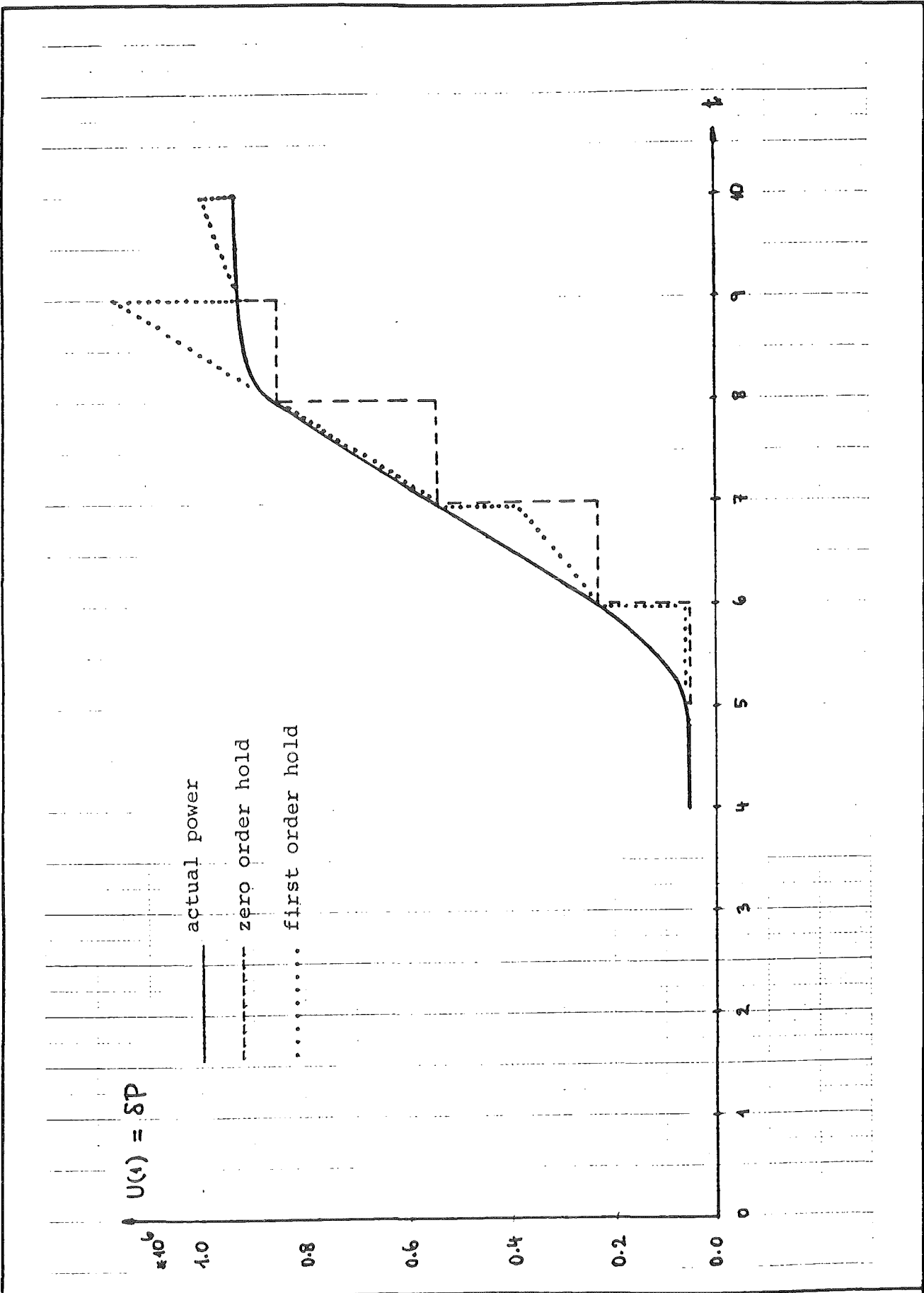
It has been shown in section 6.3, that

$$\Lambda_1^*, \Lambda_2^*, \Lambda_3^*, \Lambda_4^*, \Lambda_7^*$$

are observable, in principle, if only bank position is disturbed, and that

$$\Lambda_1^*, \Lambda_2^*, \Lambda_3^*$$

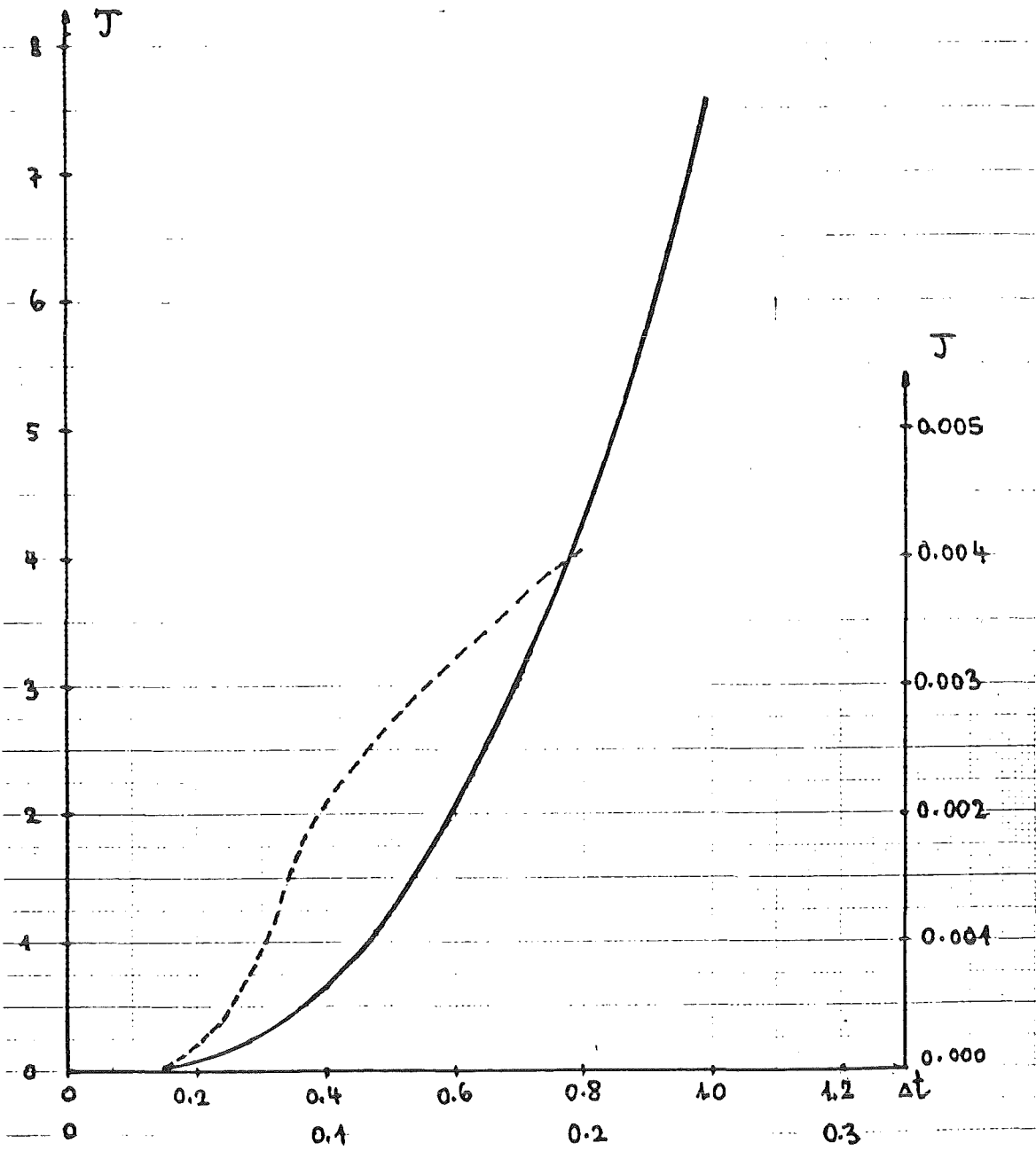
are at the borderline of being unobservable as a consequence of insufficient excitation. Unfortunately, the remaining errors in Λ_1^* , Λ_2^* and Λ_3^* affect the estimates of the observable parameters Λ_4^* and Λ_7^* via the observation residual.



SCHEMES OF INTERPOLATION BETWEEN MEASUREMENT-SAMPLES

Fig. 63

$\tau_M = 1.0 \text{ s}$, $K = 2000$



EFFECT OF SAMPLING INTERVAL ON ESTIMATION ACCURACY IN Λ_4^* , Λ_7^*

Fig. 64

The attempt will be made in the sequel to work with the erroneous Λ_4^* and Λ_7^* estimates, since the experiment cannot be repeated with a more appropriate excitation profile during this study. First we note, that (Appendix A6.3):

$$\Lambda_4^* = \gamma \cdot \Lambda_3 (k, C_f, C_c, x_p, x_w)$$

$$\Lambda_7^* = \gamma \cdot \Lambda_6 (k, C_f, C_c, x_p, x_w)$$

The heat capacities are fairly well known. Hence, it is practical to look upon Λ_4^* and Λ_7^* as nonlinear functions of the fraction of flow, x_w , and the fraction of power, x_p , of the central fuel element. But the equation system is still underdetermined, because k , x_M and τ_M are unknown. The gain factor x_M is assumed to deviate only negligibly from 1.

If a small sampling interval of $\Delta t = 0.1$ second is implemented (by means of interpolation), then Λ_7^* becomes very small, since

$$\Lambda_7^* = \gamma \Lambda_6 = 2 \gamma \Gamma_{2,1} \approx 0$$

and the estimate Λ_7^* is unreliable. We are left, therefore, only with the estimate $\hat{\Lambda}_4^*$.

The basic idea in eliminating the bias in $\hat{\Lambda}_4^*$ caused by erroneous values of k and τ_M is to minimize their effect on the criterion function:

$$J = \sum_{i=1}^N \Delta y_i^2 \quad \Delta y_i = \text{observation residual}$$

Figure 65 gives a coarse picture of the error sensitivity. The criterion, J , has a minimum for $k \approx 1250$, whereby τ_M was set equal 1 second. It decreases with increasing τ_M , but becomes unreliable below 0.002. Hence, the true τ_M is expected to lie between 1 and 1.25 seconds. It did not seem feasible to carry this procedure any further.

The functional dependence of Λ_4^* upon the physical core parameters can be expressed in a simple closed form expression for small Δt :

$$\Lambda_4^* = \gamma \Lambda_3 = 2\gamma \cdot (\phi_{21} \Gamma_M - \phi_M \Gamma_{21}) \cong 2\gamma \phi_{21} \Gamma_M$$

or

$$\Lambda_4^* = 2 \Delta t^3 \frac{x_M k x_P}{\tau_M C_C C_F}$$

Assuming, for instance, that the true values of x_P , x_M , C_C and C_F coincide with the computed nominal values, we obtain

$$\frac{k}{\tau_M} \cong 1.8 \cdot 10^3$$

where

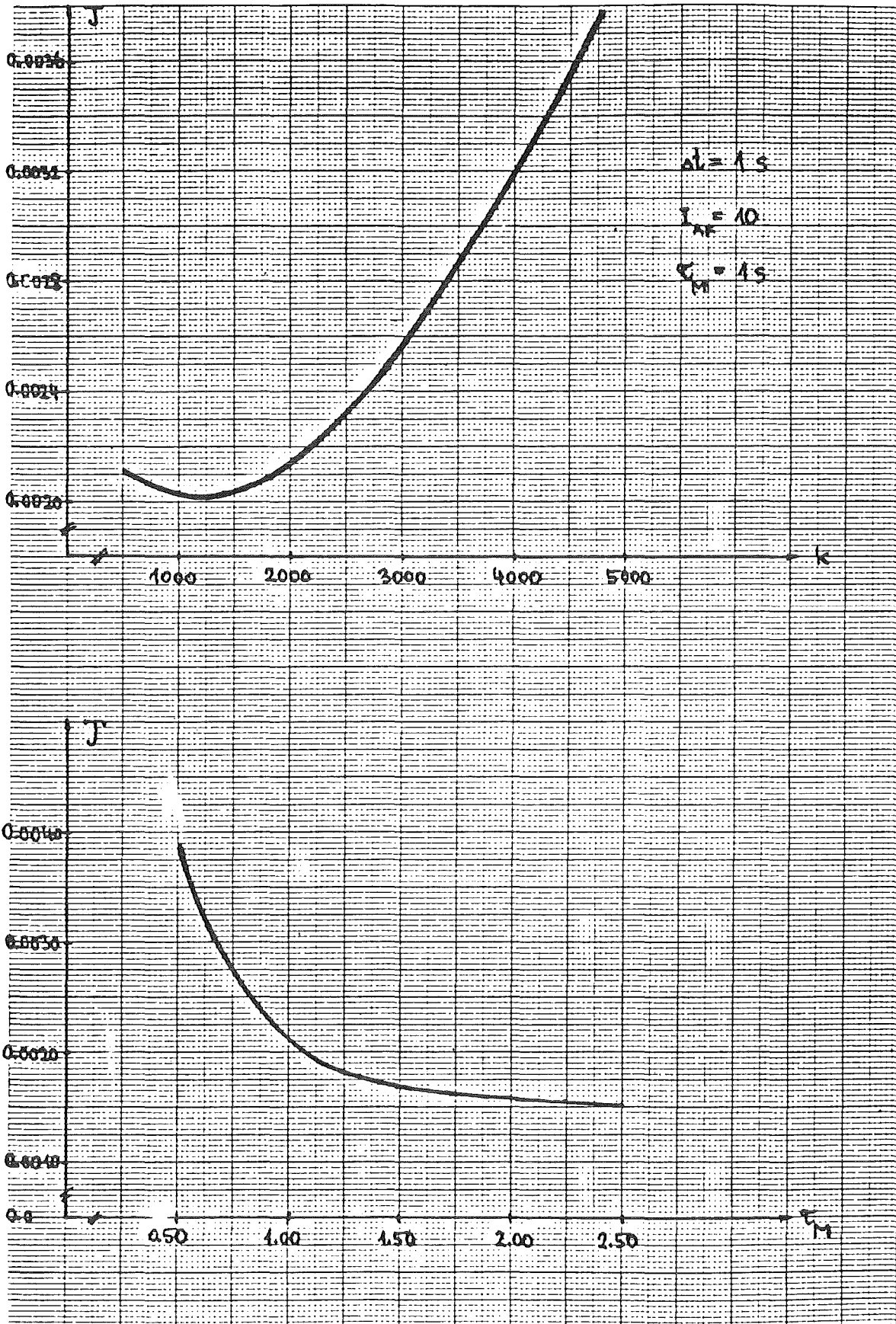
$$C_C = 10185, C_F = 6144, x_P = 0.0486, \Delta t = 0.1, \hat{\Lambda}_4^* = 0.281 \cdot 10^{-8}$$

Since τ_M was found to fall between 1 and 1.25 seconds, the heat transfer coefficient estimate must lie between 1750 and 2195.

With $\Delta t = 0.05$, we obtain the estimate $\hat{\Lambda}_4^* = 0.341 \cdot 10^{-9}$ and the range for k becomes:

$$1809 \leq k \leq 2261$$

Hence, the result is nearly independent of the sampling interval, which confirms the choice of Δt .



EFFECT OF NOMINAL PARAMETER VALUES
ON ESTIMATION ACCURACY

Fig. 65

Appendix A6.1: Generalized System-Matrices for the Case with Non-ideal Temperature Measurements

The state equations for the continuous case are

$$\begin{pmatrix} \delta \dot{T}_p \\ \delta \dot{T}_c \\ \delta \dot{T}_0 \end{pmatrix} = \begin{pmatrix} -\frac{k}{C_F} & \frac{k}{C_F} & 0 \\ \frac{k}{C_F} & -\frac{k + 2h\alpha_w W}{C_F} & 0 \\ 0 & \frac{2\alpha_m}{C_M} & -\frac{1}{\tau_M} \end{pmatrix} \cdot \begin{pmatrix} \delta T_p \\ \delta T_c \\ \delta T_0 \end{pmatrix}$$

$$\begin{pmatrix} \frac{\alpha_p}{C_F} & 0 & 0 \\ 0 & \frac{2h\alpha_w W}{C_F} & -\frac{2h\alpha_w (T_c - T_I)}{C_F} \\ 0 & -\frac{\alpha_m}{C_M} & 0 \end{pmatrix} \cdot \begin{pmatrix} \delta P \\ \delta T_I \\ \delta W \end{pmatrix}$$

and the observational equation become

$$y = \delta T_{0,j}^* = M^* \cdot x$$

where

$$M^* = [0 \quad 0 \quad 1]$$

The discrete version of the state equations for the zero order hold case has the structure

$$x^{k+1} = \Phi^* x^k + \Gamma^* u^k$$

$$y^k = M^* x^k$$

Augmented Transition-Matrix

$$\Phi^* = \left[\begin{array}{c|c} \Phi & 0 \\ \hline \xi^1 & \xi^2 \end{array} \right]$$

Φ = original transition matrix, where the outlet-temperature is measured with an ideal thermocouple

$$\xi^1 = [\xi_1^1, \xi_2^1] \quad , \quad \xi^2 = [\xi_1^2]$$

where

$$\xi_j^j = A_1^j e^{a_{33} \Delta t} + A_2^j e^{s_1 \Delta t} + A_3^j e^{s_2 \Delta t} \quad j = 1, 2$$

$$A_1^1 = a_{32} \cdot \frac{\gamma}{\tau_2} \cdot \frac{1}{(s_1 - a_{33}) \cdot (s_2 - a_{33})}$$

$$A_2^1 = a_{32} \cdot \frac{\gamma}{\tau_2} \cdot \frac{1}{(s_2 - s_1) \cdot (a_{33} - s_1)}$$

$$A_3^1 = a_{32} \cdot \frac{\gamma}{\tau_2} \cdot \frac{1}{(s_2 - s_1) \cdot (s_2 - a_{33})}$$

$$A_1^2 = a_{32} \cdot \frac{a_{33} + 1/\tau_1}{(s_1 - a_{33}) \cdot (s_2 - a_{33})}$$

$$A_2^2 = a_{32} \cdot \frac{s_1 + 1/\tau_1}{(s_2 - s_1) \cdot (a_{33} - s_1)}$$

$$A_3^2 = a_{32} \cdot \frac{s_2 + 1/\tau_1}{(s_2 - s_1) \cdot (s_2 - a_{33})}$$

and

$$\xi_1^2 = e^{a_{33} \Delta t}$$

Augmented Input-Matrix

$$\Gamma^a = \begin{pmatrix} \Gamma \\ \Gamma^1 \end{pmatrix}$$

Γ = original input matrix

$$\Gamma^1 = \begin{bmatrix} \Gamma_1^1 & \Gamma_2^1 & \Gamma_3^1 \end{bmatrix}$$

$$\Gamma_j^1 = \psi_j^1 \cdot e^{a_{33} \Delta t} + \psi_j^2 \cdot e^{s_1 \Delta t} + \psi_j^3 \cdot e^{s_2 \Delta t} + \psi_j^4$$

$j = 1, 2, 3$

$$\psi_1^1 = \frac{a_{32}}{a_{33}} \cdot \frac{\gamma}{\tau_2} \cdot \frac{b_{11}}{(s_1 - a_{33}) \cdot (s_2 - a_{33})} = \frac{A_1^1 b_{11}}{a_{33}}$$

$$\psi_1^2 = \frac{a_{32}}{s_1} \cdot \frac{\gamma}{\tau_2} \cdot \frac{b_{11}}{(s_2 - s_1) \cdot (a_{33} - s_1)} = \frac{A_2^1 b_{11}}{s_1}$$

$$\psi_1^3 = \frac{a_{32}}{s_2} \cdot \frac{\gamma}{\tau_2} \cdot \frac{b_{11}}{(s_2 - s_1) \cdot (s_2 - a_{33})} = \frac{A_3^1 b_{11}}{s_2}$$

$$\psi_1^4 = -b_{11} \cdot \left(\frac{A_1^1}{a_{33}} + \frac{A_2^1}{s_1} + \frac{A_3^1}{s_2} \right)$$

$$\psi_2^1 = \frac{A_1^2 b_{22} + b_{12}^1}{a_{33}}$$

$$\psi_2^2 = \frac{A_2^2}{s_1} \cdot b_{22}$$

$$\psi_2^3 = \frac{A_3^2}{s_2} \cdot b_{22}$$

$$\psi_2^4 = -b_{22} \cdot \left(\frac{A_1^2}{a_{33}} + \frac{A_2^2}{s_1} + \frac{A_3^2}{s_2} \right) - \frac{b_{12}^1}{a_{33}}$$

$$\psi_3^1 = \frac{A_2^1}{a_{33}} \cdot h_{23}$$

$$\psi_3^2 = \frac{A_2^2}{s_1} \cdot h_{23}$$

$$\psi_3^3 = \frac{A_3^2}{s_2} \cdot h_{23}$$

$$\psi_3^4 = -h_{23} \cdot \left(\frac{A_1^2}{a_{33}} + \frac{A_2^2}{s_1} + \frac{A_3^2}{s_2} \right)$$

Appendix A6.2: Elimination of State for the Case with Non-ideal Temperature Measurements

We proceed similar to the example already described in section 4.2. The structure of the system matrices in canonical space is:

$$\bar{\Phi}^* = \begin{pmatrix} 0 & 1 & 0 \\ 0 & 0 & 1 \\ \bar{\Phi}_{31}^* & \bar{\Phi}_{32}^* & \bar{\Phi}_{33}^* \end{pmatrix}$$

$$\bar{\Gamma}^* = \begin{pmatrix} \bar{\Gamma}_{11}^* & \bar{\Gamma}_{12}^* & \bar{\Gamma}_{13}^* \\ \bar{\Gamma}_{21}^* & \bar{\Gamma}_{22}^* & \bar{\Gamma}_{23}^* \\ \bar{\Gamma}_{31}^* & \bar{\Gamma}_{32}^* & \bar{\Gamma}_{33}^* \end{pmatrix}$$

$$\bar{M}^* = \begin{pmatrix} 1 & 0 & 0 \end{pmatrix}$$

The state can be expressed in terms of measurements as follows:

$$(A6.2-1) \begin{pmatrix} \bar{x}_1^k \\ \bar{x}_2^k \\ \bar{x}_3^k \end{pmatrix} = \begin{pmatrix} y^k \\ y^{k+1} \\ y^{k+2} \end{pmatrix} - \begin{pmatrix} 0 & 0 & 0 \\ \bar{\Gamma}_{11}^* & \bar{\Gamma}_{12}^* & \bar{\Gamma}_{13}^* \\ \bar{\Gamma}_{21}^* & \bar{\Gamma}_{22}^* & \bar{\Gamma}_{23}^* \end{pmatrix} \cdot \begin{pmatrix} u_1^k \\ u_2^k \\ u_3^k \end{pmatrix} - \begin{pmatrix} 0 & 0 & 0 \\ 0 & 0 & 0 \\ \bar{\Gamma}_{11}^* & \bar{\Gamma}_{12}^* & \bar{\Gamma}_{13}^* \end{pmatrix} \cdot \begin{pmatrix} u_1^{k+1} \\ u_2^{k+1} \\ u_3^{k+1} \end{pmatrix}$$

The details of transformation to canonical space are given next for the case, where the discrete model of the fuel-element and the thermo-couple are serially connected.

Observability Matrix (observability index $v = 3$):

$$V^* = \begin{pmatrix} 0 & 0 & 1 \\ 0 & 2\gamma & \varphi \\ 2\gamma\phi_{21} & (\phi_{22} + \varphi)2\gamma & \gamma^2 \end{pmatrix}$$

Its inverse

$$V^{*-1} = \begin{pmatrix} \frac{\varphi\phi_{22}}{2\gamma\phi_{21}} & -\frac{\phi_{22} + \varphi}{2\gamma\phi_{21}} & \frac{1}{2\gamma\phi_{21}} \\ -\frac{\varphi}{2\gamma} & \frac{1}{2\gamma} & 0 \\ 1 & 0 & 0 \end{pmatrix} \triangleq P^*$$

The elements of the system matrices in canonical space in terms of the original system matrices are

$$\bar{\phi}_{31}^* = -\varphi \cdot (\phi_{12}\phi_{21} - \phi_{11}\phi_{22}) = -\varphi \cdot \bar{\phi}_{21}$$

$$\bar{\phi}_{32}^* = (\phi_{21}\phi_{12} - \phi_{11}\phi_{22}) - \varphi \cdot (\phi_{11} + \phi_{22}) = \bar{\phi}_{21} - \varphi \bar{\phi}_{22}$$

$$\bar{\phi}_{33}^* = \phi_{11} + \phi_{22} + \varphi = \bar{\phi}_{22} + \varphi$$

$$\bar{\Gamma}_{11}^* = 0 \quad \bar{\Gamma}_{12}^* = -\gamma \quad \bar{\Gamma}_{13}^* = 0$$

$$\bar{\Gamma}_{21}^* = 2\gamma \Gamma_{21} = \gamma \bar{\Gamma}_{11}$$

$$\bar{\Gamma}_{22}^* = \gamma \cdot (2\Gamma_{22} - \varphi) = \gamma \cdot (\bar{\Gamma}_{12} - \varphi)$$

$$\bar{\Gamma}_{23}^* = 2\gamma \Gamma_{23} = \gamma \bar{\Gamma}_{13}$$

$$\bar{\Gamma}_{31}^* = 2\gamma \cdot [\phi_{21} \Gamma_{11} + \phi_{22} \Gamma_{21} + \varphi \Gamma_{21}] = \gamma \cdot (\bar{\Gamma}_{21} + \varphi \bar{\Gamma}_{11})$$

$$\bar{\Gamma}_{32}^* = 2\gamma \cdot [\phi_{21} \Gamma_{12} + \phi_{22} \Gamma_{22} + \varphi \Gamma_{22} - \frac{\varphi^2}{2}] = \gamma \cdot (\bar{\Gamma}_{22} + \varphi \bar{\Gamma}_{12} - \varphi^2)$$

$$\bar{\Gamma}_{33}^* = 2\gamma \cdot [\phi_{21} \Gamma_{13} + \phi_{22} \Gamma_{23} + \varphi \Gamma_{23}] = \gamma \cdot (\bar{\Gamma}_{23} + \varphi \bar{\Gamma}_{13})$$

The elements with bar but without asterisk denote the case with ideal temperature measurements.

Inserting (A6.2-1) into

$$y^{K+3} = \bar{M}^* \bar{x}^{K+3}$$

gives after some manipulations:

$$y^{K+3} = \Lambda^{*\top} \cdot z^*$$

where

$$z^{*K\top} = \left[\begin{array}{ccc|ccc|ccc} y^k & y^{k+1} & y^{k+2} & u_1 & u_2 & u_3 & u_1 & u_2 & u_3 & u_1 & u_2 & u_3 \\ \hline & & & & & & & & & & & \end{array} \right]$$

and

$$\Lambda^* = \begin{bmatrix} \Phi_{31}^* \\ \Phi_{32}^* \\ \Phi_{33}^* \\ \bar{r}_{31}^* - \Phi_{32}^* \bar{r}_{11}^* - \Phi_{33}^* \bar{r}_{21}^* \\ \bar{r}_{32}^* - \Phi_{32}^* \bar{r}_{12}^* - \Phi_{33}^* \bar{r}_{22}^* \\ \bar{r}_{33}^* - \Phi_{32}^* \bar{r}_{13}^* - \Phi_{33}^* \bar{r}_{23}^* \\ \bar{r}_{21}^* - \Phi_{33}^* \bar{r}_{11}^* \\ \bar{r}_{22}^* - \Phi_{33}^* \bar{r}_{12}^* \\ \bar{r}_{23}^* - \Phi_{33}^* \bar{r}_{13}^* \\ \bar{r}_{11}^* \\ \bar{r}_{12}^* \\ \bar{r}_{13}^* \end{bmatrix}$$

Appendix A6.3: Relationship between Λ^* and Λ

The Λ^* -parameters for the case of non-ideal temperature measurements can be expressed in terms of the original Λ -parameters and the time constant and gain factor of the thermo-couple at the outlet. The following table gives expressions for the parameter set No. 1 in terms of set No. 2 and in terms of the elements of the transition matrix and input matrix. The thermo-couple is characterized by

$$\varphi = e^{-\frac{(t-t_0)}{\tau_M}}$$

$$\gamma = \alpha_M \cdot (1 - \varphi)$$

New Parameter Set	Relation With Original Parameter Set	Transition Matrix Formulation
Λ_1^*	$\varphi \cdot \Lambda_1$	$\varphi \cdot (\phi_{12} \phi_{21} - \phi_{11} \phi_{22})$
Λ_2^*	$\Lambda_1 - \varphi \Lambda_2$	$\phi_{12} \phi_{21} - \phi_{11} \phi_{22} - \varphi \cdot (\phi_{11} + \phi_{22})$
Λ_3^*	$\Lambda_2 + \varphi$	$\varphi + \phi_{11} + \phi_{22}$
Λ_4^*	$\gamma \Lambda_3$	$2\gamma \cdot (\phi_{21} \Gamma_{11} - \phi_{11} \Gamma_{21})$
Λ_5^*	$\gamma \cdot (\Lambda_1 + \Lambda_4)$	$\gamma \cdot [\phi_{12} \phi_{21} - \phi_{11} \phi_{22} + 2 \cdot (\phi_{21} \Gamma_{12} - \phi_{11} \Gamma_{22})]$
Λ_6^*	$\gamma \Lambda_5$	$2\gamma [\phi_{21} \Gamma_{13} - \phi_{11} \Gamma_{23}]$
Λ_7^*	$\gamma \Lambda_6$	$2\gamma \Gamma_{21}$
Λ_8^*	$\gamma \cdot (\Lambda_2 - \Lambda_7)$	$\gamma \cdot (\phi_{11} + \phi_{22} - 2 \Gamma_{22})$
Λ_9^*	$\gamma \Lambda_8$	$2\gamma \Gamma_{23}$
Λ_{10}^*	0	0
Λ_{11}^*	$-\gamma$	$-\gamma$
Λ_{12}^*	0	0

The dependence of the Λ^* , upon the physical core parameters can be seen easily for small sample intervals. Expanding ϕ and Γ in a Taylor-series and retaining only linear terms in Δt gives:

$$\phi = I + A \cdot \Delta t$$

$$\Gamma = B \cdot \Delta t$$

Hence,

$$\phi_{11} = 1 - \frac{k}{C_f} \Delta t$$

$$\phi_{12} = \frac{k}{C_f} \Delta t$$

$$\phi_{21} = \frac{k}{C_c} \Delta t$$

$$\phi_{22} = 1 - \frac{k + 2h x_w W}{C_c} \Delta t$$

$$\Gamma_{11} = \frac{x_p}{C_f} \Delta t$$

$$\Gamma_{12} = 0$$

$$\Gamma_{13} = 0$$

$$\Gamma_{21} = 0$$

$$\Gamma_{22} = \frac{2h x_w W}{C_c} \Delta t$$

$$\Gamma_{23} = - \frac{2h x_w \cdot (T_c - T_f)}{C_c} \Delta t$$

7. Conclusions

This study consists of two parts.

The first part is concerned with existing separate core surveillance techniques. Starting from the analysis of these techniques, a rough concept for an integrated microprocessor-based core surveillance system is given.

The second part of this report describes the application of a parameter adaptive Kalman filtering technique to core surveillance. Its main features are, that all the surveillance variables which are relevant to classifying core dynamics status into normal-uncertain-abnormal can be provided to the decision making subsystems and that the cause of anomaly can be identified. Further exposure to reactor data will increase confidence in the diagnostic potentials and early warning capability of the "Global Core Surveillance Procedure".

Based on these results subsequent research and development work should concentrate on the following topics:

From the cause-consequence diagram for disturbances(cp. Fig. 1-1) appropriate algorithms aimed at combining the results of separate core surveillance techniques and gaining additional information through correlation of results should be identified.

These newly developed algorithms and existing surveillance methods will form the basis for a systems analysis. This analysis should clarify the detailed requirements for the microcomputer system with respect to speed, capacity, redundancy, diversity, reliability and the use of buses as a communication medium etc. Alternative approaches to the diagnosis of plant status, fault pattern classification and the automization of decision making should be explored particularly in situations where an earlier decision, whether resulting from greater individual measuring sensitivity or the combination of different measurements, could result in reduction of the stresses placed upon the plant. Techniques for the processing of uncertain information already applied to traffic control and medical diagnosis might be helpful.